DESIGN AND FABRICATION OF CLAY NANOCOMPOSITES FOR CONTROLLED RELEASE OF PLANT NUTRIENTS

Stanslaus Manyengo Lusambili

Reg No. SCH/H/02/2015

A thesis submitted in partial fulfillment of the requirements for the award of Doctor of Philosophy in Chemistry degree in the Faculty of Science of Masinde Muliro University of Science and Technology.

JUNE, 2021

DECLARATION

This report bears my original research work and prepared with no other than the indicated sources and support and has not been presented elsewhere for a degree or any other award.

Signature..... Date.....

Stanslaus Manyengo Lusambili

Reg No. SCH/H/02/2015

APPROVAL

The undersigned certify that they have read and hereby recommend for acceptance of Masinde Muliro University of Science and Technology a thesis entitled' Design and Fabrication of Clay Nanocomposites for Controlled Release of plant Nutrients'.

Dr Benard Omondi Omogo,

Chemistry Department,

Masinde Muliro University of Science and Technology,

Signature ……. Date…….

Professor Dickson Mubera Andala,

Chemistry Department,

Multimedia University of Kenya,

Signature……Date ……

Dr George Simiyu Manyali,

Department of Mathematics and Science,

Kaimosi Friends University College,

Signature ……. Date…….

COPYRIGHT

DEDICATION

I dedicate this thesis to my mother Veronika Achekulwa Lusambili for having very strong foresight of the value of education.

ACKNOWLEDGEMENT

May I thank the almighty God for giving the gift of life that enabled me to undertake PhD work. I am also very grateful to Masinde Muliro University of science and Technology for the opportunity to study this doctor of Philosophy degree in Chemistry and securing financial support from National Research Foundation (NRF). I appreciate the academic and moral support i received from my supervisors; Dr Benard Omondi Omogo, Professor Dickson Mubera Andala, and Dr George Simiyu Manyali during the course of my study. My gratitude also goes to the entire chemistry staff both academic, colleagues and technicians for all assistance offered to me during the course of study. Also I acknowledge assistance of laboratory technicians at JKUAT, Justus Omuga Musakala and entire chemistry staff at Materials Testing and Research Division of Ministry of Transport, Infrastructure, Housing, Urban Development and Public Work for EDX characterization, Jerom Katweo and staff at The Geology Laboratory-Nairobi, for XRD mineralogical and XRF analysis and the entire staff of Soils analysis laboratory at Kalro, Kabete, Nairobi. I am also grateful to BITRI laboratory in Botswana and Gaponik Laboratory, Technische Universitat, Dresden in Germany for analysis of my samples.

TABLE OF CONTENTS

LIST OF TABLES

LIST OF FIGURES

LIST OF PLATES

ABSTRACT

This study was necessitated by low crop yields on farms and pollution effects of leached unused fertilizers into the environment, challenges that can be solved by nanotechnology. Clay was modified by surfactant and stabilizers into multifunctional nanocomposite material used as carriers for fertilizers. The multifunctional nanocomposites were optimized in water and in maize planted in a greenhouse. The pH of the white and black clay soils used were 6.5 and 5.3 respectively while the soil that was used in optimization had pH 7.1. The CEC of white, black and soil used in optimization was 6.0, 20.2 and 19.6 me% respectively. X-Ray Diffraction (XRD) mineralogical analysis showed that the clay soils contained; kaolinite at 16.8%, muscovite at 21.7%, illite at 55.1%, and petalite at 5.9%. The Energy Dispersive X-ray spectroscopy (EDX) results showed major compositions of SiO_2 at 46.3%, Al_2O_3 at 29.8% and K_2O at 13.7% in the clays. The percentage of sulphur in the organoclay MOC2 increased by 0.3% after intercalation. The increase in percentage potassium in SRF2 from 24.8% to 45.6% and phosphorus from nil to 21.3% confirmed dispersion of NPK fertilizer into the organoclay. Fourier Transform Infra-red (FTIR) confirmed presence of clay minerals in the raw materials and showed intercalation into multifunctional nanocomposites. Furthermore, FTIR done on starch-polyvinyl alcohol (PVA) showed that the starch and PVA had polymerized to form superabsorbent polymer (SAP). The starch-PVA had higher water absorbency of 9.03 g as compared to the other superabsorbent starch-Gum Arabic (GA) that had 4.47 g after 8 hours. Starch-PVA had a fickian factor; n of 4.95 as compared to 4.49 for starch-GA. Scanning Electron Microscopy (SEM) and Transmission Electron Microscopy (TEM) pictures showed presence surface pores and interlayers in the clay materials which were confirmed by Branauer- Emmette-Teller (BET) isotherms. Analysis of XRD data points showed shifts in d-spacings after modification into nanocomposites. Moreover the clays showed high thermal stability with Thermogravimetric Analysis (TGA) of black and white clay showing stability of up to 459.7°C and 565.9°C respectively. The rate of water absorption of SAPs and dissolution in water fitted into the pseudo first order equation while the one for sorption of nutrients into soils during optimization fitted into pseudo second order. The simulation in water showed slightly lower dissolution of nitrogen and potassium in the 70-30 formulas than the 50-50 while phosphorus showed slightly lower dissolution in the 50-50 formula than 70-30 formula. The greenhouse optimization showed that the SRF2 and CRFs released lower unused nutrients into the soils after 14 weeks of study. The study achieved conversion of clay into nanocomposite slow release fertilizer and recommends these treatments for sustainable agriculture that would also ensure conservation of soil resources through reduced leachates from excess fertilizers in soils.

LIST OF ABBREVIATIONS

AFC	Agricultural Finance corporation
BET	Brunauer Emmett and Teller
BJH	Barrett Joyner and Halenda
CAN	Calcium Ammonium Nitrate
CEN	Comite European de Normalization
CRF1	Coated slow Release Fertilizers using starch PVA coating in 50-50 formulation
CRF2	Coated slow release fertilizer using starch-acacia Arabic coating in 50-50 formulation
CRF3	Coated slow Release Fertilizers using starch PVA coating in 70-30 formulation
CRF4	Coated slow release fertilizer using starch-acacia Arabic coating in 70-30 formulation
CSRF	Coated Slow Release Fertilizer
CS-PMAA	Chitosan Potassium Methacrylic acid
MOC	Modified organonanoclay
CTAB	Centyltrimethylammonium bromide
DAP	Diammonium Phosphate
DMSO	Dimethyl sulfoxide
EDX	Energy Dispersive X-ray spectroscopy
FTIR	Fourier Transform Infrared Spectroscopy
FAO	Food and Agriculture Organization
HA	Hydroxyapatite
Hap	Hydroxyapatite particles
IFDC	International Fertilizer Development Centre
K	Potassium
KEBS	Kenya Bureau of Standards
KNBS	Kenya National Bureau of Statistics
MMTs	Montimorillonite
N	Nitrogen
NEF	Nanotechnology Enabled Fertilizer
NEMA	National Environmental Management Authority
NP	Nitrogen Phosphorus fertilizer
NPK	Nitrogen Phosphorus Potassium compound fertilizer
P	Phosphorus
SAP	Superabsorbent polymer
S-PVA	Starch Polyvinyl alcohol
SRP	Slow Release Pesticide
S-GA	Starch Gum Arabic
SRF	Slow Release Fertilizer
SEM	Scanning Electron Microscopy
SSP	Single Super Phosphate
TEM	Transmission Electron Microscopy
TO	Tetrahedral Octahedral layers
TOT	Tetrahedral Octahedral Tetrahedral layers

TGA	Thermogravimetric Analysis
TPS	Thermoplastic Sugar
TPSUR	Thermoplastic Sugar with Urea
UVS	Ultra Violet Spectroscopy
UR	Urea
XRD	X-Ray Diffraction
WHO	World Health Organization

CHAPTER ONE

INTRODUCTION

1.1 Background information

The world population stands at 7.8 billion (WPC, 2019) and is expected to reach 9.1 billion people by 2050 (Naderi & Danesh-Shahraki, 2013). The provision of food to such a big population requires new technology that gives more yield in shorter period (Rameshaiah, *et al.,* 2015). As a result, agronomists are left with the critical duty of feeding more people from agricultural yields which are decreasing yearly (Owino, 2010) (Kihanda, 1996).

Food scarcity is a major problem in developing countries especially those that depend on rainfall for agriculture. Kenya with a population of 47,564,296 (KNBS, 2019) has suffered droughts caused by delayed rains or loss of crop due to flooding as is perennially experienced in Turkana County, North Eastern Counties, coastal part of the country, Kano plain in Kisumu County, Budalangi in Busia County. In general, only about 15 % to 17 % of Kenya is arable under the present farming practice since about three quarters is arid and semi-arid (Mwanda, 2008).

Maize is a staple food crop in Kenya (Owino, 2009) with a consumption of 103 kg per annum per head (Hugo *et al.,* 2005) and a second most important cereal in Asia (Majumdar *et al.,* 2017). Maize is also an important food crop in sub-Saharan Africa (Ngosong *et al.,* 2019) and strongly contributes to the food security and income generation (Cairns *et al.,* 2013). Maize is used in processed form for ugali and porridge, githeri; a meal of maize and beans with by-products used for manufacture of animal feeds (Owino, 2010) and manufacture of corn oil for cooking.

In Kenya almost all people plant cereals; like maize, beans, wheat which are planted using recommended fertilizers majorly diammonium phosphate, DAP, composite nitrogen phosphorus and potassium, NPK and calcium ammonium nitrate CAN.

According to (Maxim *et al.,* 2019) it was noted that nitrogen, N uptake has been on the increase. Almost 111.6 million tons of N fertilizer was used in 2005 (FAO, 2015) and is expected to reach 130-150 million tons by 2050 (Matson *et al.,* 1997). But still the yields remain on decline (Raun & Johnson, 1999). A lower N uptake from the soils by plants results into serious environmental pollution (Maxim *et al.,* 2019). A study done by (Akenga *et al.,* 2014) on the levels of potassium, phosphorus, calcium and nitrogen in Kakamega County was determined as 39-163, 93-111, 2-400 and 30-104 mg/kg against the recommended levels of 1-100, 2000-5000, 235-891 and > 100 mg/kg respectively. This shows that the soils are deficient in Potassium, calcium and Phosphorus.(Kenyanya *et al.,* 2013) reported in their research in Nyamira County that there is a threshold for potassium acreage dosage below and above which the yields are below the optimum. This potassium requirement in soil solution for maximum maize yield was determined as 7.9 mg/L in the study.

The decline in the crop yield discussed above arises largely from soil fertility decline which may occur through leaching, soil erosion and poor crop harvesting practices (Dorovan & Casey 1998). Unless if the soil nutrients are replenished by application of organic or mineral fertilizers, this nutrient decline continues (Mucheru-Muna *et al.,* 2007) over time. In some parts of central Kenya, research showed a nutrient depletion of exceeding 30 Kg nitrogen due to continuous cropping (Mucheru-Muna *et al.,* 2007) which is not unique to Kenya.

Though nitrogen is the most limiting nutrient for plants, up to 75 % is lost due to denitrification (Abera *et al.,* 2013) and a lot is equally lost through runoffs and leaching during heavy rain season while some more is lost through volatilization (Anbessa & Justiw, 2012). (Wu & Liu, 2008) approximated these losses as 40-70 % N, 80-90 % P and 50-70 % K. It has also been noted that some small scale farmers use less than the recommended 60 Kg N ha^{-1}. Some even use as low as 20 Kg N ha^{-1} (Mucheru-Muna *et al.,* 2007). (Kihanda, 1996) reported that replenishing of nutrient to yield above 16 bags of 90 kgs/3.5Mg ha^{-1} required application of both farm yard manure and NP fertilizers since inorganic fertilizers lowered soil pH. The added farmyard manure in the Kihanda research increased the soil pH by reduction of the exchangeable soil aluminium. This is achieved through aluminium precipitation or chelation on the organic colloids by complexes (Mucheru-Muna *et al.,* 2007). There are other factors which affect agriculture other than deficiencies in macro and micro soil nutrient content, like industrialization, depletion of water source and erosion of top soil.

In order to overcome these difficulties, a soil incorporation of a smart fertilizer is essential. These slow coated release fertilizers, CRFs are a green technology due to their low negative impact to the environment (Trinch & KuShaari, 2006). CRFs are slow release fertilizers that release nutrients in balance with plant need (Xiaoyu, *et al.,* 2013); (Maxim *et al.,* 2019). A nanostructured formulation can extend effective duration of nutrient supply of fertilizers into soil by reducing the loss rate of fertilizer nutrients into soil by leaching, run off and denitrification (Naderi & Danesh-Shahraki, 2013).

When comparing to chemical fertilizer requirement and cost, nanofertilizers are economically cheap and are required in lesser amount (Rameshaiah, *et al.,* 2015). Their

symbiotic exchange between soil and the plant system is very efficient (Kottegoda, *et al.,* 2011). When the fertilizer is applied in slow and efficient way all the required nutrients are taken up by the plant which restores the required plant energy increasing the yield drastically (Rameshaiah, *et al.,* 2015). Slow release fertilizers, SRFs have the ability to maintain elevated concentrations for longer periods (Grillo *et al.,* 2014) while Coated Slow Release fertilizers, CRFs help increase the nutrient use efficiency, NUE preventing negative effects to the environment by formed greenhouse gases and ground water contamination (AlZaharani, 1999). When a polymer nutrient formulation is fixed between interlayers of clay mineral, the stability of the polymer composite increases, which further improves the slow-release property of the product (Basak *et al.,* 2012). To make a CRF, a fertilizer can be dispersed into a nanocarrier matrix that has an interlayer that can host the fertilizer and control its release. Clay minerals are environmentally friendly, stable and cheap materials for the synthesis of SRFs and CRFs (Ni *et al.,* 2011); (Borges *et al.,* 2009) in which the clay mineral acts as an inhibitor for the fertilizer particles.

1.2 Statement of the problem and justification of study

In Kenya, production of cereals grew from 1.4 million tons in 1961 to 4.1 million tons in 2011 while the population increased from 8.4 million to 41.6 million respectively (Dietz *et al.,* 2014). Therefore while the population grew by 7.9 % per annum the cereals production only grew by 2.8 % per annum in spite of continued application of best farming practices including inorganic fertilizers such as C.A.N, N.P.K and D.A.P that are normally used to give high yields of cereals. The decreasing yield of maize due

to exhausted soils, low access to fertilizers, effects of weeds is similar for other food crops around the country.

Inorganic fertilizers have also have some negative effects to farming. Like when urea is added on the soil surface it loses 50 % to 90 % of its initial amount of nitrogen within few hours of addition due to volatization and denitrification rather than being absorbed by plants, if it is not protected (Wijesinghe & Weerasinghe, 2015). In addition, fertilizers leach and run off into natural water bodies (Vila, *et al.*, 2012). This creates eutrophication of surface water bodies by increasing the growth of algae and vegetation (Naderi & Danesh-Shahraki, 2013). The leached or run off fertilizers pollute the waterways destroying aquatic ecosystem (Himmah *et al.*, 2008). These issues have affected the performance of soil due to lack of better technologies to solve plant nutrients.

Fertilizer useage should be considerate of economic, environmental and social sustainability of the agricultural sector (Chagas *et al.*, 2018). It is against this background that this study was undertaken to ascertain the design and fabrication of clay nanocomposite materials to be used for controlled release of plant nutrients.

1.3 General objective

To design and fabricate clay nanocomposite materials to be used for controlled release of plant nutrients.

1.4 Specific objectives

The study was guided by the following specific objectives:

i. To fabricate and characterize multifunctional nanocomposite materials made up of clay, biopolymer and stabilizers.
ii. To carry out the physicochemical and kinetics studies on formed nanocomposite nutrient formulations.
iii. To determine nutrient retention and release capacity by the formed multifunctional nanocomposite in deionized water.
iv. To apply multifunctional nanocomposite in release of selected fertilizers.

1.5 Hypotheses

This study was guided by the following set of hypotheses:

i. The clay minerals do not possess suitable physical and chemical properties hence cannot be modified into multifunctional carriers of fertilizers and nanocomposites.
ii. The rate of sorption of formulas and SAPs in water do not fit into the first order kinetics
iii. The dispersion and encapsulation of fertilizers into clay nanocomposites does not enhance an efficient release of plant nutrients.
iv. Slow release fertilizer is not significantly different in discharge of plant nutrients from the starch-PVA coated and starch-GA coated nutrient formulations.

1.6 Significance of the study

The findings of this study may be important in sustainable agricultural practices that ensure conservation of soil resources and mitigate environmental pollution. The results of this research may also seek to increase food production and food security.

Nanocomposites have been tested in slow release capacities and also as nutrient carriers. Urea lazed into a smectite-polymer composite resulted into a 38% N recovery and 62% P recovery from conventional urea and DAP respectively (Datta, 2011). Organic substances have largely also been used to intercalate and exfoliate the layers in kaolinite into nanosized layers (Liu *et al.*, 2005a). Therefore the data collected may add value to clays in the area of nanocomposites apart from the traditional use in pottery.

1.7 Scope and limitation

The soils used in optimization was sourced from Masinde Muliro University of Science and Technology and standardized by Kalro to follow the absorption of the nutrients by plants. Also standard NPK formulation from supplier were used in development of the clay fertilizer nanocomposite. The study was limited to non-leguminous crops like maize crop, white imported clay and black clay from Ilesi. This study was conducted in Kenya between January, 2017 and April, 2020.

1.8 Justification

There is a worrying trend on food insecurity as world population increases and increase in pollution from inorganic fertilizers. It is therefore necessary to research on and develop an effective and efficient nutrient formula without impacting negative environmental and health effects.

CHAPTER TWO

LITERATURE REVIEW

2.1 Fertilizer and Nanotechnology

A fertilizer is a chemical or natural material added to soil or land to increase availability of plant nutrients essential for plant growth otherwise known as fertility. The macronutrients for plant development are; nitrogen which promotes leaf growth and forms proteins and chlorophyll (Gu *et al.,* 2009), phosphorus that contributes to flower and fruit development (Gu *et al.,* 2009) and also stores energy and generate processes that allow growth to occur (Cifuentes *et al.,* 2017) and lastly potassium contributes to stem and root growth and synthesis of proteins (Mandal *et al.*, 2009) it also helps avoid invading organisms that attack the plant (Cifuentes *et al.*, 2017).

The agricultural sector around the world utilizes fertilizer to improve food productivity. In a number of countries like India (Thirunavukkarasu, 2015) and Kenya the cost of fertilizer is subsidized. This promotes over application of fertilizer leading to environmental pollution due to leaching. Because of this most farmers are turning to organic fertilizers in order to reduce the amount of plant nutrients leaching into the waterways. However it is not practical to generate large quantities of organic fertilizers for large scale commercial farms.

Due to limited availability of arable land and clean water for irrigation, nanoscale science is being brought in order to provide novel solutions to many challenges facing agriculture (Chana & Yala, 2011). The most practical remedy to these problems could be in nanotechnology.

Nanotechnology is manipulation of individual atoms, molecules, molecular clusters into structures that create materials with new enhanced properties (Manjunatha *et al*, 2016). It deals with materials at atom or molecule level which involves manipulation of the material into the nanoscale which is 10^{-9}m. A nanoparticle is atomic or molecule aggregates or agglomerate with at least one dimension within the scale, 1-100 nm (Alexandre & Dubois, 2000). They have three major physical properties of high mobility in their free state, enormous specific surface areas and may exhibit quantum effects.

Nanotechnology looks at opportunities for improving efficiency, sustainability and speed of existing processes. It is a multi-disciplinary science with wide applications in medicine, water treatment, engineering, catalysis and agriculture. The applications in agriculture include; products that enhance plant nutrient absorption, remediation of aquatic and soil pollutants, design and fabrication of fertilizers, pesticides and rapid disease detection. These agricultural inputs are meant to improve productivity without negative environmental side effects. Normally the rate at which soils lose both macro and micronutrients is faster than the rate at which the soils regenerate these nutrients naturally.

While nitrogen may easily be replenished from atmospheric nitrogen and nitrogen fixing bacteria and enzymes, potassium and phosphorus depend on the abiogenic character of the rocks in the area. Therefore Nanotechnology Enabled Fertilizers, NEPs are being researched on to generate nanocomposite polymers, CRFs, nanobiosensers which are usually embedded into a biopolymer fertilizer coating to release nutrients in response to chemical signals from soil microbes in plant's root system and amend soils

with nanoclays that would delay nitrate runoffs, leaching of nitrates and volatilization of ammonia and nitrous oxide. This would largely convert farming into precision agriculture. It should be noted that large scale industrial fertilizers have not yet been realized but even then the toxicity of the materials producing NEFs need to be researched on to eliminate all challenges. It is worth noting that chemical fertilizers are made in chemical processes with very little input from the knowledge of plant physiology and need for agro-ecological specificity of crop nutrition needs (Suppan, 2017).

The challenge of the CRFs is that they are more expensive than the conventional ones. For example between 2009 and 2015 the prize of conventional urea was on average USD 0.54 per pound (453.6 g) while the coated urea was averagely between USD 0.72 to 0.74 per pound in US (Suppan, 2017). In 2014 fertilizer costs were about 40 % of all the US farm operating costs for planting maize (Suppan, 2017). However the cost benefits of the coated urea and economy of numbers was expected to lower this price over time of production.

2.2 Classification of plant minerals

Potassium is an element required by plants in large amounts. Recent estimates show that sub-Saharan Africa faces what the World Bank study referred to as “an escalating soil fertility crisis” (Nambiro & Okoth, 2013) due to rapid dissolution of potassium from the soils. Plant macronutrients are listed as carbon, oxygen, hydrogen supplied by carbon dioxide and water in the atmosphere while nitrogen, potassium, calcium, magnesium, phosphorus and sulphur are absorbed from soils. The micronutrients are chlorine, boron, iron, manganese, zinc, copper and molybdenum. The element required in abundance,

nitrogen is essential for plant growth and is the nutrient taken up in largest amount by all plants. Sources of nitrogen include ammonia, diammonium phosphate, ammonium nitrate, ammonium sulphate, calcium cyanamide, calcium nitrate, sodium nitrate and urea (Booze-Daniels & Schmidt, 1997). Urea is easily available with rapid action (Rameshaiah, *et al.,* 2015).

2.3 Fertilizer types

As indicated a fertilizer is an organic or inorganic material, either synthetic or natural containing one or more essential nutrients, which is applied to soils or to plant tissues, usually leaves to supply one or more plant nutrients to enhance plant growth, increasing productivity and quality of agricultural products (Nguyen, *et al*., 2015; Zhang *et al.,* 2010). It comes in either or both solid and liquid forms.

2.3.1 Solid

Some of the single, straight fertilizers are, CAN, UREA, SSP while multinutrients, are DAP, NPK. Organic fertilizers are on the other hand slow releasing technology that are more efficient and reduce impact on the environment. The major fertilizers are classified into;

2.3.1.1 Nitrogen fertilizers

The rule of the thumb (Zenawi & Mizan, 2019) describes nitrogen as being responsible for leafy top growth, phosphorus for root and fruit production while potassium is for disease resistance, drought tolerance and general plant durability (Chagas *et al.,* 2018). The growth of plants is dependent on availability of adequate nitrogen in the soils. Nitrogen is replenished in the soils through nitrogen fixing bacteria and nitrates formed during rainfall with thunderstorms. Most of the soil nitrogen is generated from primary

minerals of calcium nitrate, sodium nitrate and potassium nitrate. Nitrogen is most used up during growth of plants and may be rapidly replenished by chemical fertilizers like CAN, AN, DAP, AS and urea, or nitrogen generating microorganisms.

Nitrogen use efficiency is influenced by health of the crop and nitrogen loses (Zenawi & Mizan, 2019). All nitrogen eventually convert to the mobile nitrate-N form which is available to crop roots in two days while the immobile ammonium form takes 7-20 days to avail at the roots (Zenawi & Mizan, 2019). In the research of (Zenawi & Mizan, 2019), sandy soils leached 60 % of the nitrogen fertilizer while clay soils leached 20-30 % under heavy rainfall in 2 weeks. Urea on the other hand easily volatilizes during sunny days. Urease enzymes and plant residues are also known to convert urea into free ammonia gas. On sunny days and pH of above 7 about 50 % of nitrogen fertilizer volatilizes in the tropics (Zenawi & Mizan, 2019) hence need for split application of deep soil fertilization.

2.3.1.2 Phosphorus fertilizers

Phosphorus fertilizers are usually drawn from phosphorus rocks like apatite. The manufactured fertilizers are SP, TSP and DAP. Superphosphate, SP is a higher phosphorus content fertilizer manufactured from action of concentrated sulphuric acid on a phosphate rock like fluoroapatite ($Ca_5(PO_4)_3F$).

$$2Ca_5(PO_4)_3F + 7H_2SO_4 \longrightarrow 7CASO_4 + 3Ca(H_2PO_4)_2.H_2O + 2HF$$

The triple superphosphate, TSP is a concentrated superphophate with P_2O_5 content above 40 %.

Phosphorus in the soils exists as a heterogeneous mixture of adsorbed, absorbed and mineral species (Weeks & Gange, 2019). Permanent phosphorus loses from soils include leaching, soluble runoffs and erosion of phosphorus particles from the soil minerals. When phosphorus is added or removed from the soil all the components of the soil system respond accordingly towards a new phosphorus solution equilibrium providing crops with adequate phosphorus at all times. Products like SP, TSP and DAP are very soluble hence crops should access the phosphorus fast due to its rapid dissolution which does not necessarily synchronize well with plant phosphorus uptake (Weeks & Gange, 2019). This necessitates introduction of slow phosphorus releasers (Barrow, 2015), coatings (Weeks & Gange, 2019) and nanoparticles (Montalvo *et al.,* 2015a).

The effectiveness of the phosphorus fertilizers depends on the fertilizer properties; the rate and method of application, soil and climatic conditions (Mokwunye & Bationo, 2002). On small scale farming a mixture of fertilizer and manure is advised (Ademba *et al.,* 2015) to increase extractable phosphorus. In (Ademba *et al.,* 2015) research, phosphate fertilizer and manure mixture increased growth vigour, grain and dry matter yields, harvest index and achievement of the critical phosphorus level for maize of 10mg/kg soil (Weeks & Gange, 2019).

2.3.1.3 Potash fertilizers

Apart from nitrogen and phosphorus, potassium is the third essential macronutrient required by plants for growth and metabolism. Its deficiency causes poorly developed roots, low resistance to diseases, delayed maturation, small seed and lower yields (Rawat *et al.,* 2016). Potassium in soils is found as soil solution potassium,

exchangeable potassium, non-exchangeable potassium and potassium in minerals (Akbas *et al.,* 2017); (Ashley *et al.,* 2006). Most sources of potassium are from deposits of potassium in soils as feldspars and micas which are alumino silicates. Potassium feldspar is the most common source of potassium that gets converted into exchangeable potassium. This exchangeable potassium occurs in the forms of potassium ions in soil solutions, potassium ions as exchangeable cation on clays and organic matter, potassium from weathering of micas and potassium in lattices of primary minerals like potassium chloride and potassium nitrate. Some bacterial and fungal strains like Paenibacillus, acidithiobacillus, pseudomonas, burkholderia, aspergillus and clostridium have high ability of potassium solubilization (Rawat *et al.,* 2016) enriching the soils.

There are several types of potassium in soils; the soluble potassium absorbed directly by plants; the exchangeable potassium which is the fraction of potassium that occupies sites in soil colloidal complexes. This is the major bioavailable (Schroeder, 1974) source of plant potassium. The levels of this form easily reduce due to leaching, crop uptake or microbial activity (Sparks, 2000). Replenishment of this potassium depleted soils is effected by release of exchangeable potassium from clay minerals or fixed potassium which is usually found in layers of micas or feldspars. This structural potassium is mostly found bound covalently to the structure of micas, feldspars and volcanic glasses. It can only become available on weathering (Rawat *et al.,* 2016).

Low plant potassium is signaled by reactive oxygen species and phytohormones triggers expression of high affinity K^+, transporters that regulate K^+ channels to drive the K^+ to the xylem (Ashley *et al.,* 2006).

Most potash fertilizers are found in form of; Glauconite sand that contains 4-8 % K_2O (Yadav *et al.,* 2000). Potassium chloride is another common potassium fertilizer with 60-63% K_2O and 46 % Cl, potassium sulphate fertilizer is 48-53 % K_2O and 17-18 % S, potassium magnesium sulphate 20-22 % K_2O and 21-22 % S and 10-11 % Mg and lastly potassium nitrate one 44 % K_2O and 13 % N (Rawat *et al.,* 2016).

Availability of potassium depends on transport from soils to plants to root zone then to the plants (Islam *et al.,* 2018). Potassium has several functions in plants which include regulatory development that includes osmoregulation, plant water relation and internal cation to anion balance, enzyme activation in formation of organic substances, protein and starch synthesis, respiratory and photosynthetic mechanisms. Enzyme regulation is also needed in metabolism of carbohydrates into aminoacids, proteins and tolerance to stress of drought, frost heat and light. This enzyme regulation also triggers the growth of young tissues and cell enlargement (Wang *et al.,* 2013). (Wang *et al.,* 2013) documented that abiotic stress factors like heat, cold, drought and salinity have huge impact on world agriculture. Drought and low moisture can be overcome by inducing deeper rooting, larger absorption surfaces, greater water retention and application of potassium fertilizers (Rawat *et al.,* 2016). During drought stress aquaporins, could be regulated to help the plants to maintain their water balance (Kaldenhoff *et al.,* 2008). Waterlogging stress reduces the concentration of oxygen levels, dilutes the K^+ severely damaging the root cell processes (Wegner, 2010). So poorly drained soils can retard root growth reducing the K^+ uptake.

K^+ is very soluble and mobile and is transported to the xylem fast (Lack & Evans, 2005). Therefore any deficiency in the soil solutions immediately records zero balance

in the xylem of the plants causing chlorosis, poor growth, reduced yield and increased susceptibility to diseases (Amtmann *et al.,* 2008) and pests (Trouffland *et al,* 2010). Potassium regulates the osmotic pressure and hydraulic conductivity of membranes and altering water permeability (Heinen *et al.,* 2009). Adequate potassium amounts help in lowering of the osmotic pressure improving the ability of plants to tolerate drought. This could also be achieved by stomatal closure by rapid release of K^+ from the guard cells of the plants (Kant & Kafkati, 2002).

Large amounts of potassium are required to maintain the health of plants (Rawat *et al.,* 2016). It is seen in research that plants in potassium deficient soils were more susceptible to infestation than those with adequate potassium levels (Wang *et al.,* 2016). In another research of (Survar, 2012) it was discovered that rice borer infestation increased with decrease in potassium levels and increased potassium, decreased fungal diseases by 70%, bacterial by 69 %, viral by 41 %, nematodes by 33 % and pests by 63 % (Perrenoud, 1990).

Use of plant growth-promoting microorganisms is suggested as possible solution to improved plant nutrient and food production though most of the microorganisms in the market are nitrogen and phosphorus based (Rawat *et al.,* 2016).

2.3.2 Liquid

Foliar feed fertilizers are liquid nutrient formulations that are applied directly to the leaves and stem of plants. These solutions avail plant nutrients directly as opposed to the solid ones. Normally trace elements, growth hormones, vitamins are added to make them balanced. They are formulated to meet specific requirements like temperature or age of plant that may affect absorption.

2.3.3 Nanofertilizers

Slow release fertilizers can be classified into coated or encapsulated CRFs, matrix CRFs with nutrient dispersed into polymer matrices like in gels, inorganic materials of low solubility prepared from chemically and biodegradable materials. A lot of research has been done on reservoirs of guar gum coating, starch-g-poly(L-lactide) coating(Chen *et al.,* 2008), tapico starch (Sarwono, 2013), chitosan binder (Roshanravan *et al.,* 2015). These CRFs are economical, physiologically and environmentally friendly (Shaviv *et al.,* 2001); (Pack *et al.,* 2006). Limitations of these fertilizers include; complex processing technologies, unclear impact factors on release and higher prices for the materials when compared to conventional fertilizers (Shavit *et al.,* 1997).

Nanofertilizers are slow and controlled release fertilizers which can be classified into; nutrient nanoparticles, coating nutrients with nanomembranes, use of nanocomposites (Datta, 2011) as carriers of the nutrients, use of high exchange capacity zeolites and carbon nanotubes (Ahmed *et al.,* 2019). Controlled Release Fertilizers, CRFs can be classified into three; organic fertilizers that are residues of plant and animals (Azeem *et al.,* 2014), slow solubility nitrogen fertilizers created from soluble nitrogen and aldehydes and coated fertilizers which are normally wrapped into a water insoluble layer under normal environmental conditions (Fujinuma *et al.,* 2009) whose composition and thickness determine rate of release of nutrients (Hanaji *et al.,* 2000). These coated fertilizers improve nutrient availability throughout the productive cycle (Azeem *et al.,* 2014). It was noted in a research that NPK(10-5-5) encapsulated into sodium alginate, acrylic acid, acrylamide and montmorrillonite coating had good release properties as well as good water retention (Rashidzadel & Olad, 2014). In another

research it was found that when poly vinyl alcohol, PVA coating was used on NPK, absorption and water permeability of the films increased (Han *et al.,* 2009).

Polysaccharides like starch are available and biodegradable natural polymers that have extensively been used as encapsulating matrices. The starch polymer has been in other cases enhanced by vinyl ethylene or polyvinyl alcohol. Polycaprolactone, PCL is degraded slowly by micro-organisms. PCLs, montmorillonite and urea in CRFs pellets (Suppa, 2017) and polyacrylamide hydrogel have been used to bind exfoliated clays like attapulgite with good results. Polysaccharides can be physically cross linked to form three dimensional networks that swell into water. The polymer molecules in solution are random chains but adopt an ordered conformation of double helix structure which on addition of a crosslinking agent it enables polymerization. When a plasticizer like glycerol is added it opens the structure into pore-like jelly liquid. Hydrogels like linear sulfated polysaccharide kappa carrageenan have been evaluated and found to possess good fertilizer coating properties (Cifuentes *et al.,* 2017). Coating and binding of nano and subnano-composites is able to regulate the release of nutrients from the fertilizer capsule (Liu *et al.,* 2006). Both release rate and release pattern of nutrients for water-soluble fertilizers might be precisely controlled through encapsulation in envelope forms of semi-permeable membranes coated by resin-polymer, waxes and sulphur.

Encapsulation of fertilizers within a nanoparticle is one of these new technologies which are done in three ways. The nutrient can be encapsulated inside nanoporous materials, coated with thin polymer film, or delivered as particle or emulsions of nanoscale dimensions (Rai *et al.,* 2012). The controlled release ones are usually encapsulated in shells that degrade at specific rate or have a coating of thermoplastics

like ethylene-vinyl acetate. The rate of decomposition of the fertilizer may further be reduced by nitrogen stabilizers like 1-carbonyl-1, 3-methylpyrazole (CMP), dicyandiamide and nitrapyrin whose IUPAC name is 2-chloro-6-trichloromethylpyridine. In addition, nanofertilizers will synchronize the release of nitrogen and phosphorus with their uptake by crops, so preventing undesirable nutrient losses to soil, water and air via direct internalization by crops, and avoiding the interaction of nutrients with soil microorganisms, water and air (DeRosa *et al.*, 2010). Previous studies with pillared clay-modified phosphate fertilizers reported decreased fixation and increased bioavailability of soil phosphorus (Basak *et al.,* 2012).

2.3.4 Slow release potash fertilizers

For the slow release of potash fertilizer, polyacrylamide based coating of pellets are preferred. In research of (Rameshaiah, *et al.,* 2015) potash and clay were mixed together and dried for an hour before being coated with a tooth paste for proper attachment of the polymer. When the potash amount used was less, the release was slowed down (Guang-huo & Qi-chun, 2005). Studies were conducted on wheat and corn (Subbarao *et al.,* 2013) which showed slow release and effective recovery of nitrogen fertilizer

2.3.5 Nano porous Zeolite fertilizers

They usually help in slow release of the fertilizer to the plant which makes the plant to grab the entire amount of nutrients from the fertilizer supplied rather than the minimal uptake (Rameshaiah, *et al.,* 2015). Since they have larger surface area many fertilizer molecules could fit into them and get released whenever the plant requires the nutrients (Naderi & Danesh-Shahraki, 2013). Studies have shown that phosphorus zeolites

release phosphate in a slow manner (Bansilwal *et al.*, 2006). In fact zeolite based nanofertilizers are known to be efficient releasers of both macro and micronutrients into soils (Subramanian & Sharmila, 2013). The tunnels and cages in the structure of zeolite can be loaded with nutrients. The zeolite reservoir then releases the nutrients to the soil on need. Accordingly the zeolite slows the NO_3^- uptake from urea by preventing leaching from the root zone, slowing conversion of the urea in the soil by enzymes and adsorption of NH_4^+ onto the zeolite exchange sites protecting them from nitrogen fixing bacteria.

2.3.6 Carbon nanotube fertilizers (CNTs)

Tubes are in cylindrical shape and mostly made up of carbon molecule with the difference in number of wall construction. These carbon molecules are held in position by strong Van der Waals forces (Rameshaiah *et al.*, 2015). When it comes to agriculture sector, these multi walled carbon nanotubes play a beneficial role in increasing the growth rate, water intake, uptake of essential nutrients from the soil. Multi walled carbon tubes with concentration of 50 µg/mL were tested in research and the result showed increase in length of root and shoot, seed germination time, enhancement in growth and well developed root system in crops like maize, wheat, peanut and garlic (Anita & Rao, 2014). CNTs have been used in seed germination of tomatoes. The pores in the tubes serve as a storage and passage of water from the substrate to the seed over a long period of time (Khodakovskaya *et al.*, 2009).

2.3.7 Advantages of nano fertilizers

Nano coatings and nanotechnology can help in numerous ways to reduce costs and increase productivity around the farm. Nanomaterials could even be used to control the

release of the fertilizer such that the nutrients are only taken up by the plant, and not lost to unintended targets like soil, water, or microorganisms. Coated slow-release fertilizers with the granular fertilizer at its core (Gao *et al.,* 2014), change nutrient solubility characteristics, lengthens and controls nutrient release (Chagas *et al.,* 2018). Studies on CRFs have provided new ideas for improving fertilizer use, efficiency and minimizing pollution to the environment due to fertilizer losses (Hongtao *et al.,* 2014). CRFs are mostly polymer coated whose thickness and polymer‘s nature determines the rate of the nutrient release. Proper application of optimum quantities of fertilizers maximize nutrient uptake and minimize pollution.

Current practices of application are broadcasting, banding (Omodi & Saigusa, 2000) and side dressing, all of which face problems of run-off, leaching and evaporation. It has been estimated that 40-70 % N, 80-90 % P and 50-90 % K content of applied fertilizers are lost to environment hence do not reach the plant (Trenkel, 1997). Root application therefore has an efficiency of only 20-80 %. (Amanda *et al.,* 2017) collaborated this when they found out that 40 % to 70 % N and 80-90 % P were lost to the environment or chemically bound in soil hence unavailable in soils (Amanda *et al.,* 2017). This causes substantial economic loss and serious environmental problem. The soil application has serious environmental impact; leaching, runoffs into lakes, reservoirs, ponds ending in proliferation of algae that suppress other plants and aquatic animals. On the other hand denitrifying bacteria converts nitrite into greenhouse gases of nitrogen monoxide and dinitrogen oxide causing air pollution. Leached soil fertilizers increase salinity which again inhibits plant growth generating degradation and decline in agricultural production (Meena *et al.,* 2016). Soil PO_4^{3-} concentration is typically

low, due to formation of Fe- and Al-based oxides especially in tropical soils. Consequently encapsulation of nutrients done by putting them inside nanoporous materials, covering with a thin polymer film and mixing them into emulsions of nanoscale reduces nutrient losses and negative environmental impact of the conventional fertilizers (Rai *et al.*, 2012).

Research has equally been done on nanoporous synthetic layered double hydroxides loaded with NO_3^- into the interlayers that act as slow release fertilizers (Komarneni, 2010). Urea-HA , hydroxyapatite nanoparticles were reported in a field trial in Sri-Lanka and showed a 50 % reduction in urea use with a yield of 7.9 tons per hectare higher than the expected 7.3 tons per hectare using conventionally recommended urea (Suppa, 2017). Nanocomposites have also been extensively tested in slow release capacities. Urea lazed into smectite polymer composite resulted into a 38 % N recovery and 62 % P recovery from conventional urea and DAP respectively (Datta, 2011).

Organic substances have largely also been used to intercalate and exfoliate the layers in kaolinite into nanosized layers (Liu *et al.*, 2005a). These have been used to hold nutrients into the interlayers and trapped pockets in the exfoliated layers. These pieces of research have been directed at an attempt to improve the efficacy of the CRFs and SRFs. A good proportion of the research on nanocomposites has been done on clay minerals. Studies have been done on the clay minerals as slow release nanomatrices, nutrient encapsulating materials and preparation of SAPs for coating of fertilizers.

2.3.8 Superabsorbent polymer coating materials (SAPs)

SAPs are long chain polymers which are cross-linked with an ability to swell and maintain bulky water and aqueous solutions after being absorbed (Liu & Gao, 2001).

They are materials that can appear in gel form as a result of absorbing huge amounts of water and aqueous solutions (Auda, 2017). They are generally cross-linked polymeric chain networks making them overcome their dissolution and supporting their water diffusion. Some of these SAPs and hydrogels respond to external factors like pH, heat, electric fields and chemical environments making them smart. These smart SAPs are used in pharmacy, biotechnology, agriculture, drug delivery systems, diapers among many (Sadeghi & Hossein Zadeh, 2008). These biodegradable polymers have advantage since they are broken down by enzymes and microorganisms into carbon dioxide, water and biomass (Schaffazick *et al.*, 2003).

There are two important processes in SAPs, the swelling process, which occurs when the SAPs interact with nature. The degree of the swelling depends on the polarity of the SAP, the level of crosslinking, solvent properties, the particle size and environmental conditions like temperature and pH (Sadeghi, 2012). The solvent molecules penetrate the network structures causing molecular chains in cross-linked points to expand as seen in the ionic cross-linked SAP in Figure 2.1.

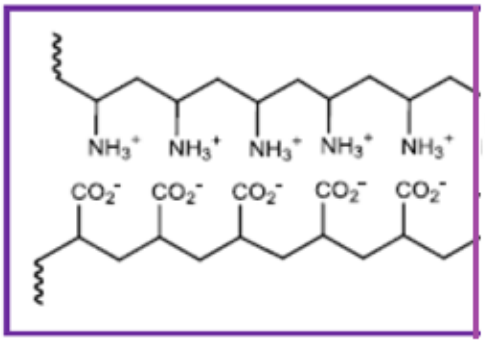

Figure 2. 1: Ionic cross-linking (Jaber 2012)

Alternatively, the hydrogen bonds in the structure create cellular structures in the SAP network that can store water as seen in Figure 2.4. Then crosslinking process, in which the crosslinks form 3-D network that makes them insoluble in water and opens pockets to trap and store water is seen in Figure 2.2.

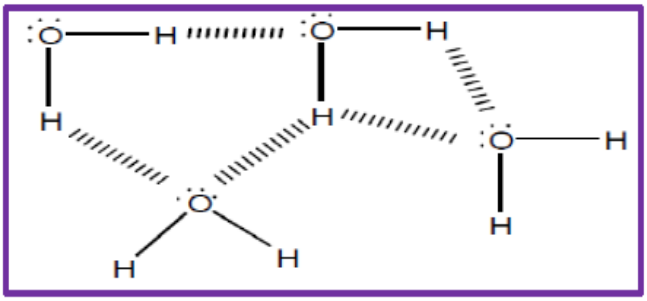

Figure 2. 2: Hydrogen bonds (Elliot, 2010)

Surface crosslinking of SAP particles improves flow and absorption of water against any pressure (Jocksusch *et al.*, 2009) protecting the shapes during swelling process. These crosslinks prevent the SAP from swelling to infinity which would cause dissolving. The coiled dry SAP stretches out into a uniform pattern on absorption of water as seen on Figure 2.3.

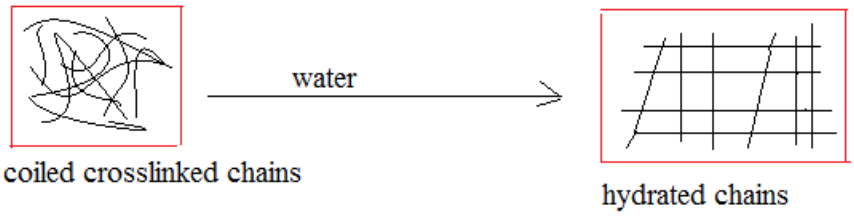

Figure 2. 3: Absorption of water by SAPs

SAPs have hydrophilic groups such as COO^-, OH^-, NH_2^- or NHCO (Ferfera-harrar *et al.*, 2015). Because of their ionic nature they absorb large quantities of water through

hydrogen bond interactions increasing the molecule disorder in the polymer network which swells them dramatically (Daungtawan *et al.,* 2011). The high water absorption of these materials is attributed to the interconnected super pore structures of diameters several hundred microns that create open channels for capillarity (Ghazali *et al.,* 2017). Carbon synthesized from biomass can greatly improve the physical properties of SAPs due to their high CEC and water holding capacity (Jamari *et al.,* 2015). (Ghazali *et al*., 2017) studied properties of controlled-release-water retention fertilizer coated with carbonaceous-g-poly (acrylic acid-co- acrylamide) superabsorbent polymer. They noted that the main factor that affect growth of plants and their quality include the amount of water and fertilizer that can be absorbed by the plant. They used superabsorbent polymer, SAP on Controlled Release and Water Retention fertilizers (CRWR).

Corn starch is a polysaccharide of large polymeric carbohydrate molecules comprising glucose molecule monomers joined in α-1.4 linkages, the unbranched amylose while the branched one is amylopectin. Corn starch contains 25% amylose and 75% amylopectin (Rahul *et al.,* 2017); (Masakuni *et al.,* 2014).

PVA is frequently used in the preparation of various membranes and hydrogels (Young-Chang *et al.,* 2009). The PVA hydrogels have received increasing attention in biomedical and biochemical applications because of their permeability, biocompatibility and biodegradability (Young-Chang *et al.,* 2009). In another research it was observed that when xylan is blended into PVA using plasticizers like polyols, the mechanical properties of the biopolymer were improved (Cuan-dian *et al.,* 2014) blended xylan which is derived from a hemicellulose with PVA which greatly improved its mechanical properties. The use of biodegradable polymers for Packaging offers an alternative and

partial solution to the problem of accumulation of solid waste composed of synthetic inert polymers (Fahmida *et al.,* 2010).

PVA is polymerized from vinyl alcohol and acetyl acetate since the vinyl alcohol is very unstable. These chains can crosslink both the amylose and amylopectin to form starch-PVA reinforced polymer.

Corn starch can also be polymerized with gum Arabic to form starch-Gum Arabic polymers. There are more than 1000 species of gum acacia extracted from acacia trees. Gum Senegal and gum seyal are the most used species for extraction of gum arabic for commercial uses. Gum arabic or acacia, GA is an exudate tree gum (Jamaludin *et al.,* 2017) obtained in the stems and branches of these trees as seen on picture 2.1.

Plate 2. 1: Gum acacia (Musa et al., 2018)

GA is a natural branched multifunctional hydrocolloid, an arabino-galactan-protein complex that contains calcium, magnesium and potassium. Hydrolysis of GA produces 88% arabinogalactan polysaccharides, 10% arabinogalactan protein and 2% glycoproteins (Mikhailenko *et al.,* 2016). GA is a natural product having hydrophilic carbohydrate and hydrophobic protein parts (Verbeken *et al.,* 2003). It is used in

pharmaceutical industry as an antioxidant and drug carrier since it contains several aminoacids like lysine, tyrosine and histidine. It is also used in food industry especially confectioneries and smoothener in lotions (Ray *et al.,* 1995).

2.4 Classification of Clays

It is important to understand the structures of clays so as to be able to discuss their physicochemical properties. Figure 2.4 represents the 2-D layer structure of the kaolins, known as T-O layout. A sheet consists of a tetrahedral silicate layer bonded to the gibbisite layer through the tetrahedral oxygen of the silicate. The distance between two TOT or TO sheets is referred to as the interlayer or the gallery. This gallery hosts many ions mostly cations like K^{+}, Na^{+}, Ca^{2+}, Si^{4+}, Al^{3+} , $Fe^{2+/3+}$ and Mg^{2+}. The c-spacing from the T of one layer to the T sheet of the other layer is approximately equal to the interlayer distance referred to as d-spacing. This distance measures approximately 0.72 to 0.95 nm for kaolins. If 139 sheets which is normally the approximate number of sheets in a platelet, are stacked together into a platelet, the vertical distance covered would be 99.38nm which qualifies it nanoparticle irrespective of the length of its horizontal distance which could measure up to several microns.

The other common structure is referred to as T-O-T in which one gibbisite sheet is sandwiched by two silicate sheets. This structure is prominently found in smectites and micas. The interlayer distance here is approximately 0.75 to 0.95nm. On comparison the gallery in this structure is bigger than in the kaolins and hence hosts more ions and undergoes a lot of polymorphic substitution due to the negative charge on the sheets.

Kaolinite like other clays are important minerals with uses ranging from traditional pottery to nanocomposites. Kaolinite is a phyllosilicate of 1:1 structure. It consists of 1 layer of tetrahedral silicate sheet- TO_4 ($T=Si^{4+}$, Al^{3+}) as Si_2O_5 and an octahedral aluminate sheet- MO_6 ($M= Al^{3+}$, Fe^{3+}) as $Al_2(OH)_4$ (Aoroko *et al.,* 2013). This structure is due to isomorphic substitution that occurs in the sheets with ions of similar size from the interlayer distances which is approximately 0.72 nm. It is difficult for Na^+ or K+ to substitute the Al and Si due to large difference in ionic sizes. However these ions readily coordinate with the oxygen of silicate and OH of aluminate (Benco *et al.,* 2001). The 2 sheets are held together by intra-layer hydrogen bonds and hydrogen bonds associating H_2O and the sheets O and OH. The 2 sheets form a layer of $Al_2Si_2O_5(OH)_4$ with a host of ions like K^+, Na^+, Fe^{3+}, Ca^{2+} and CO_3^{2-}.

2.4.1 Kaolins

Kaolins are plastic clays formed by hydrothermal alteration and chemical weathering of feldspar and muscovite. Deposits are both primary and secondary. Kaolins include kaolinite, dickite, nacrite, and halloysite which are polymorphs i.e. they have the same chemical compositions $Al_2Si_2O_5(OH)_4$ but different structures which can only be distinguished by XRD. Kaolins are mostly pure, with high brightness, relatively low viscocity at high concentration. They are hexagonal crystals with triclinic crystal unit that form 1:1 silicate to aluminate structures. The structural bonds are strong hence not easily broken down which explains their low plasticity, shrinkage and swelling properties (Tan, 2011). These structures have d_{001} spacings of 0.72-0.95 nm and lateral dimension of between 30 nm to about 70 nm (Jiang-Jen *et al.,* 2010). The kaolin layers are held together by hydrogen bonds between the oxygen of the silicate and hydroxide

of the aluminate that prevent expansions and entry of polar molecules into the interlayer. They have low CEC of between 10 and 100 mmolkg^{-1} (Alexandre & Dubois, 2000). The d-spacings can be increased up to 1.5 nm if a surfactant used as plasticizer is dispersed into the layers (Pieter, *et al.*, 2015).

Figure 2.4 shows structure of kaolinite.

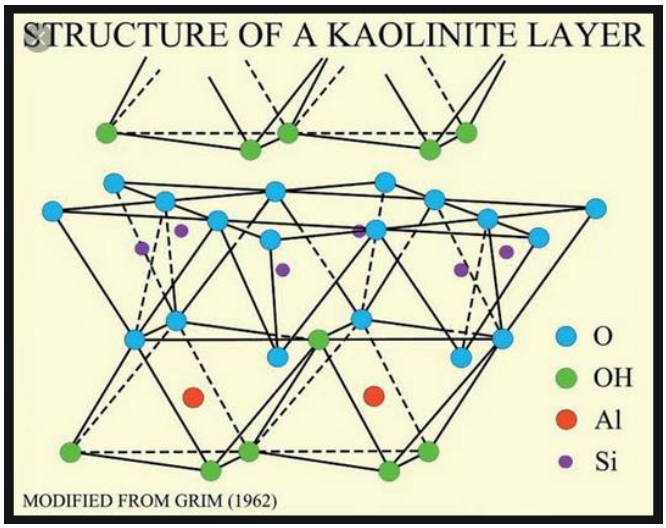

Figure 2. 4: Kaolinite structure (Grim 1962)

2.4.2 Micas

2.4.2.1 Illite

Illite is a general term for clay constituents or argillaceous sediments that belong to hydrous mica group. It is a significant rock forming mineral being a main component of shales and other argillaceous rocks with a formula, $(K, H)Al_2(Si,Al)_4O_{10}(OH)_2.xH_2O$, where x represents the variable amount of water that exists in illites (Greenland & Hayes, 1991).

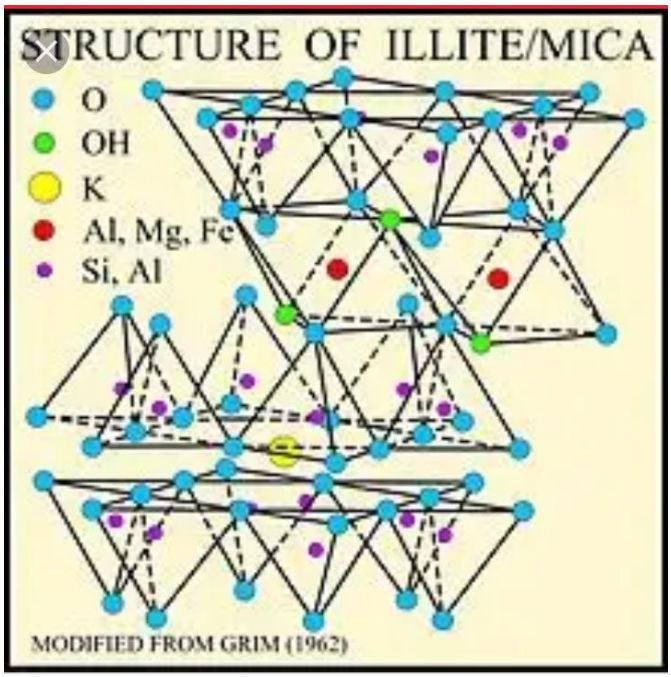

Figure 2. 5: Structure of illite

2.4.2.2 Muscovite

Is a common Mica, a hydrated phyllosilicate of $KAl_2(Si_3AlO_{10})(F,OH)_2$ (Amanda *et al.*, 2011). It has high basal cleavage yielding alstic sheets. It is usually used as fillers and extenders in paper manufacture. Figure 2.6 is a 2-D structure of muscovite.

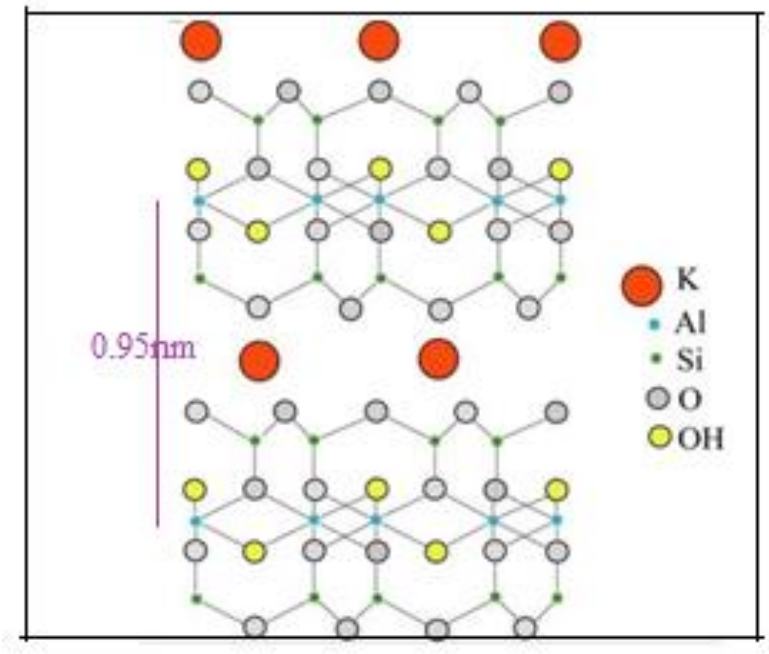

Figure 2. 6: Structure of Muscovite

Muscovite is a dehydrated dioctahedral structure. The gallery is populated with K^+ and Na^+ ions. The structure has collapsed layers at d=9.8 nm (Marian *et al.*, 2009)

2.4.3 Petalite

It is a castorite, lithium aluminium phyllosilicate mineral of formula $LiAlSi_4O_{10}$. It is usually used for in manufacture of glass-ceramic cooking ware. Figure 2.7 shows the structure of petalite

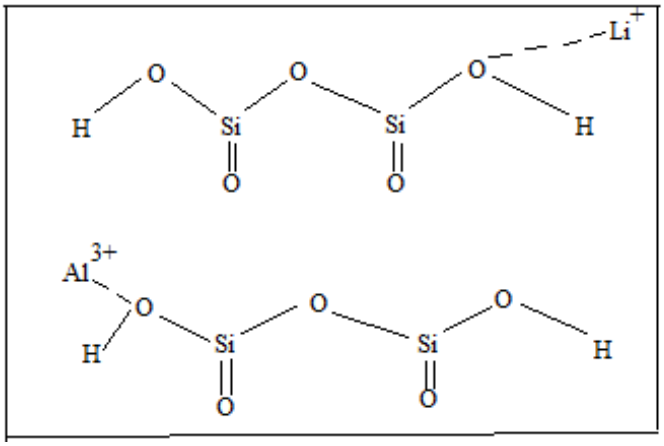

Figure 2. 7: Structure of petalite

2.4.3 Smectites

These are clays that are able to expand and contract their structures in one dimension as they absorb water or dry. The layers have a negative charge hence attract water molecules and other polar molecules into the interlayer hence very plastic. Their 2.1 structures are arranged in silica-aluminate- silica lattices. The aluminium in the $Al(OH)_3$ sheet is heavily substituted by iron and magnesium that have comparable ionic size, which give the sheet a negative charge (Gieseking, 1975). The low layer charge causes a lot of isomorphic substitutions. The d-spacings changes between 0.95 to 1.0 nm depending on the degree of interlayer solvation and higher exchangeable cation activity (Bohn *et al.*, 2001). They have a CEC of between 800 to 1200 $mmolkg^{-1}$ and highly PH dependent (Alexandre & Dubois, 2000). Examples of smectites are montmorillonite, beidellite, nontronite. The crystal lattice of smectite group clay consists of two-dimensional, 1 nm thick layers which are made up of two tetrahedral sheets of silica fused to an edge-shaped octahedral sheet of alumina, T-O-T. The lateral dimensions of these layers vary from 30 nm to several micrometres depending on the particular silicate (Jiang-Jen *et al.*, 2010). Because of the relatively weak Van der Waals forces existing

between the layers, intercalation and exfoliation of various molecules, and even the polymer is easily feasible.

Montmorillonite, MMT is a smectite of 2.1 structure, T-O-T (Alexandre & Dubois, 2000) with a structure of $(Na, Ca)_{0.3}(Al, Mg)_2(Si_4O_{10})(OH)_2.nH_2O$. They have a CEC OF 80-100 Mequiv/100g (Alexandre M & Dubois P, 2000). They are easily modified using quarternary ammonium salts into Cloisites.

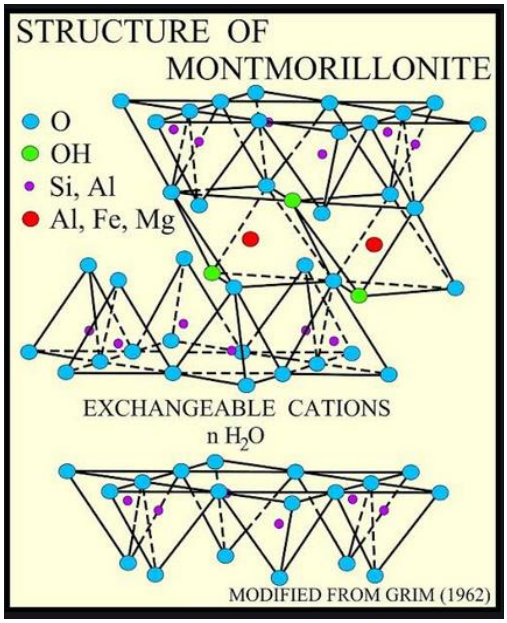

Figure 2. 8: Structure of MMT (Grim 1962)

Types of quarternary ammonium compounds used to modify clays are trimethylbenzyl ammonium, dimethylbenzyl ammonium, benzyl dimethyl ammonium. The swelling of the clay are altered by varying length of quartenary ammonium compounds. The nonpolar organic compounds are adsorbed onto the clay surface by weak Van der Wall's forces. Polar organics occupy similar sites to the polar water molecules at the silicate surface to satisfy the negative charge on the layers. The organic cations and the

negative charged clay surface form through electrostatic forces. The activities in the interlayer swell the clay platelets.

The Cloisites are organoclays. They are prepared by replacing the inorganic cations with organics in the interlayers. In many cases the organic cations are stabilized with some agents. In nature smectites have negative charge on their layers arising from isomorphous substitution in which the Al in the gibbsite is replaced with ions of lower charge like K^+ or in few cases replacement of Si in the silicate. This swells the organoclay and increases the interlayer distance. The organic cations have very big adsorption capacity for both inorganics and organics like petroleum pollutants. The figure 2.9 below shows the difference between unmodified and modified smectite clay minerals.

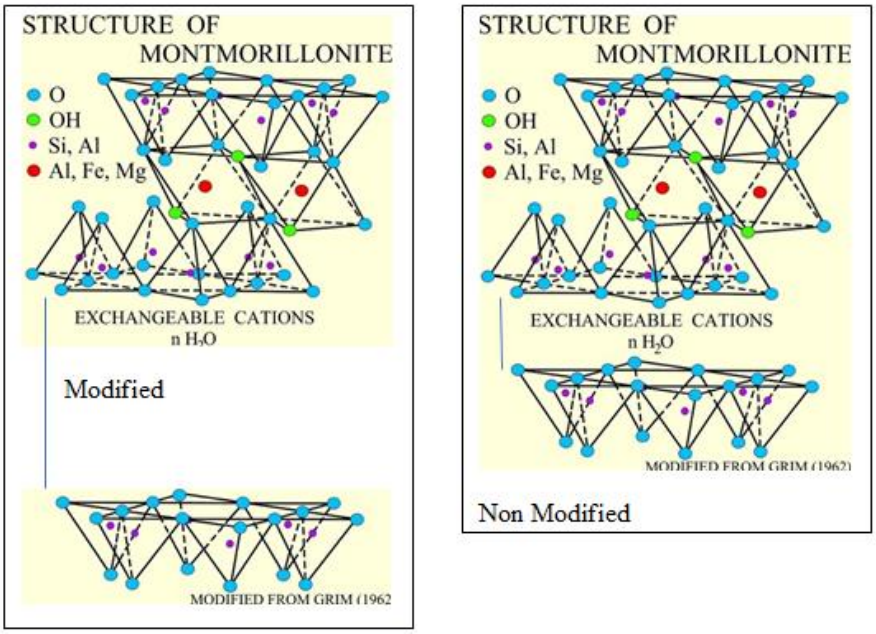

Figure 2. 9: Modified smectite clay mineral (Grim 1962)

2.5 Methods of clay polymer fabrication

Fabrication is the process of manufacturing, setting up or inventing something from raw materials. There are a number of methods that are presently employed to modify and polymerize clay minerals. Each of the methods has its own merits and demerits.

2.5.1 Melt intercalation

Melt intercalation is a polymer dispersion done in 4 steps; wetting of the initial polymer agglomerates, infiltration of the polymer chains into agglomerates, dispersion of agglomerates by erosion and rupture and distribution of the fillers or nanotubes into the matrix (Shafaq *et al.,* 2017). Usually the last step consists of blending the layers of the silicates with matrix of the polymer at high temperature conditions. The polymer disperses into the interlayer space forming either intercalated or exfoliated nanocomposite. The clay is usually mixed with molten polymer whose chains enter inside the layers to intercalate.

2.5.2 Synthesis with aid of supercritical CO_2

This method is usually applied in food and pharmaceutical industry. Supercritical liquids have advantages of lower viscocity, lower surface tension, lower liquid-like density and lower gas-like diffusivity over other organic solvents (Shafaq *et al.,* 2017). The polymer and clay are mixed in the supercritical-CO_2 at high pressures which enables the sc-CO_2 and the polymer to diffuse into the inorganic layers and intercalate.

2.5.3 Sol-gel

Sol-gel is a process done in two steps in which the sol or suspension of particles mixes with the gel. The gel usually consists of organometallics, organics, $Mg(OH)_2$, silica gel

and LiF. This gel promotes dispersion of layers of the clay in the polymer matrix. The solution, sol consists of particles of clay and polymer.

2.5.4 Intercalation of polymers from solutions

A solvent is applied to swell and disperse the clays into the polymer solution. The process consists of two phases, the aqueous and clay phase and the non-aqueous monomer or pre-polymer. The polymers intercalate between the layers of the inorganic clay mineral (Alexandre & Dubois, 2000)

2.5.5 In-situ/in position polymerization

In this polymerization the polymer clays are swollen with a monomer solution followed by polymerization in between the intercalated sheets (Shafaq *et al.,* 2017). The nanofillers are swelled in the monomer solution. A low molecular weight solution of monomer easily seeps through into the layers causing swelling

2.6 Synthesis of clay nanocomposites

For any clay monomer to be dispersed into any matrix, the interlayer distances must be increased through a pillaring process. This pillaring process requires either phosphonium ions PH_4^+ or its organic derivatives; R_3PH^+, RPH_3^+ some of which are tetraphenylphosphonium bromide, bis(triphenylphosphoranylidene)ammonium chloride, tetrabutylphosphonium bromide, tetrakis(hydroxymethyl)phophonium chloride tetraphenylphosphonium bromide and or alkylammonium ions like CTAB (centyl trimethylammonium bromide) to intercalate or exfoliate the layers. These ammonium ions on the surfactant are easily exchanged with ions situated in the clay interlayers (Giannelis, 1998). Depending on the layer charge these ions may adopt different structures reducing the electrostatic interactions between the layers by

expanding the clay galleries which facilitate diffusion of molecules, monomers and polymers into the galleries (Kornmann, 2000). The longer the surfactant, the further apart the clay layers are forced (LeBaron *et al.*, 1999). The ability to retain cations on the surfactant is defined in terms of the cation exchange capacity.

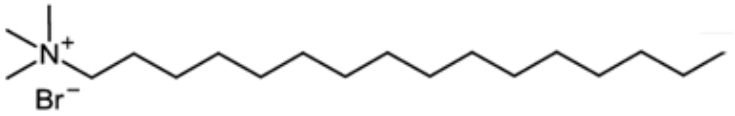

Figure 2. 10: Centyltrimethylammonium bromide,$C_{19}H_{42}NBr$, CTAB

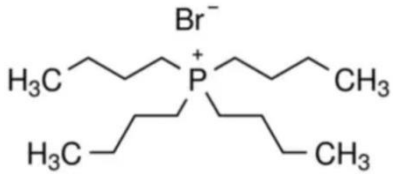

Figure 2. 11: Tetrabutylphosphonium bromide

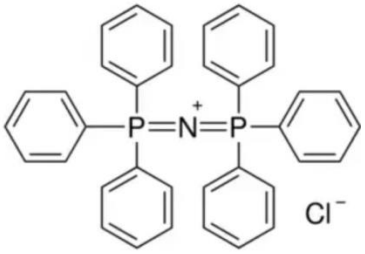

Figure 2. 12: Bis(triphenylphosphoranylidene)ammonium chloride

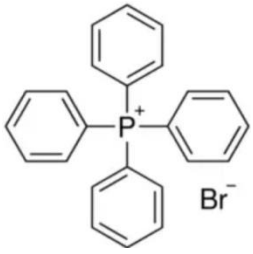

Figure 2. 13; Tetraphenylphosphonium bromide

There is some research done on preparation of nanocomposites. (Amanda *et al.*, 2017) that reported on' the Role of Slow Release Nanocomposite Fertilizers on Nitrogen and

Phosphate Availability in soil', prepared nanocomposites of urea by mixing urea and HA at 20 and 50 wt % ww^{-1} HA ratios using a melt-processing method. The nanocomposites were produced on a torque rheometer at 60 rpm for 10min at 100°C and then dried at room temperature for 24 hours. The composites were designated as UrHap20 and UrHap50.

Nanocomposites containing thermoplastic starch, TPS as a matrix were obtained from physical mixture of corn starch, urea and distilled H_2O at ratios of 56: 24: 20 respectively. Stearic acid 1 % wt ww^{-1} and 1 % wt ww^{-1} citric acid were added. The final combination was processed on co-rotating twin screw extruder. The heating rods on the extruder were set at 110 °C, 115 °C, 120 °C, 125 °C, 130 °C and 135 °C. The extruder was operated at 150 rpm to obtain the TPSUr (TPS+Ur) as blends that were then pelletized. The TPSUr/Hap nanocomposites with Hap50 and Hap20 were produced in the extruder by mixing the urea, starch, citric acid stearic acid with relevant Hap. The nanocomposites were designated as TPSUr/Hap50 and TPSUr/Hap20.

(Corradini *et al.,* 2010) considered the review 'a preliminary study of the incorporation of NPK fertilizer into chitosan nanoparticles' in which they outlined preparation of CS-PMAA nanoparticles; the Chitosan was dissolved into 0.5 % (v/v) methacrylic acid solution for 12 hours under magnetic stirring into a concentration of 0.2 % (w/v) then 0.2% mmol $K_2S_2O_8$ was added to the solution with magnetic stirring for 1 hour at 70°C until the solution became clear. The solution was cooled on an ice bath. They incorporated of NPK fertilizer into the chitosan nanoparticles. Nitrogen was sourced from urea, phosphorus from calcium phosphate and potassium from KCl. Different

amounts of the NPK were dissolved into 50 mL of the nanoparticle solution under magnetic stirring for 6 hours at 25°C.

(Ghazali *et al.,* 2017) studied, 'The properties of controlled- Release- Water Retention Fertilizer Coated with Carbonaceous-g-poly (acrylic acid-co- acrylamide) superabsorbent polymer'. They prepared carbonaceous particles by putting biomass of empty dry fruit bunches into the pyrolysis furnace with flow of nitrogen at 250 mL/min. The temperature was raised at 10 °C/min until all the matter charred. Acrylic acid-AA monomer and acrylamide-AM co-monomer were neutralized in sodium hydroxide solution in distilled water. Methylene bisacrylamide-MBA crosslinker was added into the mixture flask. The flask was immersed into a water bath at 70 °C. Ammonium Perosodisulfate-APS initiator was added and mechanically stirred at 300 rpm for 2 hours until a gel forms. The gel was dried in an oven at 60 °C in the synthesis of carbonaceous-SAP. The SAP was prepared into a gel then 0.5 % wt of the carbonaceous particles were added as filler. The commercial fertilizer granules were mixed into a starch solution. This mixture was immediately added into a freshly prepared SAP gel with stirring. The product CRWR is dried in an oven at 60 °C.

2.7 Analysis Methods and Techniques

The characterization of nanostructured materials formed is crucial in understanding their properties and their application in discharge of plant nutrients. Specific techniques were used to analyze morphology, particle size, structures of the materials, physical and chemical properties of the nanocomposites. The morphology and structure of the nanocomposites were analyzed by electron beam probe methods of Scanning Electron Microscopy (SEM) and transmission Electron Microscopy (TEM). Spectroscopic probe

techniques were used to measure optical and magnetic properties of the materials as well as their elemental and electronic structures. These methods included; UV-Vis Spectroscopy (UV), Fourier Transform Infrared Spectroscopy (FTIR), Powder X-ray Diffraction (XRD), Energy Dispersive X-ray Spectroscopy (EDX) and X-ray Flourescence (XRF).

Thermodynamic methods were used to determine temperature, surface area and volume. This characterization is also used to measure other physical properties like surface tension, pressure and porosity. These techniques include Brunauer-Emmet-Teller (BET) for surface area, Barret-Joyner-Halenda (BJH) for pore volume and Thermogravimetric analysis (TGA) for temperature gradient.

2.7.1 The electron beam probe techniques.

This is a technique in which high energy electron beams are directed into a sample for imaging, chemical analysis and determination of structure of the nanocomposite. They are divided into two, the scanning electron microscopy (SEM) and the transmission Electron Microscopy (TEM). The electron beam probe technique of Scanning Electron Microscopy and Transmission Electron Microscopy were used to analyze morphology of raw materials.

2.7.1.1 Scanning electron microscopy

Is a high resolution imaging of the surface of a solid sample. In SEM, accelerated electrons with certain amounts of kinetic energy are passed through a combination of lenses and apertures and then directed into a solid sample. On interaction with the sample atoms the speed of electrons reduces releasing some of their energy as a signal. The signals produced are used to give information about surface topology and

composition of the sample by creating an image from the reflected or the electrons that are knocked off from the sample.

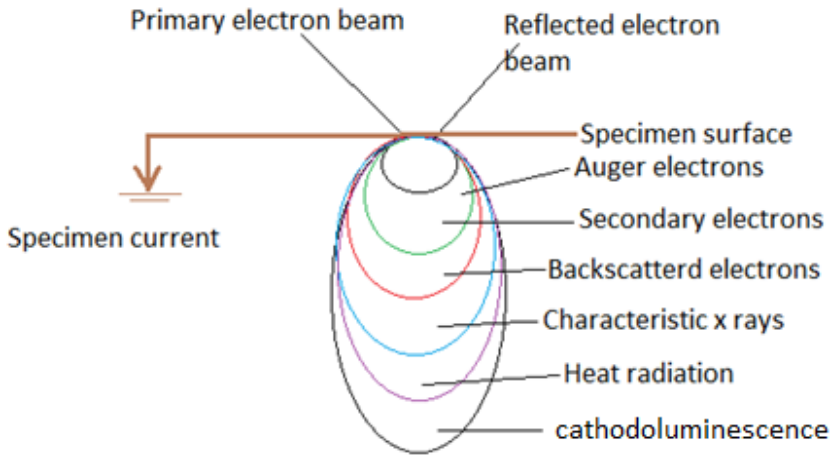

Figure 2. 14: Electron beam interaction with surface

In this technology, finely focused beam of electrons scans across the surface of the specimen. The interaction of the primary electron beam with the surface atoms excites several types of scattered or emission electrons which are then used to map the image or elemental composition of the material (Hornyark *et al.*, 2008).

The most important secondary beam effects exploited in SEM investigations are: the secondary, backscattered electrons for imaging and characteristic x-rays for simultaneous elemental analysis. The appearance and clarity of the image depends on the electron-matter interaction volume involved, the detector and the signal processing speed, pixels (Goldstein *et al.,* 2003). The spatial resolution is limited by the size of the interaction region in the specimen from which the signal is derived.

The backscattered electrons originate from an elastic scattering of the primary beam electrons by nuclei on the specimen surface. On the other hand, secondary electrons are due to inelastic scattering following interaction with specimen electrons.

Since backscattered electrons originate from elastic scattering they are equivalent in energy to primary electrons compared to inelastic scattered secondary electrons hence the image from backscattered electrons gives excellent compositional contrast since backscattered electrons yield depends on atomic number. Given that the high-energy backscattered electrons can escape from a larger interaction volume of the specimen than secondary electrons, the resolution is lower at fixed accelerating voltages. This is as a result of knock out effect of electrons from beam trajectory during elastic scattering. The SEM image is formed from low-energy secondary electrons after they exit from sample surface. Since the scattering event is inelastic the energy of the secondary electrons is reduced relative to that of primary beam electrons. In addition, secondary electrons originate from few nanometers 1 - 50 nm in depth and can be used to determine surface morphology and topography. Tilting of the surface enhances secondary electron generation because a larger specimen volume interacts with the beam, resulting in increased secondary electron emission. If the primary electron beam falls into a pit on the surface, fewer secondary electrons escape because the specimen reabsorbs the electrons. The difference in density of generated secondary electrons reaching the detector is responsible for topographical contrast during SEM imaging.

The pictures taken in this study are usually were magnified at resolutions like; of 500, 2000, 10000, 30000 and 100000. The samples were prepared by being mounted on an aluminum stub using a double sided carbon tape, and then coated with a thin layer of about 10-30 nm of gold-palladium alloy by means of vacuum sputtering coating using a Denton Desk 1 Sputter-Coater under a 70 mtorr pressure vacuum.

2.7.1.2 Transmission Electron microscopy

A beam of high energy electrons is irradiated into a solid sample. Here a beam of electrons are directed through two lenses of electromagnetic coils and focuses the beam into the sample. This powerful beam of electrons passes through the solid sample producing an image of the surface and inner structure of the sample. The lighter areas represent areas where larger number of electrons pass through while the darker ones are those that allow lesser number of electrons hence denser in terms of particles present. This provides topology, morphology and crystallinity of the sample. Figure 2.13 shows a schematic representation of the transmission electron microscopy.

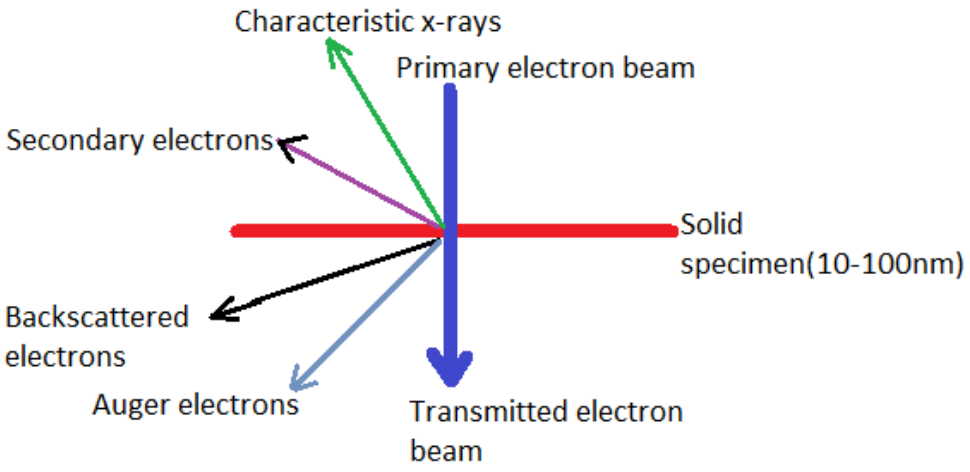

Figure 2. 15: Transmission Electron beam interaction with the solid

TEM functions on the same principle as SEM except the detector is a phosphor plate able to capture images formed by transmitted electrons. However, TEM utilizes a higher accelerating voltage hence achieves far greater resolution compared to SEM. The resolution and quality of TEM image are dependent on proper sample preparation since specimen thickness is restricted to less than 100 nm. The type of image contrast formed during TEM analysis depends on the mode of operation. The

most common mode of operation is the bright field image mode. In this mode image contrast is attributed to transmission and absorption of primary electrons by the sample. Thicker regions of the sample or regions with heavy elements will appear dark, whilst regions with no sample or with light elements in the beam path will appear bright.

The interaction of the primary electron beam in TEM with matter similarly results in inelastically scattered electrons which are transmitted obliquely through the sample with loss in energy. Electron energy loss value is element specific and unique to bonding or coordination environment hence important in elemental analysis. TEM instruments coupled to Electron Energy Loss Spectroscopy (EELS) allow for this functionality. Similarly, characteristic x-rays result following a release of secondary electron, usually from K-shell creating a vacancy. Electrons with higher energy cascade to fill the void. In the process, x-rays are emitted that are characteristic of the energy transition and element specific. These x-rays are used for qualitative and quantitative compositional TEM analysis.

2.7.2 Spectroscopic probe techniques

These are instruments that involve interaction of the material with electromagnetic radiation.

2.7.2.1 Powder X-ray Diffraction (PXRD)

An x-ray powder diffraction pattern is a plot of the intensity of X-rays scattered at different angles by the sample. The detector is set at angle two theta from the incident ray. Bragg's law provides a simple model on the relationship between the diffraction

and crystallinity. A family of planes produces a diffraction peak only at specific angle 2θ.

Xrd provides information on structures, phases, crystallinity, crystal orientation, crystal defects and grain size. The peaks are produced by constructive interference of a monochromatic beam of X-rays scattered by lattice planes in a sample. It shows periodic arrangements of the sample (Bunaciu *et al.,* 2015). The interaction of the incident ray with sample produces constructive interference that satisfies Bragg's Law,

$n\lambda=2d\sin\theta$ …… equation 2.3

where n is order of reflection, λ is the wavelength of incident ray, d is inter-planar spacing, θ is angle of incidence.

This technique has been used in a number of areas; pharmaceutical industry, forensic science, geology, glass manufacture and microelectronics among many. It has been used to identify and quantify minerals present in soils.

In XRD a fabric is the geometrical arrangement of particles and associated voids; classified into micro, mini and macrofabric. The nature of the fabric determines the angle at which the monochromatic X-ray is reflected.

The x-rays, similar to electron beams, can also be reflected at the net plane of a crystal lattice. The spacing between atoms and planes in crystalline solids show long-range periodic structure on the order of the wavelength of X-rays exhibited as Bragg's diffraction peaks. Bragg's law forms the foundation of X-ray diffraction.

Irradiating a crystal with a collimated and mono-energetic X-ray source gives rise to constructive and destructive interference via scattering of the X-rays at the crystal planes. To obtain constructive interference the path length A-B-C has to be equal to an integer multiple of the incident wavelength. Different crystal planes will have different diffraction angle.

For nanostructured materials XRD is not always appropriate in determination of structure since the coherence length of the structure is limited. The identification of a given crystal structure is usually done by correlating the diffraction pattern obtained with known standard diffraction files. X-ray diffraction was an important analytical tools utilized in structure, crystallite size and shape determination in crystalline metal oxide materials fabricated.

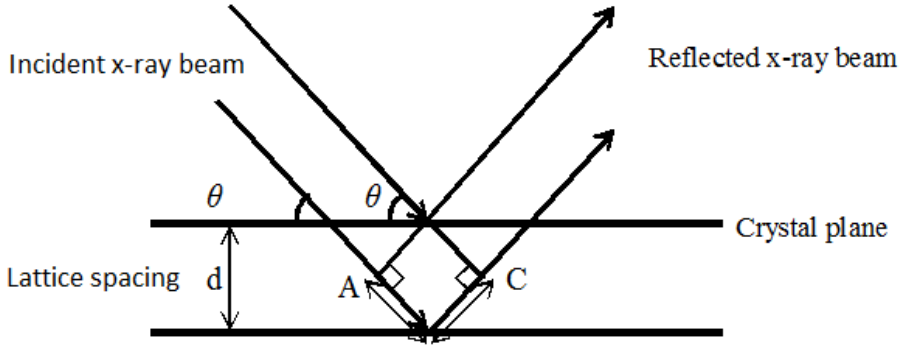

Figure 2. 16: Diffraction of X-rays from a set of crystal planes

In order to understand changes in the interlayer distances, it is important to have a clear picture of the planes that affect the x-rays in a crystal. In a cuboid the top and the bottom surfaces represent the basal 001 plane described by length a by width b. The parallel plane that passes in the middle of these two planes is the basal 002. In a TO clay mineral, an incident X-ray illuminated on the top and 002 basal planes with the same angle will be diffracted at slightly different angles known as two theta. The difference is caused by the different interaction between the ray and the silicate on one

end of the layer and an aluminate on the other layer. However if the incident ray is irradiated on the silicates of the TOT at same angle of incidence, the two theta value will be the same. The two theta value is known to increase when the top and bottom layers of a clay mineral have their interlayer distance reduced. The two theta values for the 002 basal planes will differ from an incident ray of the same angle to basal 001. The 010 prism planes represent the height surface of the unit cell described by c by b. An incident ray that will be diffracted by this plane in a clay mineral will either show the interlayers in which case the peaks will be low and in region above two theta greater than 40°, unless when it is on the b edges. Similarly the middle plane to these two planes is 020 prism planes. Multiples of these 010 and 020 define the length of the clay mineral sheets whereas the basal planes describe the height of the interlayers. A study on the heights and widths of the interlayer distances of the clay minerals and the height modified tells of a process referred to as intercalation and exfoliation.

2.7.2.2 Fourier Transform Infrared Spectroscopy (FT-IRS)

Fourier Transform Infrared (FTIR) spectroscopy provide information on fundamental vibrations of characteristic functional groups within polymeric and metal oxide materials fabricated. Analysis by IR spectroscopy was limited to energies between 4000 – 400 cm^{-1} (Liu, 2009) to some extent the far IR region of electromagnetic spectrum (Silverstein, 1998)

Functional groups common in polymeric materials include: hydroxyl, carbonyl, ester, methyl, epoxy, phenol and aromatic ring. For inorganic materials metal oxides and metal hydroxide lattice vibrations were responsible for the observed IR active bands. The analysis by FTIR spectroscopy is limited to molecules having permanent dipole

moments or phonons in crystalline materials. The FTIR spectrum is collected as absorbance or the percent transmittance of light as a function of wavelength (λ) or often its inverse, the wavenumber (cm^{-1}) is usually used. Quantitatively, the amount of energy absorbed at a given frequency depends on both molecular concentration and molecular structure. FTIR was used to identify functional groups in the multifunctional clay nanocarriers, polymer nanofiber templates and the SAPs. Data interpretation of characteristic bands was by simple correlations and reference to generalized charts of characteristic group frequencies.

2.7.2.3 Energy-Dispersive X-ray Spectroscopy (EDS)

This is an analytical method to determine the chemical composition of all kinds of materials. Energy dispersive (EDXRF) has a range of Na to U while the wavelength dispersive (WDXRF) has a range from Be to U. Here X-ray source irradiates the sample extracting a lower energy shell electron to a higher level leaving a hole. Such an atom is excited and relaxes the electron back into the hole with a characteristic energy or color. The emitted fluorescent X-ray radiation is measured for energy hence determining the element as a percentage.

The electron beam-specimen interaction equally generates X-ray photons. These characteristic X-rays are caused by the ionization of inner shell electrons when the electron beam energy exceeds critical ionization energy. The relaxation of outer shell electrons into holes generated by ejected inner K shell electron yields characteristic X-rays, specific to each element. Energy-dispersive X-ray (EDXRF) spectroscopy measures the X-ray intensity as a function of energy whereas wavelength dispersive X-ray (WDXRF) spectroscopy measures X-ray intensity as a function of

wavelength dispersion based on Bragg's diffraction.

2.7.2 4 Thermogravimetric Analysis (TGA)

Thermogravimetric analysis (TGA) involves the measurement of the change in weight of a sample under investigation with temperature increase at set rate. The sample may either lose weight to the atmosphere or gain weight by interaction with atmosphere. The two techniques used in TGA are: dynamic TGA and static TGA (Khandpur, 2007). In dynamic TGA, the sample is subjected to continuous temperature changes with time, while in static TGA the sample is maintained at constant temperature for a period of time and any changes in weight recorded. The TGA curve obtained is usually recorded in the form of integral curve, with absolute weight as the y-axis and time or temperature as the x-axis. TGA curve is influenced by several factors: heating rate, sample and atmosphere.

2.7.2.5 UV-Visible Spectroscopy (UV-VIS)

UV-Visible Spectroscopy (UV-VS) offers information in particular to the density of states in nanostructured materials. It was used to establish the nutrient release concentrations of the samples from water and soil. Ultra-violet visible spectroscopy (U-Vis) is an optical method that involves interactions of UV radiation with a sample. Molecules with pi-electrons or nonbonding electrons absorb this radiation in the range 200-400nm. The electrons are then excited to higher anti-bonding molecular orbitals. The absorption depends on the gap between Highest Occupied Molecular Orbitals, HOMO and Lowest Unoccupied Molecular Orbitals, LUMO. The absorbance of a solution is directly proportional to the concentration of the absorbing species and the path length (Yogita *et al.,* 2014).

The Ultra-Violet/Visible spectrum of a material provides information about its optical properties, which are directly related to its electronic properties. These include the optical band gap and sub-band gap absorptions. The optical transitions across the fundamental band gap of semiconductors can be related to band structure and in particular to the density of states in nanostructured materials (Mark, 2001).

Electronic absorption spectra is recorded on a Hewlett Packard 8452A UV- Visible spectrophotometer interfaced to an IBM computer. This device incorporates a rapid scanning microprocessor-controlled diode array detector in the range 190-900 nm. The detector consists of 200 diodes each in the ultra-violet and visible, which measure small amounts of current and then converts the values into absorbance units. It utilizes both deuterium and a 20-watt tungsten-halogen common axis radiation lamp source for the UV and visible region, respectively.

2.7.2.6 X-Ray Fluorescence-XRF

In UV spectroscopy photo-excitation causes promotion of electrons from the ground state to permissible electronically excited states. When these electrons return to their equilibrium ground states, the excess energy is released by either emission of light in a radiative process called luminescence or by relaxation in a non-radiative process. The energy of the emitted light relates to the energy difference between two electronic states involved in the transition between the excited state (Ef) and the equilibrium state (E_i), The quantity of the emitted light is related to the relative contribution of the radiative process (K_r). In semiconductors, inter-band luminescence occurs between the conduction and valence bands with the energy difference being known as the band gap, as illustrated in Figure 2.15

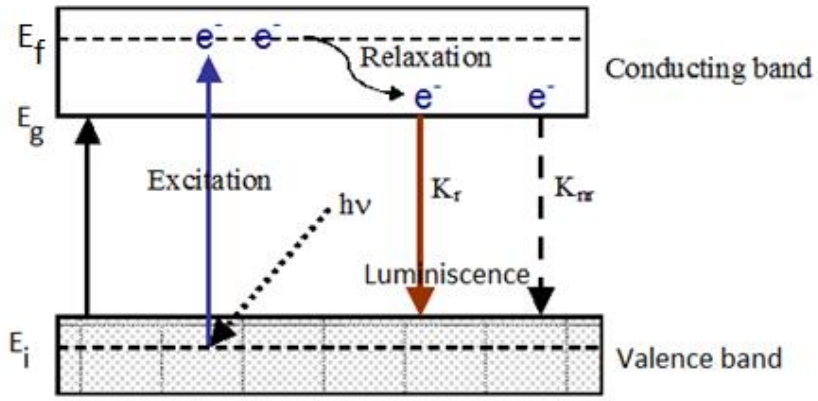

Figure 2. 17: Schematic representation of photoluminescence

XRF was used to collaborate the information of elemental composition of the materials which was determined by EDX.

2.7.2.7 Particle size

It determines porosity and pore size affects most behavior of elastic movements, mechanical movements and flow of fluids. Gas sorption method is popular for determining the surface area, total pore volume and pore size distribution of nanostructured materials. Specific surface area of a material is usually determined by physical adsorption of a gas in Brunauer-Emmet-Teller Method (BET). Whereas BET is used to determine the surface area, Barret-Joyner-Halenda (BJH) determines the total pore volume. BJH is the procedure of calculating pore size/pore volume distributions from experimental isotherms using the Kelvin model of pore filling. This model applies to mesopore and small macropore size range. The material is first heated and degassed by vacuum force or inert gas purging to remove adsorbed foreign molecules. The sample material is then placed in a vacuum chamber at a constant and very low temperature, usually at the temperature of liquid nitrogen at -195.6 °C,

and subjected to a wide range of adsorbate pressures, to generate adsorption and desorption isotherms.

Micromeritics ASAP 2010 operate by measuring the quantity of gas usually nitrogen or krypton adsorbed onto or desorbed from a solid surface at some equilibrium vapor pressure (Leddy, 2012). The pore size and surface area was calculated from equation 2b.

In linear form: $\frac{P}{V(P_0-P)} = \frac{P}{V(P_0-P)} = \frac{1}{V_M} \text{ x } \frac{P}{P_0}$; …….. equation 2b

where P is the equilibrium experimental pressure, P_o is the vapor pressure of the adsorbate gas at the experimental temperature, V ($m^3.g^{-1}$) is the standardized experimental volume of the adsorbed gas of adsorbent, V_m ($m^3.g^{-1}$) is the volume of the adsorbate monolayer of adsorbent and c is the constant that relates to heat of adsorption.

BET is based on assumptions that; the surface is energetically homogenous, only vertical interactions between adsorbed molecules are considered, and that the molecules adsorbed on the surface demonstrate the strongest energy of adsorption and heat of adsorption of the subsequent layers is the same as the latent heat of condensation of the adsorbate gas. BET remains an extremely popular method of determining surface area and henceforth was applied in analysis of the fabricated metal oxide nanofibers catalyst supports.

CHAPTER THREE

METHODS AND MATERIALS

3.1 Study site

The research laboratory for this study was set at the chemistry laboratory of Masinde Muliro University of Science and Technology while the greenhouse optimization was done at the University agricultural research farm. This study targeted black clay from Ilesi market in Kakamega County and a white clay soil sourced through the coordinator of ilesi potters.

3.2 Research design

The study followed experimental design in which the soil samples for determination of physicochemical parameters were collected from the university farm using the randomized model. Samples of the red loamy soils and the decomposed cow dung soil were air dried, mixed, ground and sieved on 2 mm mesh. The simulation of products in deionized water and absorption of the nutrients from the soils was performed in three replicates for the independent variables. The NPK was used as a control for the release capacity while tins with NPK and without any fertilizer were controls in field optimization. The design for field optimization followed randomized complete block experimental consisting groups of SRF2, CRF3 and CRF4 nanofertilizers and NPK control sample as in (Islam *et al.,* 2018). The simulation in water followed a randomized block experimental design in which the groups NPK, SRF1, SRF2, CRF1, CRF2, CRF3 and CRF4 were treated with deionized water for release of nutrients.

3.3 Sample collection and preparation.

3.3.1 Farm samples

Ten kgs of top soil was dug up to a depth of 15 cms from ten spots randomly selected on the research farm. The soil was put on a large gunny bag and mixed with 10 kgs of cow dry dung. The mixture was physically crushed using a wooden stick and thoroughly mixed using a spade. The soil was then sieved on 2 mm standard mesh in order to remove the gravel, rock and organic matter like humus, roots and stems. The soil that passed through the sieve was stored in dry polythene lined gunny sacks for planting of maize and physicochemical analysis.

3.3.2 Clay samples

The area of the clay soil was marked with assistance of local members. A pit of 1.5 m by 1.5 m square was dug on the site past the black clay sheet. Using a spade and a shovel, about 100.0 kg of the black clay soil was excavated from the sides of the pit (Moreno-Tovar *et al.,* 2017) (Njoka *et al.,* 2015). The clay soil sample was wrapped into polythene papers for transportation to the laboratory (Andala & Wachira, 2015).

3.3.2 Treatment of clay soil sample

The 100.0 kg black clay sample was air dried and crushed using wooden sticks. The crushed dry black soil was first sieved on 1mm mesh. About 20.0 kg of dry clay sample was mixed with 10.0 L of 25 % sodium hexametaphosphate solution to deflocculate the clay particles in batch one. The humus and organic matter was poured out. The clay mixture was filtered and dried.

This dry clay sample was crushed again, mixed with water and beneficiated using 75 µm mesh into a plastic bucket. The mixture was left for two weeks to sediment. The

solution part was decanted into a plastic bucket. The remaining sediment was washed on filter paper with distilled water and stored in dry polythene paper bags for characterization and preparation of nanoclays. The remaining 80.0 kg raw clay was treated in similar manner to produce more beneficiated clay samples.

3.3.4 White clay soil sample.

White clay was sourced through the Ilesi pottery group was dried and stored in dry polythene bag which was stored into a gunny bag.

3.4 Laboratory soil analysis

3.4.1 The pH of the clay soil

The pH was determined using a glass and reference electrode with a pH meter on a suspension of 5.0 g of clay soil to 5 mL of water. The 1:1 water and soil mixture was stirred vigorously using a stirring rod for 60 seconds and let to stand for 10 minutes. The pH meter was inserted into the mixture and read. This worked for the black clay sample however the red soil and white clay showed higher pH values. These white clay and red loamy soil samples were therefore analyzed further using the lime requirement test. The SMP buffer index known as the lime requirement test was determined by adding 10 mL of buffer solution to such 1:1 sample by volume. The buffer index of the suspension was determined using a pH meter, after the sample had been stirred intermittently for 15 minutes.

3.4.2 Cation exchange capacity.

Five grams of the black soil was put into a centrifuge tube, 30.0 mL of 1.0 M sodium acetate was added stoppered and shaken using a mechanical shaker for 5 minutes. The

mixture was centrifuged at 2000 rpm until the supernatant liquid became clear. The supernatant liquid was discarded. This was repeated 3 more times.

The soil in the tube was treated with 30.0 mL of 95 % ethanol, stoppered and shaken in a mechanical shaker for 5 minutes. The mixture was centrifuged at 2000 rpm for 5 minutes for at least 5 times. The exchange capacity of decanted solution from the 5^{th} batch was tested by flame photometer to ensure that it reads less than 40 ms/cm.

Exactly 30.0 mL of ammonium acetate was added to the treated soil in the tube, stoppered and shaken for 5 minutes. The mixture was centrifuged for 5 minutes. The decanted liquid was collected in a 100.0 mL volumetric flask. This was repeated two more times to collect a decanted liquid of 90.0 mL. The last run was of 10.0 mL of ammonium acetate. This decanted solution was tested for the concentration of sodium ions using a flame photometer against sodium standards between the range 0-4 meq/L. This was repeated for the other two soil samples.

3.4.3 Determination of pore size and surface area of beneficiated clay

Exactly 1.0 g of each sample was weighed and degassed at 250 °C and 10^{-6} torr overnight prior to nitrogen adsorption-desorption isotherm measurements. The 1.0 g dry beneficiated black clay sample was pushed into the micromeritics ASAP 2010 analyzer cell using the rod for Brunauer, Emmet and Teller, BET analysis (Webb & Orr, 1997). The surface area and pore size was determined using isotherms which are graphical representation of the nitrogen gas uptake quantity as a function of pressure at a constant temperature of 77 K (Trunschke, 2013).

3.4.4 Carbon concentration

Total organic carbon was done by calorimetric method in which the crushed sample was sieved on 0.5 mm mesh and dried in an oven to 40 °C. The dried sample was oxidized by acidified potassium dichromate at 150 °C for 30 minutes. Barium chloride was added to cool the digest. The solution was analyzed on spectrometric method.

3.5 Synthesis of nanocomposite fertilizers

The synthesis of the CRF and SRF involved 3 steps, synthesis of starch-PVA and starch-GA (Han *et al.,* 2009), design of a clay organonanoclay (Siafu *et al.,* 2015) and lastly fabrication of the nanocomposite fertilizer and encapsulation **(**Siafu *et al.,* 2015).

3.5.1 Starch-PVA film synthesis

Exactly 10.0 g of corn starch, 200.0 mL of 40 wt % polyvinyl alcohol and exactly 10.0 ml of glycerin was added to the corn starch and PVA mixture. The mixture was added to 100.0 mL distilled water in a 500 mL glass beaker at room temperature with stirring. The temperature of the suspended mixture was raised to 80 °C by placing it into a hot water bath. A little butanol was added to the mixture to avoid frothing. Exactly 200.0 mL of 20 wt % formaldehyde was added and stirred for 3 hours to completely gelatinize the starch. Little water was added continuously to maintain the total volume of the mixture. The temperature was then raised to 95 °C for 20 minutes. Any foam that formed on the mixture was skimmed off and the starch-PVA solution poured and leveled into a glass mold. The jelly solution dried at room temperature. The films were removed and dried at 60 °C in an oven for 24 hours. The dried starch-PVA films were removed from the mold and stored in polythene bags.

3.5.2 Starch-Gum arabic synthesis

Exactly 50.0 g of gum acacia was mixed with 20.0 g corn starch in a 250 mL glass beaker. Accurately measured 100.0 mL methanol was added into the mixture. The mixture was manually stirred with temperature being raised at 2 °C per minute until temperature reached 60 °C. About 10.0 mL glycerine was added and the mixture continually stirred until it formed a gel.

3.5.3 Nanoclays

The nanoclay was prepared by intercalation of polymers from solutions in which methanol solvent was applied to swell and disperse the clays into the polymer solution. The process consists of two phases, the aqueous and clay phase and the non-aqueous monomer or pre-polymer. The polymers intercalate between the layers of the inorganic clay mineral (Alexandre & Dubois, 2000). Exactly 150.0 g of the dry beneficiated clay in ratio of 2:1, white to black, was dispersed into 1.0 L of deionized water in a 4.5 L aluminium jug. This dispersion was sealed and mechanically stirred for two days. The beneficiated clay mud was modified by adding 3.5 L of 0.1 M NaCl solution. The mixture was then mechanically stirred at 50 °C for nine days at eight hours a day to deflocculate the particles (Huey-Rong and Donald, 1960) and populate positive charge into interlayers. The product was filtered and washed several times by distilled water to remove excess chloride. The mixture was constantly tested with $AgNO_3$ until no white precipitate showed. The washed product was dried in an oven at 60 °C and the powder stored as NaDp, sodium beneficiated clay. This was repeated in ten batches to raise 1500.0 g.

Exactly 500.0 g of the formed NaDp was mixed with 3.0 L of distilled water and 454 mL of DMSO liquid in a 4.5 L aluminium jug, and then mechanically agitated at 80 °C for 8 hours in a day for 84 days. Deionized water was added after every 1 hour to the 3.5 L mark to hinder desiccation of the stirring mixture. After 84 days of continuous stirring the suspension was aged for one week by way of stirring at room temperature. Exactly 100.0 mL of propyl alcohol was mixed with this mixture and mechanically stirred for another three days to remove excess solvent after which it was dried in an oven at 40 °C for 2 days and labeled clay-DMSO (Pieter *et al.*, 2015). This was done once over time of study to yield 500.0 g organic modified clay.

Exactly 500.0 mg per 1.0 L aqueous solution of CTAB surfactant was mixed slowly with the aqueous clay-DMSO in ratios of 70.0 mL: 30.0 mL and 50.0 mL: 50.0 mL. In the case of the 70-30, 0.5 kg clay-DMSO formula was mixed with 1.2 L of deionized water. This mixture was added to 2.8 L of CTAB and stirred. The mixture in each batch was stirred for 24 hours at 60 °C to attain maximum adsorption (Olejnik, *et al.*, 1970). The resultant suspension was washed with excess isopropyl alcohol and dried at 60 °C in an oven. This was repeated two times over the period of study to yield 1 kg. The powdered product obtained was labeled clay-CTAB 2.

Similarly, in the second ratio, 2.0 L deionized water was added to 0.5 kg clay-DMSO. This was mixed with 2.0 L CTAB and stirred for 24 hour at 60 ºC. The resultant suspension was washed with excess isopropyl alcohol and dried at 60 °C in a vacuum oven. Each ratio was repeated two times over period of study to yield 1 kg. The powdered product obtained was labeled clay-CTAB 1.

Exactly 200.0 g of clay-CTAB1 was weighed and dispersed into a 4.0 L of methanol solution then stirred for 5 days at room temperature. After 5 days of continuous stirring the suspension was left to mature for 3 days. It was washed with excess isopropyl alcohol, dried at 60 °C in a vacuum oven and named MOC 1. This was repeated two times during the course of study to yield 400 g MOC1.

Similarly 200.0 g of clay-CTAB2 was weighed and dispersed into 4.0 L of methanol solution and stirred for 5 days at room temperature. After 5 days of continuous stirring the suspension was left to mature for 3 days. It was then washed with isopropanol. The washed organoclay was dried at 60 °C in a vacuum oven and named MOC2. The procedure was repeated four times to yield 800.0 g MOC2.

3.5.4 Slow Release Fertilizers; SRF 1 and SRF 2.

Exactly 80.0 g of commercial Baraka N.P.K fertilizer was mixed with 3.0 L methanol in a 4.5 L aluminium jug and stirred at 60 °C for 5 days. The mixture was mixed with excess isopropanol to wash excess solvent. This mixture was stirred at 60 °C until it formed a thick suspension. The suspension was dried in an oven until it solidified. This procedure was repeated thirteen times during the period of study to yield 1040.0 g of the modified NPK.

Exactly 240.0 g of MOC 1 was mixed with 240.0 g of powdered modified NPK and each dispersed into a 3.6 L of methanol solvent in a 4.5 L aluminium jug. The mixtures were stirred for 8 hours in a day for 15 days at 40 °C. After 15 days of stirring, excess isopropanol was used to wash the intercalated compound obtained in order to remove unreacted matter and organic impurities. The new NPK fertilizers produced were dried at 40 °C in a vacuum oven yielding 480 g SRF1.

Exactly 480.0 g of the formed SRF1 was crushed and mixed with 100 mL methanol to form a paste. The SRF1 paste was rolled into twenty 10.0 g spheres, twenty 4.0 g spheres, twenty 2.0 g spheres and twenty 1.0 g spheres.

Exactly 240.0 g of MOC 2 was mixed with 240.0 g of powdered modified NPK and each dispersed into a 3.6 L of methanol solvent in a 4.5 L aluminium jug. The mixtures were stirred for 8 hours in a day for 15 days at 40 °C. After 15 days of stirring, excess isopropanol was used to wash the intercalated compound obtained in order to remove unreacted matter and organic impurities. The new NPK fertilizers produced were dried at 40 °C in a vacuum oven labeled SRF2. The procedure was repeated two times to yield 960.0 g SRF2. Exactly 900.0 g of the formed SRF2 was crushed and mixed with 400.0 mL methanol to form a paste. The SRF2 paste was rolled into fifty 10.0 g spheres, fifty 4.0 g spheres, fifty 2.0 g spheres and twenty 1.0 g spheres.

3.5.5 Coated slow Release Fertilizers

3.5.5.1 CRF 1

Five 10.0 g and five 4.0 g dry spheres of SRF1 were dropped into 200 mL of starch-PVA jelly in a 1000 mL glass beaker and slowly stirred at 40 °C for 8 hours until the jelly solidified on the SRF1. The SRF1 coated with starch-PVA was labeled CRF1. The CRF1 was left in the beaker for 3 days for it to solidify into thick jelly. The products were dried in an oven at 40 °C for 2 days.

3.5.5.2 CRF2

Similarly, five 10.0 g and five 4.0 g dry spheres of SRF1 were dropped into 200.0 mL of starch-GA jelly in a 1000 mL glass beaker and slowly stirred at 40 °C for 8 hours until the jelly solidified on the SRF1. The SRF1 coated with starch-GA was labeled

CRF2. The CRF2 spheres were left in the beaker for 3 days for it to solidify into thick jelly. The products were dried in an oven at 40 °C for 2 days.

3.5.5.3 CRF 3

Fifteen 10.0 g, fifteen 4.0 g and ten 1.0 g dry spheres of SRF2 were dropped into 200.0 mL of starch-PVA jelly in a 1000 mL glass beaker and slowly stirred at 40 °C for 8 hours until the jelly solidified on the SRF2. The SRF2 coated with starch-PVA was labeled CRF3. The CRF3 was left in the beaker for 3 days for it to solidify into thick jelly. The products were dried in an oven at 40 °C for 2 days.

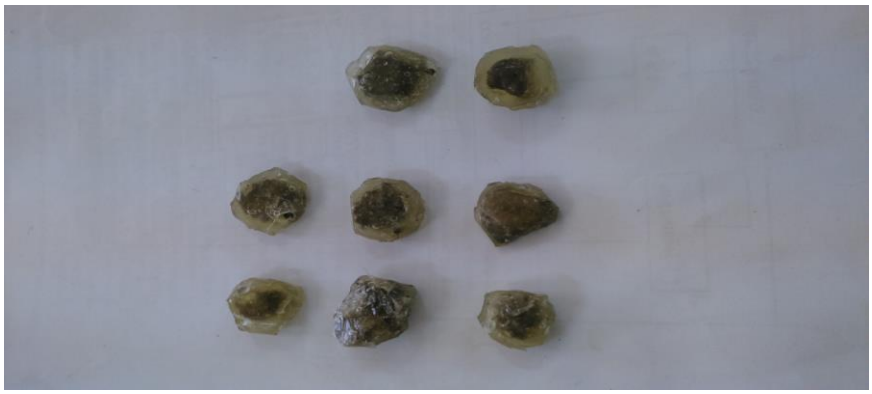

Plate 3. 1: CRF3 pieces

3.5.5.4 CRF4

Fifteen 10.0 g, fifteen 4.0 g and ten 2.0 g dry spheres of SRF2 were dropped into 200 mL of starch-GA jelly in a 1000 mL glass beaker and slowly stirred at 40 °C for 8 hours until the jelly solidified on the SRF2. The SRF2 coated with starch-GA was labeled CRF4. The CRF3 was left in the beaker for 3 days for it to solidify into thick jelly. The products were dried in an oven at 40 °C for 2 days.

Plate 3. 2: CRF4 pieces

3.6 Physicochemical nature of clays and formed formulas

3.6.1 Characterization of raw clay samples

The white and black clay soil were characterized by; XRD for mineralogy and crystallinity, FTIR for determination of functional groups, EDX and XRF for approximation of elemental composition, SEM and TEM determine the morphology, TGA for analysis temperature gradient and BET for particle size analysis.

3.6.2 Characterization of sodium modified clay sample

The sodium beneficiated clay sample, NaDp was crushed and characterized by; XRD, EDX, XRF, FTIR, TGA and BET.

3.6.3 Characterization of organonanoclay; MOC1 and MOC2

Both MOC1 and MOC2 were characterized by; XRD, EDX, FTIR, XRF and BET.

3.6.4 Characterization of Slow Release Fertilizers

Both SRF1 and SRF2 were characterized by; FTIR, XRD, XRF, BET and EDX.

3.6.5 Characterization of starch

The sample was characterized by; FTIR, XRD, TGA and SEM.

3.6.6 Characterization of PVA

This sample was characterized by; FTIR, XRD, TGA and SEM.

3.6.7 Characterization of starch-PVA

The sample was characterized by FTIR.

3.6.8 Characterization of NPK

NPK was characterized by; FTIR, EDX and XRF.

3.6.9 Rate of nutrient dissolution in water

The N, P and K nutrient release analysis was done by using the modified methodology of (Ramos Campos *et al.,* 2015) on water solutions.

3.6.9.1 Release from 50-50 formulas

Exactly 2.0 g of NPK was added into the first one, 4.0 g of SRF1, 4.0 g CRF1 and 4.0 g CRF2 were dropped into the remaining three 1 L beakers. Exactly 1.0 L of deionized water was poured into each of the four beakers and stirred mechanically for 2 minutes. After 24 hours, 20.0 mL solution was pipetted from each beaker and transferred into a 20 mL plastic bottle. The remaining solution in each beaker was thoroughly stirred and kept over another 24 hours. This procedure was repeated for 30 days.

3.6.9.2 Dissolution of 70-30 formulas

Exactly 2.0 g of NPK was added into the first one, 4.0 g of SRF2, 4.0 g CRF3 and 4.0 g CRF4 were dropped into the remaining three 1 L beakers. Exactly 1.0 L of deionized water was poured into each of the four beakers and stirred mechanically for 2 minutes. After 24 hours, 20.0 mL solution was pipetted from each beaker and transferred into a 20 mL plastic bottle. The remaining solution in each beaker was thoroughly stirred and kept over another 24 hours. This procedure was repeated for 30 days.

3.6.10 Spectroscopic analysis

The concentrations of N, P and K were determined and compared on CEN (Comite European de Normalization) standards (Farida *et al.*, 2014). The standard for CRFs is dissolution in deionized water of less than 15 % after 24 hours and 75 % after 30 days (Farida *et al.*, 2014).

3.6.10.1 Testing of phosphorus 50-50

Potassium dihydrogen phosphate of analytical grade was opened and placed into an oven set at 80 °C for one hour to remove all moisture. The phosphorus standard was prepared by dissolving 1.403 g KH_2PO_4 in 1.0 L of distilled water in a 1L volumetric flask to make a 1000 ppm $H_2PO_4^{-1}$ solution. This solution was diluted into 20 ppm, 15 ppm, 12 ppm, 10 ppm, 8 ppm, 6 ppm, 4 ppm, 2 ppm and 1 ppm. The 6 ppm solution was put into the cuvette and inserted into the machine to set the wavelength. The wavelengths were read to establish the maxima.

A combined reagent was prepared to color the samples for the UV-VIS spectrophotomer's reading during the phosphorus analysis. A ration of 50 mL 2.5 M sulphuric acid was transferred into a plastic beaker, 15.0 mL of ammonium molybdate solution was added, 30.0 mL ascorbic acid solution was then added with mixing. Lastly 5.0 mL of potassium antimony tartrate was added and thoroughly mixed. 2.0 mL of this combined solution was added into the samples and left for 2 minutes for a light blue colour to form. The blue coloured phosphorus sample was filled into the cuvette, inserted into the UV-VIS spectrophotometer and read at 450 nm. Care was taken to ensure the samples were at the same light blue colour. These blue solutions were read at 450 nm

3.6.10.2 Testing of potassium 50-50

The potassium standard was made by dissolving 1.912 g of potassium chloride into 1.0 L distilled water in a 1L volumetric flask to make a 1000 ppm K^+ standard solution. This solution was diluted into 20 ppm, 15 ppm, 12 ppm, 10 ppm, 8 ppm, 6 ppm, 4 ppm, 2 ppm and 1 ppm. The 6 ppm solution was put in the cuvette and inserted into the machine. The wavelengths were read to establish the maxima.

A combined reagent was prepared to color the samples for the UV-VIS spectrophotomer's reading during the potassium analysis. The combined solution that was used in reading of phosphorus was also used in reading of potassium. Care was taken to ensure the samples were at the same light blue color.

3.6.10.3 Testing of nitrate 50-50.

The nitrate standard was prepared by dissolving 1.629 g potassium nitrate into 1.0 L distilled water to form a 1000 ppm solution. This solution was diluted into 20 ppm, 15 ppm, 12 ppm, 10 ppm, 8 ppm, 6 ppm, 4 ppm, 2 ppm and 1ppm. The 6 ppm solution was put in the cuvette and inserted into the machine. The wavelengths were read to determine the UV maxima which was at 518 nm.

A combined solution was prepared to give the solution a yellow colour. Exactly 0.5 mL of the sample was put into a 50.0 mL conical flask. One mL 1.0 mL of a 5 % salicyclic acid was mixed with this solution and kept for 20 minutes. 5.0 mL portion of 4 M sodium hydroxide was added and mixed to form a yellow color. The samples were read at 518 nm.

This combined solution was prepared by dissolving 160.0 g oven dried sodium hydroxide pellets into 1.0 L distilled water in a 1L volumetric flask and the 5 % salicyclic acid was prepared by dissolving 5.0 g oven dried salicyclic acid into 95 mL of 2.5M sulphuric acid. Exactly 5.0 mL of distilled water was added. This solution was kept for 2 days. The yellow samples were read at 518 nm.

3.6.10.4 Testing of phosphorus 70-30

Potassium dihydrogen phosphate of analytical grade were opened and placed in an oven set at 80 °C for one hour to remove all moisture. As in the 50-50 sample the phosphorus standard was prepared by dissolving 1.403 g KH_2PO_4 in 1.0 L of distilled water in a 1.0 L volumetric flask to make a 1000 ppm $H_2PO_4^-$ solution. This solution was diluted into 20ppm, 15 ppm, 12 ppm, 10 ppm, 8 ppm, 6 ppm, 4 ppm, 2 ppm and 1ppm. The 6 ppm solution was put in the cuvette and inserted into the machine. The wavelengths were read to determine the maxima. These solutions were read at 450 nm.

A combined reagent for the blue clour was prepared as in section *3.6.10.1.* The blue coloured phosphorus sample was filled into the cuvette, inserted into the uv-vis spectrophotometer and read at 450 nm. Care was taken to ensure the samples were at the same light blue color.

3.6.10.5 Testing of potassium 70-30

The potassium standard was made by dissolving 1.912 g of potassium chloride into 1000 mL distilled water in a 1.0 L volumetric flask to make a 1000 ppm K^+ standard solution. This solution was diluted into 20ppm, 15 ppm, 12 ppm, 10 ppm, 8 ppm, 6 ppm, 4 ppm, 2 ppm and 1ppm. The 6 ppm solution was put in the cuvette and inserted

into the machine. The wavelengths were read to determine the maxima. These solutions were read at 450 nm. A combined reagent was prepared as in section 3.6.10.4. Care was again taken to ensure the samples were at the same light blue color.

3.6.10.6 Testing of nitrate 70-30

The nitrate standard was prepared by dissolving 1.629 g potassium nitrate into 1.0 L distilled water to form a 1000 ppm solution. This solution was diluted into 20ppm, 15 ppm, 12 ppm, 10 ppm, 8 ppm, 6 ppm, 4 ppm, 2 ppm and 1ppm. The 6 ppm solution was put in the cuvette and inserted into the machine. The wavelengths were read to find the maxima. These solutions were read at 518 nm. The colouring combined solution was prepared as in section 3.6.10.3.

3.6.11 Controlled optimization of maize plants

After studying the release characteristics of the three formed products, it was necessary to study their nutrients absorption ability in soils. This was done in a greenhouse of 4 meters by 2.5 meters with a slanting roof from the door side. The door side was 3 meters high while the backside was 1.5 meters high. A greenhouse was used so as to control most of the conditions required for the maize plant. The conditions to be controlled were pests, adverse factors like wind, excess water from rain, hailstones and farm animals that are housed at the same farm space. The controlling of the conditions was necessitated by the fact that little study has been recorded on this front. The planting tins were of varying capacities as shown on Table 3.1

Table 3. 1: Mass in grams of soil packed in planting tins

Sample	FP	NPK	SRF2	CRF3	CRF4

treatment					
1	518	679	510	304.5	571
2	513	215	801	567	521
3	500	460	506	523	523
4	510	723	769	612	723
5	495	789	820	770	796
6	843	818	832	899	787
7	849	830	800	883	887

The tins were packed with sieved ground loose red loamy soils in the masses shown. All the tins were planted with pioneer maize crop on 2.5.2019. The order from 1 to 7 represented the order in which the tins would be removed for analysis. The first tin was removed after 2 weeks, 2^{nd}, 3^{rd}, 4^{th}, 5^{th}, 6^{th} and 7^{th} were removed after 4, 6, 8, 10, 12 and 14 weeks respectively. The first column on the right from the door was treatment 1 representing maize crop planted without a fertilizer, the second column referred to as treatment 2 was planted with 14.0 g of NPK, the third column had a treatment of 28.0 g SRF2, the fourth column's treatment was 28.0 g CRF3 and the last treatment 5 had 28.0 g CRF4. The tins were arranged in the greenhouse in an ascending order of the sample numbers, that is the tins for sample number one were put where the greenhouse height was shortest while the ones in sample number 7 were arranged where the greenhouse had the highest height.

Plate 3. 3: 3 Greenhouse for planting maize

The greenhouse was constructed slanting uniformly to one side as seen on plate 3.3. A wire mesh door was put in front of the greenhouse to allow sufficient circulation of air. The open mesh wire door reduced maximum temperatures in the greenhouse during daytime to 35-45 ^{o}C. Research showed that increase in temperature up to 55 ^{o}C farvoured release rate of N from 4-6 days, with a similar trend for P and K (Ding *et al.*, 2016). This finding was corroborated one by (Morgan *et al.,* 2009).

Maize seeds were planted into tins that had been filled with prepared red loamy planting soils. The crop was watered to fill the tin every 3 days this was to avoid drying of the crop since the greenhouse temperatures peaked at 50 °C. In the research of (Ding *et al.,* 2016), higher moisture content of above 45 % had less benefit to controlled nutrient release over a long period. The tins were watered periodically to minimize the percentage water content in the tins.

Plate 3. 4: Spacing of planting tins

The tins were arranged at equidistance from each other towards the entrance as seen in picture 3.4. This was to ensure that the crops being removed from the greenhouse had a similar height from the roof since with controlled conditions the growth rate was expected to be equal as seen from plate 3.5. (Jeffrey & Sinclair, 1998) noted that the size of the planting pot did not affect the transpiration from the soil water. Transpiration was affected by the soil drying until about one third of the available water remained in the pot which then transpires linearly until all the water is exhausted (Jeffrey & Sinclair, 1998). This means the size of the pots did not affect the transpiration of the water from the pots by their size (Tong *et al.*, 2018). The NPK was ringed 2 cm from the planted pioneer PHB 30g19 seed in the tins (Mirjana *et al.*, 2012) while the SRF spherical formulas were put 2 cm from the maize seed and 5 cm under the soil level from the seed for all the tins.

Plate 3. 5: Maize at 7 weeks

The picture on plate 3.5 shows maize crop at 7 weeks. The row along the polythene paper at the far end is the crop that shall be removed at week eight for analysis.

3.6.12 Analysis of nutrients in the greenhouse soil samples

3.6.12.1: Testing of phosphorus greenhouse crop soil samples

Potassium dihydrogen phosphate of analytical grade were opened and placed in an oven set at 80 °C for one hour to remove all moisture. The phosphorus standard was prepared by dissolving 1.403 g KH_2PO_4 in 1.0 L of distilled water in a 1.0 L volumetric flask to make a 1000 ppm $H_2PO_4^-$ solution. This solution was diluted into 20ppm, 15 ppm, 12 ppm, 10 ppm, 8 ppm, 6 ppm, 4 ppm, 2 ppm and 1ppm. The 6 ppm solution was put in the cuvette and inserted into the machine. The wavelengths were read to find the maxima. The blue solutions were read at 450 nm.

A combined reagent was prepared as in section *3.6.10.1*. The blue coloured phosphorus sample was filled into the cuvette, inserted into the UV-VIS spectrophotometer and read at 450 nm. Care was taken to ensure the samples were at the same light blue color.

3.6.12.2: Testing of potassium in greenhouse crop soil samples

The potassium standard was made by dissolving 3.490 g of potassium dihydrogen phosphate into 1.0 L distilled water in a 1.0 L volumetric flask to make a 1000 ppm K^+ standard solution. This solution was diluted into 20 ppm, 15 ppm, 12 ppm, 10 ppm, 8 ppm, 6 ppm, 4 ppm, 2 ppm and 1 ppm. The 6 ppm solution was put in the cuvette and inserted into the machine. The wavelengths were read to establish the maxima. These solutions were read at 450 nm.

A combined reagent was prepared as in section 3.6.10.1. The blue coloured phosphorus sample was filled into the cuvette, inserted into the UV-VIS spectrophotometer and read at 450 nm. Care was taken to ensure the samples were at the same light blue color.

3.6.12.3: Testing of nitrate in greenhouse crop soil samples

The nitrate standard was prepared by dissolving 1.629 g potassium nitrate into 1000 mL distilled water to form a 1000 ppm solution. This solution was diluted into 20ppm, 15 ppm, 12 ppm, 10 ppm, 8 ppm, 6 ppm, 4 ppm, 2 ppm and 1 ppm. The 6 ppm solution was put in the cuvette and inserted into the machine. The wavelengths were read to find the maxima. These solutions were read at 518 nm to calibrate the UV-VIS spectrophotometer. A combined colouring solution was prepared as in section 3.6.10.3.

3.6.13 Water absorbency of starch-PVA

Water absorbency was determined by gravimetric method (Cun-dian *et al.,* 2014) in which three pieces of starch-PVA films each weighing 2.0 g were cut and each was put into dry clean tea bag. They were lowered into a 250 mL glass beaker containing 100.0 mL tap water. Three tea bags were removed after intervals of I hour and weighed. This

was repeated until there was no change in mass. The water absorbency was calculated from equation 3b below.

$W_A=\frac{M_1-M_0}{M_0}$ …… equation 3b, where M_1 is mass of the starch-PVA at time t and M_0 initial mass of the starch-PVA which was 2.0 g.

3.6.14 Water absorbency of starch-Gum arabic

Three pieces of starch-GA films each weighing 2.0 g were cut and each of them put into dry clean tea bag. They were lowered into a 250 mL glass beaker containing 100.0 mL tap water. Three tea bags were removed after intervals of I hour and weighed. This was repeated until there was no change in mass. The water absorbency determined by gravimetric method as in research of (Cun-dian *et al.,* 2014) was calculated from equation 3b below (Ghazali *et al.,* 2017).

$W_A=\frac{M_1-M_0}{M_0}$ …….. equation 3b, where M_1 is mass of the S-GA at time t and M_0 initial mass of the starch-Gum acacia which was 2g.

3.6.15 Kinetic diffusivity of starch-Gum acacia

Two pieces of starch- Gum acacia films weighing 2.0 g were weighed. Each of the pieces was put into a dry clean tea bag. They were lowered into a 250 mL glass beaker containing 100.0 mL tap water. The tea bags with starch-gum acacia were removed and their masses taken at intervals of 5 minutes until there was no change in mass of the pieces. The readings were taken up to 120 minutes. The diffusivity was calculated from the formula below (Ghazali *et al.,* 2017).

$F=\frac{M_t}{M}=kt^n$…….. equation 3c

where M_t= amount of solvent diffused into the SAP at t and M=amount of solvent diffused at equilibrium, that is until there is at change in mass.

3.6.16 Kinetic diffusivity of starch-PVA

Two pieces of starch- PVA films weighing 2.0 g were put into a dry clean tea bag. They were lowered into a 250 mL glass beaker having 100.0 mL tap water. The tea bags with starch-PVA were removed and their masses taken at intervals of 5 minutes until there was no change in mass of the pieces. The readings were taken up to 340 minutes. The diffusivity was calculated from the equation 3c.

3.6.17 Water retention of SRF, CRF3 and CRF4

Exactly 2.0 g SRF was mixed with 200.0 g of uniformly ground red loamy soil that was used in the greenhouse and put into a 250 mL glass beaker. Accurately measured 100.0 mL of tap water was added slowly to avoid loss of any of the powdered soil. The glass beaker was covered with polythene paper and weighed, W_1. Similarly 2.0 g coated fertilizers, CRF3 and CRF4 were put into 250 mL glass beakers 2 and 3 respectively with red loamy soil used in the greenhouse. Again 100.0 mL of tap water was slowly added in each of the beakers and then covered with polythene paper. The beakers were weighed, W after every 2 days for 31 days. The water retention of the product was calculated from the equation 3d (Ghazali *et al.,* 2017).

$$WR = \frac{W}{W1} x100\% \quad \text{..... equation 3d}$$

CHAPTER FOUR

RESULTS AND DISCUSSION

4.0 Introduction

The results will be discussed in chronological order of the objectives. The discussion starts with the physical constants of the soil materials used in the study including the soil that was used in the process of maize optimization.

4.1. Physical constants of samples

The loamy red soil collected from Masinde Muliro University of Science and Technology farm and the dry sieved clay soils were analyzed for their physical constants. This analysis was conducted at Kalro Laboratories in Nairobi and the constants are given on Table 4.1.

Table 4. 1: Physical constants of used soil samples

Property	Black clay	White clay	Red Loamy Soil
Ph	5.30	6.50	7.10
Elect.cond. mS/cm	0.13	0.06	0.63
Total organic C%	2.85	0.41	3.42
Sand %	48.00	44.00	64.00
Silt %	22.00	28.00	8.00
Clay %	28.00	30.00	28.00
CEC me %	20.20	8.00	19.60
Ca me %	16.80	1.00	29.40
Mg me %	2.70	0.20	4.50
K me %	0.20	1.60	2.80
Na %	0.70	0.50	0.60
P /ppm	20.0	5.00	22.30
N%	0.25	0.06	0.28
Fe/ ppm	387	34	69.5

Soil particle size was done by use of the pipette method with sodium hexametaphosphate as the dispersing agent. The black soil pH was done in water while

the white and red loamy soils were done in lime solutions. Calcium and Magnesium were determined by AAS. The results of the tests mentioned above compared well with those of (Puge *et al.,* 1982).

Soil available phosphorus was done by Bray II method. Soil organic content was done by loss on ignition. Total nitrogen was determined by Kjeldahl digestion. Potassium and sodium were determined by flame photometry. The above methods were also used in determination of these physical constants in the (Nsosong *et al.,* 2019) with similar results. The carbon concentration is determined on a spectrophotometer at 600nm with similar results to research by Anderson and Ingram (Anderson & Ingram, 1993).

Comparison of the organic carbon, pH values, total N content and the mehlich P of the samples shown on Table 4.1 show that the white imported soil is more beneficiated than the local black soil that was sieved on 75µm.

The CEC for black soil is the largest which means this soil would pick cations from a solution medium around it and exchange with the cations in the interlayer distances. Considering that the black and white soils will be used to store K^+, then this black soil will more readily desorb the K^+ with other cations in the red planting soil than the white one. On this account the black soil will be preferred to the white soil as the clay for modification. On the other hand the red planting soil shows a CEC, 19.6 which is high enough to sustain absorption of plant nutrient like K^+, Ca^{2+} and $Mg^{2+}$from the fertilizer material.

The amounts of P and N in the black and red soils are comparable at 20 ppm, 0.25 % and 22.5 ppm, 0.28 % respectively and significantly different from the white soil at

5ppm, 0.06 %. This could mean that the white clay soil is concentrated into a mineral when the black one is still raw clay form.

The soils that were used to plant the maize crop had significantly different chemical properties to a similar maize research in Trans Nzoia whose soil had pH 5.1, N content 0.17 %, P content 8.1 ppm and K^+ content 0.09% (Owino, 2010).

4.2 Spectroscopic characterization

Clays are very heterogeneous materials whose characteristics depend on their geological formation as well as the extraction location (AlvarezAcevedo *et al.*, 2017). The raw materials and products were characterized as follows;

4.2.1. Energy Dispersive X-ray spectroscopy (EDX)

The materials tested were BC, WC, MOC2, NPK and SRF2 and their mean elemental percentages displayed as oxides are shown on Table 4.2.

Table 4. 2: Elemental composition of materials using EDX

% Elements	BC±SE	WC±SE	MOC2±SE	NPK±SE	SRF2±SE
SiO_2	46.26±0.21	24.23±0.11	24.55±0.13	0.00	15.41±0.14
Al_2O_3	29.78±0.65	37.23±0.56	38.63±0.58	0.00	0.00
Fe_2O_3	8.19±0.11	0.42±0.01	1.83±0.01	1.34±0.01	5.72±0.03
K_2O	13.72±0.01	35.93±0.07	32.49±0.07	38.49±0.01	45.60±0.12
P_2O_5	0.00	0.00	0.00	41.65±0.15	21.34±0.14
CaO	0.73±0.01	0.00	0.00	16.69±0.03	8.39±0.03
TiO_2	1.19±0.02	1.90±0.02	1.86±0.02	0.00	1.91±0.03
SO_3	0.07±0.00	0.00±0.00	0.32±0.00	1.19±0.01	0.79±0.01
ZrO_2	0.00	0.04±0.00	0.00	0.00	0.08±0.00
Rb_2O	0.03±0.00	0.06±0.00	0.06±0.00	0.00	0.06±0.00
SrO	0.04±0.00	0.00	0.00	0.126±0.00	0.09±0.00
Br	0.00	0.00	0.10±0.00	0.033±0.00	0.15±0.00

Key: n = 3, BC=Ilesi black, WC= white clay, MOC2= modified organoclay 2, NPK= fertilizer, SRF2= slow release fertilizer.

Table 4.2 compares the raw clays, the modified organoclay and formed slow release fertilizer. The silica percentage in black clay is higher than in white clay because of its beneficiation. The major components in the two clay samples were SiO_2, Al_2O_3, K_2O and Fe_2O_3 as also observed in (Maxim *et al.,* 2019). The SiO_2 composition in both white and black clays ranged between 24 % and 47 %, Al_2O_3, 29 % and 38 %, K_2O ranged between 13-36 % and lastly Fe_2O_3, 0.416 % and 8.1 %. Both samples have appreciable percentage of TiO_2 of between 1.2 and 1.9 %. This data is similar to research on chemical composition of different clays and pure kaolin in Saudi Arabia (Mohsen & El-Maghraly, 2010), common clays of Yola Bentoni in Nigeria (James *et al.,* 2008) and Adiabo clays in Nigeria (Abuh *et al.,* 2004), clays in Odupani in South eastern Nigeria (Osabar *et al.,* 2009), kaolinitic clays from Mukurwe-ini-kenya (Andala & Wachira, 2015) and natural clays from Brazilian southeast region (Alvarez Acevedo *et al,* 2017).

Whereas the percentages of SiO_2, Al_2O_3, K_2O, TiO_2 and Fe_2O_3 in MOC2 did not change significantly, the percent sulphur increased from 0.07 % to 0.32 %. The MOC2 sample also has bromine which due to presence of the CTAB pillaring molecules which again is proof of intercalation of the clay layers but also an indication that the isopropyl alcohol did not remove all the organics.

4.2.1 X-ray fluorescent spectroscopy (XRF)

Whereas the EDX reads the silicon it excites from the phyllosilicate, XRF will see and measure the SiO_2 as sand that was present in the sample hence recording larger percentages for SiO_2. These percentages are determined as oxides as shown in the Table 4.3

Table 4. 3: Elemental composition of samples using XRF

% Element	BC±SE	WC±SE	NaDp±SE	Clay-DMSO±SE	MOC2±SE	SRF2±SE
SiO_2	72.7±0.01	44.7±0.01	69.2±0.34	64.9±0.00	50.4±0.01	32.1±0.01
Al_2O_3	19.9±0.01	40.0±0.01	22.9±0.01	30.3±0.01	35.8±0.02	18.1±0.01
Fe_2O_3	2.6±0.02	0.2±0.01	3.0±0.01	1.7±0.09	0.7±0.02	1.3±0.01
K_2O	2.8±0.01	9.3±0.01	3.1±0.01	6.2±0.00	8.0±0.01	9.1±0.02
P_2O_5	0.0±0.00	0.0±0.00	0.0±0.00	0.0±0.00	0.1±0.00	22.1±0.01
CaO	0.7±0.02	0.3±0.01	0.6±0.01	0.4±0.01	0.3±0.01	5.7±0.02
TiO_2	0.6±0.01	0.8±0.00	0.7±0.0.01	0.7±0.28	0.8±0.00	0.8±0.03
SO_3	0.1±0.01	0.0±0.00	0.2±0.01	4.9±0.00	2.7±0.01	6.0±0.01
BaO	0.1±0.00	0.0±0.00	0.1±0.00	0.0±0.00	0.0±0.00	0.0±0.00
Cl_2O	0.0±0.00	0.1±0.00	0.5±0.00	0.2±0.01	0.2±0.01	4.3±0.11
MgO	0.0±0.00	2.5±0.00	0.0±0.00	0.0±0.00	0.0±0.00	0.0±0.00

Key: n = 3, BL= black clay, WC= white clay, NaDp= Na modified clay, DMSO= DMSO pillared organoclay, MOC2= CTAB modified organoclay and SRF2= slow release fertilizer.

The major compositions in black and white clay on Table 4.3 are silicon, aluminium, potassium, iron, calcium while titanium, sulphur and chlorine are in small percentages. It is evident from the table that BL and WC picked other substances to form NaDp, clay-DMSO and MOC2. A spike in the composition of sulphur in clay-DMSO indicates the introduction of the DMSO in the interlayers of the clay minerals this is because some of the DMSO molecules were not replaced by CTAB and removed from the interlayers by the isopropyl alcohol. The percentage of potassium, phosphorus, calcium, chlorine increased in SRF2 due to NPK that was dispersed into the organoclay nanocomposite. This XRF result collaborate the data that was collected by EDX. In both cases sodium and nitrogen do not show since they are out of range for both instruments. It is also worth noting that the data of SRF2 in XRF shows presence of aluminium unlike in the case of the EDX which missed it probably due to the high

lattice energy that the EDX, X-ray could not break. These results compare well with the work on XRF analysis of Maghnia clays by (Khelifa *et al.,* 2018).

4.2.2 FTIR data

The raw clays were characterized on FTIR to establish the functional groups in the raw clays and consequently establish if the materials had clay minerals for intercalation. Figure 4.1 is the IR spectrum of black clay and white clay.

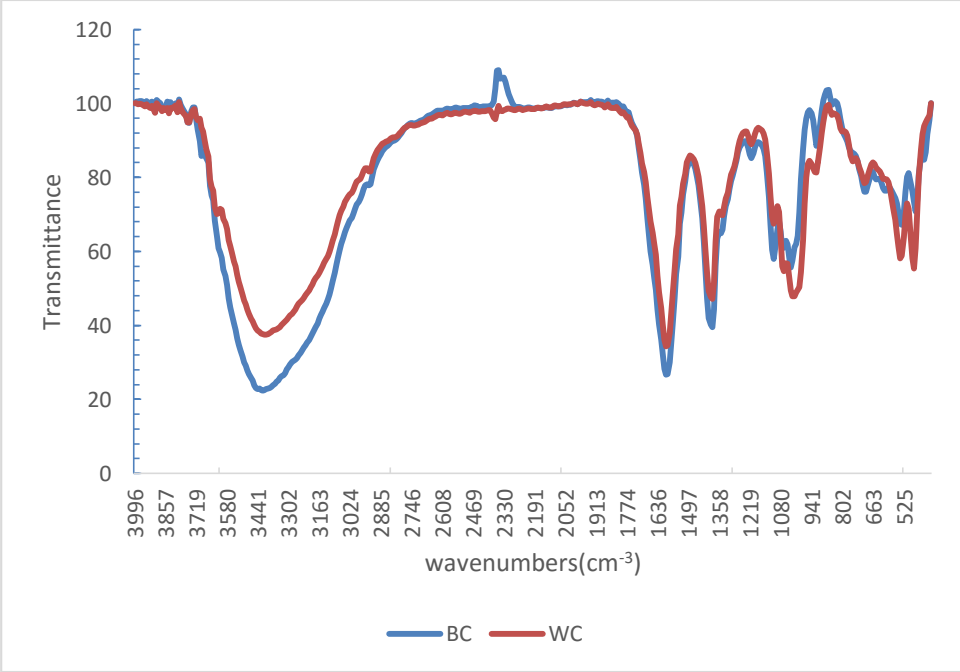

Figure 4. 1: FTIR spectrum for black and white clay

The spectra of black and white clay are similar with five major peaks. The two peaks between 450 and 500 cm^{-1} have shoulders and are usually assigns stretching vibrations for Si-O-Al, Si-O and Fe-O as in (Mohan & Lakhwant, 2016). The shoulders are due to

SiO_2 impurities which affect the stretching vibrations of Si-O affecting these major peaks. The broad bands on Figure 4.1 at between 3600 cm^{-1} and 3000 cm^{-1} correspond to typical OH stretching on Al-OH. (Bhaskar & Gopalakrishnarao, 2010) theoretically placed these OH stretching on Al-OH bands at 3697 cm^{-1}, 3669 cm^{-1} and 3645 cm^{-1} in his research. The small peak at 3632 cm^{-1} in the figure could be O-H stretching involving the inner OH in the gibbsite sheet as it compares with the expected 3620 cm^{-1} which is associated with Al-O-H stretching

The peaks in the fingerprint at 1016 cm^{-1} and 1024 cm^{-1} can be assigned to Si-O and Al-O-H bending respectively. The absorption peaks at between 949 cm^{-1} and 932 cm^{-1} could be assigned to Al-OH bending while those at 728 cm^{-1} and 798 cm^{-1} can be assigned to Si-O bridging bond in quartz-SiO_2 as they compare closely with 770 cm^{-1} and 750 cm^{-1} in the research of (Aroke *et al.*, 2013). The characteristic 778 cm^{-1}, 695 cm^{-1} and 468 cm^{-1} associated with Si-O stretching are observed in Figures 4.1 for both clays. The bands 728 cm^{-1} and 754 cm^{-1}, 499 cm^{-1} and 478 cm^{-1} confirm presence of silicates as also observed in (Bhaskar & Gopalakrishnarao, 2010).

The peak at 2509 cm^{-1} with its fingerprint at 574 cm^{-1} in Figure 4.1 points to presence of Fe-O stretches in the crystalline impurities as also observed in (Parthasarathy *et al.*, 2001). The two spectra in Figure 4.1 represent the gibbsite and silicate sheets in the samples confirming presence of functional groups of clay minerals. Figure 4.2 shows the spectra of an overlay of the raw clays, modified organoclays and the nanocomposites in order to trace the effect of intercalation.

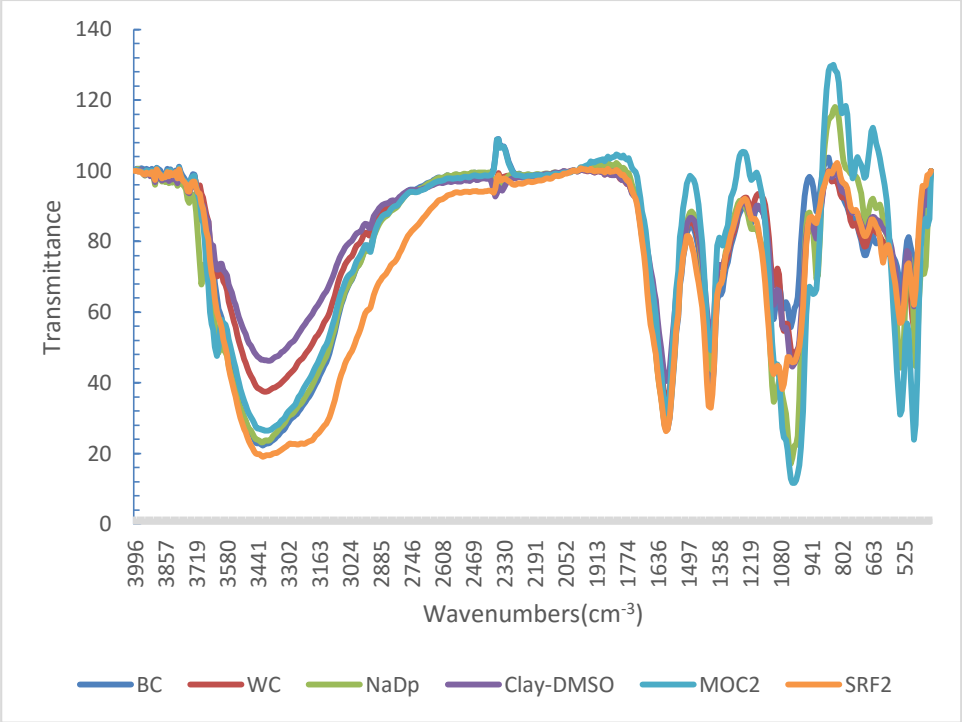

Figure 4. 2: FTIR spectrum for the clays and nanocomposites

Key: BC = black clay, WC= white clay, NaDp = sodium modified clay, clay-DMSO = DMSO modified clay, MOC2 = CTAB modified clay, SRF2 = Slow release fertilizer.

The FTIR spectrum of NaDp is quite similar to the ones of black and white clays. The positions of the peaks have not changed much except for the degree of absorbance. Any distortion of this spectrum from the raw clays could arise from attraction of the Na^+ to O forming Si-O-Na and Fe-O-Na. The peak at 1414 cm^{-1} in Figure 4.2 can be assigned to CO_3^{2-} interacting with Na^+ (Benco *et al.*, 2001). The other peaks remain at the positions as observed in the white and black clays.

The solvent, DMSO, with a formula $(CH_3)_2SO$ is a liquid at room temperature that dissolves both polar and nonpolar compounds hence described as an aprotic solvent. This enables it to dissolve into the interlayer distances of clay minerals easily which is hosting inorganics. It combines with the high population of Na^+ in the gallery forming

short pillars within the interlayers and also introduces a non-polar end of an organic molecule into the gallery.

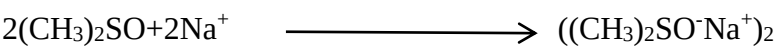

The formed modified organoclay can pick both polar and nonpolar molecules. The distances opened by DMSO are typically small from 0.72 nm to 0.76 nm (Mohd *et al.,* 2014) due to the small size of the molecule unit (Siafu *et al.,* 2015). However the clay structure is now well modified to enable entry of larger surfactants that can pillar the layers at larger distances. The nonpolar part of the CTAB enters the gallery by dissolving its polar end into the polar part of the DMSO as shown below.

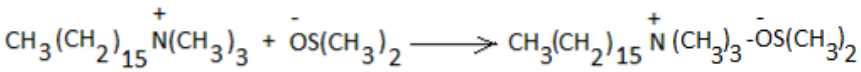

The larger CTAB molecules coalesce into large molecule units developing strong forces of cohesion as opposed to the existence of forces of adhesion. This pushes the smaller DMSO molecules out of the interlayers. When the product is washed with excess isopropyl alcohol the smaller DMSO molecules are washed out.

The spectrum of MOC2 is similar to that of DMSO except for varied absorbance readings. This is expected since the only bond introduced is an N-C replacing the S-C-O that was in the DMSO. These bands of N-C and S-C-O happen to occur at similar band length of 800-784 cm^{-1} for N-C and 840-820 $cm^{-1}$for S=O which makes the two spectra similar.

This CTAB molecule attaches to the aluminate sheet through interaction with OH and to the silicate sheet through an interaction with O.

$CH_3(CH_2)_{15}N^+(CH_3)_3\text{-}O^-S(CH_3)_2 + HO\text{-}Al(OH)_2 \longrightarrow CH_3(CH_2)_{15}N\text{-}O\text{-}Al(OH)_2 + (CH_3)_2SOH$

As discussed earlier the peaks at 3461 cm^{-1}, 3497 cm^{-1} and 3371 cm^{-1} on Figure 4.2 can be assigned to OH stretching of Al-O-H observed also in research of (Mohd *et al.,* 2014). The distortion from the 3600-3500 cm^{-1} of this band could be due to the high coordination from Na^+ introduced into the sample. The interference of this peak by SiO_2 is seen in fingerprint at 959 cm^{-1} and 926 $cm^{-1}$for Si-O and OH respectively. The number of shoulders on the peaks in NaDp at 1096 cm^{-1} to 443 cm^{-1} is high which is an indication of modification of the interlayer by Na^+ which has increased in positive charge. This increase in positive charge polarizes the hydrogen bonds that hold the layers of the sheets together. Figure 4.2 shows peaks between 3498 cm^{-1} and 3295 cm^{-1} which are all associated with the OH stretching on Al-O-H with a fingerprint at 954 cm^{-1} which compares with (Aroke *et al,* 2013).

The peaks at 1636 cm^{-1}, 1074 cm^{-1} and 1096 cm^{-1} can also be assigned to C-O which was introduced into the sample by the methyl groups on clay-DMSO which was also reported by (Csernatoni *et al.,* 2013). The alkyl groups on CTAB repel each other decreasing the crystallinity of the layers in MOC2 and SRF2. The interaction between OH group and SO_3 introduced by DMSO confirms an intercalation of the interlayers. The number of peaks increased tremendously owing to the above interferences.

The DMSO pillars do not hold the entire interlayer due to their small sizes. This makes the structure less crystalline and weak since the layers are held together by weak Van

Der Waals forces in addition to the existing hydrogen bonds. This makes some parts of the sheets to slide over each other.

The spectrum of MOC2 has a peak at 671 cm^{-1} that can be assigned to C-Br in low bond concentrations. The peak at 1436 cm^{-1} represents the C-H stretching arising from the centyltrimethyl group. The peak at 1064 cm^{-1} represents the S=O stretching. The peaks are sharp and distinctive which points to higher crystallinity since the CTAB pillars the layers at single positions.

The SRF2 spectrum has some defined differences from the previous ones. For example the band at 3500-3000 cm^{-1} is broad and neat. The band at 1300-1400 cm^{-1} has larger transmittance. The peak between 950 cm^{-1} and 1000 cm^{-1} has several fingers at the tip and lastly the band at 500-450 cm^{-1} has been distorted up to 800 cm^{-1}. These distortions can only be explained if an introduction of new molecules from NPK into the MOC2 occurred.

This spectrum for SRF2 has marked differences from those of the raw materials as had been discussed before. The transmittance of OH band in SRF2 at 3500-3440 cm^{-1} was the lowest which means it had the highest absorbance. This implies that the product had the highest number of free OH that were introduced by the NPK as NO_3^-, K^+, NH_4^+ and $H_2PO_4^-$. The structure of $H_2PO_4^-$ has two OH units that increases the OH groups. The spectrum also had C-H stretching bands that arose from CTAB that was used to intercalate and traces from DMSO that remained in the formula after washing the SRF2 with propyl alcohol.

Comparing the spectrum of the white clay which was more pure and in larger proportions in the blend as our starting material with the rest, one can trace the effect of modifications on this spectrum. For example the transmittance of the band between 3700 and 3500 cm^{-1}, when modified by Na^+ decreases from a transmittance of 40 to 20 which means a stronger absorbance from the O-H bond which could have been modified into free Na^+ and $O\text{-}H^-$ from the fixed Al-O-H increasing the concentration of free O-H. Secondly the introduction of DMSO generates strong hydrogen bonds with the OH of the octahedral Al on the clay-DMSO mineral molecule causing reduction in the number of free OH units. This in turn reduces absorbance causing an increase in transmittance as seen on the spectrum transmittance from 20 to 50. Introduction of CTAB decreases the transmittance from around 50 to around 23. This could mean that as the DMSO is expelled from the organoclay, the hydrogen bonds are also reduced as the N of the CTAB molecule bonds with the sheets especially to the negatively charged TOT, the oxygen of the OH on the octahedral sheet and the oxygen of the O on the silicate sheet. This increases the free OH in the interlayers increasing the absorbance. The steps below propose the reactions between the CTAB and the aluminate in which free OH is generated that causes the increase in absorbance.

i) 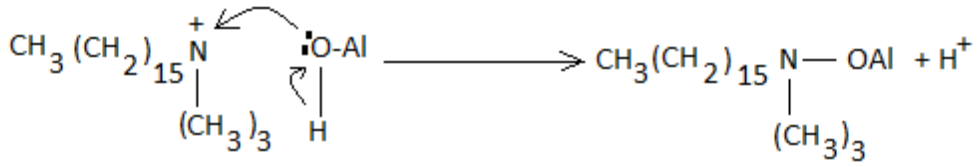

ii) $H^+ + Br^- \longrightarrow HBr$

iii) $Si\text{-}O + HBr \longrightarrow Si\text{-}Br + OH^-$

The transmittance of this band is lowered when NPK is infused into the organoclay to form the SRF2 nanocomposite. This introduction also broadens the band. The introduced NO_3^- combines with water as seen in equation 4w which forms very many free OH units which absorb more IR radiation which reduces transmittance drastically.

$NO_3^- + H_2O \longrightarrow HNO_3 + OH^-$……. Equation 4w

The two bands on SRF2 at 1400-1600cm^{-1} are not affected much by the modifications. However the loops of these two bands show increased transmittance for MOC2. This could be caused by formation of C-Br arising from a substitution of a hydrogen on the methyls attached on N of the CTAB. A drift of the electrons on the N-C bond to quench the N^+ generates a partial positive on the carbon facilitating this substitution of hydrogen. The band at 1100-900 cm^{-1} shows decrease of the transmittance of MOC2 to 10 but when the NPK is dispersed into the MOC2 modified organoclay this transmittance increases tremendously to 60. This could be due to the bonds that are formed between the N^+ on the CTAB and NO_3^- or $H_2PO_4^-$ in the nanocomposite. The band at 450-1000 cm^{-1} is again heavily involved in the modification process in which MOC2 has the biggest variation. There are a lot of distortions to this band arising from the Si-O impurities.

NPK composite fertilizer was dispersed into the MOC to yield SRF. The spectrum of NPK is given on Figure 4.3.

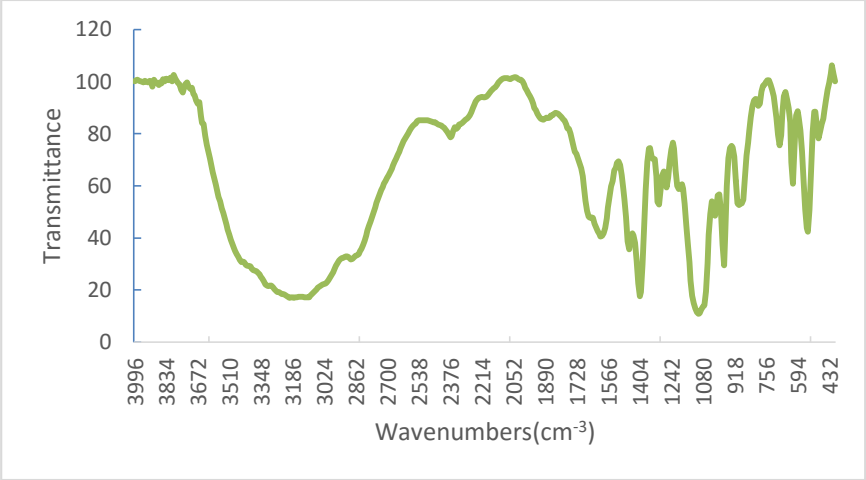

Figure 4. 3: FTIR spectrum for NPK

This spectrum has a number of different features from the one of MOC2. There is a band at 3500-2900 cm^{-1} with a shoulder on the left as opposed to the one in MOC2 at 3600-3200 cm^{-1} with a shoulder on the right. There is a very small band at 2400 cm^{-1} which is a total reverse of what is observed on MOC2 band. Each of the bands at 1600 cm^{-1} and 1400 cm^{-1} has a shoulder on the right, the one at 1100 cm^{-1} has two shoulders on the left, the one at 500 cm^{-1} has three shoulders on the right. In the case of MOC2 each of the bands at 1600 cm^{-1}, 1400 cm^{-1}, 1000 cm^{-1}, 450 cm^{-1} has two shoulders on the right.

A comparison of these two spectra with the spectrum of SRF2 shows that a totally new substance with a broad band at 3000-3600 cm^{-1}, narrow one at 1400 cm^{-1}, one at 1300 cm^{-1}, a narrow one at 1050 cm^{-1} and one at 550 cm^{-1} with two shoulders on right were formed as in (Mahendra *et al.*, 2015) research. This comparison shows that a new nanocomposite crystalline solid formed between NPK and MOC2. This nanocomposite would discharge its nutrients slowly owing to the nature of dissolution from the material. Basically the nutrients are locked into the interlayers by TOT or TO sheets

while the horizontal layers are partially closed by the CTAB pillars and perpendicular crystal units of the clay minerals.

The band at 2300 cm^{-1} on NPK spectrum is assigned to O=P-OH symmetric stretching while the one at 1836.1 cm^{-1} can be asigned to N=O stretching. The NO_3 asymmetrical stretch falls in the range1358-1350 $cm^{-1}$and the band at 972.1 cm^{-1} in the fingerprint could be assigned to C-N-H bending. The band at 3116 cm^{-1} shifted to this lower band from 3494 cm^{-1} due to strong interactions between the OH of Al-O-H and the K^+ from NPK fertilizer. These functional groups assigned compared and matched with the ones assigned by (Mahendra *et al.,* 2015) and (Maxim *et al.,* 2019) during their researches. The variations are caused by the composition of the nutrients and the additives in the NPK.

The peaks on Figure 4.2 show presence of a kaolinite mineral as is supported by the research of (Bhashar & Gopolakrishnarao, 2010), muscovite collaborated by (Marian *et al.,* 2009) lastly illite which is also collaborated by the work of (Pironon *et al.,* 2003)

The bands on Figure 4.2 compare quite well with those of the research done by (Khelifa *et al.,* 2018) on intercalation of raw clays from Maghia in West Algeria in which his band 997-1000 cm^{-1} pointed at stretching vibration of Si-O, 793-795 cm^{-1} bending vibration of Al-O and 510-470 cm^{-1} as stretching vibration of Si-O-Al (Salahuddin *et al.,* 2008). The stretching of an inner Al-OH was observed at 3617-3626 cm^{-1} and the bands at 1617-1524 cm^{-1} and 1366 cm^{-1} represented stretching vibrations of C=N and C-N respectively (Khelifa *et al.,* 2018). The FTIR spectra show that the black, white

materials have clay minerals and that these clay minerals were modified into organoclays.

Whereas FTIR identified the functional groups in the raw materials that would classify them as clays, it also confirmed intercalation by changes in absorbance in the band between 3700-3500 cm^{-1} it however lacked the ability to describe the crystallinity which is fundamental in establishing the availability of interlayers leading this research to study the XRD of the materials.

4.2.3 X-ray diffraction

XRD was used to determine the clay minerals in the raw clays and indicate the modification through a study of the crystallography of the nanocomposites.

4.2.3.1: Mineralogy for black clay

The powder XRF D2 De-phaser instrument generated a diffractogram and a pie-chart of the mineral assemblage with their formulae. Table 4.4 shows the mineral assemblage of the black clay and their chemical formulae.

Table 4. 4: Formulae and mineral percentage in black clay

Mineral	Chemical formula	Mineral percentage
Berlinite	$Al\ PO_4$	15.5
Lazurite	$Al_{8.75}Ca_2Cl_{0.18}K_{0.17}Na_{9.77}S_{2.88}Si_{9.25}\ O_{44.32}$	13.2
Muscovite	$Al_{2.73}Ca_{0.01}Fe_{0.03}K_{0.78}Mg_{0.02}Na_{0.18}Si_{3.15}Ti_{0.02}\ O_{11}$	16.9
Kaolinite	$Al_2Si_2\ O_9$	11.5
Microcline	$Al_{1.03}K_{0.986}Na_{0.014}Si_{2.97}\ O_8$	21.7
Albite	$Al_{0.502}NaSi_{1.497}\ O_4$	14.6
Quartz	SiO_2	6.6

The compound showed a number of crystalline inorganic compounds including microcline and albite which are alkali feldspars. Whereas microcline is a potassium rich

tectosilicate rock with sodium impurities, albite is plagioclase feldspar with sodium alkali. Both feldspars are silicates that decompose over a period of time to form kaolins. This analysis also showed Berlinite and quartz that remained after beneficiation process of the raw clay soil. Lazurite on the other hand is a tectosilicate with sulphur, sulphate and chloride in the formula. The analysis of the minerals showed that the soil had muscovite clay and kaolinite clay at 16.9 % and 11.5 %, with a total clay percentage of 28.4 %. Figure 4.4 shows that if the quartz and alkali feldspars are further removed the clay mineral percentage would improve.

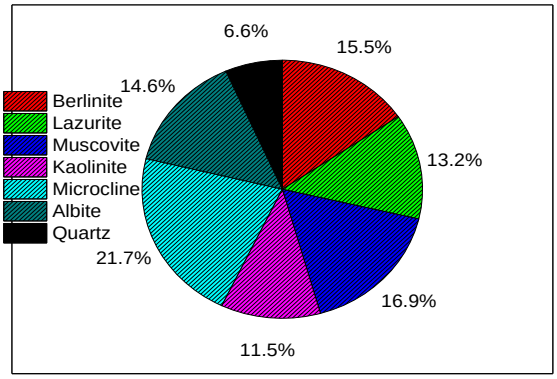

Figure 4. 4: Pie-chart for mineral assemblage in the black clay

Key; The colours; pink, blue = clay minerals.

4.2.3.2: Mineralogy for white clay

The Table 4.5 and Figure 4.10 give the mineral assemblage and instrument generated chemical formula for the white clay sample. This sample identified seven minerals of which microcline and albite are alkali feldspars. The major clay compositions are illite at 55.1% which is a tetrahedral-octahedral- tetrahedral, TOT structure, kaolinite at 5.3% and petalite at 5.9%. The total clay mineral assemblage is 66.3%. Unlike in the black clay this one has a much higher percentage of clay minerals. It is due to this higher

mineral assemblage that the study decided to give the white clay a higher percentage in the blend.

Table 4. 5: Formulae and composition of mineral in white clay

Compound name	Chemical formula	Mineral percentage
Illite	$Al_4K\ Si_2O_{12}$	55.1
Petalite	$A1LiSi_4O_{10}$	5.9
Ulvospinel	$Fe_{2.247}Ti_{0.751}O_4$	4.9
Kaolinite	$Al_2H_4Si_2O_9$	5.3
Microcline	$AlKO_8Si_3$	11.2
Albite	$Ga_{1.001}NaSi_3O_8$	11.1
Quartz	SiO_2	6.6

Figure 4.5 shows the mineral assemblages. Removal of the quartz and alkali feldspars would improve greatly the percentage of the clay mineral material.

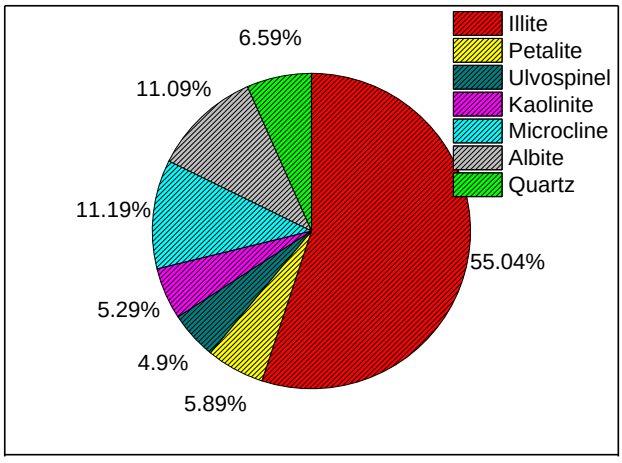

Figure 4. 5: Pie-chart for mineral assemblage in the white clay

Key: pink, red, brown= clay minerals

4.2.3.2 Crystallography of clay samples

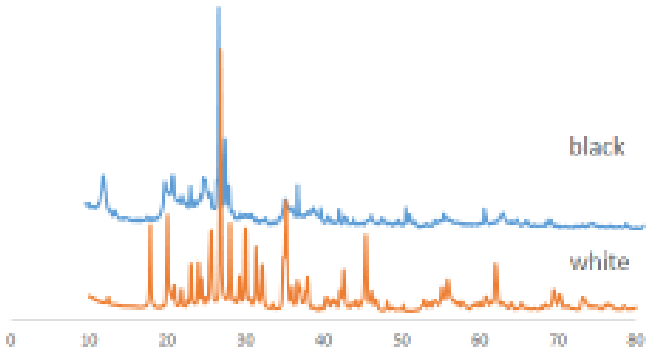

Figure 4. 6: XRD diffractographs for white and black clay

Kaolinite clay minerals have theoretical basal peaks, reflected from the basal planes of 001, 002, 003 and 004 with two theta values of 12.3°, 24.4°, 37.6° and 51.1° respectively and prism peaks reflected from prism planes of 020, 110, 130, 202 at two theta 19.8°, 20.3°, 35.1° and 38.3° respectively (Sachan & Penumadu, 2007).

Figure 4.6 shows that the black clay soil consists of two clay minerals. The basal plane 001 observed at 12.3°, 002 at 24.4°, 003 at 37.6° and 004 at 51.1° compare with value in literature for Kaolinite. These planes were also observed at these two theta in (Peng *at al.*, 2020) research. The prism planes 020 at 20.3°, 040 at 38.3° which are observed on Figure 4.6 are associated with kaolinite as also observed in (Peng *at al.*, 2020). This confirms presence of kaolinite in the black clay sample. Similarly the basal planes; 001 observed at two theta 17.8°, 002 at two theta 26.8° and 003 at two theta 35.1° and the prism planes 010 at two theta 20.1°, 020 at two theta 27.0°, 030 at two theta 46.0° and 040 at two theta 55.1° are characteristic of muscovite. These planes were also observed

in research of (Mohd *et al.,* 2014). Figure 4.6 collaborates the mineral assemblage on Table 4.4

The white clay contains seven minerals with illite and kaolinite as the only clay minerals as seen on Figure 4.4. The diffractograph of the white clay in Figure 4.6 has the basal peaks of the planes 001, 002 and 003 corresponding to two theta 12.3°, 24.3°, 38.5° respectively and prism planes of 020, 030 and 040 at two theta 20.3°, 35.1° and 38.5°respectively. These peaks are characteristic to illite and compare closely with peaks at two theta of 17.8°, 26.7° and elevated 35.2° observed in (Sachan & Penumadu 2007) The basal planes; 002 at 24.4°, 003 at 37.6° and prism planes of 020, 110, 130, 202 at two theta 19.8°, 20.3°, 35.1° and 38.3° respectively confirm presence of kaolinite much as the basal peak at 51.1° and prism peaks at 12.3° are missing. Figure 4.6 confirms presence of clay minerals that can be intercalated.

For basal reflections d spacing for plane 001 is a constant. The order of reflections is 1, 2, 3, ……, L. For lower angles less than 40° two theta peaks occur at "evenly" spaced intervals. Note that when the 2-theta increases by 2, the d-spacings will reduce by 2. For example the d-spacing for Kaolinite for the 004 plane is 1.8 with a two theta of 51.1°, if the X-ray is reflected at 25.6° then the d-spacing will be 1.8x2=3.6. This closely compares with the recorded two theta 24.4° on Figure 4.6, with d-spacing of 3.6. This relationship shows that the data collected in this research is credible and can be used to discuss the effect of modification on the d-spacing distance as in (Mohd *et al.,* 2014). A same relationship is observed in the muscovite in which basal d-spacing of 9.95 is associated with two theta of 8.9°. A half of this d-spacing is 4.975 and would be

associated with a two theta of 8.9x2=17.8°. Table 4.12 gives a two theta of 17.8° and d-spacing of 4.97 which is quite comparable to the "evenly" relationship.

As discussed earlier the white clay had a very large proportion of illite with minor ones of kaolinite and petalite. A study of the changes in the d-spacings of these minerals during the modification will tell whether the process of intercalation was achieved.

Figure 4.6 has basal peaks at two theta 12.3°, 24.4°, 37.6° and 51.1°and prism peaks at two theta of 19.8°, 20.3°, 35.1° and 38.5° that are characteristic to kaolins as also reported by (Yakaya *et al.,* 2017); (Sachan & Penumadu, 2007). This study observed basal peaks at two theta 17.9°, 26.8° and 35.1° and prism peaks 20.2°, 27.1°, 46.1° and 55.8° assigned to prism planes for muscovite. These peaks however show poor resolution, due to impurities that arises from close reflection by the other minerals of microcline, albite, lazurite, berlite and quartz in the sample. The peak of two theta 27.4° and those observed at 62° represent sodium and potassium feldspars and are found normally in the region of d-spacing of 0.630-0.645 nm and 0.310-0.325 nm (Tan, 2011). This finding is also collaborated by XRD data of natural clays from Brazilian southeast region (Alvarez Acevedo *et al,* 2017). The poor resolution is also explained by variable compositions and degree of crystallinity that causes mutual interference with the diffraction pattern's analysis.

4.2.3.3 Intercalation of clay minerals

In formation of the multifunctional organoclay organic surfactants were utilized. The overlay of the XRD diffractographs show the shifts in the two theta and d-spacings.

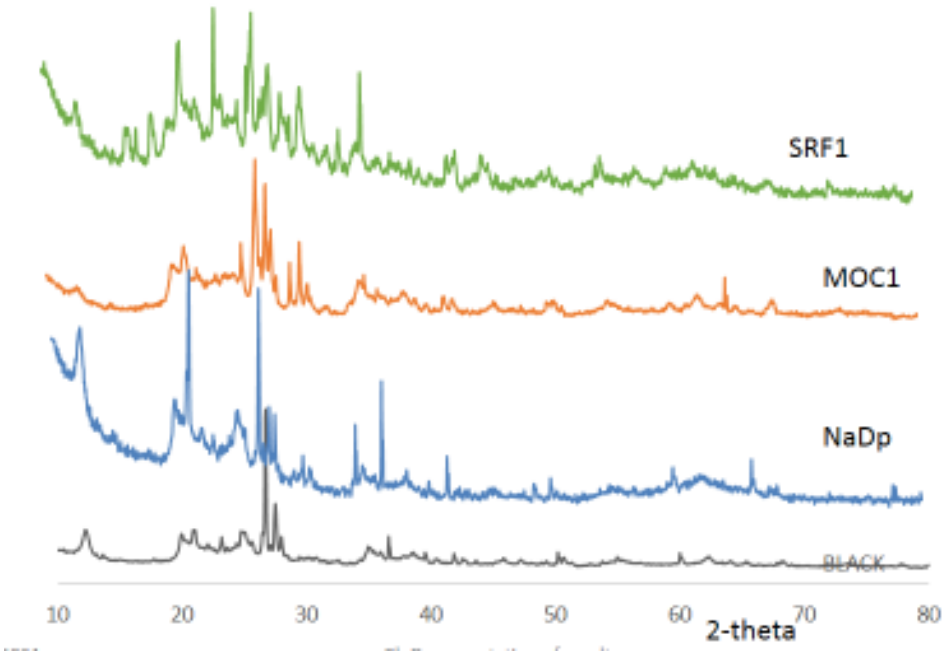

Figure 4. 7: XRD diffractographs for 50-50 nanocomposites

This XRD overlay figure has similar features to the overlay of (Maxim *et al.*, 2019). The peak on Figure 4.7 at two theta representing the plane 001 shifts slightly to bigger two theta in NaDp. It then shifts to lower two theta in MOC1 and SRF1 which indicates an increase in the interlayer distance in SRF1 and MOC1 as compared to the raw clay. The prism peak at plane 020 at two theta 20.3° in the black clay shifts to lower two theta in NaDp indicating an increase in the interlayer distance. The peak at two theta 20.3° in NaDp shifts further to a lower two theta in MOC1. The intensity of this prism peak at 20.3° is lower than of NaDp which suggests that there is increased concentration of atoms at the plane. Both the silicate layer and the aluminate layer are bound to Na^+ through their oxygen atoms. The increase in d-spacing in NaDp can be explained by the crowding of the interlayer by Na^+ (Khaldi *et al.*, 2014). So the crowded Na^+ in the gallery develop forces of repulsion increasing the interlayer distance. The increase in the interlayer distance in MOC1 is due to pillaring of the sheets at bigger length after

intercalation and the slightly collapsed peak can be explained by increase in concentration of organics at the sheets that lower the number of reflected X-rays. The intensity of this peak improves in SRF1 which could be due to filling of the gallery with nutrient inorganics that positively respond to the incident X-ray.

Similarly the prism peak at two theta 37.8° in the black clay becomes more defined in NaDp but shifts to a lower two theta of 35.3° in MOC1 and SRF2 a characteristic observed in (Khaldi *et al.,* 2014). As discussed earlier this shift in the position of planes 001 and 002 confirms an increase in the inter plane distance. Therefore an increase in both the basal and prism planes of the same clay unit cell causes an increase in the volume that can be occupied by the nutrients in the gallery. This variation in the unit cell can only have arisen out of an intercalation reaction of the clay minerals in the clays. Clay minerals like MOC1 have multiple advantages among them is chemical interaction with organics like in clay nanocomposite polymers and dispersion of inorganics like NO_3^-, $H_2PO_4^-$ and K^+ into the gallery. In the later, a unit cell can have its gallery shielded by two perpendicular unit cells on both sides which would lock the nutrients in the gallery. Nutrients in such a unit cell can only desorb out through the pores in the clay mineral.

On the overall there is an increase in the d-spacing in the nanocomposites that can be explained by intercalation, pillaring in MOC1 and additional effect in SRF1 due to population of the fertilizer nutrients. Figure 4.8 shows a comparison of the crystallinity in the 70-30 nanocomposites with the white clay.

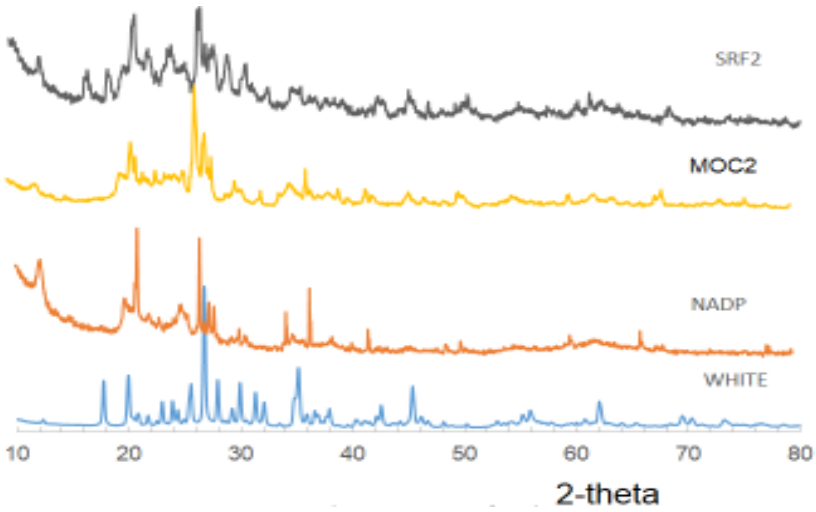

Figure 4. 8: XRD diffractograph for 70-30 nanocomposites

The clay blende was first modified by populating the gallery with sodium ions. The basal peak at plane 002 in illite collapses from the NaDp while the prism peak of kaolinite slightly increases in two theta showing an increase in d-spacing. The basal peak of 003 at two theta 26.8° in illite shifts to a lower two theta which implies an increase in the d-spacing. The basal peak at the plane 004 is observed at lower two theta so is to the prism plane 040 of muscovite that shifts to lower two theta value in NaDp. The kaolinite basal peaks of two theta 37.6° at $d_{3.579}$ is prominent in NaDp. Generally this explains slight increase in the interlayer distance caused by the strong repulsion forces set by the high concentration of Na^+ on the sheets. The shifting of two theta in NaDp as seen from the Miller's indices observed in Figure 4.8 compares with typical intercalation as also seen in research of (Khaldi *et al.*, 2014) which was explained by the large number of positively charged Na ions introduced by clay mineral modification step that set strong interlayer repulsion forces. The large concentration of positive

charges in the interlayer enabled the clay minerals to attract the strongly polar DMSO molecules into this gallery.

The DMSO reacts with the Na^+;

$$(CH_3)_2S{=}O + Na^+ \longrightarrow (CH_3)_2S^+\text{-}O^- Na^+$$

This polar molecule can interact and stick onto the sheets through the Na^+. This slightly increases the length of the molecule causing slight intercalation in both the TO and the TOT sheets. This intercalation is enhanced by introduction of the longer CTAB molecules to replace the DMSO ones as in (Mohd *et al.*, 2014).

Most of the peaks collapse due to the organic in the gallery. The peak at plane 003 is observed at slightly higher two theta from its position in NaDp. The peak at 27.3° in the clay mineral is depressed to 25.6°. All the peaks in the MOC2 reduced from their original position which confirms that CTAB had pillared and increased the distance between the galleries (Min *et al.*, 2011); (Mohd *et al.*, 2014). A number of the peaks have poor resolution but still represents a crystalline compound a case also noted in the research in modified montimorillonite (Khelifa *et al.*, 2018); (Min *et al.*, 2011).

As discussed earlier the diffractograph of SRF2 shows more crystallinity than MOC2 due to population of inorganics in the interlayer distance. The study sort to also compare the effect of the percentage surfactant to the intercalation output. Figure 4.9 compares the diffractographs of MOC1 and MOC2.

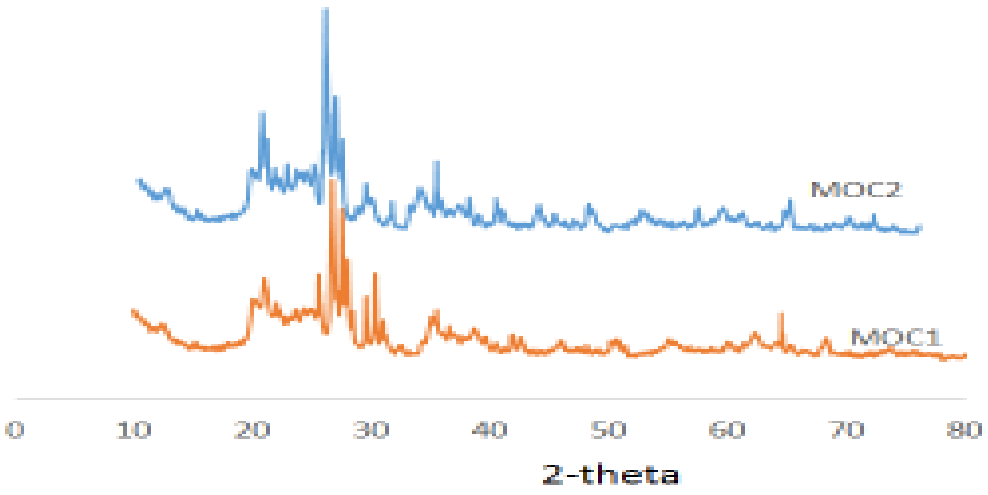

Figure 4. 9: Comparison of diffractographs of MOC1 and MOC2

The peak at two theta 27.6° has shifted slightly to 27.1° the shoulder on the peak at 29.5° on MOC1 has shifted to a smaller two theta of 29.1°. The peak at two theta 20.3° is more defined in MOC2 than MOC1. There is also a peak at 38.3° that was depressed in MOC1 but can clearly be seen on MOC2. The peak at 35.4° on MOC1 shifts to a lower two theta of 35.1°.On the overall, MOC2 has its d-spacing slightly increased as compared to MOC1. An analysis of the data points shown on Table 4.6 confirms that there is an increase in the interlayer distances from MOC1 to MOC2 structure.

Table 4. 6: Basal planes for kaolinite

Plane	Theoretical 2-theta/degree	MOC 1	2θshift value	MOC2	2θshift value
Basal	12.3	11.988	0.312	12.191	-0.203
	24.4	24.149	0.257	24.068	0.081
	37.6	37.201	0.399	37.079	0.122
	51.1	50.982	0.118	50.577	0.405
Prism	19.8	19.608	0.192	19.366	0.242
	20.3	20.257	0.043	20.136	0.121
	35.1	35.093	0.007	35.215	-0.122
	38.3	38.225	0.075	37.768	0.457

These data points are extracted from the XRD data points that were machine generated and used to draw the diffractographs. The 2θ shift value in the last column indicates the difference in two theta between MOC1 and MOC2. The two negative values in the column represent decrease in d-spacing as compared to six points that show an increase in d-spacing.

The XRD mineralogical characterization shows that the clay materials used had clay minerals and XRD crystallography confirms intercalation of the clay materials and dispersion of nitrogen, phosphorus and potassium into the layers. Figure 4.10 shows the comparison between XRD of SRF1 and SRF2.

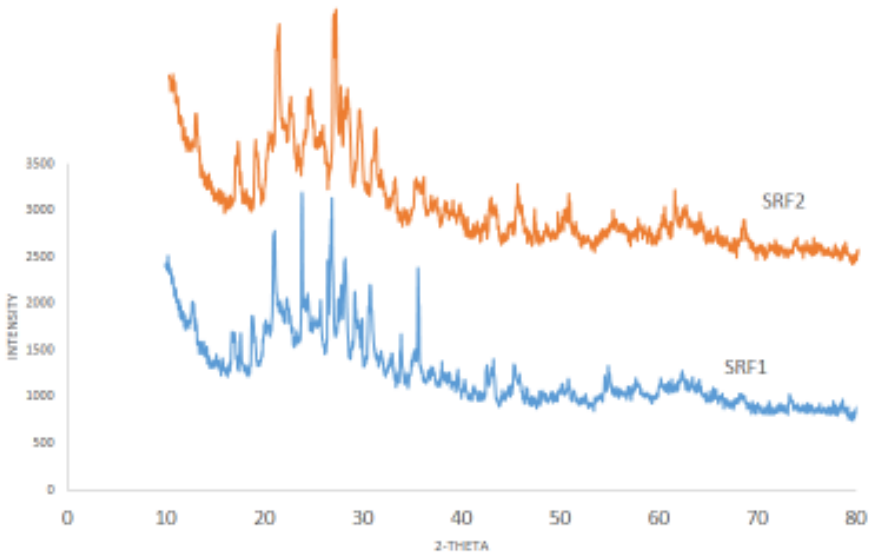

Figure 4. 10: Comparison of diffractographs of SRF1 and SRF2

The boldness in both diffractographs indicate crowding of ions into the interlayer distances. The peaks at two theta 17.7° and 18.3° in SRF2 are more defined than in

SRF1. Also the peak at the angle two theta 24.4° on SRF1 has shifted to 23.6° in SRF2 while the one at 20.2° on SRF1 has moved to 20.8° on SRF2 which implies that SRF2 will host more nutrient concentration due to the bigger volume of the gallery. Most importantly, the peaks at 20.2°, 24.4°, 27.8° and 35.5° on SRF1 are neat which implies that the incident X-ray is irradiating planes containing the aluminate and silicate sheets. These peaks are wide and less defined in SRF2 because the incident X-rays are reflected by the N, P, K ions crowded at the planes in SRF2 which confirms higher concentration of the nutrients in SRF2 as opposed to SRF1.

4.2.4 Thermal Gravimetric Analysis (TGA)

TGA measures mass of a sample over time as temperature changes. It provides information about physical phenomena as phase transitions, absorption and desorption. It can be used to evaluate the thermal stability of a material. A negligible mass loss corresponds to little or no slope in the TGA trace diagram. Figure 4.11 displays the TGA for the black clay.

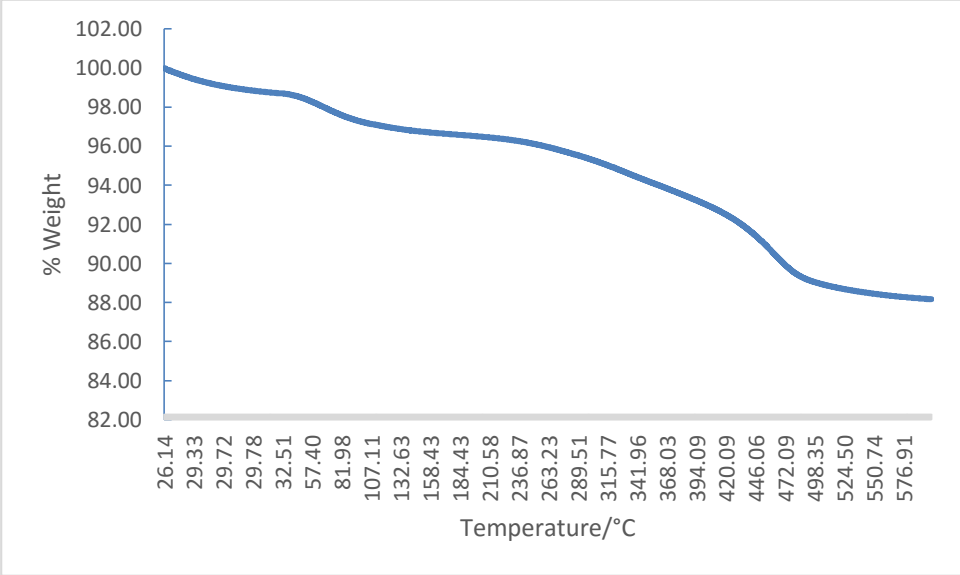

Figure 4. 11: TGA for black clay

The loss in weight on Figure 4.11 can be divided into four parts. The first part is from 26.14 °C to 35.51 °C in which the loss can be attributed to removal of moisture on the beneficiated raw clay (Mohd *et al.,* 2014). The region 35.51 °C to 103.12 °C has approximately 1 % loss that is attributed to removal of free water held on the sheets and into the interlayers which is held in the system by the London forces (Khelifa *et al.,* 2018). The loss in weight observed between 103.12 °C to 496.09 °C could be due to decomposition of the high organic or carbon matter in the clay recorded on Table 4.1 and the removal of coordinated water. This was also observed in Maghia clays (Khelifa *et al*, 2018). The remaining stretch up to 576.91 °C could represent removal of inorganics as hydroxides. Figure 4.12 shows the TGA for white clay.

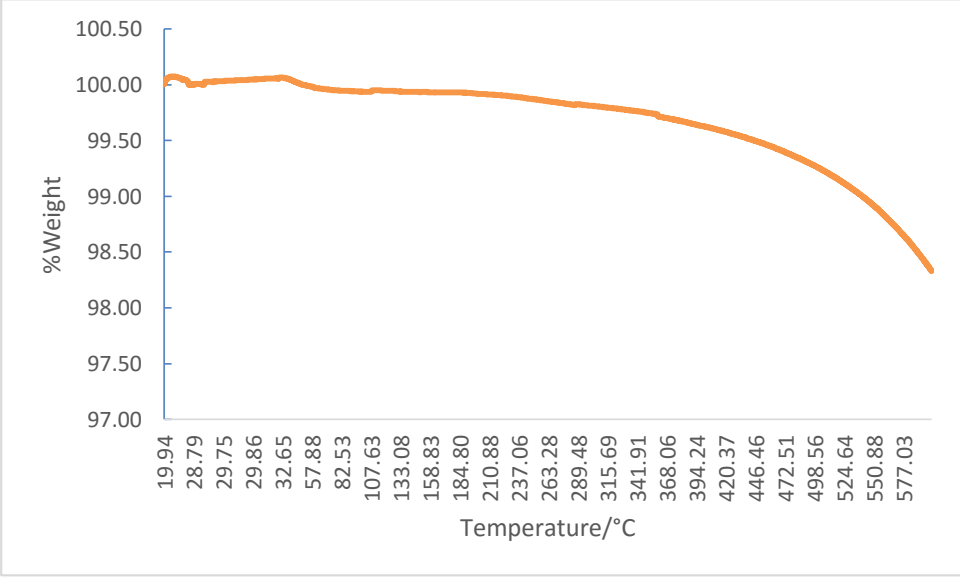

Figure 4. 12: TGA for white clay

The TGA curve on Figure 4.12 for white clay material is stable up to about 30 °C then there is a slight weight increase which could be because of expansion caused by the

movements of free water into the sheets. However there is a slight weight loss from 41.26 °C to 226.24 °C that can be attributed to removal of free water and water that is adsorbed to the sheets which compares well with the record of (Belmokhtar *et al.*, 2012). The free water adsorbed on the white clay by weak van der waal's forces is removed at lower temperatures of up to about 113.08 °C (Mohd *et al.*, 2014). The steady loss in weight from 226.24 °C to 566.05 °C could be due to loss of water coordinated to the clay sheets either adsorbed to oxygen of the silicate or OH of the gibbsite by hydrogen bonds. This is also observed in the research of (Khelifa *et al*, 2018) on the Maghia raw clays (Choul *et al.*, 2012) (Mohsen & El-Maghraly, 2010). The loss in weight of the white clay is only 1.5 % as compared to 12 % for the black clay which indicates that the black clay soil has a higher percentage of organics which is collaborated by its higher carbon percent of 2.85 to 0.41 of the white one as seen on Table 4.1. Both black and white clay are stable up to 500 °C as is observed on Figures 4.12 and 4.11 which implies that if the nutrients are dispersed into these clays, they can survive a bush fire on the farm.

4.2.5 SEM analysis

The morphology of the materials used in this study was important so as to establish existence of layers and pores in the multifunctional clay structure. The microscopic pictures helped see the structure in these materials. Plate 4.1 displays the SEM picture of white clay material.

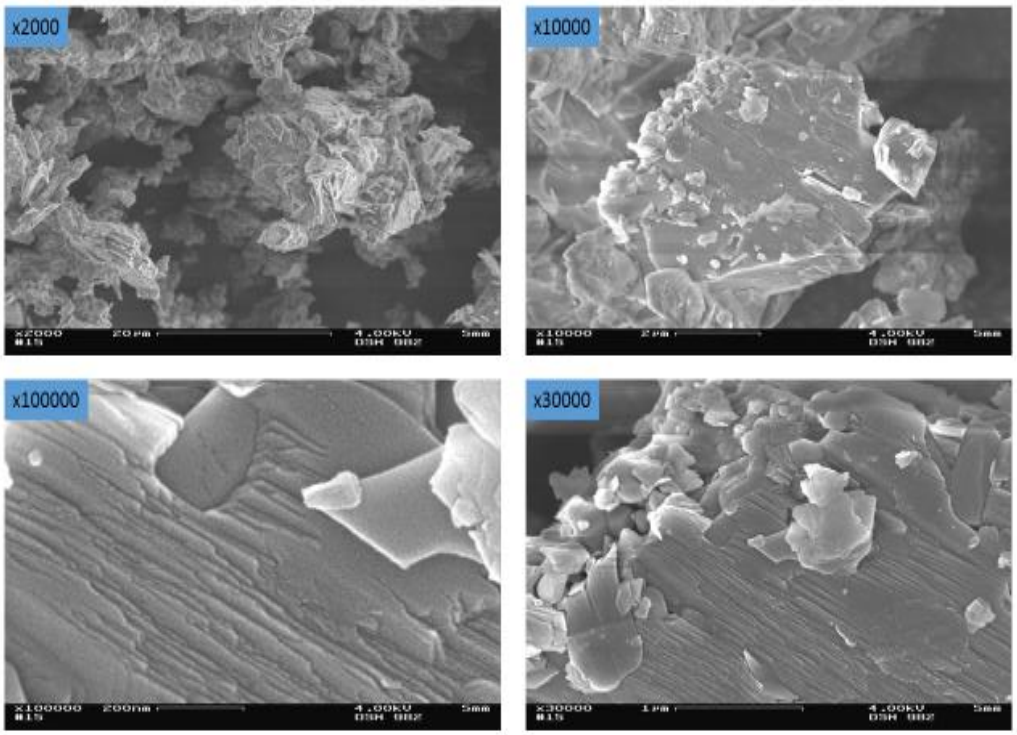

Plate 4. 1: SEM for white clay

Key: x2000, x10000, x30000, x100000 are picture magnifications

Plate 4.1 displays scanning electron microscopy pictures for the white clay. The x2000 picture shows crystals of the powder. Picture x10000 shows platelets and stacks of parallel stacks. The x30000 picture shows parallel stacks of the clay sheets. The picture makes plain platelets on the stacks of different sizes scattered around. Layers of packing within crystals with some individual layered pieces splashed on the stacks in the x100000 picture are seen. This x100000 displays single clay mineral polymers consisting of sheets and interlayer distances packed at approximate distances of 0.9-1.0nm. The plate confirms presence of a layered structure of phyllosilicates (Maxim *et al.,* 2019). The other clay material used was black clay whose morphology is given by four pictures with different magnifications on picture on Plate 4.2.

4.2.5 SEM analysis

The morphology of the materials used in this study was important so as to establish existence of layers and pores in the multifunctional clay structure. The microscopic pictures helped see the structure in these materials. Plate 4.1 displays the SEM picture of white clay material.

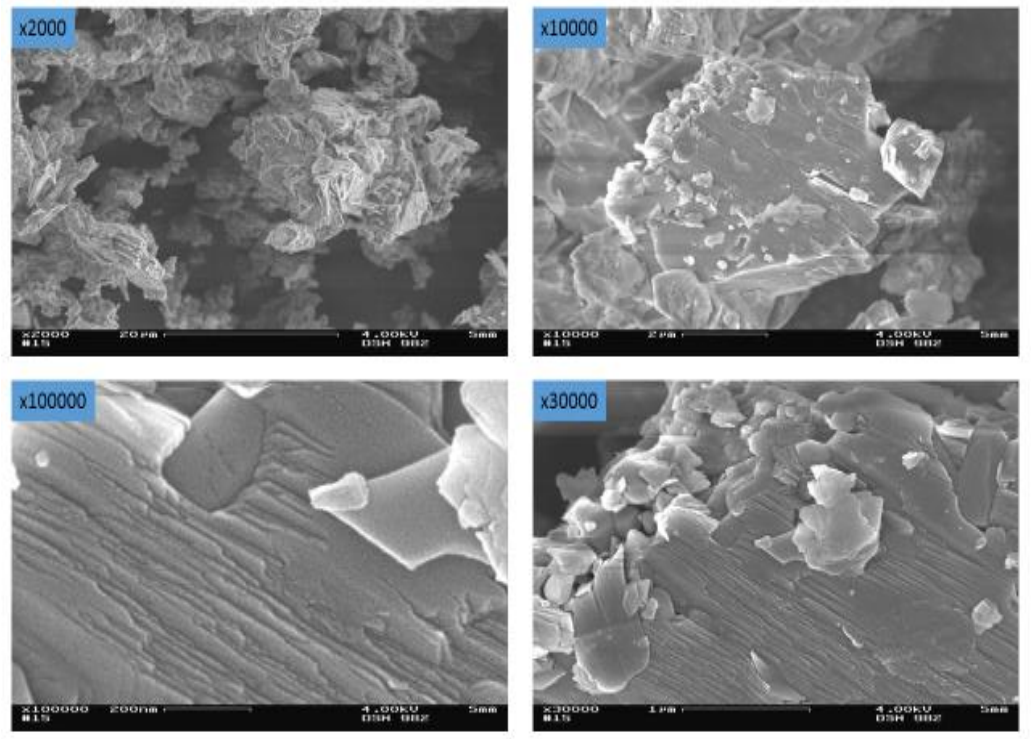

Plate 4. 2: SEM for white clay

Key: x2000, x10000, x30000, x100000 are picture magnifications

Plate 4.1 displays scanning electron microscopy pictures for the white clay. The x2000 picture shows crystals of the powder. Picture x10000 shows platelets and stacks of parallel stacks. The x30000 picture shows parallel stacks of the clay sheets. The picture makes plain platelets on the stacks of different sizes scattered around. Layers of packing within crystals with some individual layered pieces splashed on the stacks in the

x100000 picture are seen. This x100000 displays single clay mineral polymers consisting of sheets and interlayer distances packed at approximate distances of 0.9-1.0nm. The plate confirms presence of a layered structure of phyllosilicates (Maxim *et al.*, 2019). The other clay material used was black clay whose morphology is given by four pictures with different magnifications on picture on Plate 4.2.

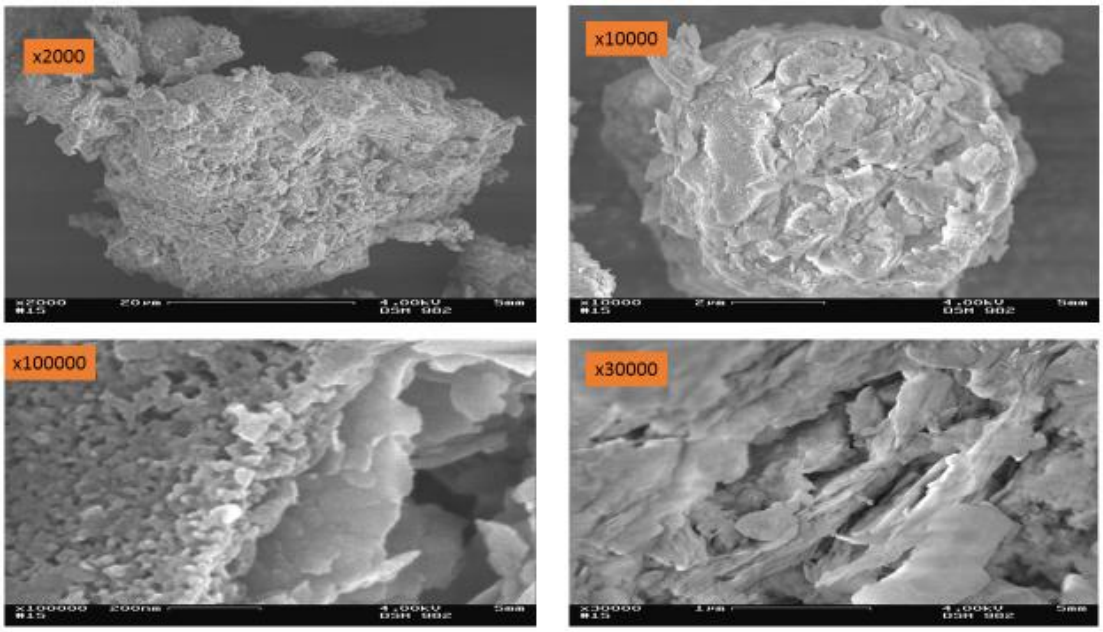

Plate 4. 3: SEM for black clay

Key: x2000, x10000, x30000, x100000 magnification

Plate 4.2 shows the scanning electron microscopy of black clay at various magnifications. The pictures at magnification of x2000, x10000, x30000 and x100000 illustrate the petrological properties of the sample. The x2000 picture shows irregular crystal nature of the clay mineral that is packed together into large solid units. The x10000 magnification, observed from the top surface of the crystal shows the nature of a platelet of clay with indications of sheets that appear to be peeling off. Layers and large number of pores on the top sheet are observed in the x30000 picture as in (Maxim

et al., 2019). The x100000 picture confirms presence of layers though not as defined as in the white clay due to the level of beneficiation in this sample. There are large gullies and holes seen on top of this x100000 picture that represent interlayer distances and surface pores respectively. This set of pictures at various magnifications reveal phyllosilicate nature of the sample that was also observed by (Alvarez-Acevedo *et al.*, 2017).

4.2.6. TEM analysis

TEM analysis was performed to understand the internal morphology of the clay samples. These TEM pictures were characterized by darker and lighter regions.

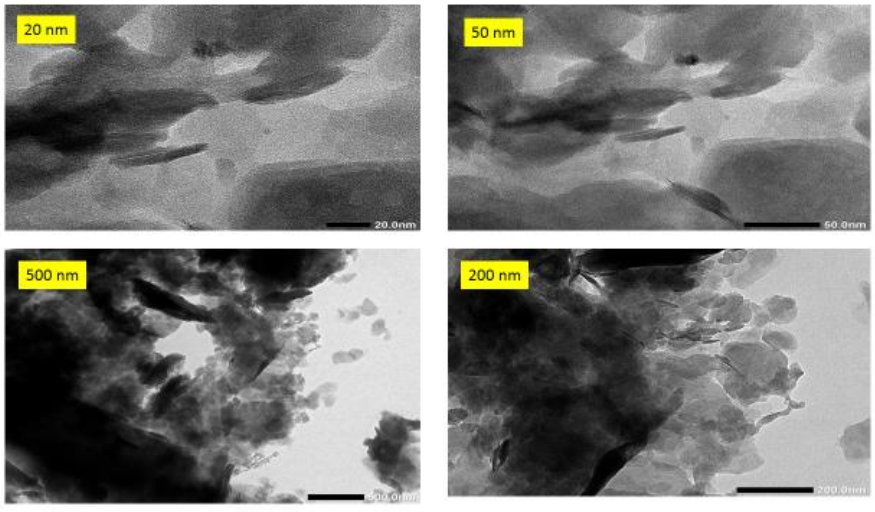

Plate 4. 4: TEM for black clay

Key: 20 nm, 50 nm, 200 nm and 500 nm magnification.

There are light spots in the 20nm picture which represent regions that are either pores or interlayer distances. The darker regions in the 50 nm picture represent the sheets and the region with interlayer gallery ions. The 200 nm picture shows platelets and pores for the

much lighter spaces (Mohd *et al.*, 2014). Lastly the 500 nm picture confirms presence of crystals and a pore at the centre of the picture.

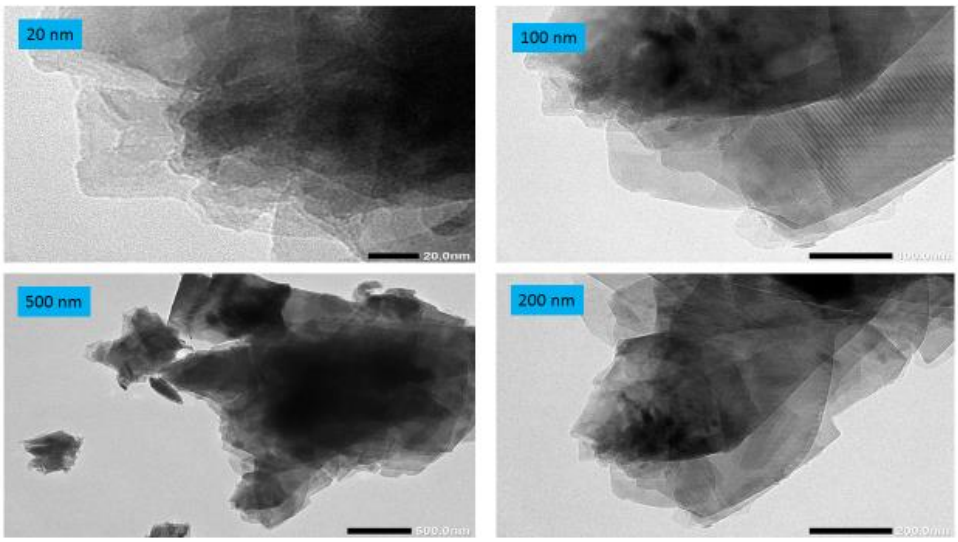

Plate 4. 5: TEM for white clay

Key: 20 nm, 100 nm, 200 nm and 500 nm magnifications

The picture, 20 nm on plate 4.4 shows presence of stacks of the clay minerals. The lighter areas in this picture show presence of pores in the morphology of the clay material. The 100 nm picture dark parallel regions representing the layered sheets and parallel lighter regions representing the interlayer distances. The 200 nm picture confirms presence of layers and existence of tachoids. We see platelets and stacks on 500 nm picture in addition to pore spaces in the middle of this picture. Both SEM and TEM present materials that have layers and surface pores which can be modified to allow entry of nutrient formulas. The presence of pores on the surface of the materials is supported by Table 4.8 which is also observed in (Utpalendu & Manika, 2013).

4.2.7 BET analysis

The importance of interlayer distances and surface pores in the clays has been reiterated in previous discussions. Clays have many layers in their structures that make adsorption and desorption a little complicated hence require the Brunauer-Emmett- Teller, BET and Barrett-Joyner-Halenda, BJH to describe the equilibrium between the adsorbate and adsorbent systems. Figure 4.13 shows the isotherm for the white clay.

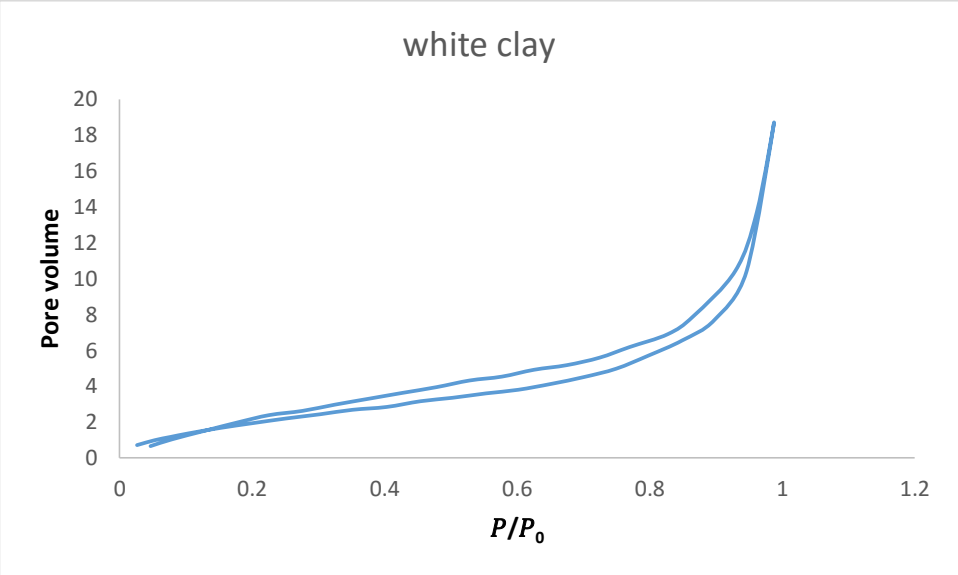

Figure 4. 13: BET isotherm for white clay

The nitrogen adsorption isothermal of white clay in Figure 4.13 follows largely a type II (Utpalendu & Manika, 2013) with a hysteresis, H4 that suggests presence of mesopores. The hysteresis which differs slightly from type IV one is narrow indicating higher proportion of macropores. The amount of $\frac{P}{P_0}$ below 0.01 is very low indicating absence of micropores. This type of hysteresis is not quite reversible between the adsorption and desorption which implies it does not perfectly fit into type II (Utpalendu & Manika, 2013). It is then reasonable to classify it as type IIB (Rouquerol *et al.*, 1998) which suggests that the material contains high percentage of the mesopores. The hysteresis

does not have a plateau at $\frac{P}{P_0}$ that is more than 0.8 but instead has a steep rise and drop. The sample contains some mesopores responsible for generation of the hysteresis above 0.4 but the higher percentage of macropores is responsible for absence of the plateau as also observed in (Alvarez-Avevelo *et al.*, 2017) research on Brazilian clays. There is some indication of micropores due to $\frac{P}{P_0} < 0.05$ due to irreversibility in this segment. Such pores could be like of illite or muscovite mixed into kaolin. This $\frac{P}{P_0} < 0.05$ implies some capillary condensation and evaporation taking place in the mesopores. This isotherm shows a large presence of illite due to the narrow hysteresis above 0.4 and small amount of kaolins due to lack of plateau at relative pressure of above 0.8 supporting Figure 4.10 that gave total percentage for kaolinite and petalite as 11.2 % and 55.1 % for illite. Figure 4.14 shows the BET isotherm for black clay.

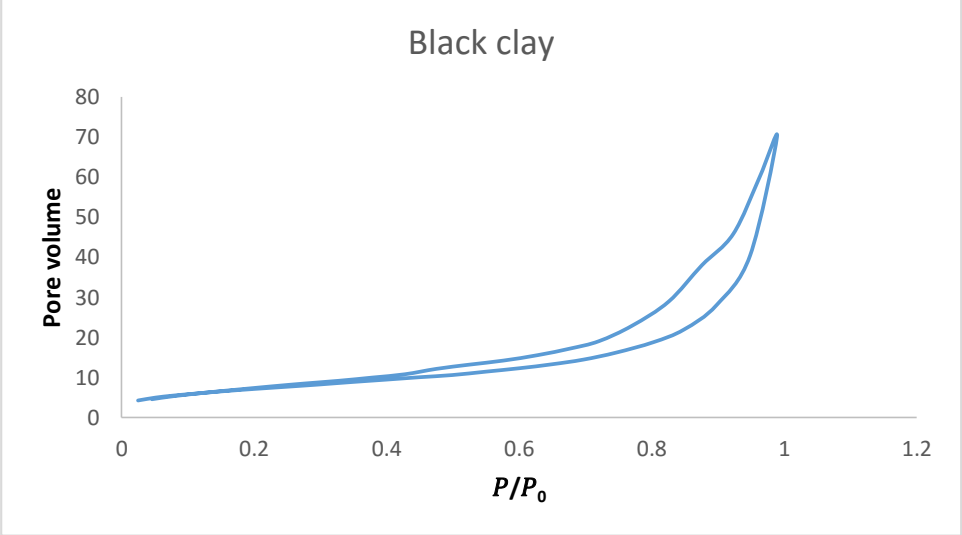

Figure 4. 14: BET isotherm for black clay

The isotherm on Figure 4.14 fits into the type IIB model (Rouquerol *et al.*, 1998). It compares well with that of Niobrara chalk D 3150 North shale due to prominent

hysteresis at higher relative pressures (Rouquerol *et al.,* 1998). It has a steep slope for $\frac{P}{P_0}$ of between 0.98 and 1.0 which suggests absence of micropores and forced closure at $\frac{P}{P_0}$ = 0.37 which falls in 0.35< $\frac{P}{P_0}$ > 0.55 due to tensile strength effect normally associated with samples with large fraction of mesopores of <4nm (Groen *et al.*, 2003). The lower segment with low volume of nitrogen adsorbed and lower hysteresis indicate presence of macroporous samples. (Utpalendu and Manika, 2013) proposed presence of fine mesopores, larger mesopores and macropores from their isotherms which compare closely with that of black clay in Figure 4.14. The prominent hysteresis, H3 at higher $\frac{P}{P_0}$ > 0.7, indicates low quantity mesopores in a large proportion of macropores. This supports Figure 4.9 which gives the clay mineral sample as only 28.3 % of the sample.

The white clay sample consists small proportion micropores, smaller sized mesopores and macropores while the black clay has a broader hysteresis indicating larger sized mesopores and macropores. The white sample must therefore have some smectites or micas while the black is of kaolins. These raw clay materials were modified into a MOC1 which is shown on Figure 4.15.

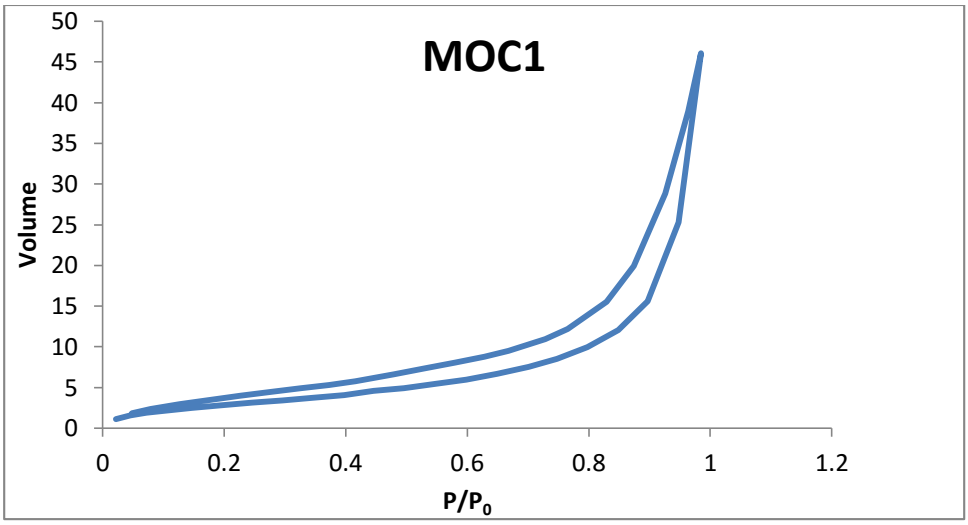

Figure 4. 15: BET isotherm of MOC 1

Figure 4.15 shows an isotherm of MOC1 in which the multilayers are filled with CTAB. The curve has a hysteresis up to $\frac{P}{P_0}$ of 0.1 and a steep slope at $\frac{P}{P_0}$ of 0.98 to 1.0 and is missing the forced closure. The steep slope at $\frac{P}{P_0}$ of 0.98 to 1.0 hints at absence of micropores and small size mesopores. The absence of the plateau alludes to presence of macropores but the narrow hysteresis at relative pressure of below 0.5 means there is some presence of mesopores. The fact that the hysteresis runs down to 0.1 could mean that the surfactant had opened more pores either on the surface or within the interlayer space. The uniform nature of the hysteresis suggests that the CTAB molecules in the interlayer increase the inner pressure which reduces the nitrogen gas interaction with some of the pores by increasing filled up pores. The combined effect means increased pores on the monolayer, multilayer and the interlayer (Alvarez-Acevedo *et al.*, 2017). NPK was dispersed into this organoclay yielding SRF1 whose isotherm is shown on Figure 4.16.

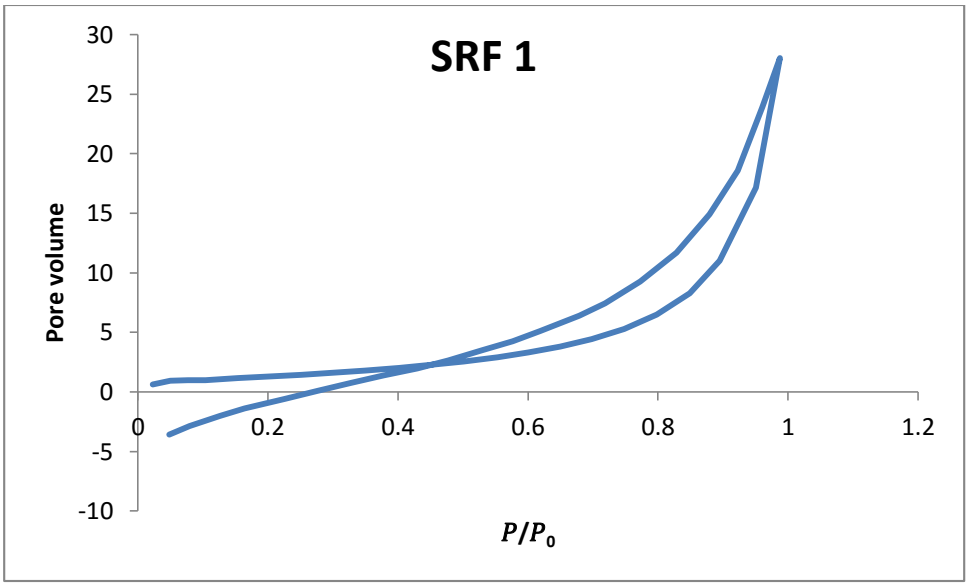

Figure 4. 16: BET isotherm of SRF1

Figure 4.16 represents an isotherm of the slow release fertilizer SRF1. The nature of the hysteresis from $\frac{P}{P_0}$ >0.43 is identical to the one of MOC1 but gives a totally different curve below. The desorption curve below $\frac{P}{P_0}$ = 0.43 is steep into the negative while the adsorption is less steep. From $\frac{P}{P_0}$ = 0 to 0.43 the nitrogen molecules adsorb into the available pores since a number of the mesopores have already been filled with the NPK molecules. As the relative pressures increases, the nitrogen absorbs and desorbs at relatively equal volumes. The higher relative pressures 0.98 to 1.0 show absence of micropores. The higher relative pressures 0.98 to 1.0 show absence of micropores. Figure 4.17 represents the isotherm for MOC2.

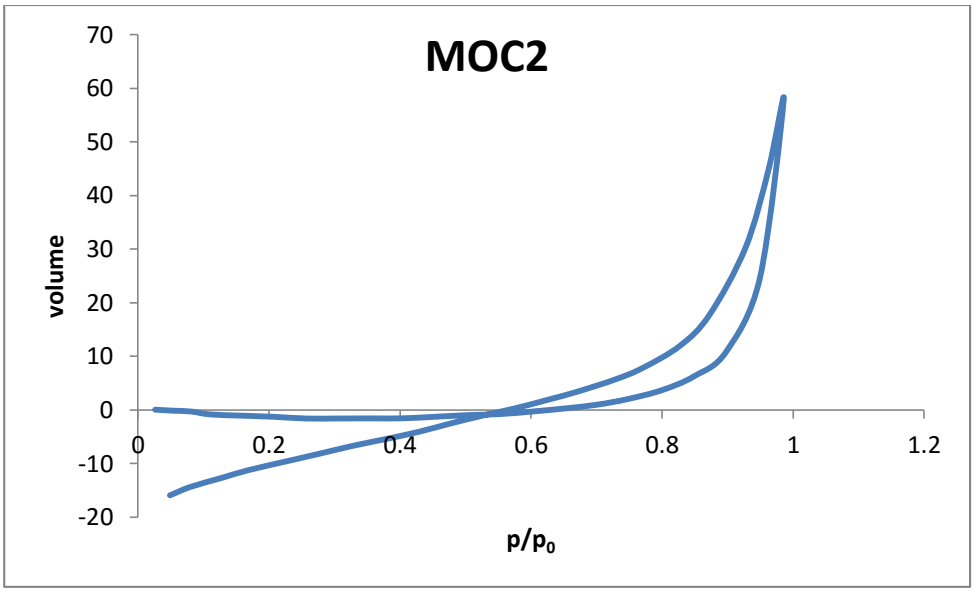

Figure 4. 17: BET isotherm for MOC 2

Figure 4.17 which represents MOC2 closes down into the negative. The curve below relative pressure of below 0.6 cannot be explained by the assumptions of BET as explained by (Alvarez-Acevedo *et al.*, 2017). The curves have hysteresis up to $\frac{P}{P_0}$ of 0.6. They have a steep slope at $\frac{P}{P_0}$ of 0.98-1.0 and missing the forced closure. The absence of the plateau implies presence of macropores but the wide hysteresis means some presence of mesopores and probably a small percentage of micropores. The fact that the hysteresis runs down to $\frac{P}{P_0}$ of 0.6 could mean that the surfactant has opened more pores either on the surface or within the interlayer space. The uniform nature of the hysteresis could point to the CTAB molecules in the interlayer increasing the inner pressure reducing the nitrogen gas interaction with some of the pores due to increased pores on the monolayer, multilayer and the interlayer.

The general occupation surface area is 0.345 for SRF1 as compared to 0.423 of MOC1 which supports the previous statement that SRF would disperse more nutrients enabling

the fertilizer to take a long time supplying nutrients to the plants. The Table 4.7 gives a summary of adsorption on the BET isotherms for the samples.

Table 4. 7: Adsorption summary BET

Sample	Correlation Coefficient	Constant, C	Surface area, M^2/g	Total pore volume, cc/g
White	0.9989	16.07	8.38	7.16
Black	0.9999	59.47	26.46	29.68
MOC1	0.9999	27.78	11.26	7.13
SRF1	0.9952	52.04	4.82	4.34

The correlation coefficient shows that the data have sufficient linearity for all the samples analyzed. The surface area for black soil sample was largest due to the impurities in the clay which coalesced into the solid. The surface area reduces to 11.26 M^2g^{-1} in MOC1 as some of the CTAB breaks the large clay polymeric molecules into shorter units that the pillars can sustain. The increase in the population of the interlayers by NPK reduces the polymeric clay units even further. The total volume has similar trend to the surface area. The black clay sample has the largest total pore volume which can be attributed to the porosity opened by the silt particles on the surface of the sample. The reduction of this volume in MOC1 and SRF1 could be due to fragmentation of the populated molecules in order to sustain the forces of cohesion.

Table 4. 8: Desorption summary on BJH isotherms

Sample	Surface area M^2/g	Pore volume(cc)	Pore diameter/nm	Total pore volume c.c/g
White	7.21	0.03	3.24	0.03
Black	30.36	0.09	3.62	1.08
MOC1	17.88	0.07	1.79	55.15
SRF 1	17.49	0.05	1.82	8.95

There is a decrease in surface area for MOC1 caused by the reduction of the pores by the CTAB. Similarly the pore diameter reduces in MOC1 and SRF1 due to the filling by the surfactant molecules. The columns on Figure 4.18 are extracted from data in Tables 4.7 and 4.8.

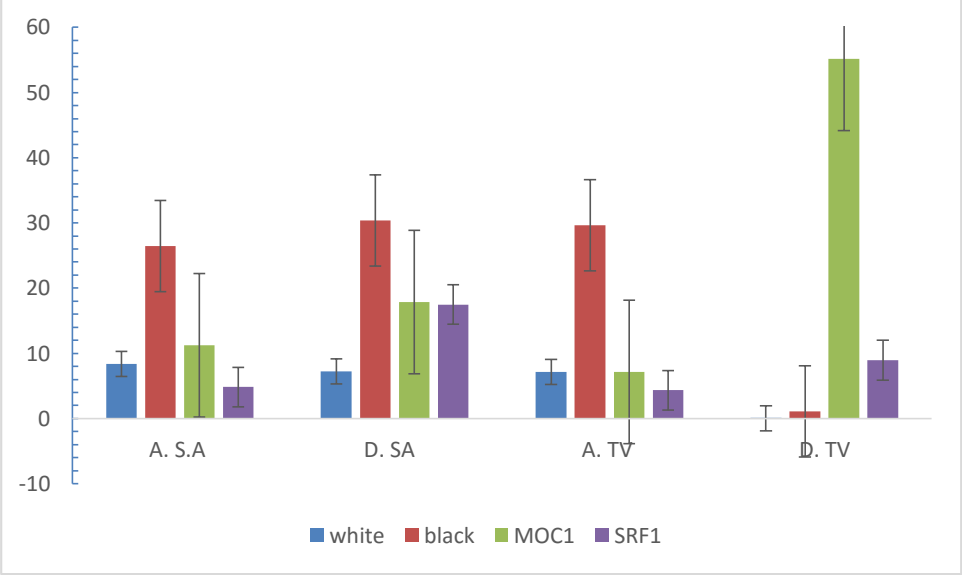

Figure 4. 18: column for comparison of surface area and total pore volume

Figure 4.18 compares surface area and total pore volume for the raw materials and finish product. The error bars verifies that white clay and SRF1 do not have significantly different adsorption surface area. Similarly the black clay and MOC1 do not have significantly different adsorption surface area but white clay has significantly different desorption surface area to black, MOC1 and SRF1. Figure 4.18 establishes that the adsorption total volume is significantly similar for white, MOC1 and SRF1 which are different from black clay. Furthermore, MOC1 recorded very high desorption total volume as compared to SRF1. The white and black clay have very low desorption total volume as compared to MOC1. The white clay has similar surface area relationships for adsorption and desorption. This is because the adsorption and desorption on the surface

have narrow hysteresis due to pores that are uniformly packed, since from Table 4.5 66.3% of the minerals are involved in the process of adsorption and desorption. The number of total pore volume involved in adsorption is far more than the one for desorption. The white clay mineral has larger percentage of the TOT structure hence easy to adsorb on the tetrahedral structure since adsorption closes the pores on the surface of TOT. As the nitrogen adsorbs into the octahedral layer, the pressure on top fills those pores on the tetrahedral surface (Rouquerol *et al.,* 1998). This process opposes desorption one since the inner nitrogen pressure is lower.

The black clay on Figure 4.18 has larger desorption surface area than adsorption. This could be because adsorption only occurs on the surface of a clay mineral while desorption will also occur through the pores caused by porosity. The total adsorption is higher than desorption which could be due to the multilayer nature of the sample. The nitrogen gas pressure exerted from out will adsorb the molecules which fill the pore volume making it difficult for the desorption process.

The total pore volume for desorption is much larger than the adsorption pore volume due to the effect of the CTAB pillars forcing more pores in addition to the larger exposure arising from the fragmenting polymeric layers.

The surface area for desorption on Figure 4.18 is significantly higher than for adsorption on the MOC1 because organics in the interlayer develop sufficient pressure on the nitrogen to desorb opening more pores from the gallery along the TO and TOT.

The bar errors indicate that adsorption surface area and total pore volumes for SRF1 on Figure 4.18 is similar to that of the MOC1. However the total pore volume for

desorption is much lower in SRF1 than was for the MOC1 as displayed by the error bars. This could be because of the large number of molecules contributed by the NPK into the interlayers which in turn reduces the nitrogen and nitrogen pressure from these interlayers reducing desorption.

From the correlation coefficient on Table 4.7, the data fits well into the adsorption t-plot. The samples have high specific surface area of 4.8 for SRF1 which is the smallest and 26.46 of black clay as the largest which compares well with the data on the clays in America whose lowest specific surface area was 2.82 for mancos B shale to 31.81 of montimorillonite (Alvarez Averedo *et al.*, 2017).

Table 4. 9: Data for t-plots

Sample	Slope	Intercept	Correlation Coefficient
White	389.87	2.59	0.9989
Black	130.41	2.23	0.9999
MOC1	298.08	1.11	0.9999
SRF1	708.19	1.39	0.9952

As discussed before, the correlation values show data with good linearity. The white clay has higher slope hence faster filling by the absorbate due to open pores as opposed to the black clay where most of the pores are filled by silica impurities. This illustrates that the white clay has more mesopores than the black which is consistent with data on Tables 4.4 and 4.5. The intercepts on the t-plots for MOC1 and SRF1 are smaller which could be explained by reduced pores due to the pillar ends of the CTAB molecules and the filling of these pores by the nutrient molecules. The higher slope of SRF1 is due to the faster filling of the pores by the absorbate. The isotherms show presence of

mesoporous and macroporous materials both of which relate to clays with good adsorptive properties materials

4.3 Characterization of Superabsobent polymer

The effect of the slow release formula may be dampened if the farm for the crops receives a lot of water especially in areas where farming depends largely on rain. In such scenario it becomes imperative to protect the SRF product. Coating materials were analyzed for their effectiveness by studying their morphology using SEM, crystallography using XRD and the particle size that would be responsible for desorption and adsorption in order to enhance the slow release capability of the NPK nanocomposite. The prepared coating materials were characterized to establish their efficiency.

4.3.1 Characterization of corn starch

The SAP polymer molecules are held together by both Van der Waals forces and strong hydrogen bonds into a quasi-crystalline form due to the corn starch granules.

4.3.1.1: XRD analysis

This analysis was performed to establish whether the solid granules of corn starch have any crystalline patterns. Figure 4.19 shows the XRD peaks for corn starch powder.

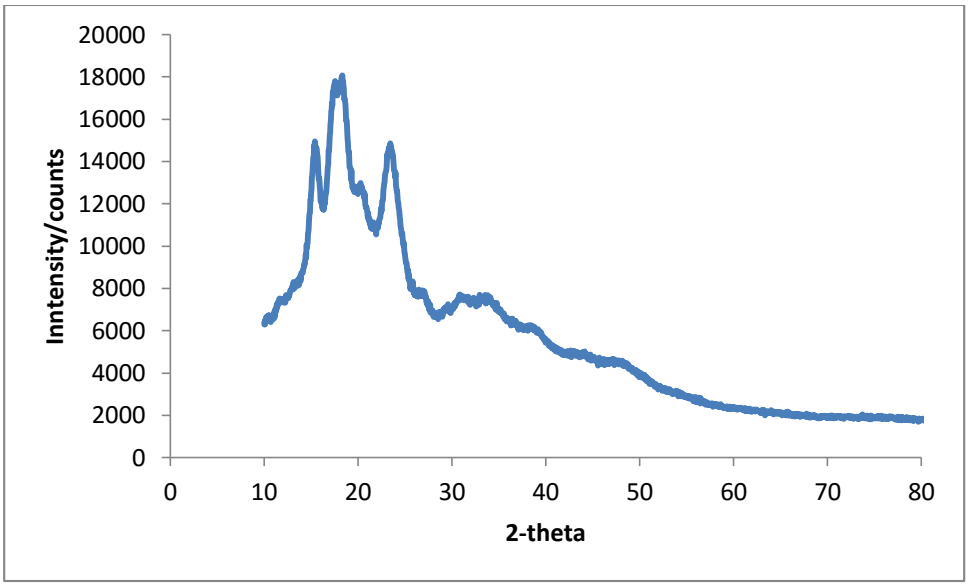

Figure 4. 19: Diffractograph of corn starch

Figure 4.19 has wide peaks at two theta 14.6°, 18.3° and 23.4° just like in the research of (Aytung, 2014). This implies that this covalently bonded compound has semi-crystalline nature in solid state. However it is not possible to establish existence of the basal and prism planes as normally recorded in the seven crystal types of; cubic, monoclinic, orthorhombic, tetragonal, trigonal and hexagonal. A crystal structure is characterized by unit cell, containing atoms in a specific spatial arrangement and a formula. Corn starch in not crystalline compound as seen from Figure 4.19 but exists as granules in solid state. This is probably why the XRD displays only three broad peaks at two theta 14.6°, 18.3° and 23.4°. The bigger peak at two theta 18.3° represent the granular formations in the 75 % amylopectin composites which was also observed by (Sarko *et al.*, 1976). The peak at 23.4° could be due to packing together of the amylopectin molecules in the composites as it compares with one of (Perez & Vergelati, 1987) at a similar angle. The shoulder on the 18.3° peak at two theta 14.6° could represent amylose molecules packed together. The three peaks above were also reported

in (Marta *et al.*, 2019) though at slightly shifted positions due to the thermal treatments on their starch.

4.3.1.2: Thermogravimetric analysis

Figure 4.20 shows the loss of mass of corn starch on TGA analysis.

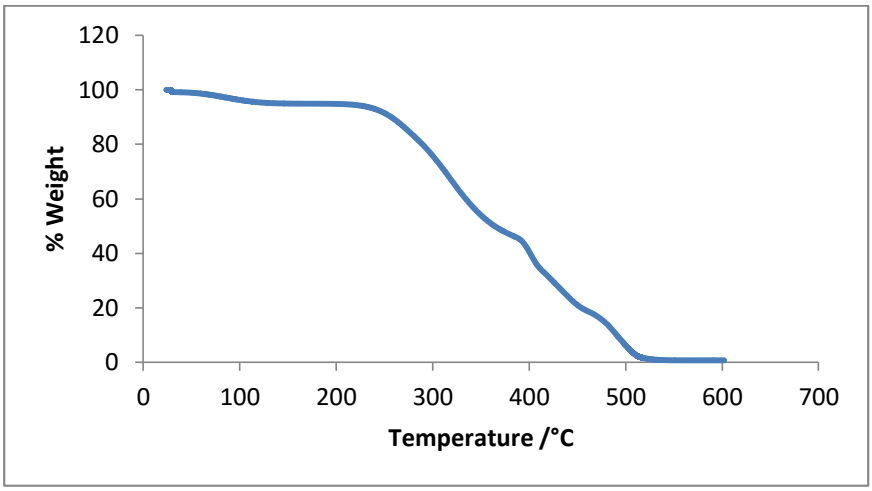

Figure 4. 20: TGA for Corn starch

This curve can be divided in three major sections as was also observed in the research of (Chagas *et al.*, 2018). The first section has very low percentage loss in mass up to around 250 °C. The next sector runs from 250 °C to around 520 °C before the curve flattens. Corn starch easily forms a gel in water due to inter and intra hydrogen bonding with water at low temperatures of up to 60 °C through a gelation process without loss in mass.

There is water desorption of about 5 % from around 60 °C to 100 °C which can be attributed to loss of all forms of water which compares well with the research of (Mano *et al.*, 2003). There is no loss of mass between 100 °C and 220 °C which can be attributed to retrogradation of both amylose and amylopectin polymer molecules that

tend to form suspensions due to extended hydrogen bonds between OH-6 and hemiacetal oxygen as also seen in the research of (Makalalu *et al.*, 2017). This is followed by about 95 % loss in mass from 250 °C up to about 520 °C in a degradation step.

This shoulder was also reported by (Mano *et al.*, 2003) which means the polymer molecules gelatinize by breaking down at α- 1, 4- hemiacetal oxygen joints up to 400 °C after which the small glucose molecules sublime. Starch gelatinization is a process of breakdown of intermolecular interactions between the molecules of amylose and amylopectin at solid state with heating which retrogrades into a gel over some time rearranging into granules. The formation of tetrahedral oxygen to water molecules with starch molecules generates the gelation of the polymer molecules.

4.3.1.3: SEM analysis

Picture on Plate 4.5 is of corn starch.

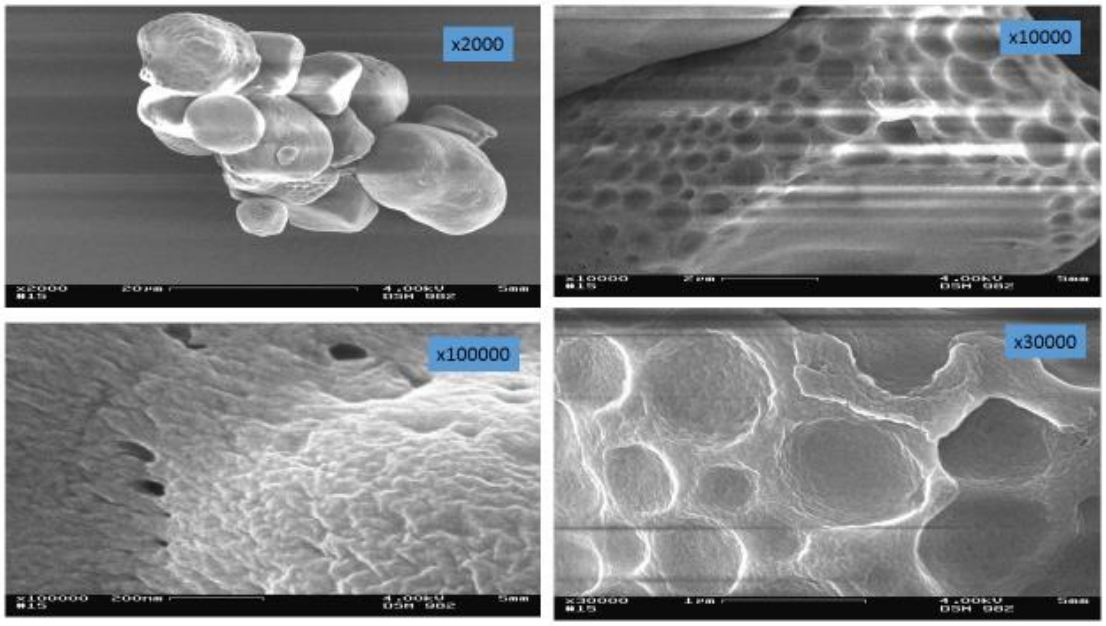

Plate 4. 6: SEM corn starch

Picture on Plate 4.5 shows the scanning electron microscopy of corn starch fine powder. The x2000 picture shows granules of irregular shape with some edges. This structure may be referred to as quasi-crystalline polymeric sugars of amylose and amylopectin chains. The smaller crystals could be representing the amylose chains while the larger ones are amylopectin units. The x10000 one shows small and large round spots which could be the pockets of crosslinks in both amylose and amylopectin respectively that absorb and store water and solutions. The x30000 picture clearly shows these pockets along with the OH crosslinks. The x100000 picture shows some porous holes that form in the structure. These pores trap solutions and generate an equilibrium with the pockets after removal from a solution enhancing both the amount and period over which the solution can be desorbed.

The corn starch developed crosslinks in the PVA material generating hydrogels. The irregular shapes seen in this picture are also observed in the research of (Marta *et al.,* 2019). The smaller pockets represent amylose while the bigger ones are amylopectin which is similar to the picture in research of (Rahul *et al.,* 2017) for corn starch and in line with another study (Tan *et al.,* 2017).

4.3.2 Characterization of PVA

Polyvinyl alcohol has form a layered polymer. The layers are held together by Van Der Waals forces. (Cuan-dian *et al.,* 2014) blended xylan which is derived from a hemicellulose with PVA which greatly improved its mechanical properties. This study cross-linked the PVA chains by corn starch molecules which introduced the hydrogels into the starch-PVA structure.

4.3.2.1: XRD analysis

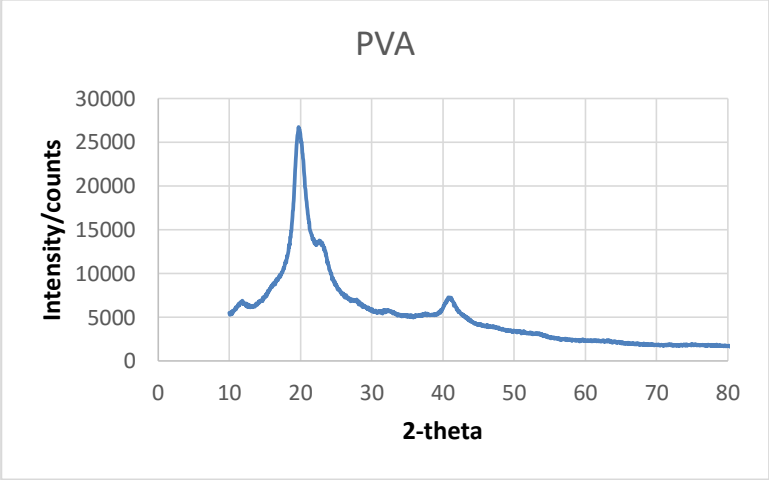

Figure 4. 21: Diffractograph of PVA

Like in the case of corn starch, PVA has a peak at two theta 20° and a small one at around two theta 41° which were also observed by (Kharazmi *et al.*, 2015). The peak at two theta 20° is usually observed in most solid compounds that have repeating pattern, occasionally referred to as semi-crystalline. This is not a crystalline inorganic compound however the peak at 19.8° as seen on Figure 4.21 provides evidence that the solid nature of this polymer which is made from ethanol and vinyl acetate. PVA has a main peak at two theta 19.8° whose d spacing is 4.4801Å and is consistent with semi-crystalline structure in (G'eminarda & Bouraya, 2000) research. This peak is identical to the one recorded by (Gulfam *et al.*, 2014), (Kaiwen *et al.*, 2016).

4.3.2.2: Thermogravimetric analysis

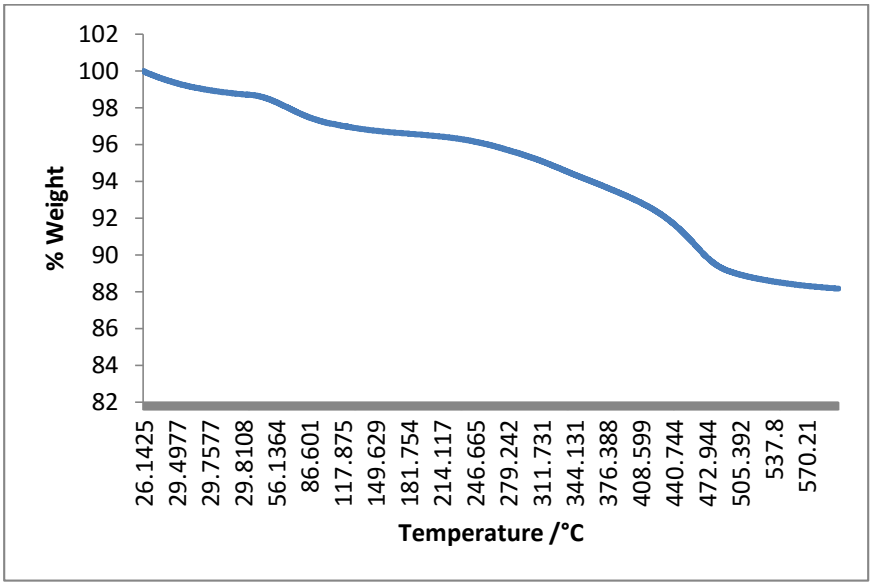

Figure 4. 22: TGA for PVA

There is steady reduction in percentage mass on Figure 4.22 which is similar to the one of (Chagas *et al.*, 2018). However it is possible to divide this reduction into 4 sections. The one from 26.1 °C to 71.3 °C, 71.3 °C to 262.9 °C, 262.9 °C to 456.8 °C then lastly 456.8 °C and beyond.

There is a loss in mass of 2 % up to 71.29 °C. This loss can be attributed to loss of moisture in the granules. The loss in mass from 71.29 °C to 262.97 °C of about 2 % represents the decomposition of the polymer followed by removal of the ethanol monomer molecules from the 262.97 °C to 456.79 °C. The final reduction in mass from 456.79 °C and beyond can be attributed to break down of the vinyl acetate polymer which is closely followed by a pyrolysis of the vinyl acetate monomers. This TGA compares with the one in the research of (Kaiwan *et al.*, 2016).

4.3.2.3: SEM analysis

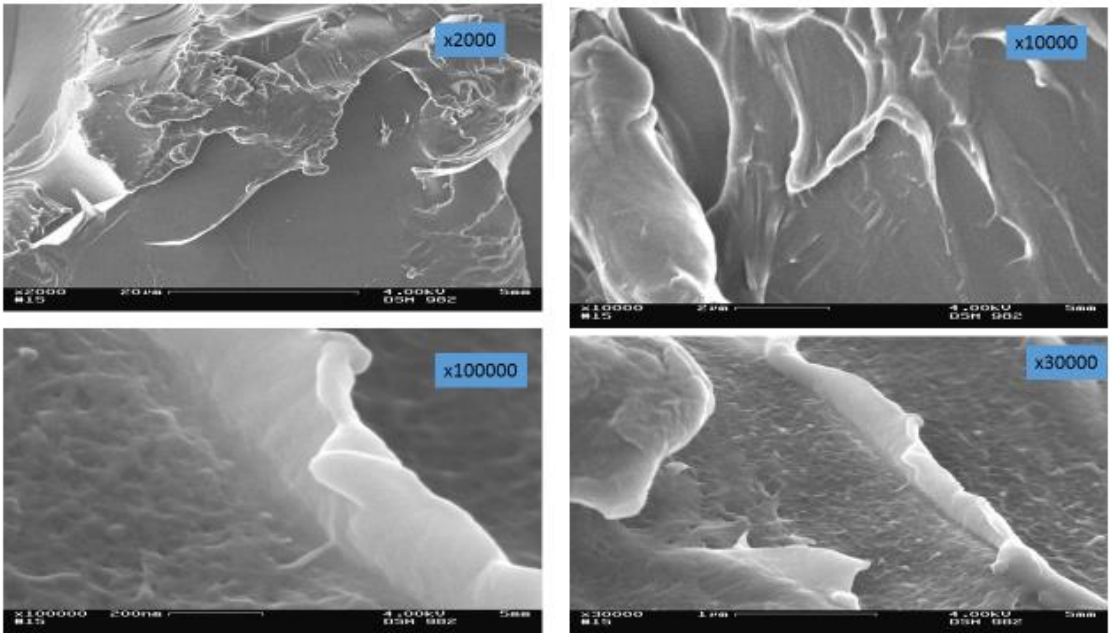

Plate 4. 7: SEM for PVA

The x2000 picture on plate 4.6 shows a polymeric solid. The x10000 picture shows presence of uniform structure in layers and homogeneous surface with ridges that represent the polymer layers. The x30000 picture shows homogeneous surface with layers that stretches from up to down could represent polymer chains with Van der Waals forces shown between the chains. The x100000 picture shows lighter regions that represent the interlayers and Van der Waals forces. There are ridges seen which could represent the polymer linkages which was also observed in (Shan *et al.*, 2011).

4.3.3 Characterization of gum Arabic

Gum Arabic is light brown crystalline solid with a polymeric structure of arabinogalactan polysaccharides and arabinogalactan proteins. These structures crosslink the polymers of starch to improve their hydrogel characteristic.

4.3.3.1: XRD analysis

XRD of the gum Arabic was performed and the diffractograph is given on Figure 4.23.

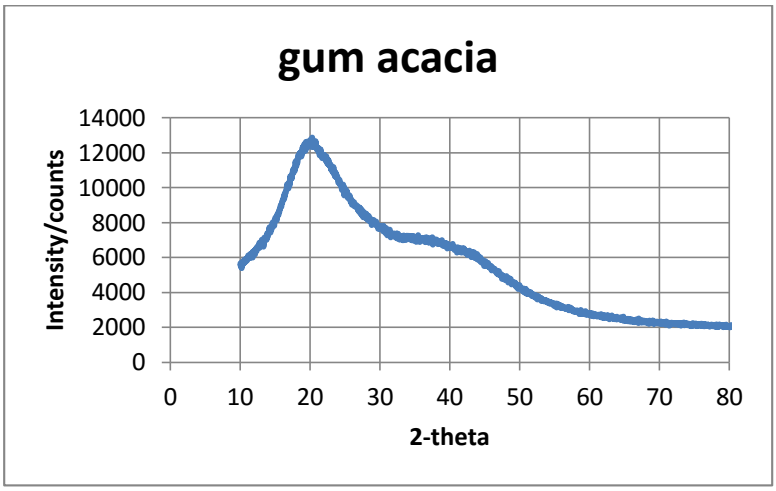

Figure 4. 23: Diffractogram for the gum acacia

The diffractograph has a broad single peak hence not easily defined on the two theta. This means it is not possible to place this molecule in a unit cell. This compound is not crystalline by any percentage. There is a two theta peak at 19.9° due to the solid nature and presence of the calcium, magnesium and potassium (Nafie *et al.*, 2012). The XRD shows that GA is an amorphous solid and it compares closely with that of (Gulfam *et al.*, 2014) with a two theta at 19.895° with a d spacing of 4.4375Å.

4.3.3.2: Thermogravimetric analysis

Thermogravimetric analysis of gum Arabic was performed to establish its level of resistance to temperature increase in case of outbreak of fires in fields where the coated formulas are used. Figure 4.23 shows the TGA of gum Arabic

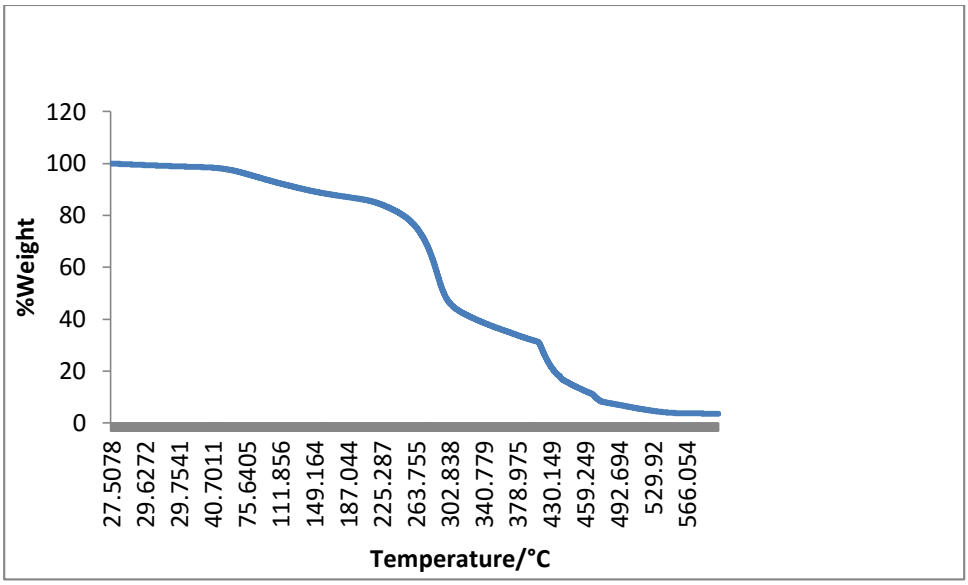

Figure 4. 24: TGA for acacia

Figure 4.24 can be divided into six sections; 27.51 °C to 68.2 °C, 68.2 °C to 242.94 °C, 242.94 °C to 324.52 °C, 324.52 °C to 408.67 °C, 408.67 °C to 485.66 °C, 485.66 °C and beyond. The TGA of the coating materials tells of the level of decomposition these products will have in the environment. For example should a fire raze through the farm after planting would one still plant without fertilizers in other words would the flame temperature break down the coat? This curve on Figure 4.24 is similar to the one reported by (Jamaludin *et al.*, 2017). There is no significant loss in mass up to 34.9 °C. The small loss in mass between 34 °C to 68.2 °C can be attributed to evaporation of moisture from the crystalline compound in a water desorption step also reported by (Mothe & Rao, 2000); (Shoralahi, 2004) and (Jamaludin *et al.*, 2017). There is however a significant loss of mass of about 19 % from 68 °C to 242.94 °C which could be due to the decomposition of the complex product into the polysaccharide and the protein residues and the degradation from 242.94 °C to 324.52 °C of about 40 % could be due to the decomposition of the polysaccharide molecules into glucose and the

decomposition of the aminoacids in the proteins. The loss in mass of around 30 % between 324.52 °C to 408.67 °C could be due to sublimation of the individual sugar monomers and 408.67 °C to 485.66 °C represent decomposition of protein molecules reaching a mass residue of about 5% a similar trend to in (Cozi *et al* ., 2009) research. Temperature of 485.66 °C and beyond represents sublimation of the residues.

4.3.3.3 SEM analysis for gum arabic

Plate 4.7 below shows the gum arabic morphology.

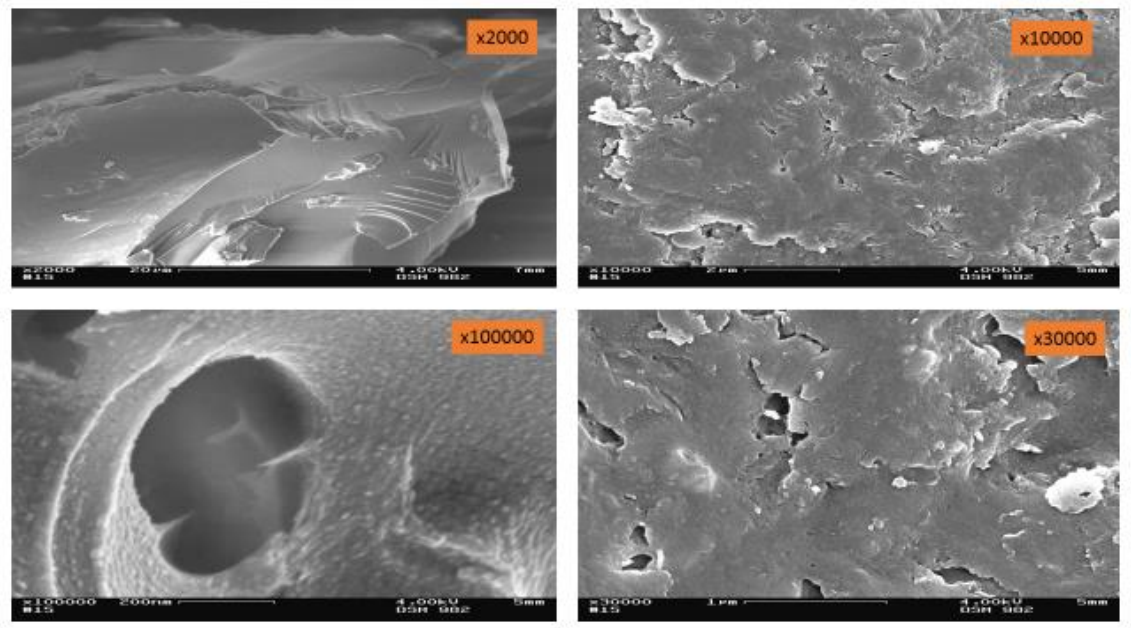

Plate 4. 8: SEM for gum acacia

The x2000 picture shows the morphology of amorphous solids. The x10000 SEM picture shows homogeneous phase of the hydrophilic seen as white ridges and hydrophobic parts of the complex. The ridges seen could be indication of intermolecular distances. The x30000 picture shows the pockets as pores on the surface. These pocket

unlike in starch are irregularly positioned and are fewer. The x100000 shows one of these pockets that trap water for desorption.

4.3.4 FTIR of the SAPs

Starch was polymerized separately with PVA and Gum Arabic. Whereas starch and gum Arabic contain polysaccharides PVA contains ethene and OH in its structure. Figure 4.25 shows combined FTIR for raw materials and one of the SAPs.

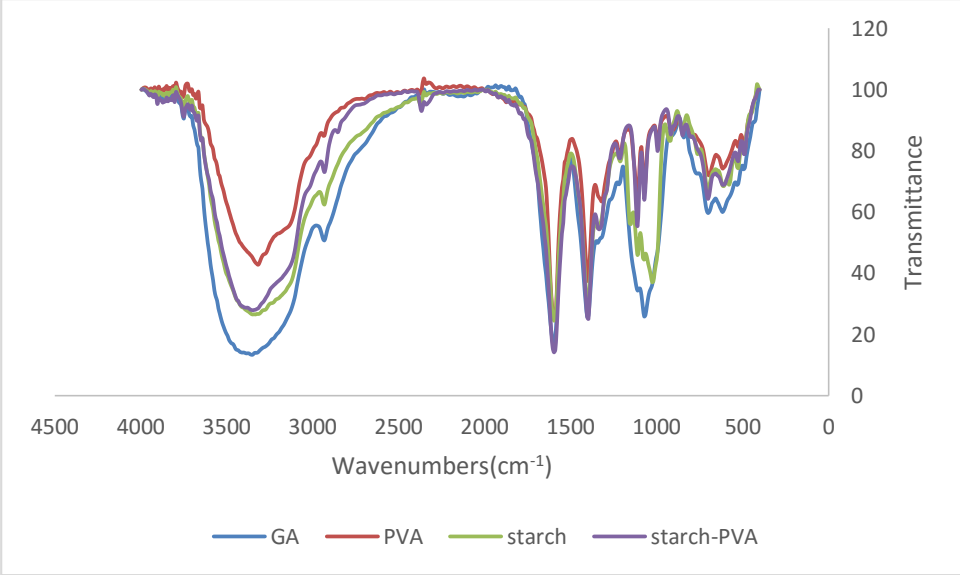

Figure 4. 25: FTIR combined spectrum for SAPs

The spectra for the four are similar. Corn starch and gum Arabic are both polysaccharides while PVA has C-C-O-H functional groups which are also found in the polysaccharides.-The IR should therefore show five spectral bands C=C, C-C, C-O, O-H and C=O. The peak on Figure 4.25 at 3400-3200 cm^{-1} of PVA corresponds to OH stretching also reported by (Kharazmi *et al.*, 2015). The peak at 3317 cm^{-1} is observed at slightly higher wavenumber of 3348.2 cm^{-1} in starch-PVA due to stronger hydrogen bonds formed between the starch and the PVA as also noted in (Kaiwan *et al.*, 2016).

Figure 4.25 of this spectrum but the peak at 500-600 cm^{-1} has a twin raising them to six. The peaks compare well with those found in the research of (Chagas *et al.,* 2018); (Daoub *et al.,* 2018)

The reaction between corn starch and PVA generated a new material starch-PVA. A study of the bands between 3600 cm^{-1} and 3000 cm^{-1} show a marked difference between the spectrum of PVA (Kharazmi *et al.,* 2015) and S-PVA which proves that a chemical reaction took place. Transmittance for PVA was around 40 for the band of O-H which reduced to around 30 when polymerized into starch-PVA. The reduction in transmittance implies an increase in absorbance that can only arise from increased free OH. The PVA formed crosslinks in the starch structure through the OH. Introduction of these OH crosslinks increased the free OH reducing transmittance. A similar trend is observed when we compare the spectrum of starch with that of starch-PVA and that of starch-GA. The spectrum bands at 1600 cm^{-1} and 1400 cm^{-1} do not show a lot of difference but the ones at 1200 cm^{-1} to 1000 cm^{-1} and 700 cm^{-1} to 500 cm^{-1} are largely affected by the formation of a SAP from the raw materials.

In conclusion, starch, gum Arabic, PVA are organic materials that can be polymerized to form strong films with crosslinks that can enable them to absorb large quantities of water. The absorbency of water would be improved if the starch is polymerized into the individual structures of PVA and GA.

4.4 Physical characterization of the coating materials

There are a number of polymer products that are used to hold solutions for a long period. They are extensively used in baby products like diapers and in sanitary towels.

The active ingredients are usually made from superabsorbent polymer materials. This study developed biodegradable (Trenkel, 2010) SAPs that are geared towards agricultural utility to reinforce the effect of the slow release fertilizer. The following physical tests were performed to test the efficiency of these SAP materials.

4.4.1 Water absorbency of the SAPs

Water absorbency was done to compare the capability of the starch-PVA and starch-GA to hold solutions up to their limits. The results of the study were recorded on Table 4.10

Table 4. 10: Water Absorbency

TIME	W1±SE	W2±SE
H0	2.2 ± 0.000^{IA}	2.067 ± 0.0333^{eB}
H1	4.3 ± 0.0577^{HA}	3.500 ± 0.0577^{dB}
H2	5.0 ± 0.000^{GA}	3.933 ± 0.0333^{cB}
H3	5.7 ± 0.000^{fA}	4.267 ± 0.0333^{bB}
H4	6.733 ± 0.033^{eA}	4.567 ± 0.0333^{aB}
H5	7.233 ± 0.033^{dA}	4.467 ± 0.0333^{abB}
H6	8.333 ± 0.0333^{cA}	4.4333 ± 0.0667^{abB}
H7	9.203 ± 0.0667^{aA}	4.5 ± 0.0577^{aB}
H8	9.033 ± 0.0333^{bA}	4.467 ± 0.0333^{abB}

Key: H= time in hours, W1=mass of starch-PVA, W2= mass of starch-GA, Mean values followed by the same capital letter(s) within the same column do not differ significantly from one another while mean values followed by the same small letter(s) within the same row do not differ significantly from one another (α=0.05, one-way ANOVA, Posthoc-Tukey-test), while the harmonic mean sample size, n=3.

Table 4.10 shows that the 2.2 g strip of starch-PVA absorbed water and increased its maximum mass of up to 9.2 g in 7 hours. There is a reduction at the 8^{th} hour to 9.0 g was noted which could be due to the saturated PVA beginning to dissolve into jelly. It takes 7.0 g water for PVA to reach its maximum equilibrium point. The starch-GA superabsorbent polymer strip of mass 2.1 g absorbed water up to 4.5 g in the same 7 hours. The amount of water absorbed was 2.4 g. Therefore starch-PVA absorbs 7.0g to

reach its equilibrium point which is more than the 2.4 g that is absorbed by starch-GA to its equilibrium. This is expected since starch-PVA has more open space between the polymer chain and hydrogen bonds of the OH crosslinks than in starch-GA. There is steady swelling of the starch-PVA from start to 7th hour. This is illustrated by significantly different mass from H0 to H8. In the case of starch-GA the values at the 5th and 6th hour are not significantly different just like at 4th and 7th hour which could be due to irregular water pockets formed by the OH crosslinks in the starch-GA structure. Lack of uniformity in the mass of water absorbed in starch-GA could be due to irregular sizes of the cross-linked pockets in its structure and the fact that GA structure does not have open space. Figure 4.26 shows the absorbency of water for the two saps.

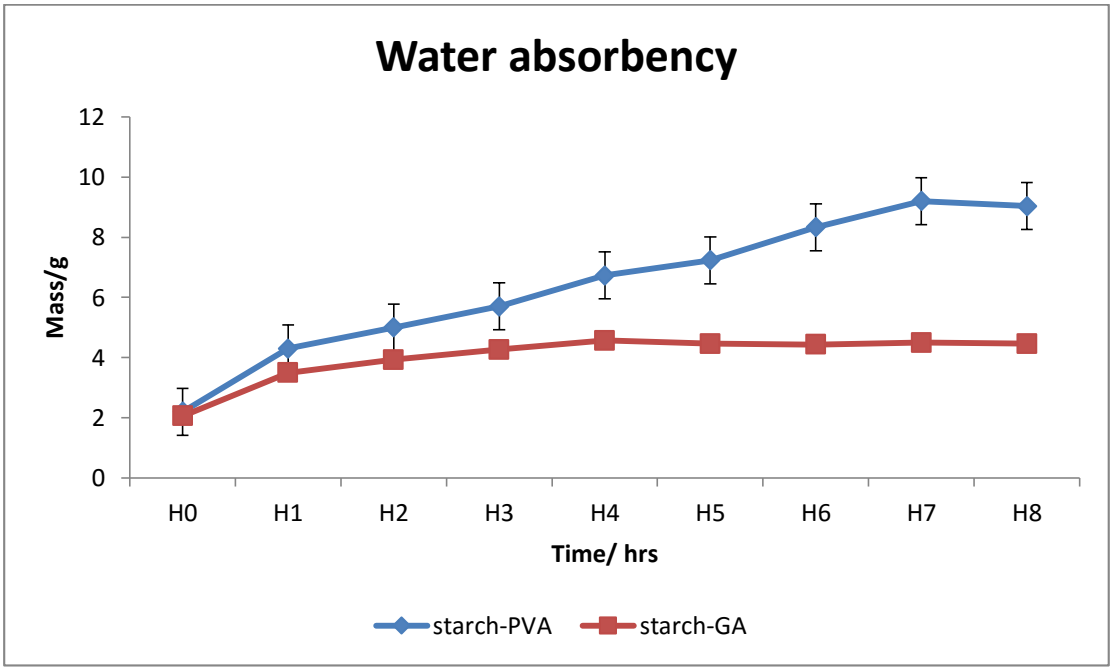

Figure 4. 26: Water absorbency

Key: H= time in hours.

The curves on Figure 4.26 on absorbency of each of the SAPs increased and reached a maximum after which a decrease in mass was recorded. The water absorbency of the first three hours between starch-PVA and starch-GA is not significantly different as shown by the error bars on Figure 4.26. From H3 the water absorbency between starch-PVA and starch-GA is significantly different with starch-PVA showing higher absorbency up to H7. Whereas starch-PVA shows a high saturation point at 7 hours, starch-GA reaches its saturation at only 4 hours. Crosslinking in starch-PVA trapped more water in addition to the water attached to the composite through hydrogen bonds but with reduced overall absorbency rate due to increased time to saturate. This is also observed in the research of (Ghazali *et al.,* 2017). (Zangi *et al.,* 2009) reported that urea fertilizer dissolved in water in about 5 minutes. From Figure 4.26 above starch-GA achieves this faster than starch-PVA. The water weight added to the SAPs can be equated to the number of pores that trap the water. These pores increase the water uptake to the coated fertilizers before slow diffusion into the plant on need takes place (Mohamad *et al.,* 2013) reducing the leaching of the nutrients. This finding was also reported in the research of (Ghazali *et al.,* 2009) on properties of Controlled-Release-Water Retention Fertilizer Coated with Carbonaceous-g-poly(acrylic acid-co-acrylamide) superabsorbent polymer.

Water absorbency into the CRFs involve the water penetration into the coating then slow penetration into the fertilizer to dissolve the nutrients and lastly penetration of the nutrients slowly out of the coating (Trinch & KuShaari, 2016). There is a lag time of about 5% of the release time before the nutrient solution is released out the fertilizer compound and a lag time of about a week for CRF in maize crop to start releasing

nutrients after the seed has germinated (Trinch & KuShaari, 2016). This reduces loss of nutrients to the soils before development of roots.

4.4.2 Water diffusivity

Water diffusivity is given as a linear relationship between the mass of absorbed water against time (Ghazali *et al.*, 2009) in the equation ln F=ln kt^n.

4.4.2.1 Water diffusivity for S-PVA

Water diffusivity was calculated from mass increase on the strips of SAPs. Table 4.11 compares the values of diffusivity and time for S-PVA and S-GA.

Table 4. 11: Water diffusivity for S-PVA

Time /minutes	lnT	Mass of H_2O in SR1(g) ±SE	$F=\frac{M_t}{M_0}$	lnF_{SR1}	Mass of H_2O in SR2(g) ±SE	$F=\frac{M_t}{M_0}$	lnF_{SR2}
M010	2.30	1.267 ± 0.033^{s}	0.174	-1.749	0.867 ± 0.033^{h}	0.334	-1.097
M020	2.71	1.667 ± 0.067^{r}	0.229	-1.474	1.000 ± 0.000^{g}	0.385	-0.955
M030	3.40	1.867 ± 0.033^{r}	0.256	-1.363	1.067 ± 0.033^{g}	0.410	-0.892
M040	3.69	2.167 ± 0.033^{q}	0.297	-1.214	1.333 ± 0.033^{f}	0.513	-0.667
M050	3.91	2.567 ± 0.033^{p}	0.352	-1.044	1.400 ± 0.058^{f}	0.539	-0.618
M060	4.09	2.633 ± 0.067^{p}	0.360	-1.022	1.733 ± 0.067^{e}	0.667	-0.405
M070	4.25	2.933 ± 0.033^{o}	0.402	-0.911	1.767 ± 0.033^{e}	0.680	-0.386
M080	4.38	3.100 ± 0.058^{o}	0.425	-0.856	1.900 ± 0.000^{d}	0.731	-0.313
M090	4.50	3.100 ± 0.000^{o}	0.425	-0.856	2.067 ± 0.033^{c}	0.795	-0.229
M100	4.61	3.500 ± 0.058^{n}	0.479	-0.736	2.367 ± 0.033^{b}	0.910	-0.094
M110	4.70	3.667 ± 0.033^{n}	0.502	-0.689	2.467 ± 0.033^{b}	0.949	-0.052
M120	4.79	3.933 ± 0.033^{m}	0.539	-0.618	2.600 ± 0.000^{a}	1	0
M130	4.87	4.033 ± 0.033^{lm}	0.553	-0.592	-	-	-
M140	4.94	4.200 ± 0.000^{kl}	0.575	-0.553	-	-	-
M150	5.01	4.333 ± 0.033^{k}	0.593	-0.523	-	-	-
M160	5.08	4.533 ± 0.033^{j}	0.621	-0.476	-	-	-
M170	5.14	4.800 ± 0.058^{j}	0.658	-0.419	-	-	-
M180	5.19	5.033 ± 0.033^{ij}	0.689	-0.373	-	-	-
M190	5.25	5.033 ± 0.033^{i}	0.689	-0.373	-	-	-
M200	5.30	5.133 ± 0.067^{hi}	0.703	-0.352	-	-	-
M210	5.35	5.333 ± 0.033^{h}	0.731	-0.313	-	-	-
M220	5.39	5.300 ± 0.000^{h}	0.726	-0.320	-	-	-
M230	5.44	5.333 ± 0.067^{h}	0.731	-0.313	-	-	-
M240	5.48	5.333 ± 0.088^{h}	0.731	-0.313	-	-	-

M250	5.52	5.833 ± 0.033^{g}	0.799	-0.224	-	-	-
M260	5.56	5.900 ± 0.058^{g}	0.808	-0.213	-	-	-
M270	5.60	6.067 ± 0.033^{efg}	0.831	-0.185	-	-	-
M280	5.63	6.200 ± 0.000^{ef}	0.849	-0.164	-	-	-
M290	5.67	6.133 ± 0.033^{ef}	0.840	-0.174	-	-	-
M300	5.70	6.333 ± 0.033^{cde}	0.868	-0.142	-	-	-
M310	5.74	6.567 ± 0.033^{cd}	0.900	-0.105	-	-	-
M320	5.77	6.733 ± 0.033^{c}	0.922	-0.081	-	-	-
M330	5.80	7.000 ± 0.058^{b}	0.959	-0.042	-	-	-
M340	5.84	7.300 ± 0.000^{a}	1	0	-	-	-

Key: M= time in minutes, SR1 is diffusivity for the PVA-SAP while SR2 is for GA-SAP, M_t=mass at time t, M_0= mass at equilibrium. Mean values followed by the same capital letter(s) within the same column do not differ significantly from one another while mean values followed by the same small letter(s) within the same row do not differ significantly from one another (α=0.05, one-way ANOVA, Posthoc-Tukey-test), while the harmonic mean sample size, n=3.

Table 4.10 shows the amount of water that the SAP absorbed over a period in minutes. The amount of water increases until the SAP begins to dissolve into jelly causing a reduction in mass. The S-PVA absorbs water from 1.3 g after 10 minutes to 7.3 g after 340 minutes. There are some timelines that do not show significant difference in diffusivity; namely the M70, M80, M90 denoted with letter o, M160, M170 with letter j, M210, M220, M230, M240 with letter h, M250, M260 with letter g and M280, M290 with letters ef. This could be caused by the position of the strip in the reaction vessel impairing free absorption of water. Starch-GA on the other hand starts at 0.9 g after the first 10 minutes and saturates at 2.6 g after only 120 minutes. This shows that starch-GA will be less effective at both the rate of absorbing plant nutrients and the rate of releasing them for plant uptake. The starch-GA product has a shortcoming since it saturates at only 120 minutes though an advantage as long as the amount of water in the farm is limited. On the other hand starch-PVA will hold more water which means it will

release the nutrients over larger period especially if the soils experience reduced amounts of water.

The diffusivity, Ln F relates with its Ln T in a linear manner. Therefore a plot of Ln F on y axis against Ln T is a straight line with an equation in the form; y= mx+c. From equation 3c, Ln F= Ln kt^n can be expressed as Ln F=n Ln kt, Hence, Ln F= n Lnt + n Lnk. Comparing this equation with y= mx+c; y=Ln F, m=n and c=n lnk. The data on Table 4.11 was used to plot the graph as Figure 4.27 which relates diffusivity with time.

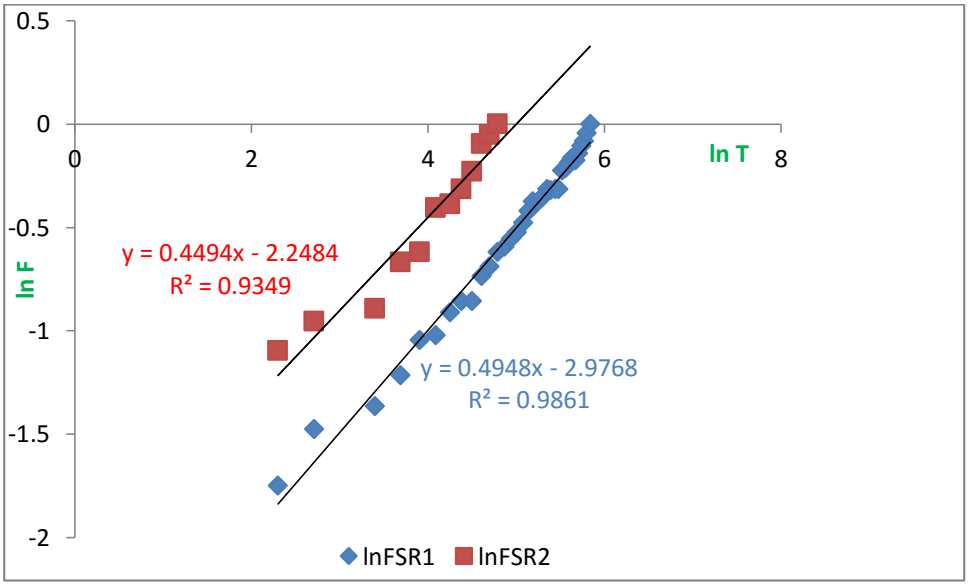

Figure 4. 27: Graph of Ln F vs Ln T

Key: axis is labeled in green

From this Figure 4.27, k for starch-PVA was calculated from the equation; y=0.4948x-0.29768; n, the slope= 0.4948, n Ln k= -2.9768, therefore 0.4948 Ln k= -2.976, Ln k = -6.016, hence $e^{-6.016}$= k= 0.00244.

While k for S-GA was calculated from the equation; y=0.4948x-0.29768; n, slope = 0.4494, n lnk= -2.2484, 0.4494 ln k= -2.2484, In k= -5.003; hence $e^{-5.003}$ = k = 0.00672. The information from Figure 4.27 is summarized into Table 4.12.

Table 4. 12: Kinetic water diffusivity summary of the SAPs

Sample	k/ $x10^{-3}$	n/$x10^{-1}$	Amount of water absorbed/g	Behavior
S-PVA	2.44	4.948	7.300±0.000	Fickian
S-GA	6.71	4.494	2.600±0.000	Fickian

Key: 0.5<n<1.0 nonfickian; n<0.5 fickian

Fickian behavior is important in describing diffusivity of solution in SAPs. Water diffuses into SAPs causing them to expand. This process involves moving of the water molecules into the hydrogel chains (Bamgbose, 2012). During swelling, movement of molecules increases which in turn increases the spaces between polymer chains (Ghazali *et al.,* 2017) in the SAP. Starch-PVA has a bigger n than starch-GA as observed on Table 4.12. This means there is increased entanglement and higher crosslinking in starch-PVA than in starch-GA which implies a reduction in space between the polymer chains in starch-GA. This crosslinking enables water to diffuse faster into its matrix composite causing bigger swelling and a larger water uptake, over a longer period of 6 hours. Both SAPs fall into the Fickian behavior considering the larger quantities of water that it absorbs. Starch-GA has a slightly lower n due to low volume of water it absorbs (Ghazali *et al.,* 2017). This could be due to the fact that the surface crosslinking in the S-GA is weak making it swell on the surface with dissolving. The arabinogalactan polysaccharide molecule has a supramolecular structure. In 0.1 % water solutions it forms associates of up to 8 nm-20 nm aggregates (Mikhailenko *et al.,* 2016) which are spherical and can increase to conglomerates of up to 200nm diameter when the concentration increases to 5 % also observed by (Mikhailenko *et al.,* 2016).

The research of (Mikhailenko *et al.,* 2016) showed that there was water molecules in the conglomerates probably attached to the molecule through hydrogen bonds and trapped

into the supramolecular structure through intermolecular interactions of the two saps The structure of arabinogalactan (Mikhailenko *et al.,* 2016) shows that the matrix formation between the gum arabic and starch had very few crosslinks generated through hydrogen bonding and that the pockets for trapping water are relatively large as is seen on x100000 of plate 4.7. This explains why the surface dissolves after picking only 2.4 g H_2O per 2 g starch-GA as opposed to starch-PVA that picks 7.1 g H_2O per 2 g.

Increased k of 6.71x 10^{-3} for starch-GA reflects increased polymer-solvent interactions. The liquid passes through starch-GA in 120 minutes which is faster than starch-PVA that takes 340 minutes (Ghazali *et al.,* 2017). Starch-PVA is therefore considered stiffer and less flexible for water to pass through which again suggests higher crosslinking in starch-PVA hence greater ability to trap and store the water or solution in addition to having increased swelling.

The mean value for starch-GA showed a reduction trend after around 30 minutes unlike in the case of starch-PVA that started showing dissolving process after 8 hours. This showed a saturation of the water absorptivity as the surface crosslinks began to dissolve uniformly. Water diffuses into the SAPs until the water pockets fill. The water then begins to desorb through the same SAP film. Mechanism of sorption often involves chemical reaction of the functional groups on the SAPs or mass-transport processes between the liquid phase containing the nutrients across the liquid film surrounding solid roots and the diffusion into the macro and micropores of the SAP and SRF2.

4.4.3 Water retention of the SAP

Water is very important in determining the ability of a plant to absorb nutrients. The water usually dissolves the formulas into solutions to enable the plants to absorb through the roots, stem or leaves. In the same manner a lot of water is known to leach nutrients away from the root zone reducing the availability of the nutrients and causing pollution to the soils and surface waterways. The ability of the coated-SRF2 to retain water was compared with non-coated-SRF2 and the data is displayed on Table 4.13.

Table 4. 13: Comparison of water retention

TIME	Water in SRF2 ± SE	Water in CRF3 ± SE	Water in CRF4 ± SE
D01	100.03 ± 0.033^{aA}	100.13 ± 0.067^{aA}	100.1 ± 0.21^{aA}
D03	99.57 ± 0.067^{abA}	98.33 ± 0.033^{bB}	99.7 ± 0.058^{aA}
D05	99.23 ± 0.088^{bcA}	95.2 ± 0.15^{cC}	96.13 ± 0.033^{Bb}
D07	98.77 ± 0.033^{cdA}	92.13 ± 0.033^{dC}	93.37 ± 0.067^{Cb}
D09	98.4 ± 0.058^{edA}	91.77 ± 0.088^{deC}	92.5 ± 0.15^{Db}
D11	97.67 ± 0.033^{fA}	91.57 ± 0.033^{dfC}	92.27 ± 0.067^{deB}
D13	97.4 ± 0.058^{fgA}	91.27 ± 0.033^{efC}	92.17 ± 0.067^{defB}
D15	97.3 ± 0.058^{fgA}	90.83 ± 0.033^{fgC}	92.03 ± 0.033^{defB}
D17	97.17 ± 0.033^{fghA}	90.6 ± 0.058^{ghC}	91.8 ± 0.15^{efB}
D19	96.97 ± 0.033^{fhA}	90.4 ± 0.00^{hiC}	91.67 ± 0.13^{fgB}
D21	96.67 ± 0.033^{hiA}	90.1 ± 0.058^{ijC}	90.97 ± 0.033^{ghiB}
D23	96.27 ± 0.088^{ijA}	89.83 ± 0.033^{jkC}	90.97 ± 0.033^{jihB}
D25	96 ± 0.058^{iA}	89.6 ± 0.058^{ijC}	91 ± 0.10^{ghiB}
D27	96.03 ± 0.038^{iA}	88.73 ± 0.12^{mC}	90.67 ± 0.033^{ijkB}
D29	95.37 ± 0.033^{kA}	88.3 ± 0.10^{nC}	90.47 ± 0.033^{jklB}
D31	95.2 ± 0.00^{klA}	87.83 ± 0.033^{oC}	90.3 ± 0.058^{klB}
D33	94.73 ± 0.12^{lmA}	87.37 ± 0.088^{Pc}	90.13 ± 0.12^{Mc}

Key: D= time in days, Mean values followed by the same capital letter(s) within the same column do not differ significantly from one another while mean values followed by the same small letter(s) within the same row do not differ significantly from one another (α=0.05, one-way ANOVA, Posthoc-Tukey-test), while the harmonic mean sample size, n=3.

The amount of water retained increased with increase in time for all the days of study as is seen on Table 4.13. The SRF decreased from 100.0 g to 94.7 g in 33 days retaining 5.3 g of water. The CRF3 decreased from 100.1 g to 87.4 g retaining 12.7 g water and CRF4 from 100.1 g to 90.1 g retained 10.0 g. More water was retained by coated SAPs because the SAPs have ability to diffuse in water and trap it into the sacks built by hydrogen bonds between the water and the OH of the SAPs forming hydrogels. CRF3 retains more due to its structure that has a higher capacity to hold larger quantities of water as seen on Figure 4.28 that compares these trends.

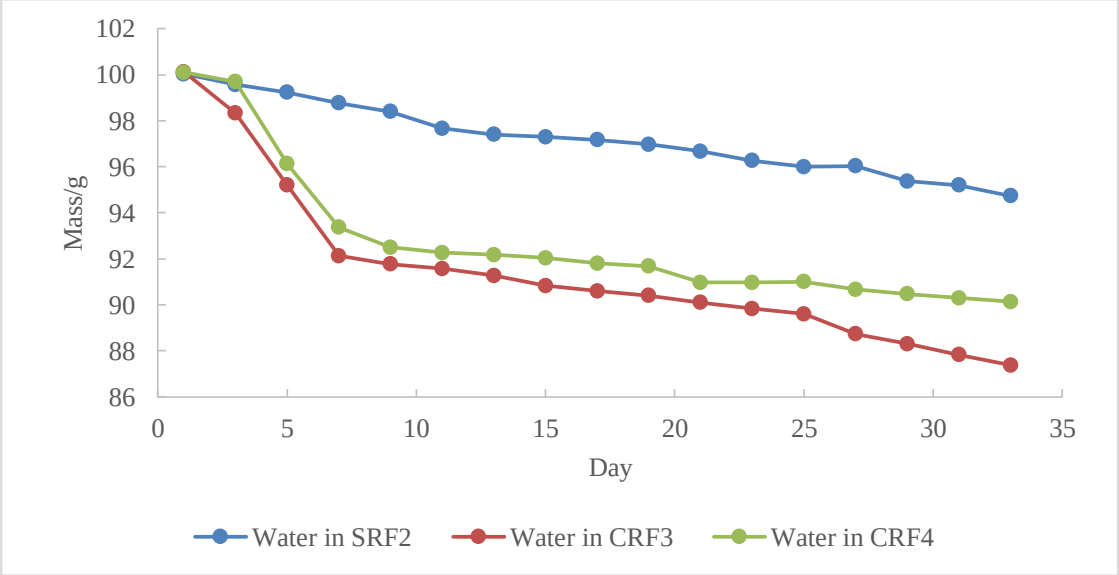

Figure 4. 28: Comparison of mass of water in products in soil

Figure 4.28 shows that CRF3 has higher retention of water followed by CRF4 and lastly SRF2. The curve for CRF3 drops from start and remains lower than CRF4 up to the 33rd day. The difference between that of CRF3 and CRF4 is generally small up to day 25 when CRF3 shows a bigger increase in retention. At this point it could that the CRF4 has started peeling off the SRF2 reducing the retention by a bigger factor than CRF3. The curve of SRF2 does not show an equilibrium point. The SRF2 starts to break up at a

point when it picks more water that it can retain which continuously increase the number of SRF2 particles hence the running without an equilibrium.

The magnitude of the retention from Table 4.13 was put on a column of Figure 4.29 for easy comparison.

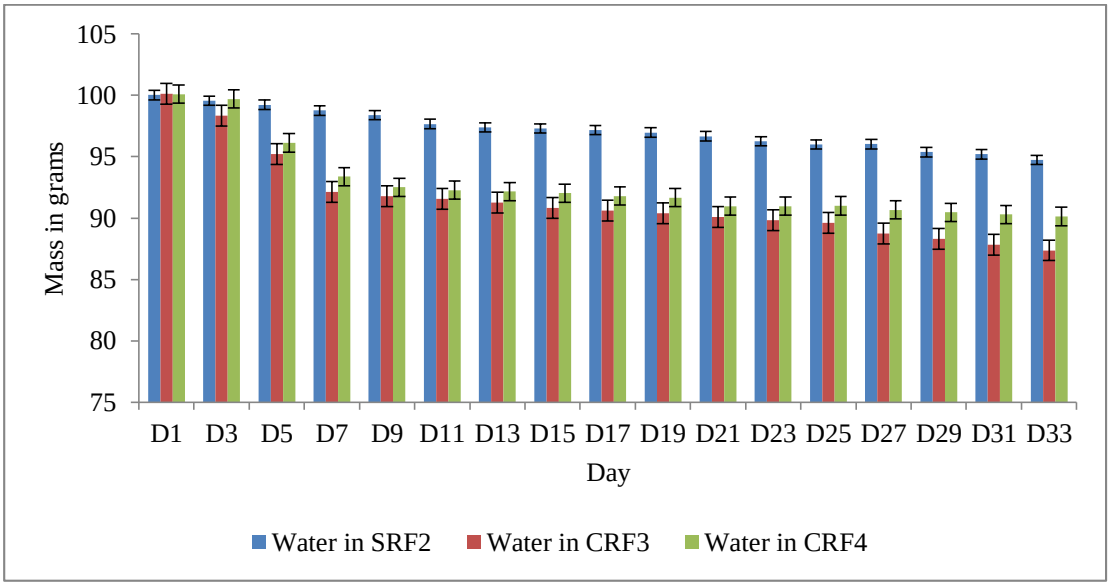

Figure 4. 29: Column of water retention

Figure 4.29 shows the differences between the product's water level retentions. The water retention for up to the 3rd day is similar for all the formulas. From the 3rd day to the 33rd day, the water retention for SRF2 is significantly different from that of CRF3 and CRF4 as is seen on error bars on Figure 4.29. The water retention for CRF3 and CRF4 is not significantly different between the 5th and 25th day beyond which the treatments are significantly different. The steady decrease in the mass of contents in SRF2 is evident. The organoclay continues to absorb water until it begins to break down. However the column for CRF3 and CRF4 reduces after the third day. CRF4 shows another steady decrease that can be attributed to the quick filling of the cross-linked space within the structure. The 21th, 23rd and 25th days do not show changes in

amounts absorbed that can be explained by the logging of the water spaces in the structure. The leveling at the 31st and 33rd day can be attributed to development of equilibrium between the water in the soil and that in the starch-GA structure. The columns of CRF3 differ significantly from that of CRF4 from day 25. This could be due to the large number of the OH crosslinks on the starch-PVA structure that allows more water to be absorbed which reduces the possibility of an equilibrium being set. This confirms that starch-PVA is a more effective and efficient than starch-GA. Picture on plate 4.8 shows some of the products that were reclaimed from the planting tins at the end of study. The row of CRF3 shows that the product in week 1 and week 6 are similar. Both have soil covering the product. This soil is attached to the starch-PVA jelly giving it long time protection. Week 13 still shows some soil texture on the product. While the CRF4 shows some soil cover on the week 2 product, after which the SAP did not hold the soil. The products had shaded off a lot of the coat with only a small film cover holding the SRF2.

Plate 4. 9: Some of reclaimed products from tins at end of study

The CRF3 formulas for weeks 1, 6, 10 and 13 have soil particles attached on starch-PVA. This confirms that the formula remained intact over the period of study. In the case of starch-GA we notice presence of soil particles on only week two of the formula. However the formula is intact providing evidence that the coating film remained on up to week 12. The SRF2 formula breaks down into smaller pieces from week 5 which increases the surface area for desorption of nutrients.

The SAPs have capacity to absorb, store water and release water with the nutrients in a slow manner with a trend similar to that of (Ghazali *et al.*, 2017). As illustrated on Figure 4.28, starch-PVA has a sharp uniform absorption trend in the first 7 days followed by slow uniform absorption up to 33 days. In the first 7 days the starch-PVA structure absorbs a lot of water causing larger stretches due to the high level of crosslinking formed through hydrogen bond interactions. After the 7^{th} day the structure develops an equilibrium that consists of a desorption rate that is slightly lower than an absorption rate. In the case of starch-GA, there is a striking difference between the 5^{th} and the 7^{th} day as observed on Figure 4.28. This is probably due to breakdown of the arabinogalactan supramolecular structures into polymers which opens the pores rapidly letting in large quantities of water. After the 7^{th} day the arabinogalactan structures develop an equilibrium shown as a slower rate of absorption.

Figure 4.28 for water retention of SRF2 is different from those of the coated SRFs. There is uniform increase in absorption of water into the SRF2 product and the amount absorbed is significantly low as compared to the coated products. In 33 days SRF2

absorbs only 5.5 g water per 2 g SRF as compared to starch-PVA and starch-GA that absorb 11.1 g and 10.1 g per 2.2 g products respectively. The extra 5.6 g for starch-PVA and 4.5 g for starch-GA was then absorbed by the coating SAPs. These final values show that starch-PVA is a better SAP than starch-GA as it shows a higher swelling capacity.

4.4.4 The kinetics of the products

The sorption of the SAPs and the fabricated products were tested on various sorption models to establish their kinetics in dissolution of nutrients into water and soils. The pseudo first order equation; $\frac{dq_t}{dt}$ = k_1 (q_e-q_t) limits into the linear form, Ln (q_e-q_t) = Ln q_e- k_1t where q_e is sorption capacity at equilibrium, q_t is sorption capacity in mg/g at time t, in minutes and k_1 is the rate constant for the pseudo first order. A plot of Ln (q_e-q_t) against time should give a straight line, though in real sense the intercept is never In q_e as expected (Ho & McKay, 2002).

After integration the pseudo second order, $\frac{dq_t}{dt}$ = k_1 (q_e-q_t)^2 generates the linear form of $\frac{t}{q_t} = \frac{1}{kq_e^2} + \frac{1}{q_e}t$. A plot of $\frac{t}{q_t}$ against t gives a linear relationship in which $\frac{1}{q_e}$ is the slope while $\frac{1}{kq_e^2}$ is the intercept.

4.4.4.1 Kinetics of water absorption into the SAPs

The nature of absorption of water and nutrients from the SAPs describes the rate of sorption through the SAPs. The dissolution of water from the SAPs was compared between starch-PVA and starch-GA. Table 4.11 was converted into table on Appendix 21 that was fitted into the pseudo first and second order, whose plots are seen on Figure 4.30 for pseudo first order and Figure 4.31 for pseudo second order respectively.

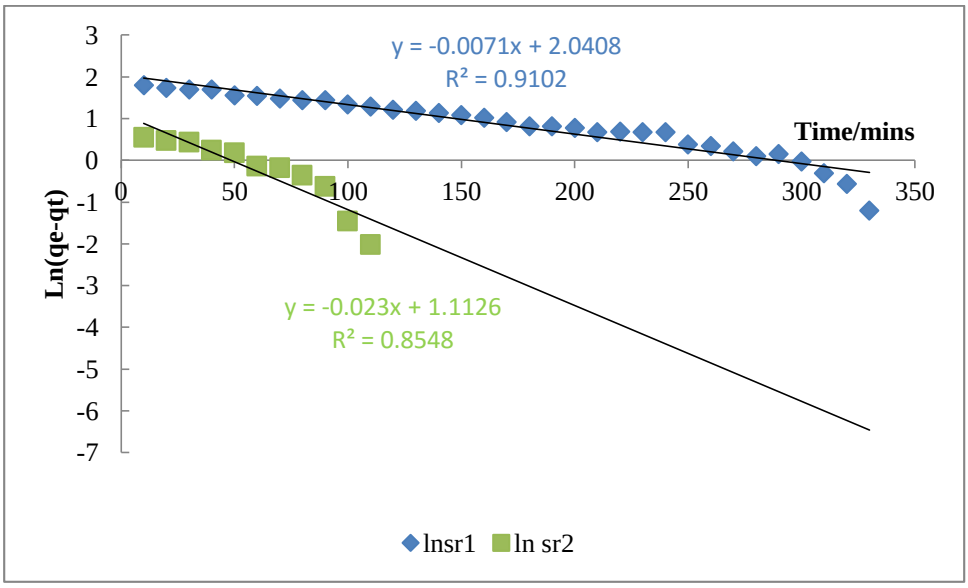

Figure 4. 30: Correlation curve for pseudo first order for SAPs

Key: SR1 is data for starch-PVA and SR2 is data for starch-GA

The two lines are characteristic of pseudo first order reactions. Starch-PVA has a smaller k_1 value than starch-GA. This curve compares well with the one reported by (Ho & McKay, 2002) in the research on sorption of Cu^{2+} ions on peats. For the pseudo second order, the two linear graphs are shown on Figure 4.31.

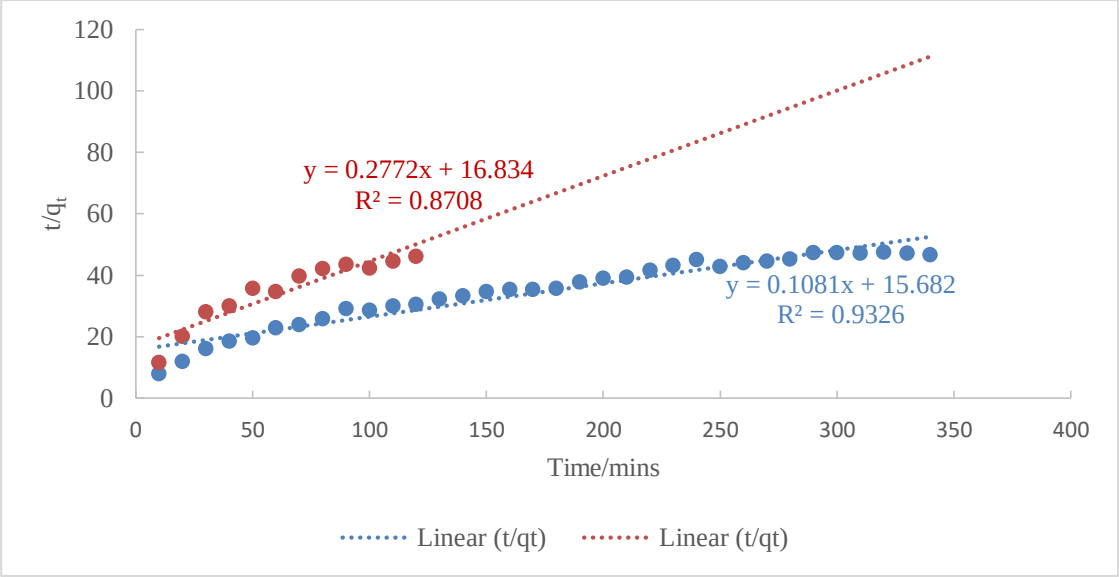

Figure 4. 31: Correlation curve for pseudo second order rate for SAPs.

Again the starch-PVA has a smaller k_2 than starch=GA. In the research of (Ho & McKay, 2002) on kinetic models for sorption of copper^{2+} ions onto peats, his pseudo first and second order reaction rates compare well with Figure 4.31. The starch-PVA shows a higher R^2 correlation of 0.9326 which supports the previous argument that starch-PVA is a more suitable SAP than starch-GA.

Table 4. 14: summary of pseudo kinetics sorption

Sample	k_1	R^2	k_2	R^2
S-GA	0.023	0.8548	0.005	0.8708
S-PVA	0.007	0.9102	0.001	0.9326

The correlation values for k_1 are slightly lower than of k_2 but the k_1 values are much bigger than those of k_2. This implies that the sorption of water to the SAPs fit better in the pseudo first order kinetics due to the large k values for pseudo first order than for pseudo second order. This finding compared well with the work of (Rashidzadeh *et al.*, 2015).

4.4.1.2 Rates of water absorption into the products

Table 4.14 gives the relationship between R^2 and rate for the products fabricated.

Table 4. 15: Comparison of rate constants for SAPs

Treatment	SRF2	CRF3	CRF4
Rate/gday^{-1}	0.3075	0.6143	0.5056
R^2	0.9795	0.7818	0.6961

The rate of uptake of water is highest in CRF3 followed by CRF4 which demonstrates that CRF3 has larger OH crosslinks and pockets to store the water. The crosslinks enable it to attract and interact with water molecules easily. The absence of hydrogels in SRF2 makes it absorb less amount of water however this uptake has higher correlation value since it is not interfered with unlike those of SAPs that are affected by the uniformity of the SAP coating. This could mean that the absorption of water by starch-PVA and Starch-GA should be fitted into pseudo first order kinetics.

4.4.4.3 Kinetics of release of nutrients into water

Release of nutrients from fertilizer products is controlled by the immediate environment. Those which are encapsulated in clay minerals desorb through the pores of the layers. The rate of release of nutrients was calculated from a graph of the nutrient released as a gradient for the 30 days in the simulations in water. Table 4.16 gives the values of rate of release of nutrients in $gL^{-1}day^{-1}$. The data in these tables were retrieved from Figures 4.51, 4.53, 4.55 for the 50-50 products, Figures 4.57, 4.59, 4.61 for the 70-30 products and lastly Figures 4.63, 4.66, 4.69 for the maize crops.

Table 4. 16: Table of rate of 50-50 products in gday-1

	NPK	SRF1	SRF2	CRF1	CRF3	CRF2	CRF4
Nutrient	50-50	50-50	70-30	50-50	70-30	50-50	70-30

NO_3^-	0.0087	0.0085	0.0074	0.0087	0.0065	0.0085	0.0069
$H_2PO_4^-$	0.0010	0.0010	0.0010	0.0006	0.0009	0.0007	0.0009
K^+	0.0016	0.0013	0.0013	0.0010	0.0011	0.0010	0.0012

Table 4.16 displays significant difference between the rate of release NO_3^-, $H_2PO_4^-$ and K^+ in NPK and the rest of the treatments. Other than $H_2PO_4^-$, both NO_3^- and K^+ have higher rate of release from NPK which is explained by the nature of release. NPK dissolves in water while SRF desorb through the pores on the surface of the organoclay mineral. The coated SRF absorbs the nutrients through the superabsorbent polymers and later release them into the water.

SRF2 has higher rate of release than the coated formulas as is evident on Table 4.16. The rate of release of coated formulas is lower because of the effect of the SAPs which absorb the solutions with nutrients into the hydrogel sacks first then into the formula before slowly releasing the nutrients into the water at equilibrium. This trend is observed in the release of both $H_2PO_4^-$ and K^+. Table 4.16 shows some difference between release of nutrients in the 50-50 products and the 70-30 ones. For instance, N-SRF2 shows a slower rate of release of 0.0074 $gL^{-1}day^{-1}$ than N-SRF1 which is 0.0085 $gL^{-1}day^{-1}$. Similarly N-CRF3 has a slower rate of release of 0.0065 $gL^{-1}day^{-1}$ than N-CRF1 which was 0.0087 $gL^{-1}day^{-1}$. Lastly N-CRF4 shows lower rate of release of 0.0069 $gL^{-1}day^{-1}$ than the N-CRF2 that is 0.0087 $gL^{-1}day^{-1}$. The slower release in the 70-30 formulas could be attributed to better intercalation in the 70-30 products due to more uniform pillaring of the layers. This means apart from being able to populate more nutrients into the 70-30 product, you expose larger pore surface area as seen from Figure 4.18 which represent the BET/BHJ columns. This is also supported by the isotherm on Figure 4.17 of MOC2 which does not have reversibility between adsorption

and desorption and illustrates higher number of closed pores which in turn reduces the adsorption of the nutrients.

CRF4 releases at a faster rate than CRF4 which is due to the higher level of crosslinks in CRF3 that enable it to retain the water and nutrients for longer periods as is supported by its higher water absorbency on Table 4.10.

Again the slower rate of CRF3 and CRF4 as compared to CRF1 and CRF2 could be due to higher efficiency in intercalation of the MOC2 that produced the 70-30 products. Generally Table 4.16 shows slower release of $H_2PO_4^-$ than the other nutrients. This can be attributed to the strong attractions between $H_2PO_4^{-1}$ and K^+, Ca^{2+} in the NPK-fertilizer used in the study which is countered by the long time the SRF remains in the soils due to its slow release nature. This is an advantage for the 70-30 product considering that phosphorus is a limiting factor for fertilizers in soils. $H_2PO_4^-$ absorption increases with higher soil pH (Owino, 2010) that is not easy to achieve due to acid rains and over use of acidic based fertilizers like CAN, DAP, SSP and TSP. Like in the case of nitrogen the R^2 of the 50-50 products of phosphorus is higher than that of the 70-30. This means for a given day the amount of nutrients dissolved from 50-50 is more that of 70-30 which again implies that the 70-30 formula is a slower release product.

It is also worth noting on Table 4.16 that the rate of release of K^+ is higher than of $H_2PO_4^-$ but lower than the one of NO_3^-. Potassium salts are very soluble, hence easily desorbs through the phyllosilicate sheets of the multifunctional organoclay. This

coupled with the interactions between NO_3^- and $H_2PO_4^-$ make it significantly easier for K^+ to be desorbed.

As for the kinetic models of release, the 50-50 and 70-30 treatments in deionized water were tested to see if they fit into the first order kinetics. The data on Appendix 22 was used to draw Figures 4.32 and 4.33. Figure 4.32 fitted the release data of 50-50 into the pseudo first order while Figure 4.33 fitted the data in pseudo second order.

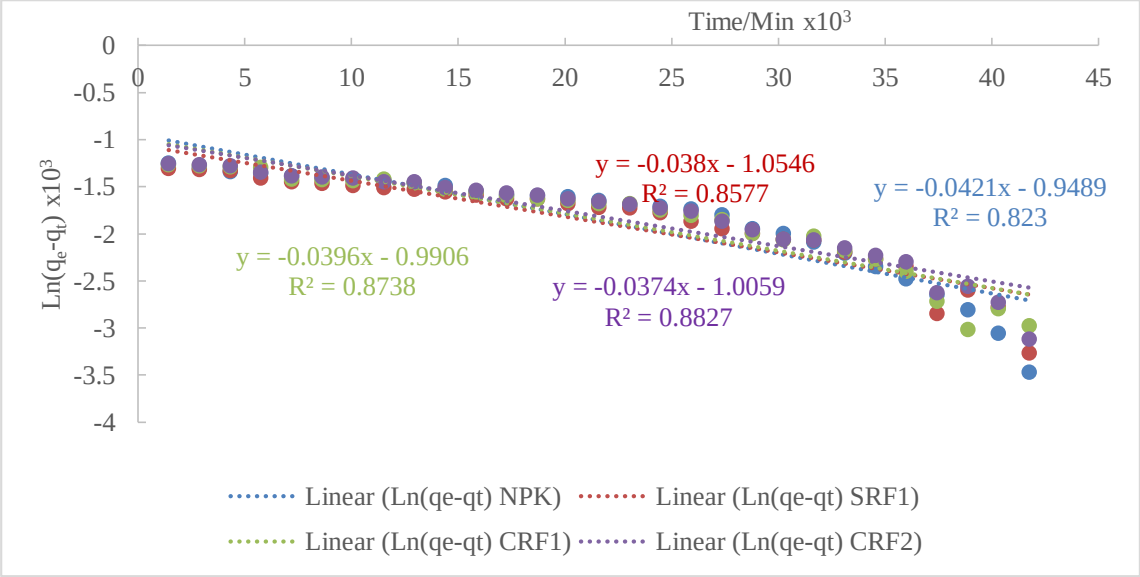

Figure 4. 32: Graphs for pseudo first order NO_3^- in 50-50

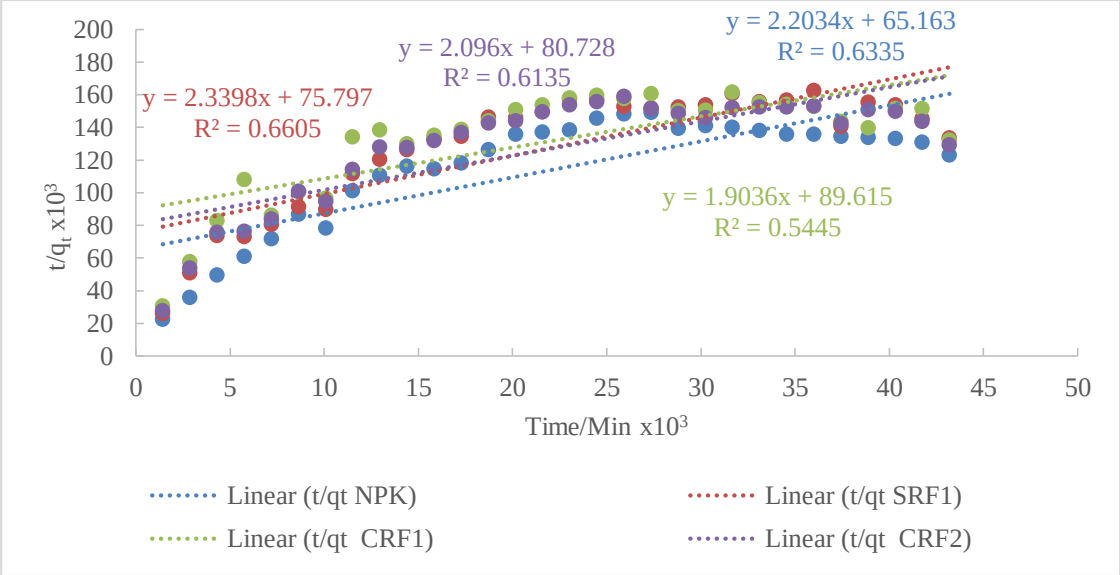

Figure 4. 33: Graphs for pseudo second order NO_3^- in 50-50

The graphs for the release of nutrients on Figure 4.32 are characteristic to those of pseudo 1st order even though the R^2 values are low. There is close correlation in R^2 values for SRF and CRFs. These R^2 values are higher than of NPK which is 0.823. This could be explained by the nature of the dissolution in the formulas. Whereas NPK formula dissolves throughout the 30 days, the SRF desorbed through the pores of the multifunctional clay sheets for about 23 days before it started dissolving. The coated formulas showed slightly higher R^2 values than the SRF1. The nutrients in the coated formulas desorbed first through the starch-PVA and starch-GA then through the pores of the clay sheets before dissolving.

Figure 4.33 shows the curves when NO_3^- release was fitted into pseudo second order. The points have a maximum at around the 20th day. The release of NO_3^- from the formulas does not fit into the pseudo second order kinetics sorption since the isotherms do not show possibility of an interception at any point in addition to having very low correlation values.

The data on Appendix 23 was used to draw the isotherms of Figure 4.34 for the pseudo first order kinetics and Figure 4.35 for the pseudo second order kinetics of $H_2PO_4^-$ for the 50-50 formulas.

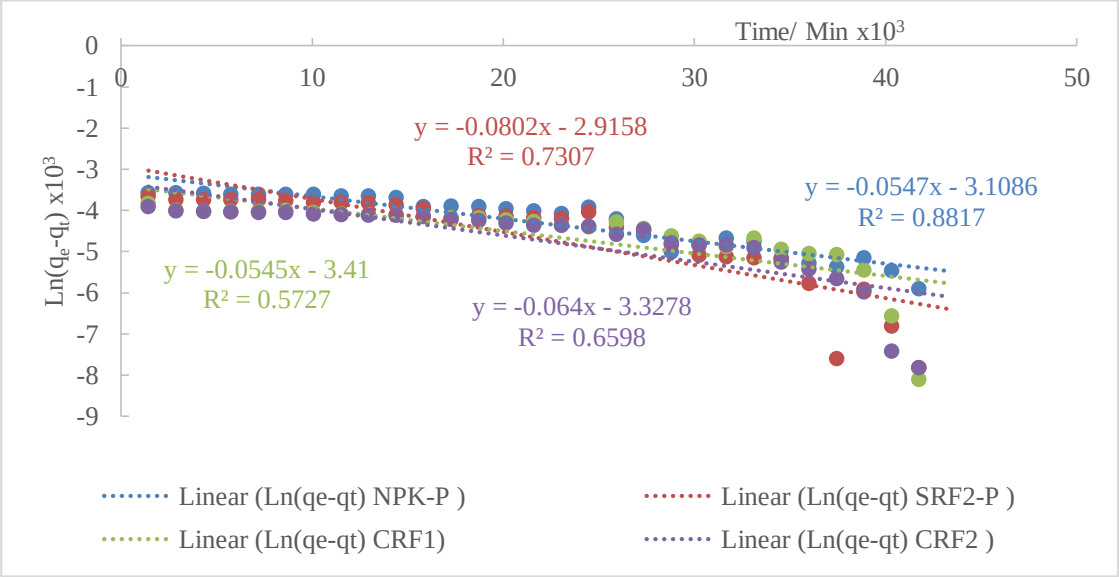

Figure 4. 34: Graphs for pseudo first order $H_2PO_4^-$ in 50-50

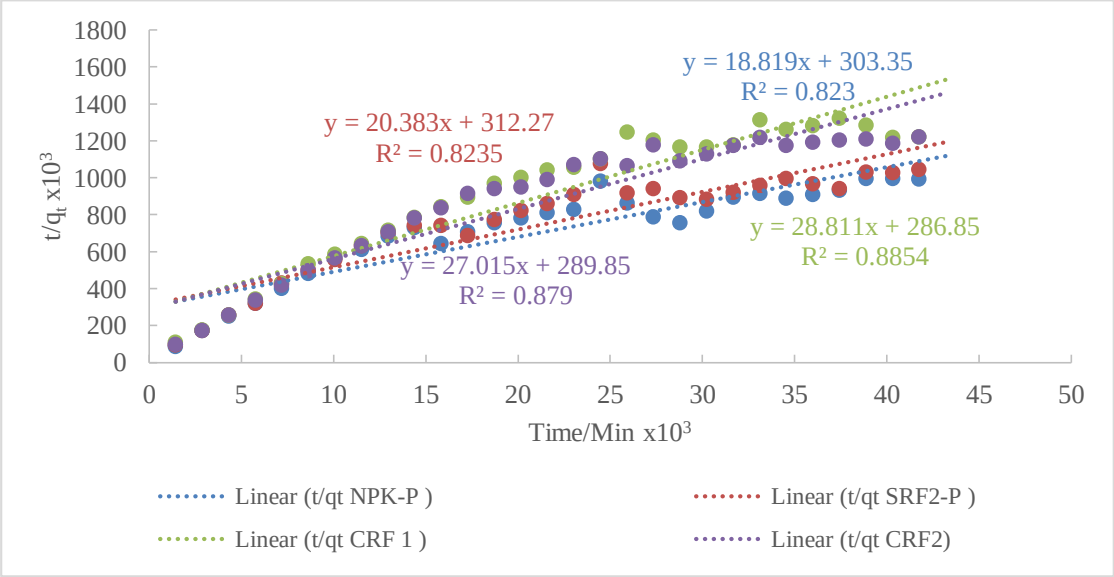

Figure 4. 35: Correlation curve for pseudo second order $H_2PO_4^-$ in 50-50

The R^2 value for CRF1-P on Figure 4.34 is lowest which could be due to rapid dissolving of the starch-GA at day 28 which affects the dissolution rate for all the days. The isotherms on Figure 4.35 are characteristic to those of pseudo 2nd order. The R^2 values show good correlation and all intercept t/q_t axis at about 215. The graphs of coated products have larger gradients which is normal for slow release formulas.

The data on Appendix 24 was prepared to analyze the pseudo first and second order kinetics of potassium 50-50. The data on this table was further used to draw the isotherms on Figures 4.36 and 4.37.

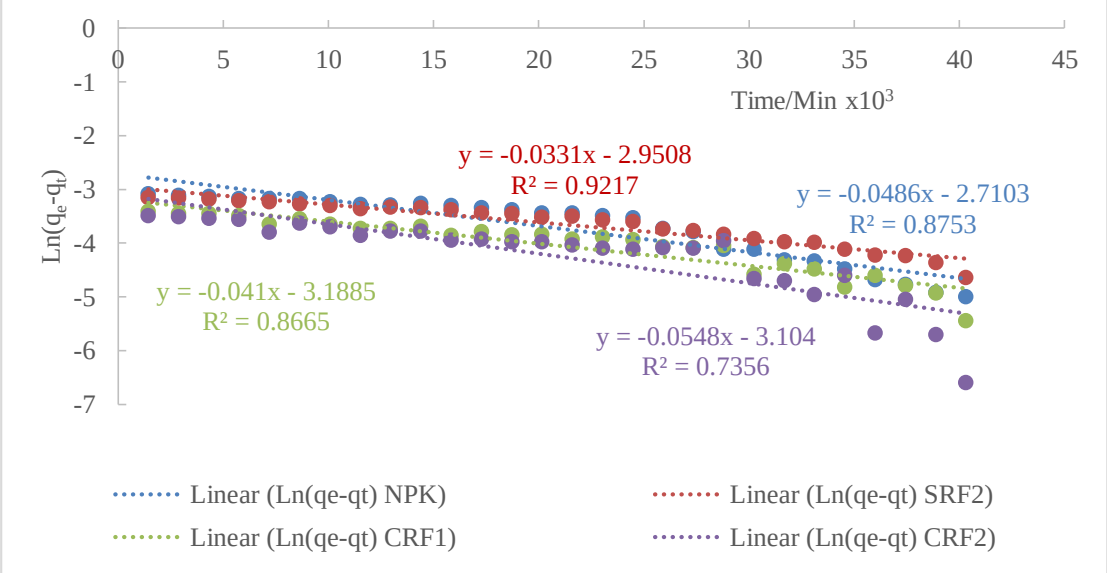

Figure 4. 36: Graphs for pseudo first order K^+ in 50-50

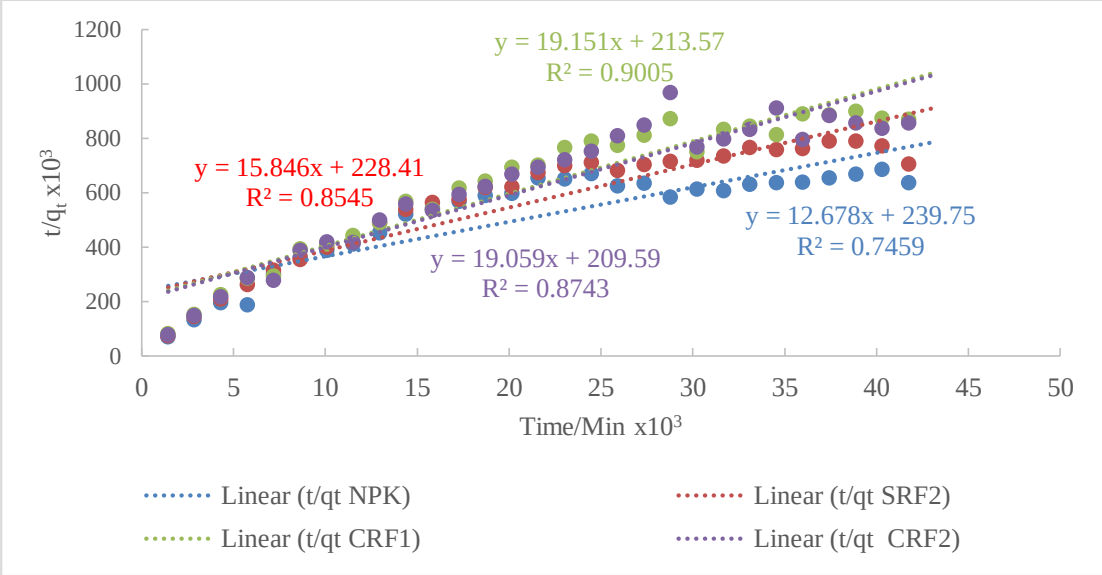

Figure 4. 37: Graphs for pseudo second order K^+ in 50-50

The graphs on Figure 4.36 fitted into characteristic pseudo first order isotherms. The low correlation value for CRF2 could be attributed to the dissolving of the starch-GA after the 20th day. The graphs on Figure 4.37 show that release of K^+ fits into the pseudo second order kinetics. The isotherms converge on about the 3rd day with a similar t/q_t value of around 230. The graphs show close correlation between the CRF1 and CRF2 which have larger gradients than of SRF1. This correlation is attributed to the effect of the coating to the release process. On the other hand, the difference in the gradients between SRF1 and NPK is due to the fact that SRF1 desorbs potassium from the formulas in the first 23 days before dissolving while the NPK simply dissolves into solution from the first day. The R^2 and k values are summarized into Table 4.17 and Table 4.18.

Table 4. 17: Pseudo first order for 50-50 release of nutrients

Treatment	NPK		SRF1		CRF1		CRF2	
Rate	k_1	R^2	k_1	R^2	k_1	R^2	k_1	R^2
NO_3^-	0.0421	0.8230	0.0380	0.8577	0.0396	0.8738	0.0374	0.8827
$H_2PO_4^-$	0.0547	0.8817	0.0802	0.7307	0.0545	0.5727	0.0640	0.6598

K^+	0.0486	0.8753	0.0331	0.9217	0.0410	0.8665	0.0548	0.6436

Table 4. 18: Pseudo second order for 50-50 release of nutrients

Treatment	NPK		SRF1		CRF1		CRF2	
Rate	k_2	R^2	k_2	R^2	k_2	R^2	k_2	R^2
NO_3^-	0.0750	0.6335	0.0720	0.6605	0.0400	0.5445	0.0490	0.5445
$H_2PO_4^-$	1.1700	0.8230	1.3300	0.8235	2.8900	0.8854	2.5200	0.8790
K^+	0.6700	0.7459	1.1000	0.8545	0.6700	0.7459	1.7300	0.8743

Table 4.16 established that the rate of release from NPK formula was higher than of the SRF and CRF fertilizers. A comparison of k_1 values for SRF1 and NPK show lower values in SRF1 for NO_3^- and K^+ corroborating the data on Table 4.16. The values for $H_2PO_4^-$ in SRF1 and NPK verifies the earlier discussion that encapsulating phosphorus in a SRF fertilizer improves the release of phosphorus. The R^2 value for the pseudo first order is higher than of pseudo second order therefore the release of nutrients fits better into the pseudo first order due to very high concentration of water.

The release of nutrients from the 70-30 treatments was tested for pseudo order. Appendix 25 gives the data for the pseudo first and second order kinetics of NO_3^- for the 70-30 formulas. The data on this table was used to draw the isotherms on Figures 4.38 and 4.39.

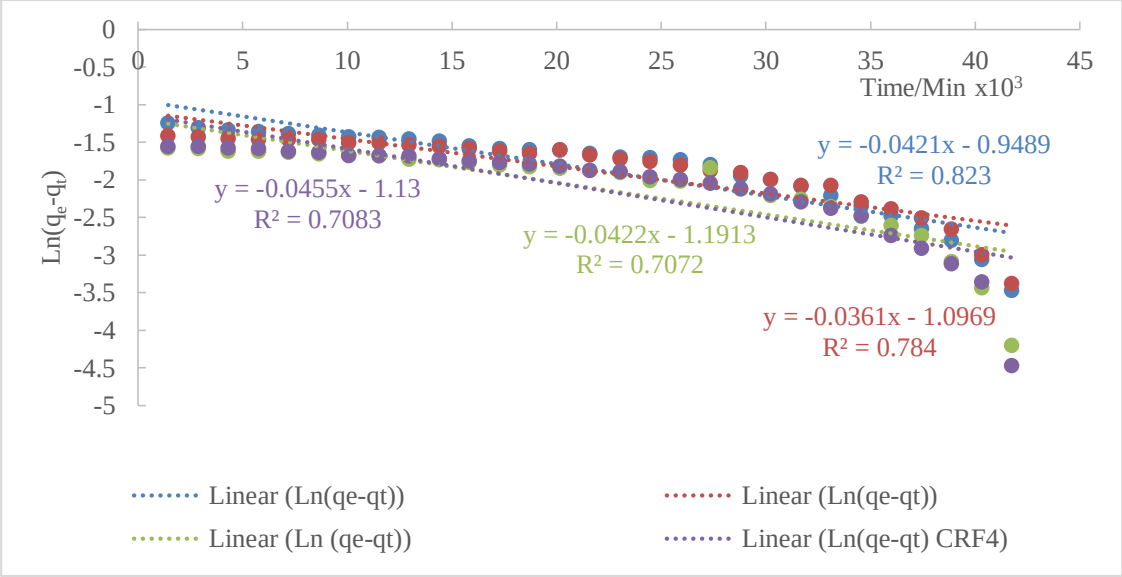

Figure 4. 38: Graphs for pseudo first order NO_3^- in 70-30

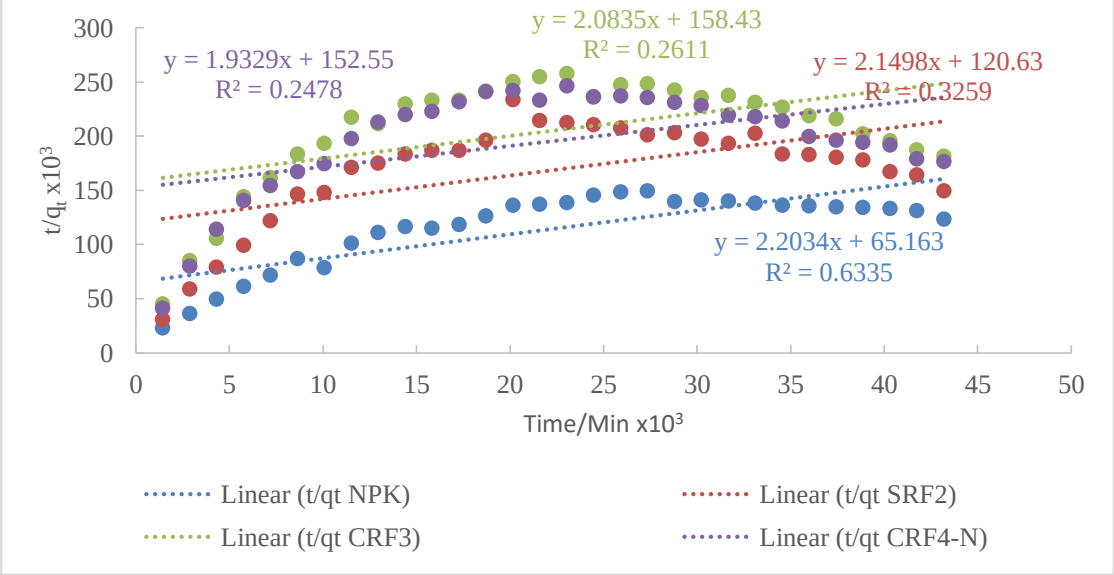

Figure 4. 39: Graphs for pseudo second order NO_3^- in 70-30

The isotherms on Figure 4.38 are characteristic of pseudo first order kinetics though with low correlation value due to dissolving of the formulas into the solution from around the 23rd day. The data on Figure 4.39 show very low correlation values of 0.3287 for SRF2, 0.2336 for CRF3 and 0.2466 for CRF4.

Appendix 26 gives the data for pseudo first and second order kinetics of $H_2PO_4^-$ for the 70-30 formulas. The data on this table was used to draw the isotherms on Figures 4.40 and 4.41.

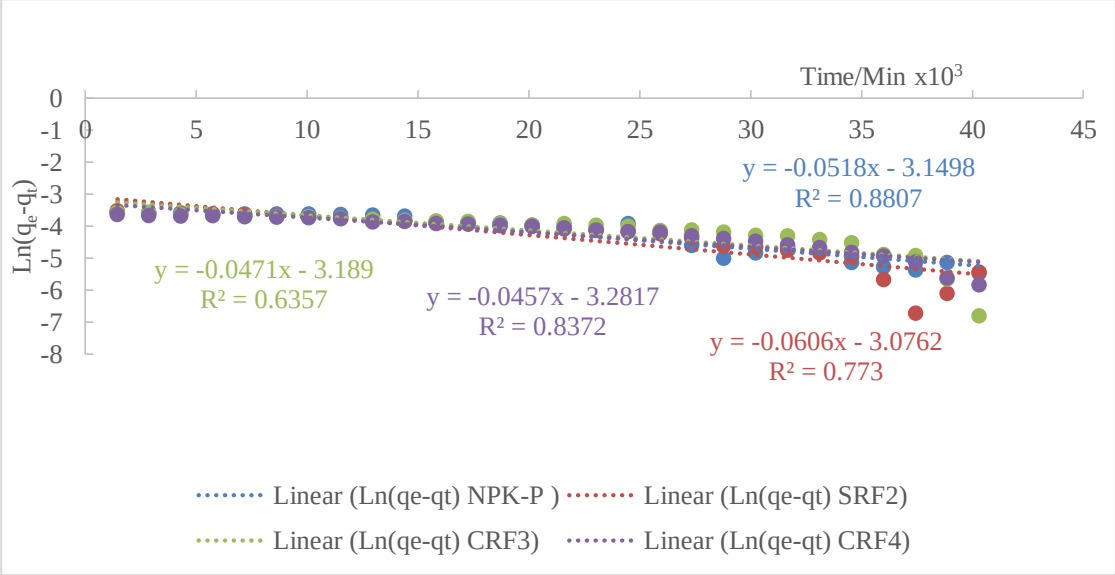

Figure 4. 40: Correlation curve for pseudo first order $H_2PO_4^-$ in 70-30

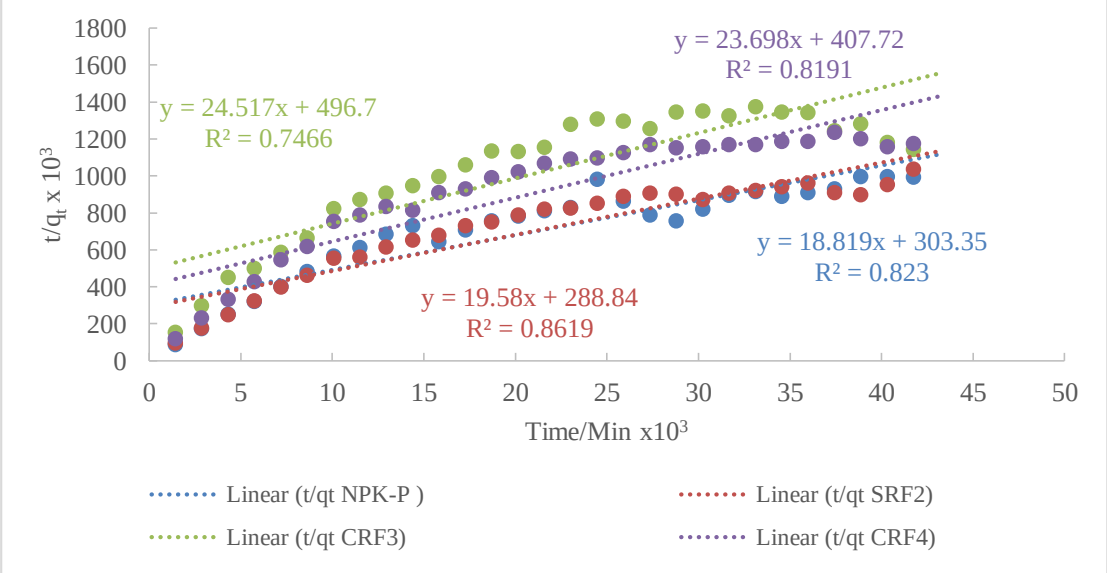

Figure 4. 41: Correlation curve for pseudo second order $H_2PO_4^-$ in 70-30

The isotherms on Figure 4.40 have characteristic trend to pseudo first order kinetics. The low R^2 value is due to the rapid dissolving of the products after the 20th day. The isotherms on Figure 4.41 have trends like other pseudo second order reactions but fail to intercept in the first quadrant. The gradients of the graphs show close relationship between the CRF3 and CRF4 which is due to the effect of the SAP coating enhancing desorption process for a longer period of time.

The data on Appendix 27 was generated to analyze for the pseudo first and second order kinetics of K^+ of the 70-30 formulas. The data on this table was used to draw the isotherms on Figures 4.42 and 4.43.

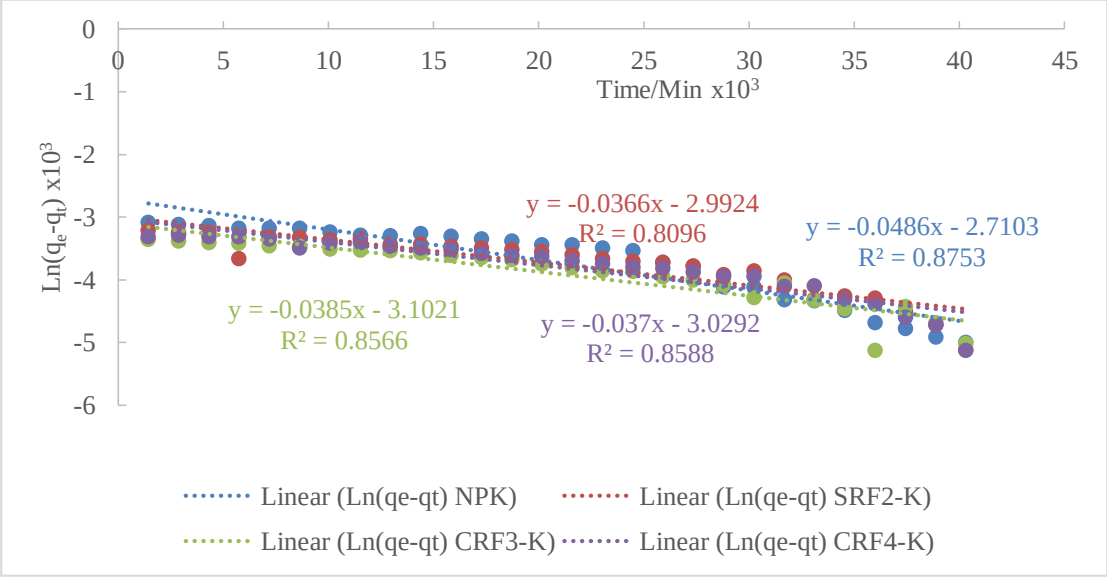

Figure 4. 42: Correlation curve for pseudo first order K^+ in 70-30

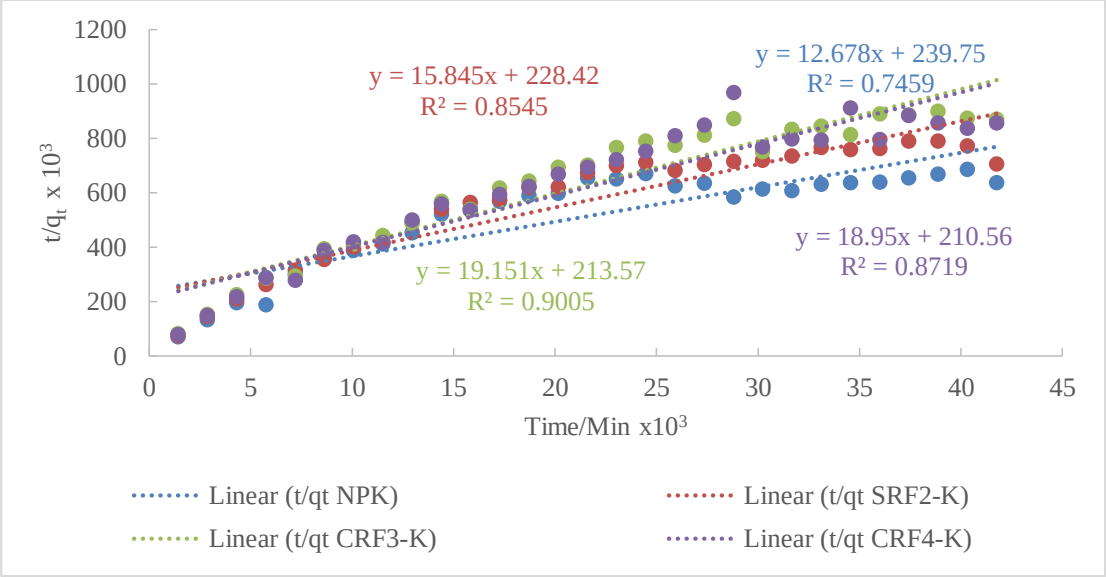

Figure 4. 43: Graphs for pseudo second order K^+ in 70-30

The isotherms on Figure 4.42 are similar to trend of pseudo first order kinetics though with low R^2 values. The gradients and R^2 of CRFs compare closely due to the similar way in which they desorb. The isotherms on Figure 4.43 are characteristic of the pseudo second order kinetics. All the isotherms converge on day one at same $\frac{t}{q_t}$ value. The gradients show that CRF3 is the slowest formula followed by CRF4 and then SRF2.

The pseudo first order equation Ln (q_e-q_t) = Ln q_e - k_1t and pseudo second order equation $\frac{t}{q_t} = \frac{1}{kq_e^2} + \frac{1}{q_e}t$ were used to calculate k_1 and k_2 values which are presented on Tables 4.19 and 4.20.

Table 4. 19: Pseudo first order summary for 70-30 release

Treatments	NPK		SRF2		CRF3		CRF4	
Rate constant	k_1	R^2	k_1	R^2	k_1	R^2	k_1	R^2
NO_3^-	0.0421	0.8230	0.0361	0.7840	0.0422	0.7072	0.0455	0.7083
$H_2PO_4^-$	0.0547	0.8817	0.0606	0.7730	0.0471	0.6357	0.0457	0.8372
K^+	0.0486	0.8753	0.0366	0.8096	0.0385	0.8566	0.0370	0.8588

Table 4. 20: Pseudo second order for 70-30 release

Treatments	NPK		SRF2		CRF3		CRF4	
Rate constant	k_2	R^2	k_2	R^2	k_2	R^2	k_2	R^2
NO_3^-	0.0750	0.6335	0.0380	0.3259	0.0270	0.2611	0.0240	0.2478
$H_2PO_4^-$	1.1700	0.8230	1.3300	0.8619	1.2100	0.7476	1.3800	0.8191
K^+	0.6700	0.7459	1.1000	0.8545	1.7200	0.9005	1.7100	0.8719

The treatments fit better into the pseudo first order which has a higher R^2. Comparison of the k_1 on Table 4.19 shows that CRF1 is the best slow release formula for $H_2PO_4^-$ followed by CRF2. This collaborate the earlier argument on Figure 4.28 that starch-PVA has better crosslinks than starch-GA hence sets an equilibrium after absorbing more solution decrease desorption. Similarly SRF1 has lower k_1 than NPK which implies that its sorption is slower. In the case of K^+, CRF2 has a higher k_1 than CRF1 which means K^+ desorbs through starch-PVA faster than through starch-GA. Again the value of k_1 for NPK shows that the formula dissolves into the solution without a desorption process.

The k_2 data on Table 4.20 show that SRF2 releases $H_2PO_4^-$ in a slower manner than the coated formulas and that release of K^+ from CRF3 is slower than CRF4. This is explained by the better crosslinks in the starch-PVA that absorb more K^+ before it begins to release it. However the r^2 values for the pseudo second order are lower than those of the pseudo first order which makes the release of nutrients from it in water fit into the pseudo first order for both the 50-50 and 70-30 formula

4.4.4.4 Rate of release of nutrients into soils

The formed products were also optimized in maize crop planted in a greenhouse. The concentration of the nutrients in the planting tins of the crops that were nurtured for 14

weeks was plotted against weeks. Optimization was undertaken to compare the rates of release of the formulas in soil media at specific pH of the soils. The following factors affect nutrient release; soil moisture, soil temperature, soil PH, and the nutrient content (Ding *et al.*, 2016). It was therefore necessary to do a greenhouse optimization so as to control the factors that control the rates of nutrient release. The gradient of the line obtained represented the rate of release of the nutrients into the soils. Evaluating the rates of nutrient release in water was not enough since soils have complex physicochemical properties (Ding *et al.*, 2016). Table 4.21 shows these gradients.

Table 4. 21: Rate of release of nutrients from maize crops

Nutrients	FP		NPK		SRF2		CRF3		CRF4	
	r^2	Rate	r^2	Rate	r^2	Rate	r^2	Rate	r^2	Rate
NO_3^-	0.906	-0.02	0.973	0.15	0.819	0.10	0.988	0.08	0.886	0.08
$H_2PO_4^-$	0.967	-0.01	0.947	0.08	0.859	0.04	0.973	0.09	0.990	0.09
K^+	0.945	-0.06	0.909	0.29	0.849	0.14	0.868	0.19	0.929	0.16

Figure 4.63 shows linear graphs for total available NO_3^- in FP, NPK, SRF2, CRF3 and in CRF4 over a period of 14 weeks. Table 4.21 shows the rate of desorption in gL^{-1} of total NO_3^- in FP , NPK, SRF2, CRF3 and in CRF4 soil samples over the study period. The container that was planted without any fertilizer showed gradual decrease in rate of release which is due to the absorption of the nutrient without replacement. The container planted with NPK shows significantly higher total NO_3^- rate of 0.1472 $gL^{-1}wk^{-1}$ desorbed into the container than the others. This value is nearly double that of NO_3^- in CRF4 which is expected since CRF4 is a coated slow release fertilizer.

Concentration of NO_3^- in maize crop can visually be approximated by the colour of the leaves. Deep green colour of the leaves and stems represents a crop that had sufficient concentration of NO_3^-. Plate 4.9 shows the crop at 4 weeks.

Plate 4. 10: Maize crop at four weeks and 2 days

The picture on Plate 4.9 shows the maize crop at four weeks and two days. There are five columns arranged as follows; maize in tins on extreme left were planted with CRF4, followed by those planted with CRF3, SRF2, NPK and lastly FP on the extreme right.

The maize in the columns of CRF4, CRF3, SRF2, NPK have similar green colour shade which implies that they have absorbed sufficient quantity of NO_3^- for growth. Table 4.34 confirms that NPK with its higher rate of desorption discharges more unused NO_3^- of 6.08 gL^{-1} into the tin than the others. The rates of desorption of NO_3^- in the soils decreases from N-NPK through N-SRF2, with 2.90 gL^{-1}, 2.75 gL^{-1} of N-CRF4 and

lastly N-CRF3 with 2.58 gL^{-1}. The lower value for N-SRF2 is attributed to the slow release effect whereas the extra slow effect in the coated materials arise from the SAPs coating.

Figure 4.66 shows the rate of deposition of total available $H_2PO_4^-$ in FP, NPK, SRF2, CRF3 and $H_2PO_4^-$ in CRF4 for 14 weeks. Table 4.34 shows decreased concentration of phosphorus released in gL^{-1} of total $H_2PO_4^-$ in FP, NPK, SRF2, CRF3 and $H_2PO_4^-$ in CRF4 soil samples over the study period. While phosphorus dissolves from NPK into the soils, the SRF2 and its coated formulas desorb slowly from the pores on the surface of the multifunctional clay mineral as was discussed under Figure 4.18. The coated slow release fertilizers that discharge NO_3^- slowly aids in the good adsorption of $H_2PO_4^-$ (Sangakhara & Cho, 2008) enhancing its dissociation into the soils. The increase in desorption of $H_2PO_4^-$ could be arising from an attraction between the $H_2PO_4^-$ anion and the OH on the SAPs which allows for capillarity of the $H_2PO_4^-$ anions. This is enhanced by the attractions of the $H_2PO_4^-$ anion to the root of the plant. The attraction and repulsion forces within the products in the interlayer distances, interactions between the nutrients and the charges on the sheets and lastly osmotic pressure set by the roots of the plants and the solutions at the root zone will determine the sorption.

Figure 4.69 shows linear graphs for total available K^+ in FP, NPK, SRF2, CRF3 and in CRF4. The rate of desorption of K^+ in FP decreases over the period of time. This rate of -0.0607 $gL^{-1}wk^{-1}$ is higher than that of phosphorus which was -0.007 $gL^{-1}wk^{-1}$ and of nitrogen at -0.0215 $gL^{-1}wk^{-1}$ due to the strong interaction between phosphates and silicates in the soils. This means the amount of NO_3^- and $H_2PO_4^-$ absorbed are higher than that of K^+. SRF2 has the slowest discharge of K^+ at 0.1428 $gL^{-1}wk^{-1}$ due to the

effect of the multifunctional organoclay which reduces the passing of the K^+ ion through the pores. However this discharge is improved by the effect of the SAPs through an interaction between the K^+ and the OH of the SAPs that eventually draws the K^+ onto the surface for desorption into the plant. CRF3 has higher rate of desorption of K^+ at 0.1881 $gL^{-1}wk^{-1}$ than CRF4 with 0.1591 $gL^{-1}wk^{-1}$. This can be explained by the uniform crosslinking (Jocksusch *et al.,* 2009) in CRF3 that enables relatively free movement of K^+ than CRF4 whose crosslinks are largely intertwined. CRF3 would however be proposed as the better formulation than CRF4 for discharge of K^+. This formula improves the K^+ discharge adequately from 4.727 gL^{-1} to 6.409 gL^{-1} while reducing K^+ discharged into the soils which reduce environmental pollution.

This study proposes that the products should be made in cylindrical form and in 4g units so as to serve at least 5 units per maize crop. The coating should be of uniform 3mm thickness to reduce peeling off with increase in weeks especially for starch-GA as observed on the picture on plate 4.8.

4.4.4.5 Kinetic models in nutrient release into soils

The nitrogen in the soil was adsorbed by plants from the FP control while in the other treatments, the nitrogen adsorbed by the plants was desorbed from the formulas. The rate of desorption from the formulas was equated to the rate of adsorption by the plants and the surplus of nutrients were deposited into the tins. Appendix 28 shows the data of the pseudo first order and pseudo second order for the nitrogen nutrient during the observation period. Figure 4.44 shows the linear relationship for the pseudo first order rates of Nitrogen.

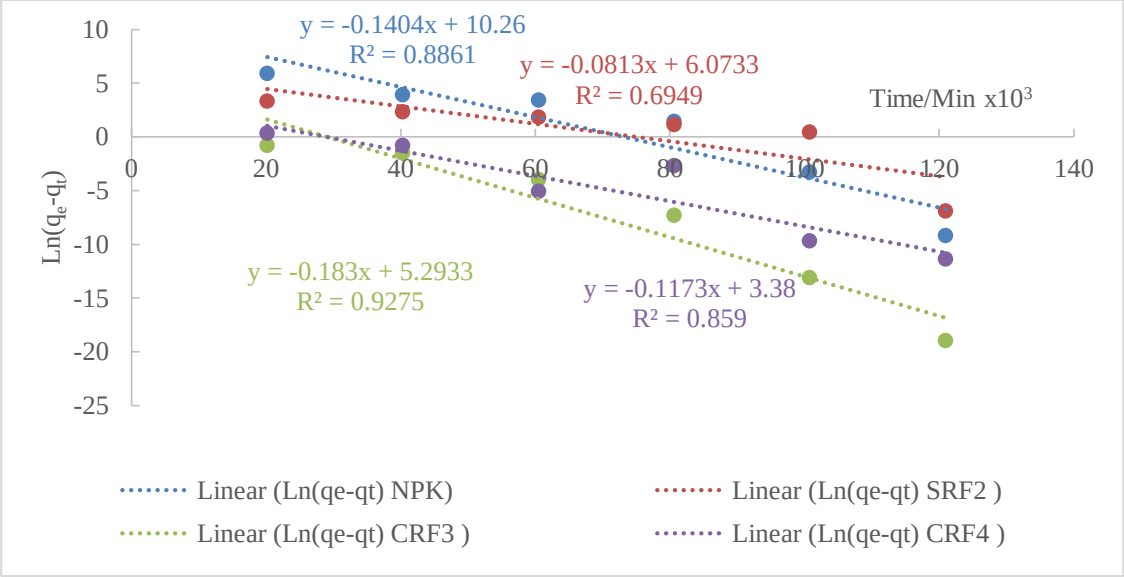

Figure 4. 44: Graph for pseudo first order NO_3^- in crops

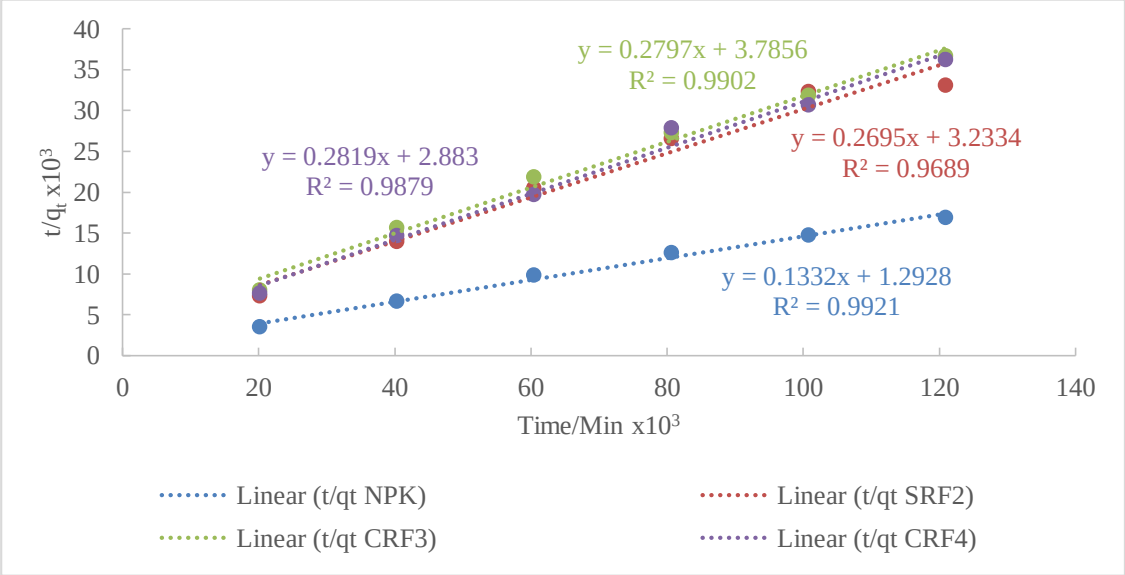

Figure 4. 45: Graph for pseudo second order NO_3^- in crops

The nature of the slope on Figure 4.44 gives a correlation with pseudo first order reactions. The R^2 values for CRF4 and SRF2 are quite low. However these curves compare with those of (Ho & McKay, 2002).

Release of NO_3^- from the SRF, CRF3 and CRF4 formulas as seen on Figure 4.45 fit better in the pseudo second order rate formula than the pseudo first order one. All the

treatments have a positive k_2 value also observed in other research findings like of (Ho & McKay, 2002); (Hongtao *et al.*, 2014). The biggest rate constant could represent the treatment with a lowest release capacity which is CRF4.

Phosphorus is a limiting element in most P fertilizers due to its low ability to dissolve into exchangeable P in soils. Appendix 29 shows the data when the treatments are fitted into the pseudo first and second order reaction rate equations which was used to draw Figures 4.46 and 4.47 respectively.

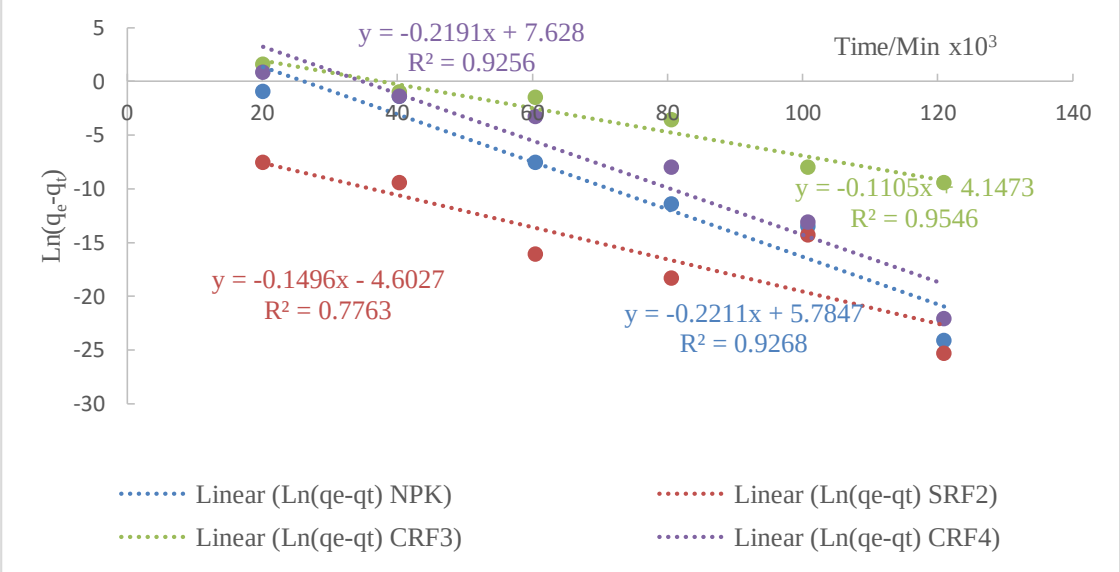

Figure 4. 46: Graph for pseudo first order $H_2PO_4^-$ in crops

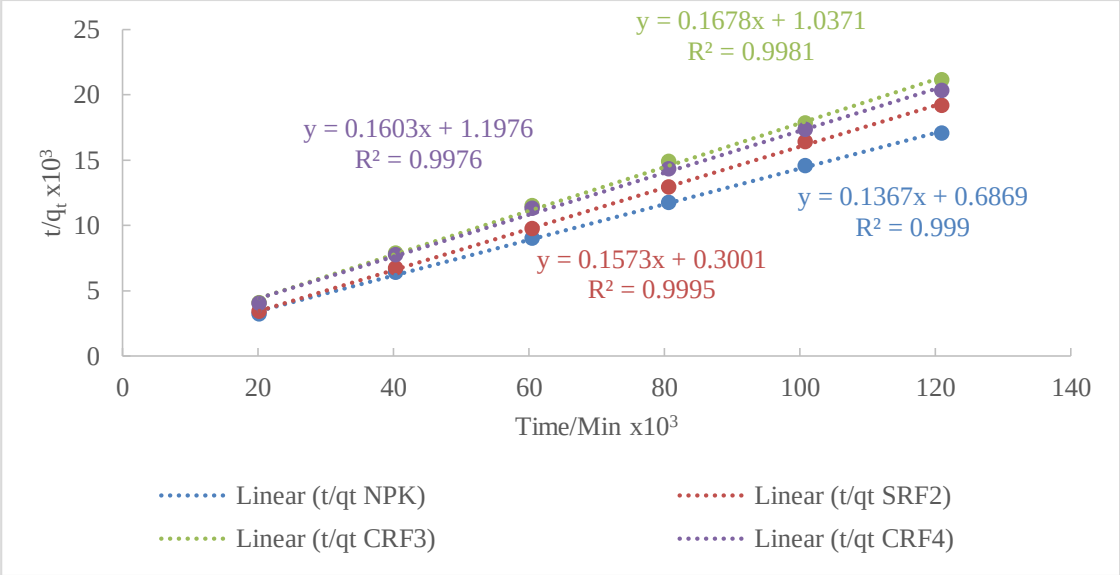

Figure 4. 47: Graph for pseudo second order $H_2PO_4^-$ in crops

The plot on Figure 4.46 is characteristic of pseudo first order rate equation. The treatments have fairly high R^2 except for SRF2 that posts a low value of 0.7763. They have positive k_1 values which are also observed in (Ho & McKay, 2002).

The treatments on Figure 4.47 have similar linear graphs that have an intercept as expected. The slopes of the line graphs are positive as expected from the pseudo second order. All the treatments post very high correlation value of R^2 0.9992 for SRF2, 0.9991 for NPK, 0.9976 for CRF4 and lastly 0.9935 for CRF3.

The rate constants are; 0.027 for NPK, 0.082 for SRF2, 0.022 for CRF4 and 0.027 for CRF3. The rate constants show that CRF3 has the lowest release capacity followed by CRF4. This is explained by the nature of the coating that slows the sorption process. Similarly SRF2 shows slow release nature than NPK. This is due the nature of the sorption in SRF2 which depends on the pore volumes of the nanocomposite material. The data on Appendix 30 was used to draw isotherms of Figure 4.48 and 4.49.

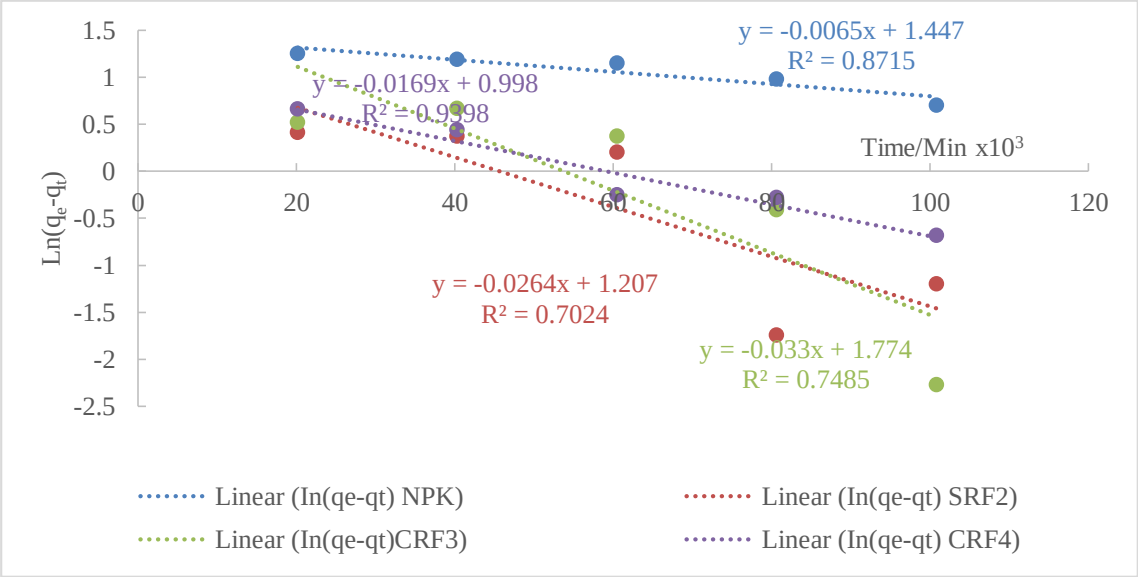

Figure 4. 48: Graph for pseudo first order K^+ in crops

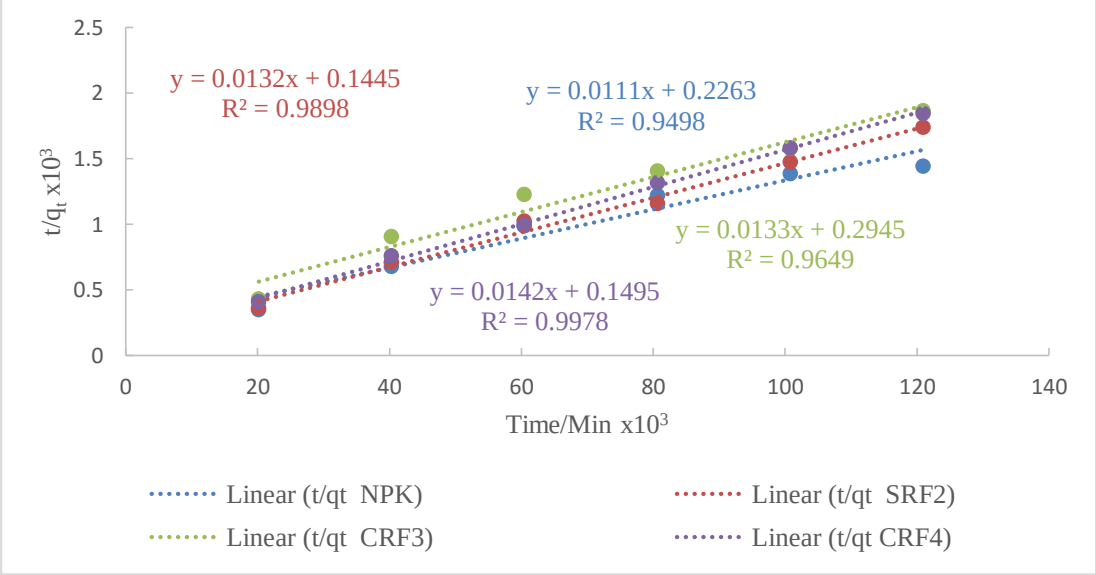

Figure 4. 49: Correlation curve for pseudo second order K^+ in crops

The data on Figure 4.48 gives curves that fit into the pseudo first order rate of reaction with however low correlation. The correlation compares with other research work like of (Ho & McKay, 2002) (Ho & McKay, 1998).

The potassium desorption from products were fitted into the pseudo second order rates of reactions graphs giving Figure 4.49. The graphs for all the treatments fitted well into the pseudo second order rate having the highest correlation of R^2 of 0.9976 for CRF4, followed by SRF2 with 0.9995, then FP with 0.992, CRF3 comes at 0.9981 and lastly NPK with 0.999. These curves relate closely with those of (Ho & McKay, 2002); (Ho & McKay, 1998).

CRF4 for K^+ has the lowest release rate which is explained by the nature of the starch-GA coating that slows the sorption process. Similarly SRF2 shows slow release nature than NPK. This is due the nature of the sorption in SRF2 which depends on the pore volumes of the nanocomposite material. CRF3 has a faster release than SRF2 which could be due to ease of decomposition of the starch-PVA that breaks the SRF2 into smaller particles that enhance the sorption process. Tables 4.22 and 4.23 give summary of the pseudo first and pseudo second order respectively.

Table 4. 22: Data for pseudo first order for crops

Treatments	NPK		SRF2		CRF3		CRF4	
	k_1	R^2	k_1	R^2	k_1	R^2	k_1	R^2
NO_2^-	0.1404	0.8861	0.0813	0.6949	0.1830	0.9275	0.1173	0.8590
$H_2PO_4^-$	0.2211	0.9268	0.1496	0.7763	0.1105	0.9546	0.2191	0.9256
K^+	0.0655	0.8715	0.2640	0.7023	0.3300	0.7485	0.1690	0.9398

Table 4. 23: Data for pseudo second order for crops

Treatment	NPK		SRF2		CRF3		CRF4	
	k_2	R^2	k_2	R^2	k_2	R^2	k_2	R^2
NO_3^-	0.0140	0.9921	0.0230	0.9698	0.0210	0.9902	0.0280	0.9878
$H_2PO_4^-$	0.0270	0.9498	0.0820	0.9898	0.0270	0.9649	0.0220	0.9978
K^+	0.0005	0.9990	0.0012	0.9995	0.0010	0.9981	0.0014	0.9996

The k_2 values for NO_3^- show that CRF4 has the slowest release capacity followed by CRF3. This supports the discussion on Table 4.12 of water retention that SAPs slows down the release of the NO_3^- into the soils by developing an equilibrium between the nutrient in the formulas and the roots of the plants. Similarly, SRF2 shows a slower release rate than NPK because the release from SRF2 is through the pores as opposed to NPK that releases through dissolution into the soil solutions. In the case of $H_2PO_4^-$, CRF3 is slower than CRF4 and SRF2 is slower than NPK for the same reasons as in the case of nitrogen. The trend in release of K^+ is the same as for NO_3^-.

4.5 Nutrient retention and release capacity for 50-50 formulas

This subsection studies the nature of the formed products, SRF, CRF1 and CRF2 in controlled release of nutrients. The 50-50 treatments were simulated in water over a period of 30 days and later compared with the 70-30 one. This simulation was used to determine nutrient retention and release capacity by the formed multifunctional nanocomposite in deionized water. The concentration of nutrients released into water was followed by a UV-VIS spectroscopy.

4.5.1 Nutrient retention and release capacity of nitrogen

The data in appendix 2 shows the absorbance of NPK, SRF, CRF1 and CRF2. Equations 4a and 4b on appendix 31 were used to convert the absorbance into concentration in g per litre. The analyzed data for concentration of NO_3^- in gL^{-1} is shown on Table 4.24 below.

Table 4. 24: Concentration of NO_3^- in 50-50 formula

DAY	NPK-N ±SE	SRF1-N ±SE	CRF1-N ±SE	CRF2-N ±SE
1	0.0640 ± 0.0001^{Az}	0.0551 ± 0.0001^{Bu}	0.0472 ± 0.0001^{Dy}	0.0518 ± 0.0001^{Cv}
2	0.0804 ± 0.0001^{Ay}	0.0565 ± 0.0001^{Bu}	0.0498 ± 0.0001^{Dxy}	0.0534 ± 0.0001^{Ctv}
3	0.0874 ± 0.0001^{Ax}	0.0586 ± 0.0002^{Bu}	0.0521 ± 0.0001^{Dx}	0.0570 ± 0.0001^{Cs}
4	0.0945 ± 0.0001^{Aw}	0.0787 ± 0.0001^{Bs}	0.0533 ± 0.0000^{Dx}	0.0754 ± 0.0001^{Cr}
5	0.1006 ± 0.0001^{Av}	0.0893 ± 0.0002^{Br}	0.0835 ± 0.0002^{Dw}	0.0858 ± 0.0001^{Cq}
6	0.1045 ± 0.0001^{Au}	0.0945 ± 0.0003^{Bqr}	0.0861 ± 0.0001^{Dvw}	0.0856 ± 0.0000^{Cpq}
7	0.1105 ± 0.0001^{At}	0.0962 ± 0.0000^{Bqr}	0.0896 ± 0.0002^{Duv}	0.0913 ± 0.0002^{Cp}
8	0.1138 ± 0.0001^{Ast}	0.1034 ± 0.0000^{Bpq}	0.086 ± 0.0001^{Dvw}	0.1011 ± 0.0001^{Co}
9	0.1172 ± 0.0001^{As}	0.1076 ± 0.0000^{Bop}	0.0938 ± 0.0000^{Du}	0.1013 ± 0.0001^{Co}
10	0.1241 ± 0.0001^{Ar}	0.1139 ± 0.001^{Bno}	0.111 ± 0.0000^{Dt}	0.1129 ± 0.0001^{Cn}
11	0.1383 ± 0.0000^{Aq}	0.1192 ± 0.001^{Bmn}	0.1172 ± 0.000^{Ds}	0.1203 ± 0.0001^{Bm}
12	0.1464 ± 0.0001^{Ap}	0.1286 ± 0.001^{Clm}	0.1247 ± 0.0001^{Dr}	0.1265 ± 0.0001^{Cl}
13	0.1482 ± 0.0000^{Ap}	0.1282 ± 0.001^{Blm}	0.1303 ± 0.0002^{Bq}	0.1312 ± 0.0001^{Bl}
14	0.1485 ± 0.0001^{Ap}	0.1382 ± 0.0000^{Bkl}	0.1338 ± 0.0001^{Dq}	0.1402 ± 0.0001^{Bk}
15	0.1575 ± 0.001^{Ao}	0.1445 ± 0.0001^{Ck}	0.1407 ± 0.0004^{Cp}	0.1444 ± 0.0004^{Bk}
16	0.1666 ± 0.0000^{An}	0.1466 ± 0.0001^{Bjk}	$0.146\pm0.0001^{C*o}$	0.1499 ± 0.0004^{Bj}
17	0.1684 ± 0.0000^{An}	0.1561 ± 0.0001^{Cj}	0.1536 ± 0.0000^{Dn}	0.1572 ± 0.0003^{Bj}

18	0.1752 ± 0.0001^{Am}	0.1697 ± 0.0001^{Ci}	0.1644 ± 0.0000^{Dm}	0.1632 ± 0.0001^{Cj}
19	0.1835 ± 0.0001^{Al}	0.1805 ± 0.0001^{Bh}	0.1704 ± 0.0001^{Cl}	0.1807 ± 0.0001^{Bj}
20	0.2066 ± 0.0000^{Ak}	0.1889 ± 0.0000^{Dgh}	0.1918 ± 0.0000^{Ck}	0.1941 ± 0.0001^{Bj}
21	0.2147 ± 0.0001^{Aj}	0.197 ± 0.0001^{Dg}	0.2012 ± 0.0002^{Cj}	0.2075 ± 0.0001^{Bi}
22	0.2262 ± 0.0002^{Ai}	0.1975 ± 0.03^{Bg}	0.1962 ± 0.0000^{Bi}	0.2085 ± 0.0018^{Bi}
23	0.2402 ± 0.0001^{Ah}	0.2128 ± 0.0001^{DCf}	0.2139 ± 0.002^{Ch}	0.2176 ± 0.001^{Bh}
24	0.2546 ± 0.0001^{Ag}	0.2205 ± 0.0003^{DCef}	0.2243 ± 0.0014^{Cg}	0.2266 ± 0.001^{Ag}
25	0.2655 ± 0.0003^{Af}	0.2217 ± 0.0002^{Be}	0.2356 ± 0.0018^{Bf}	0.2351 ± 0.0026^{Bf}
26	0.2786 ± 0.0002^{Ae}	0.2661 ± 0.0021^{Bc}	$0.2611\pm0.0006^{B*e}$	0.2631 ± 0.0054^{Bd}
27	0.2904 ± 0.0000^{Ad}	0.2502 ± 0.0001^{Dd}	0.2783 ± 0.0003^{Bb}	0.2581 ± 0.0001^{Ce}
28	0.3027 ± 0.0004^{Ac}	0.2624 ± 0.0003^{Dc}	0.2664 ± 0.0003^{Cd}	0.2695 ± 0.0002^{Bc}
29	0.3193 ± 0.0002^{Ab}	0.2879 ± 0.003^{Bb}	0.2761 ± 0.0003^{Cb}	0.2912 ± 0.0001^{Bb}
30	0.3516 ± 0.0004^{Aa}	0.3235 ± 0.0003^{Da}	0.3269 ± 0.0005^{Ca}	0.3346 ± 0.0003^{Ba}

Key: NPK is NPK fertilizer, SRF1 is 50-50 slow release fertilizer, CRF1 is starch-PVA coated SRF1, CRF2 is starch-GA coated SRF1, Mean values followed by the same capital letter(s) within the same column do not differ significantly from one another while mean values followed by the same small letter(s) within the same row do not differ significantly from one another (α=0.05, one-way ANOVA, Posthoc-Tukey-test). An asterisk (*) on a letter is used to show the lower value between values that are not significantly different in a row while the harmonic mean sample size, n=3.

Table 4.24 shows a general increase in the concentration of nutrients released from day 1 to 30th day for all the treatments. This trend is similar with the percolation test done on coated and uncoated NPK fertilizer for 4 weeks by (Himmah *et al.,* 2018). NPK dissolves from a concentration of 0.064 gL^{-1} to 0.3516 gL^{-1}, SRF1 from 0.0551 gL^{-1} to 0.3235 gL^{-1}, CRF1 from 0.0472 gL^{-1} to 0.3269 gL^{-1} while CRF2 increases from 0.0518 gL^{-1} to 0.3346 gL^{-1}. This trend is in line with the Beer-Lambert's law.

The data on Table 4.24 shows a general decrease in the concentrations dissolved across the table in order of NPK, SRF1, CRF2 and CRF1. In all the 30 days, NPK has the highest dissolution factor shown by letter A. SRF1 shows lower release than NPK in thirteen days with letter B and with letter C in 3 days. For example day 1 shows a decreasing trend of; 0.064 gL^{-1} for NPK, 0.0551 gL^{-1} for SRF1, 0.0518 gL^{-1} for CRF2

and 0.0472 gL^{-1} for CRF1. From the 11^{th} day, CRF2 shows generally higher release than SRF1. This could be due to dissolving of starch-GA jelly attracting nutrient ions strongly using an osmotic pressure especially if the intercalation was not achieved at high levels.

The slow release nature of SRF1 can be attributed to the multilayer porous clay sheets. The NO_3^- which is dispersed into the interlayer spaces desorbs through small porous pores in the surface of the nanolayers as was noted on Figures 4.16 and 4.18 on discussion of BET as opposed to NPK that dissolves. The amount of NO_3^- that desorbs in SRF1 will therefore be less and will depend on the surface area of the multifunctional organoclay.

Generally CRF1 has the lowest release of concentration of nutrients shown with letter D in 14 days, letter C in 5 days and letter B in 2 days which gives a total of 21 days out of the 30 days. This shows that the starch-PVA is a better slow release coating material. This material has larger, stronger OH crosslinks that were observed on picture x30000 of plate 4.5 which improve the water-nutrient uptake and reduces the release of the nutrients by strong hydrogen bond interactions with the $H_2PO_4^-$ and NO_3^-.

The effectiveness of SRF1 formula depends on the efficiency of the intercalation and success of the pillaring of the clay sheets. The data from day 11 to day 30 points to intercalation that was not well achieved and that is probably why some of the SRF1 values were lower than the CRF2 values. Some of these examples are; day13 SRF1 concentration is 0.128 gL^{-1} as compared to 0.131 gL^{-1} of CRF2, day 16 SRF1 has 0.147 gL^{-1} while CRF2 has 0.150 gL^{-1}.

Whereas the intercalation of the clay minerals and distribution of the nitrogen nutrient into the clay nano-matrix was achieved, the data of anomalies on days 13 and 16 on Table 4.24 shows that the fabrication factors need to be varied to improve the slow release capacity. The quantitative relationships of release of these products is featured on Figure 4.50 which shows a column of the release of NO_3^- from NPK, SRF1, CRF1 and CRF2 over the 30 days.

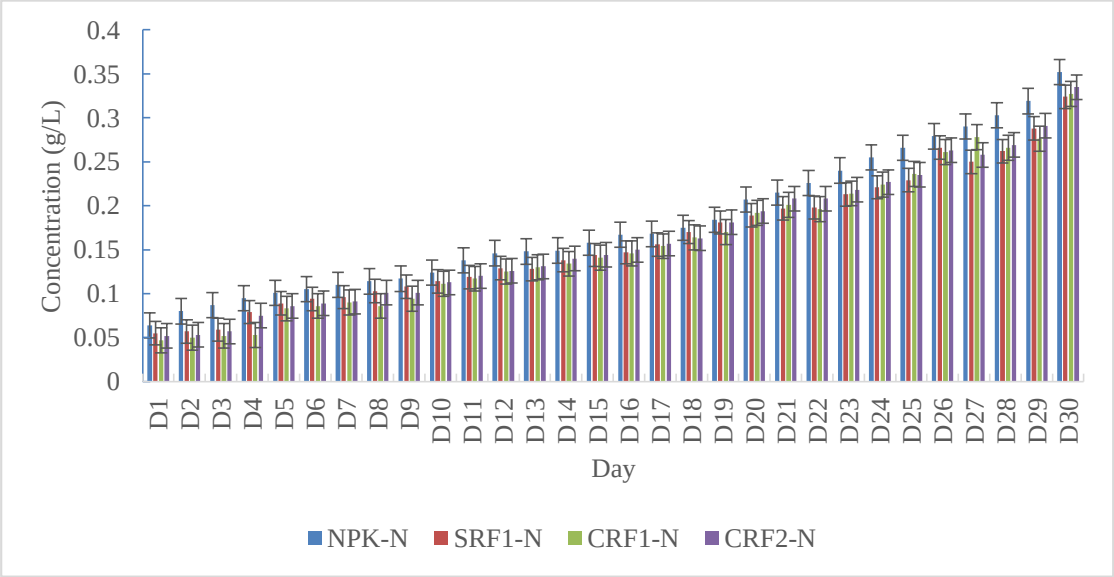

Figure 4. 50: Column of NO_3^- release from the 50-50 products

There is steady increase in the release of nutrients into the water from the first to the 30th day. The release of NO_3^- from NPK is significantly higher than the rest of the treatments during the days; 2, 3, 24, 25 and 27 as illustrated by error bars on Figure 4.50. The rate of release of NPK whose bar is given as blue shows higher concentration than the others over the period of study showing that it is comparatively a faster release product than the others. The rest of the products have significantly similar release rates except for day 4 which has a lower value of CRF1-N than would be expected. SRF1 shows slightly higher release than CRF 1 and CRF2 in 18 days which can be explained

by the effect of the SAPs that slows down the flow of NO_3^- from the nutrient formulations. Figure 4.51 shows the rate of release of the treatments.

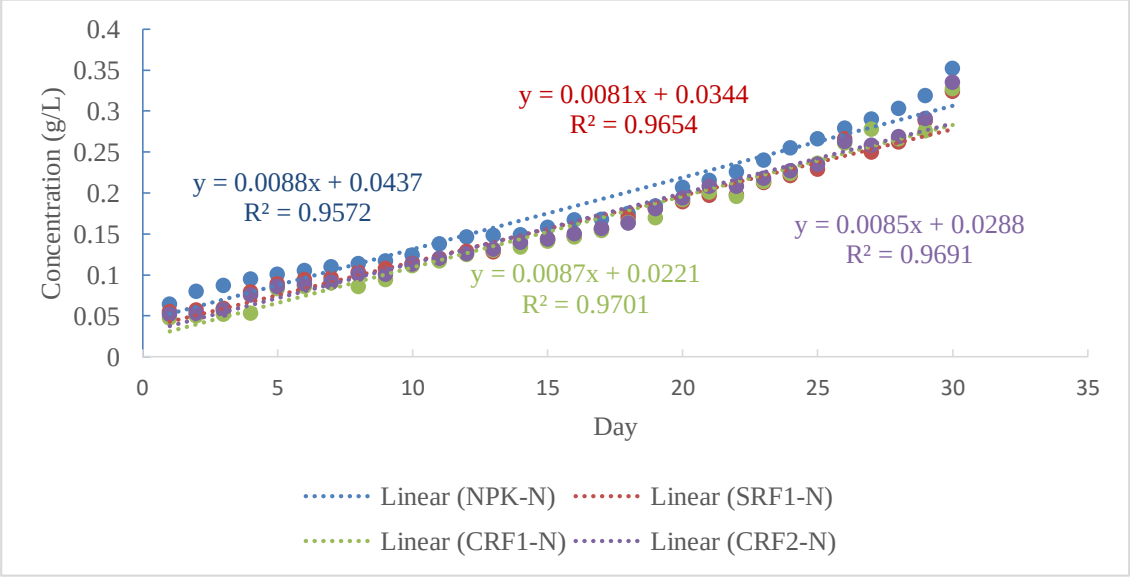

Figure 4. 51: Rate of release of NO_3^- in 50-50 formulas

Figure 4.51 shows linear relationship between the release of NO_3^- from the products in the 50-50 formula and time as in research of (Ding *et al.*, 2016). The gradient of NPK on Figure 4.51 is 0.0087 $gL^{-1}day^{-1}$ which represents the rate of release of NO_3^- from NPK sample. This is expected because as the NO_3^- in NPK dissolves directly into the water, the release of NO_3^- from SRF1 and the CRFs desorb from the organoclay mineral regulated by BET isotherms as seen on Figure 4.16 of SRF1 and Figure 4.18 column of surface area and total pore volume.

The rate of release of SRF1 on Figure 4.51 is 0.0081 $gL^{-1}day^{-1}$ and is less than that of NPK which is 0.0087 $gL^{-1}day^{-1}$ which shows that the rate of release is slower in SRF1 due to the effect of the nanoorganoclay that reduces desorption through the clay sheets.

On the overall the graphs for SRF1, CRF1 and CRF2 are not significantly different from each other as observed on Figure 4.51. The coating of starch-PVA on CRF1 absorbs a lot of water before attaining equilibrium reducing the amount that desorbs. The reduction in the rate in SRF1 and CRFs is due to the slow releasing modified nanoclay in addition to the effect of the coating SAPs that only allow the NO_3^- to pass through slowly. On average the release from CRFs experiences double effect in reduction, one from the effect of the organoclay and the other form the SAPs.

The rate of release of nutrients from CRF2 is 0.0085 $gL^{-1}day^{-1}$which is slower than that of NPK. This reduction in the rate is due to the slow release of NO_3^- from modified nanoclay in addition to the effect of the coating of starch-GA that allows the NO_3^- to slowly be attracted it.

4.5.2 Nutrient retention and release capacity of phosphorus

Phosphorus exists as PO_4^{3-}, HPO_4^{2-}, and $H_2PO_4^-$ in solutions. Equations 4c and 4d on appendix 31 were used to convert absorbance on Appendix 3 to concentration in gL^{-1}. The analyzed data is given on Table 4.25.

Table 4. 25: Concentration of $H_2PO_4^-$ in 50-50 formula

Day	NPK-P ±SE	SRF1-P ±SE	CRF1-P ±SE	CRF2-P ±SE
1	0.017 ± 0.0001^{Ah}	0.015 ± 0.0000^{Bl}	0.013 ± 0.0001^{Co}	0.015 ± 0.0001^{Bp}
2	0.017 ± 0.0001^{Ah}	0.017 ± 0.0001^{Akl}	$0.016\pm0.0001^{A*n}$	0.017 ± 0.0001^{Ao}
3	0.017 ± 0.0002^{ABh}	0.017 ± 0.000^{Akl}	$0.017\pm0.0001^{B*mn}$	0.017 ± 0.0001^{Bno}
4	0.018 ± 0.0001^{Ah}	0.018 ± 0.0001^{Akl}	0.017 ± 0.0002^{Cmn}	0.017 ± 0.0000^{Bmno}
5	0.018 ± 0.0001^{Ah}	0.017 ± 0.0000^{Ckl}	0.017 ± 0.0001^{BCmn}	0.017 ± 0.0002^{Bmno}
6	0.018 ± 0.0000^{Ah}	0.017 ± 0.0001^{ABkl}	0.016 ± 0.0002^{Cn}	0.017 ± 0.0000^{Blmn}
7	0.018 ± 0.0001^{Ah}	0.018 ± 0.0006^{Ajkl}	$0.017\pm0.0001^{A*lmn}$	0.018 ± 0.0000^{Almno}
8	0.019 ± 0.0001^{Ah}	0.018 ± 0.0002^{Bjkl}	$0.018\pm0.0000^{B*klmn}$	0.018 ± 0.0002^{Blmn}
9	0.019 ± 0.0000^{Ah}	0.018 ± 0.0001^{ABjk}	$0.018\pm0.0002^{B*klmn}$	0.018 ± 0.0002^{Blm}
10	0.020 ± 0.0001^{Ah}	0.019 ± 0.0000^{ABijk}	$0.018\pm0.0000^{B*klmn}$	0.018 ± 0.0005^{Blm}
11	0.025 ± 0.0002^{Ag}	0.0213 ± 0.0000^{Bhij}	$0.019\pm0.0000^{C*jklm}$	0.0189 ± 0.0005^{Ckl}
12	0.024 ± 0.0002^{Ag}	0.025 ± 0.002^{ABfg}	0.019 ± 0.0001^{Cjkl}	0.019 ± 0.0002^{BCjk}
13	0.025 ± 0.0001^{Ag}	0.024 ± 0.0002^{Agh}	0.019 ± 0.0003^{Cjklmn}	0.020 ± 0.0003^{Bijk}
14	0.026 ± 0.0002^{Afg}	0.025 ± 0.0001^{Bgh}	0.020 ± 0.0001^{Dijk}	0.021 ± 0.0001^{Chij}
15	0.027 ± 0.0003^{Afg}	0.025 ± 0.0001^{Bfg}	$0.021\pm0.0004^{C*hij}$	0.022 ± 0.0000^{Cgh}
16	0.028 ± 0.0001^{Afg}	0.025 ± 0.0003^{Bfg}	0.022 ± 0.0000^{Chi}	$0.022\pm0.0007^{C*hi}$
17	0.025 ± 0.0001^{Ag}	0.023 ± 0.002^{Aghi}	0.022 ± 0.0006^{Ahi}	0.022 ± 0.0001^{Agh}
18	0.030 ± 0.0000^{Af}	0.028 ± 0.0001^{Aef}	0.021 ± 0.0008^{Chij}	0.024 ± 0.0003^{Bf}
19	0.035 ± 0.0002^{Ae}	0.029 ± 0.0001^{Bde}	$0.023\pm0.0014^{C*gh}$	0.023 ± 0.0002^{Cfg}
20	0.038 ± 0.004^{Abcde}	0.032 ± 0.000^{ABcd}	$0.025\pm0.0003^{B*fg}$	0.026 ± 0.0003^{Be}
21	0.037 ± 0.0001^{Acde}	0.034 ± 0.0004^{Bbc}	$0.026\pm0.0001^{C*def}$	0.027 ± 0.001^{Ce}
22	0.035 ± 0.0002^{Ade}	0.034 ± 0.0004^{Abc}	0.027 ± 0.0001^{Bcdef}	$0.027\pm0.0001^{B*e}$
23	0.036 ± 0.0004^{Acde}	0.035 ± 0.0004^{Bbc}	0.025 ± 0.0003^{Def}	0.027 ± 0.0002^{Ce}
24	0.039 ± 0.000^{Abcde}	0.035 ± 0.0003^{Bb}	0.027 ± 0.0002^{Dcde}	0.029 ± 0.0002^{Cd}
25	0.040 ± 0.000^{Abcde}	0.037 ± 0.0002^{Bab}	0.028 ± 0.0003^{Dbcd}	0.030 ± 0.0001^{Ccd}
26	0.040 ± 0.0002^{Abcd}	0.040 ± 0.0004^{Aa}	0.028 ± 0.0003^{Cbc}	0.031 ± 0.0001^{Bbc}
27	0.039 ± 0.0000^{Aabc}	0.038 ± 0.0003^{Bab}	0.030 ± 0.0002^{Db}	0.032 ± 0.0001^{Cb}
28	0.041 ± 0.0003^{Aabc}	0.039 ± 0.0002^{Ba}	0.033 ± 0.0001^{Da}	0.034 ± 0.0000^{Ca}
29	0.042 ± 0.0000^{Aab}	0.040 ± 0.0002^{Aa}	0.034 ± 0.0002^{Ba}	0.034 ± 0.0001^{Ba}
30	0.045 ± 0.0002^{Aa}	0.040 ± 0.0002^{Aa}	$0.034\pm0.0010^{B*a}$	0.035 ± 0.0002^{Ba}

Key: NPK is NPK fertilizer, SRF1 is 50-50 slow release fertilizer, CRF1 is starch-PVA coated SRF1, CRF2 is starch-GA coated SRF1, Mean values followed by the same capital letter(s) within the same column do not differ significantly from one another while mean values followed by the same small letter(s) within the same row do not differ significantly from one another (α=0.05, one-way ANOVA, Posthoc-Tukey-test). An asterisk (*) on a letter is used to show the lower value between values that are not significantly different in a row while the harmonic mean sample size, n=3.

The concentrations of nutrients released increased as the number of days increased until it peaked at 30th day. This is expected since increase in the number of days, increases the amount of $H_2PO_4^-$ anions that accumulates in the vessel. For example in NPK the $H_2PO_4^-$ concentration increases from 0.017 gL^{-1} for day 1 to 0.045 gL^{-1} on 30th day, SRF1 increases from 0.015 gL^{-1} on day 1 to 0.040 gL^{-1} on the 30th day. Similarly CRF1 increases from 0.013 gL^{-1} on the first day to 0.034 gL^{-1} on the last day and lastly CRF2 increases from 0.015 gL^{-1} for the first day to 0.035 gL^{-1} on the 30th day. Table 4.25 shows that NPK releases the highest concentration of nutrients into water for the 30 days as indicated with letter A followed by SRF1 represented by letter B in thirteen days, letter A in 7 days and in the 5 days shown with letters AB.

The slow release of SRF 1 can be attributed to the multilayer porous clay sheets as discussed earlier in the release of NO_3^-. The $H_2PO_4^-$ which is dispersed into the interlayer spaces desorbs through the surface of the nanolayers through small pores regulated by BET isotherms as seen on Figure 4.16 of SRF1 and Figure 4.18 column of surface area and total pore volume as opposed to NPK that dissolves.

Generally Figure 4.25 shows that the CRF2 and CRF1 release lower concentrations of nutrients than SRF1 which is due to coating of SAPs which reduces the release process. The release in CRF2 for all the 30 days is lower than that of SRF1 due to the starch-GA coating on the SRF1 which protects the $H_2PO_4^-$ from dissolving rapidly. The OH in the

$H_2PO_4^-$ structure strongly attaches on the OH of the starch-GA crosslinks requiring stronger osmotic pressure to push the ion out of the product into the water.

On the other hand CRF1 displays the lowest release of nutrients for 26 of the 30 days represented with letter D for 6 days, letter C for 8 days, C* for 4 days, B* for 6 days and lastly A* for 2 days. The fact that CRF1 generally releases lower quantities of nutrients than CRF2 implies that the starch-PVA coat is more effective than the starch-GA coat. The stronger crosslinks in starch-PVA absorbs more water than those of starch-GA holding solutions for longer period than starch-GA as observed on Table 4.9 of water absorbency and 4.12 of water retention.

Figure 4.52 is derived from Table 4.25 and shows column of the concentrations of $H_2PO_4^-$ from the 50-50 products.

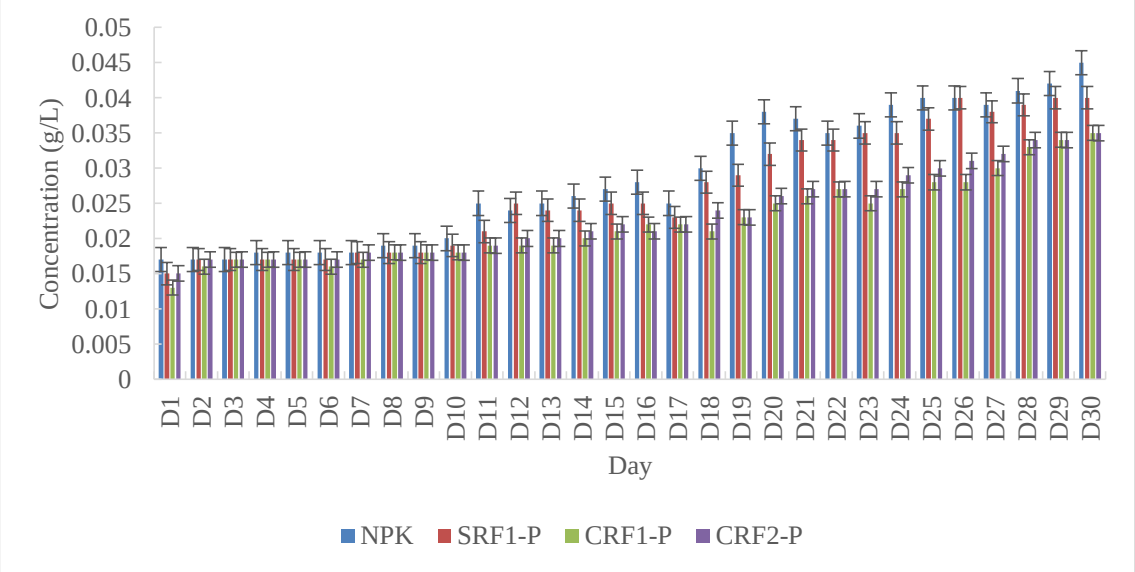

Figure 4. 52: Column of $H_2PO_4^-$ release from the 50-50 products

The error bars on Figure 4.52 show that there is no significant difference between all the treatments within the first 10 days. From the 11th day the error bars show that NPK and SRF1 do not show significance difference in release of nutrients, similarly CRF1 and

CRF2 do not show significance difference. However the concentrations of nutrients released by NPK and SRF1 are significantly higher from those of coated products. This implies that dispersing phosphorus into clay nanomatrix improves its release ability which is supported by the research of (Amanda *et al.*, 2011) on role of slow release nanocomposites on nitrogen and phosphorus availability. Figure 4.53 shows the rate of release of nutrients.

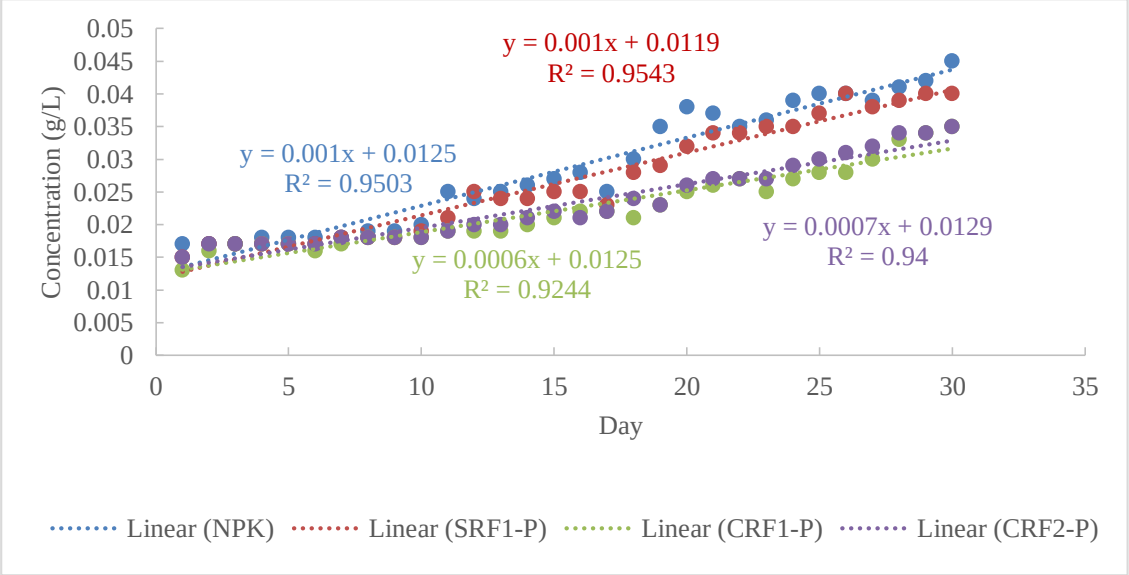

Figure 4. 53: Rate of release of $H_2PO_4^-$ in 50-50 formula

The nutrient release rates of $H_2PO_4^-$ showed linear relationship as in research of (Ding *et al.*, 2016). Generally the rate of release of $H_2PO_4^-$ into water is far less than NO_3^- which was also observed in (Himmah *et al.*, 2018) percolation tests.

The line graphs of P-NPK and P-SRF1 are close to each other and significantly far from those of the other two formulas P-CRF1 and P-CRF2. The trend shows that CRF1 has the slowest rate of release of nutrients followed by CRF2, SRF1 and lastly NPK. This is due to the difference in the way the $H_2PO_4^-$ comes out of the products. Whereas it dissolves from NPK into water, it desorbs from the surface of the organoclay mineral in

the case of SRF1 as was discussed on Table 4.25. This desorption is regulated by the total pore volume in the multifunctional material as seen on Figure 4.18. Lastly desorption from CRF1 and CRF2 is regulated by equilibrium between the solution in the sacks of the crosslinks in the SAPs and the water in addition to the effect of the total the pore volume discussed on Figure 4.26 of water absorbency.

In conclusion Figure 4.53 shows very close correlation between NPK and SRF1 with higher rates of release than CRF1 and CRF2. The phosphorus in the 50-50 formulation had low and erratic release trend which could be attributed to the decomposition of some of the $H_2PO_4^-$ into HPO_4^{2-} and PO_4^{3-} affecting the quantity of absorbance of $H_2PO_4^-$.

4.5.3 Nutrient retention and release capacity of potassium

The equations 4e and 4f on Appendix 31 was used to convert the absorbance on Appendix 4 into concentration in gL^{-1}. The analyzed data is given on Table 4.26.

Table 4. 26: Concentration of K^+ in 50-50 formula

Day	NPK-K ±SE	SRF1-K ±SE	CRF1-K ±SE	CRF2-K ±SE
1	0.020 ± 0.0001^{An}	0.019 ± 0.0000^{Bv}	0.018 ± 0.0001^{Ds}	0.019 ± 0.0001^{Csr}
2	0.022 ± 0.0003^{Amn}	0.020 ± 0.0000^{Btv}	0.0189 ± 0.0001^{Crs}	0.019 ± 0.0001^{BCt}
3	0.023 ± 0.0003^{Almn}	0.021 ± 0.0003^{Bt}	0.019 ± 0.0001^{Cqrs}	0.020 ± 0.0000^{BCst}
4	0.031 ± 0.0070^{Aghij}	0.022 ± 0.0000^{Bt}	0.020 ± 0.0003^{Cqrs}	0.020 ± 0.0002^{Cst}
5	0.024 ± 0.0005^{Aklmn}	$0.023\pm0.0003^{A*s}$	0.025 ± 0.0002^{Apqr}	0.026 ± 0.0005^{Ars}
6	0.024 ± 0.0001^{Aklmn}	0.024 ± 0.0001^{Ars}	0.022 ± 0.0010^{Aop}	0.022 ± 0.0020^{Aqr}
7	0.026 ± 0.0003^{Ajklmn}	0.025 ± 0.0002^{ABq}	0.025 ± 0.001^{ABnop}	0.024 ± 0.0001^{Bpq}
8	0.028 ± 0.0003^{Aijklm}	$0.028\pm0.0002^{A*rs}$	0.026 ± 0.001^{BCmnop}	0.028 ± 0.0020^{Aq}
9	0.029 ± 0.000^{Ahijklm}	0.027 ± 0.0003^{Apq}	0.027 ± 0.0010^{Amno}	$0.026\pm0.001^{A*op}$
10	0.028 ± 0.000^{Aijklm}	0.027 ± 0.000^{Aop}	$0.025\pm0.0020^{A*mn}$	0.026 ± 0.0020^{Ao}
11	0.029 ± 0.0002^{Ahijkl}	0.028 ± 0.0000^{Bno}	$0.029\pm0.0000^{A*lm}$	0.030 ± 0.0002^{Ano}
12	0.031 ± 0.0003^{Ahijk}	0.030 ± 0.0004^{An}	0.028 ± 0.0006^{Ckl}	0.029 ± 0.00^{ABmn}
13	0.032 ± 0.0001^{Aghj}	0.030 ± 0.0002^{Bm}	0.029 ± 0.0000^{Ckl}	0.030 ± 0.0001^{Bm}
14	0.034 ± 0.0001^{Agh}	$0.033\pm0.0006^{A*l}$	$0.029\pm0.0001^{B*jk}$	0.030 ± 0.0001^{Blm}
15	0.033 ± 0.0000^{Agh}	0.032 ± 0.0001^{Bk}	0.031 ± 0.0001^{Cij}	0.031 ± 0.0002^{Ckl}
16	0.036 ± 0.0030^{Ag}	0.033 ± 0.0001^{Bjk}	0.030 ± 0.0000^{Dhi}	0.032 ± 0.0001^{Cjk}
17	0.037 ± 0.0002^{Af}	0.035 ± 0.0003^{Bj}	0.031 ± 0.0001^{Dghj}	0.033 ± 0.0000^{Cij}
18	0.042 ± 0.0002^{Aefg}	0.038 ± 0.0000^{Bi}	0.034 ± 0.0003^{Cgh}	0.032 ± 0.0001^{Dhi}
19	0.043 ± 0.0001^{Aefg}	0.039 ± 0.0005^{Bh}	0.034 ± 0.0010^{Cfg}	$0.032\pm0.000^{C*gh}$
20	0.049 ± 0.0002^{Ade}	0.040 ± 0.0001^{Ag}	0.033 ± 0.0020^{Cef}	$0.030\pm0.002^{C*g}$
21	0.049 ± 0.0002^{Ad}	0.042 ± 0.0000^{Bh}	0.040 ± 0.0002^{Cf}	0.039 ± 0.0002^{Dg}
22	0.052 ± 0.0001^{Acd}	0.043 ± 0.0001^{Bf}	0.038 ± 0.0000^{Df}	0.040 ± 0.0000^{Cf}
23	0.053 ± 0.0003^{Acd}	0.043 ± 0.0001^{Bf}	0.039 ± 0.0000^{De}	0.042 ± 0.0000^{Cf}
24	0.054 ± 0.0004^{Acd}	0.046 ± 0.0004^{Bf}	0.043 ± 0.0001^{Cde}	0.038 ± 0.0001^{De}
25	0.056 ± 0.0003^{Ac}	0.047 ± 0.0002^{Bf}	0.041 ± 0.0000^{Db}	0.045 ± 0.0003^{Ce}
26	0.057 ± 0.0001^{Abc}	0.048 ± 0.0002^{Be}	0.042 ± 0.0003^{Ce}	0.042 ± 0.0010^{Cd}
27	0.058 ± 0.0003^{Aabc}	0.049 ± 0.0003^{Bd}	0.043 ± 0.0000^{Dcd}	0.046 ± 0.0003^{Cd}
28	0.059 ± 0.0008^{Aabc}	0.052 ± 0.0001^{Bc}	0.046 ± 0.0001^{Db}	0.048 ± 0.0003^{Cc}
29	0.066 ± 0.0001^{Aa}	0.059 ± 0.0000^{Bb}	$0.048\pm0.001^{C*bc}$	0.049 ± 0.0003^{Cb}
30	0.064 ± 0.0000^{Aa}	0.062 ± 0.0005^{Ba}	0.051 ± 0.0003^{Ca}	0.048 ± 0.0003^{Da}

Key: NPK is NPK fertilizer, SRF1 is 50-50 slow release fertilizer, CRF1 is starch-PVA coated SRF1, CRF2 is starch-GA coated SRF1, Mean values followed by the same capital letter(s) within the same column do not differ significantly from one another while mean values followed by the same small letter(s) within the same row do not differ significantly from one another (α=0.05, one-way ANOVA, Posthoc-Tukey-test). An asterisk (*) on a letter is used to show the lower value between values that are not significantly different in a row while the harmonic mean sample size, n=3.

Generally the concentration of nutrients released increases from day 1. For instance the release of K^+ from NPK for day 1 increases from 0.020 gL^{-1} to 0.064 gL^{-1} on 30th day, from 0.019 gL^{-1} to 0.062 gL^{-1} for SRF1, from 0.018 gL^{-1} to 0.051 gL^{-1} for CRF1 and lastly 0.019 gL^{-1} to 0.049 gL^{-1} for CRF2..

NPK releases the highest concentration of nutrients in all the 30 days statistically denoted by letter A. Generally SRF1 releases lower concentration of nutrients than NPK in 21 days labeled as letter B and in 5 days labeled A*. The slow release in SRF1 is attributed to the multilayer porous clay sheets. The K^+ dispersed into the interlayer spaces desorbs through the surface of the nanolayers as opposed to NPK that dissolves into the water. The amount of K^+ that desorbs will depend on the surface area of the multifunctional organoclay regulated by BET isotherms as discussed on Figure 4.15 of SRF1 and Figure 4.17 column of Surface area and total pore volume.

Both CRF1 and CRF2 have lower concentration of nutrients released than SRF1 as is observed from Table 4.26. CRF1 has the lowest concentration of nutrients released in 20 of the 30 days which confirms the argument that starch-PVA is a better SAP than starch-GA. The nutrient release rates showed a linear relationship as in research of (Ding *et al.,* 2016). Figure 4.54 gives a column for the data on Table 4.26 which establishes evidence of the trend discussed above.

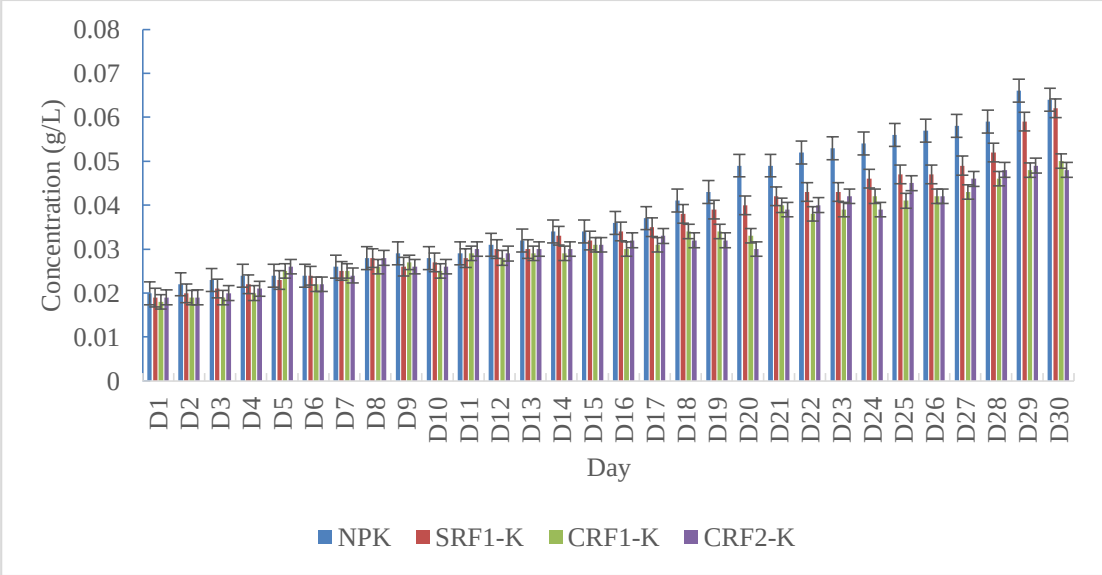

Figure 4. 54: Column of K+ dissolution from the 50-50 products

The concentrations of nutrients released from NPK shown as blue columns on Figure 4.54 are larger than the rest. The error bar analysis on Figure 4.54 shows that release of NPK was significantly higher than the other treatments for 10 days after day 18. The error bars do not show any significant difference between NPK and SRF1 on the 29th and 30th day after achieving equilibrium. The release from CRF1 and CRF2 is not significantly different for all the 30 days due to similar effect of the SAPs. Figure 4.55 shows the rate of release of K^+ from the treatments.

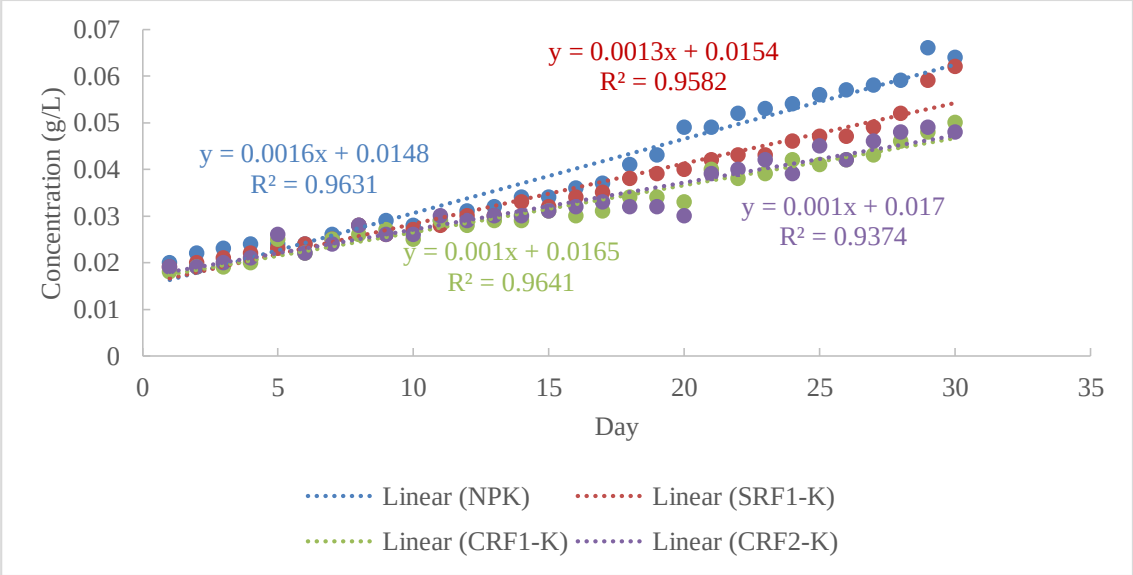

Figure 4. 55: Rate of release of K^+ in 50-50 formula

The data for the treatments on Table 4.25 was used to draw line graphs on Figure 4.55. The graphs of K-NPK and K-SRF1 significantly deviate from those of K-CRF1 and CRF2 which are relatively close to each other.

Potassium salts are very soluble in water hence their release in water can only be decreased due to attractions from the NO_3^- and $H_2PO_4^-$. Figure 4.55 shows slower nutrient release rate of K-CRF1 and K-CRF2 of 0.001 $gL^{-1}day^{-1}$ which is lower than that of SRF1, 0.0013 $gL^{-1}day^{-1}$ and NPK, 0.0016 $gL^{-1}day^{-1}$ which can be attributed to the effect of the SAP coating. NPK released the highest total of NO_3^- 0.288 gL^{-1} followed by CRF2 with 0.283 gL^{-1} then 0.280 gL^{-1} and SRF1 releases least amount of 0.268 gL^{-1}.

Table 4. 27: Analysis of treatments in 50-50 formulas

Treatment	NPK	SRF1	CRF1	CRF2
NO_3^-	0.179 ± 0.014^a	0.16 ± 0.013^a	0.157 ± 0.014^a	0.161 ± 0.014^a
$H_2PO_4^-$	0.029 ± 0.0017^a	0.027 ± 0.0026^{ab}	0.022 ± 0.0011^b	0.023 ± 0.0011^b
K^+	0.039 ± 0.0026^a	0.036 ± 0.00021^a	0.032 ± 0.0011^a	0.033 ± 0.0017^a

The data shows that CRF1 has the lowest release concentration of NO_3^- with 0.157 gL^{-1} followed by SRF1 with 0.16 gL^{-1} then CRF2 with 0.161 gL^{-1} and lastly NPK with 0.179 gL^{-1}. This is expected since SRF1 releases NO_3^- through the pores of the multifunctional organoclay as opposed to NPK that dissolves the nutrient in water. CRF1 has the lowest release of $H_2PO_4^{-1}$ with 0.022 gL^{-1} followed by CRF2 with 0.023 gL^{-1} then SRF1 with 0.027 gL^{-1} and lastly NPK with 0.029 gL^{-1}. In the case of K, CRF1 again has the lowest release capacity with 0.032 gL^{-1} followed by CRF2 with 0.033 gL^{-1}, then SRF1 with 0.036 gL^{-1} and lastly NPK with 0.039 gL^{-1}. The simulation shows that SRF1 is a slow release formula and its slow release capacity is improved with the starch-PVA that shows the lowest release capacity for all the treatments and starch-GA superabsorbent polymers.

4.6: Nutrient retention and release capacity for 70-30

A second SRF product, SRF2 fabricated from MOC2 was chemically analyzed by spectroscopic methods and physically by dissolving in deionized water. This was done to test which fabrication between the 50-50 and 70-30 formulas had better intercalation for dispersion of the nutrients.

4.6.1 Nutrient retention and release capacity of nitrogen for 70-30 formula

Equations 4g and 4h on Appendix 31 were used to convert the absorbance in Appendix 5 into concentration of NO_3^- into gL^{-1}. Table 4.28 shows the concentration of released nutrients over a period of 30 days.

Table 4. 28: Concentration of NO_3^- in 70-30 formula

DAY	NPK-N ±SE	SRF2-N ±SE	CRF3-N ±SE	CRF4-N ±SE
1	0.064 ± 0.0001^{Az}	0.047 ± 0.0000^{Bv}	0.032 ± 0.0001^{Dq}	0.035 ± 0.0001^{Cw}
2	0.080 ± 0.0001^{Ay}	0.049 ± 0.006^{Buv}	$0.034\pm0.0005^{C*pq}$	0.036 ± 0.0002^{Cvw}
3	0.087 ± 0.0001^{Ax}	0.055 ± 0.0004^{Btuv}	0.041 ± 0.0003^{Copq}	0.038 ± 0.0005^{Dvw}
4	0.095 ± 0.0001^{Aw}	0.058 ± 0.0001^{Btu}	0.040 ± 0.0002^{Dopq}	0.041 ± 0.0001^{Cv}
5	0.101 ± 0.0001^{Av}	0.059 ± 0.0001^{Bst}	$0.045\pm0.0000^{C*nopq}$	0.047 ± 0.0010^{Cu}
6	0.105 ± 0.0001^{Au}	0.059 ± 0.0006^{Bst}	0.047 ± 0.0005^{Dmnopq}	0.052 ± 0.0010^{Cu}
7	0.111 ± 0.0001^{At}	0.068 ± 0.0014^{Brs}	0.052 ± 0.0001^{Dlmnopq}	0.058 ± 0.0000^{Ct}
8	0.114 ± 0.0001^{Ast}	0.068 ± 0.0001^{Brs}	0.053 ± 0.0001^{Dlmnopq}	0.058 ± 0.0000^{Ct}
9	0.117 ± 0.0001^{As}	0.074 ± 0.0006^{Bqr}	0.062 ± 0.000^{Cklmnopq}	$0.061\pm0.0000^{C*st}$
10	0.124 ± 0.0001^{Ar}	0.079 ± 0.0000^{Bpq}	$0.063\pm0.00^{C*klmnopq}$	0.066 ± 0.0001^{Cs}
11	0.138 ± 0.0000^{Aq}	0.085 ± 0.0001^{Bop}	$0.068\pm0.002^{C*klmnop}$	0.071 ± 0.0003^{Cr}
12	0.146 ± 0.000^{Ap}	0.093 ± 0.000^{Bmno}	$0.074\pm0.0001^{C*jklmn}$	0.075 ± 0.0007^{Cqr}
13	0.148 ± 0.000^{Ap}	0.096 ± 0.000^{Bmn}	$0.078\pm0.0003^{C*jklmn}$	0.078 ± 0.0007^{Cq}
14	0.149 ± 0.000^{Ap}	0.086 ± 0.000^{Bnop}	0.081 ± 0.0003^{Djklm}	0.083 ± 0.0007^{Cp}
15	0.158 ± 0.001^{Ao}	0.101 ± 0.0002^{Blm}	0.085 ± 0.0000^{Dijkl}	0.093 ± 0.0003^{Co}
16	0.167 ± 0.000^{An}	0.109 ± 0.0001^{Bkl}	0.090 ± 0.0000^{Dijk}	0.094 ± 0.0012^{Co}
17	0.168 ± 0.000^{An}	0.116 ± 0.0009^{Bjk}	$0.104\pm0.0032^{C*hiji}$	0.104 ± 0.0001^{Cn}
18	0.175 ± 0.000^{Am}	0.125 ± 0.0011^{Bj}	0.105 ± 0.0001^{Dhij}	0.109 ± 0.0004^{Cm}
19	0.184 ± 0.0001^{Al}	0.136 ± 0.0001^{Bi}	0.079 ± 0.0338^{Djklmn}	0.116 ± 0.0002^{Cl}
20	0.207 ± 0.000^{Ak}	0.142 ± 0.0001^{Bi}	0.119 ± 0.0001^{Dghl}	0.125 ± 0.0002^{Ck}
21	0.215 ± 0.0001^{Aj}	0.154 ± 0.0001^{Bh}	0.129 ± 0.0002^{Dgh}	0.133 ± 0.0000^{Cj}
22	0.226 ± 0.0002^{Ai}	0.164 ± 0.0001^{Bg}	0.134 ± 0.0001^{Dfgh}	0.145 ± 0.0003^{Ci}
23	0.240 ± 0.000^{Ah}	0.164 ± 0.0000^{Bg}	0.143 ± 0.0001^{Defg}	0.152 ± 0.0002^{Ch}
24	0.255 ± 0.000^{Ag}	0.189 ± 0.0003^{Bf}	0.153 ± 0.0003^{Defg}	0.162 ± 0.0000^{Cg}
25	0.266 ± 0.0003^{Af}	0.197 ± 0.0001^{Bf}	0.165 ± 0.0003^{Ddef}	0.180 ± 0.0001^{Cf}
26	0.279 ± 0.0002^{Ae}	0.208 ± 0.0007^{Be}	0.174 ± 0.0016^{Dcde}	0.191 ± 0.0001^{Ce}
27	0.290 ± 0.000^{Ad}	0.219 ± 0.0048^{Bd}	$0.193\pm0.0031^{C*bcd}$	0.200 ± 0.0005^{Cd}
28	0.303 ± 0.0004^{Ac}	0.239 ± 0.0043^{Bc}	$0.206\pm0.0027^{C*abc}$	0.210 ± 0.0032^{Cc}
29	0.319 ± 0.000^{Ab}	0.255 ± 0.0003^{Bb}	0.223 ± 0.001^{Dab}	0.234 ± 0.0022^{Cb}
30	0.352 ± 0.0004^{Aa}	0.289 ± 0.0063^{Ba}	$0.238\pm0.0022^{C*a}$	0.245 ± 0.0027^{Ca}

Key: NPK is NPK fertilizer, SRF2 is 70-30 slow release fertilizer, CRF3 is starch-PVA coated SRF2, CRF4 is starch-GA coated SRF2, Mean values followed by the same capital letter(s) within the same column do not differ significantly from one another while mean values followed by the same small letter(s) within the same row do not differ significantly from one another (α=0.05, one-way ANOVA, Posthoc-Tukey-test). An asterisk (*) on a letter is used to show the lower value between values that are not significantly different in a row while the harmonic mean sample size, n=3

Like in Table 4.24 for the 50-50 there is a general increase in the concentration of nutrients dissolved from day 1. Table 4.28 shows that release of all nutrients increased with increase in days. For example NO_3^- in NPK released a concentration of 0.064 gL^{-1} on first day which increased to 0.352 gL^{-1} on the 30^{th} day, as compared to NO_3^- in SRF2 that increased from 0.047 gL^{-1} to 0.289 gL^{-1}, CRF3 from 0.032 gL^{-1} to 0.327 gL^{-1}, lastly CRF4 increased from 0.245 $gL^{-1}$to 0.035 gL^{-1}.

Table 4.28 attests to a decrease in release of NO_3^- across the table as was also observed on Tables 4.24, 4.25 and 4.26. In all the 30 days, NPK has the highest concentration released shown by letter A. The trend of NPK and SRF2 across the table for all the 30 days implies a difference between the structure of NPK and SRF2. This can only have come from effective intercalation and maximum dispersion of the NPK nutrients into the organoclay. This supports the XRD data on Figure 4.10 for SRF1, SRF2 overlay and Figure 4.9 of MOC1 and MOC2 that demonstrates that MOC2 has stronger intercalated pillars.

SRF2 has a lower released concentration than NPK for NO_3^- for the 30 days. This lower release of concentration can be attributed to the multilayer pores on the surface of the clay sheets. The NO_3^- which is dispersed into the interlayer spaces desorbs through the surface of the nanolayers through these small pores as opposed to NPK that dissolves. This release from SRF2 depends on the surface area of the multifunctional organoclay as observed on Figure 4.16 that shows presence of micropores and Figure 4.18 that compares the adsorption and desorption of surface area and total pore volume of SRF1.

CRFs show lower release than SRF2 for all the 30 days due to starch-PVA coating and starch-GA which effectively protect them from releasing the nitrogen, by slowly absorbing NO_3^- solution until its equilibrium point before slowly releasing the same into the water.

Table 4.28 submits evidence that CRF3 has the lower release of NO_3^- than CRF4 as was also established in the discussion of Tables 4.24, 4.25 and 4.26. This implies that the starch-PVA has superior water absorption and retention than starch-GA superabsorbent. Starch-PVA has a higher equilibrium for the water absorption due to its larger number of OH crosslinks. The data on Table 4.28 was used to plot a column of Figure 4.56.

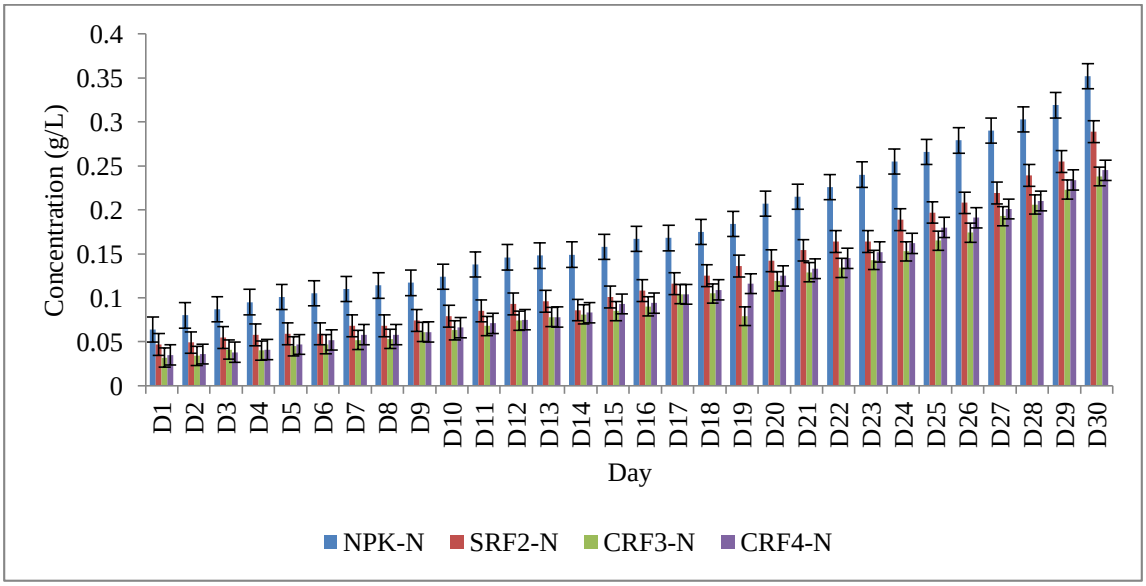

Figure 4. 56: column for release of NO3- from 70-30 formulas

The error bars on Figure 4.56 show that the release of NO_3^- from CRF3 and CRF4 are not significantly different for 29 days except for day 19. From the 22nd day SRF2 releases significantly more NO_3^- than CRF3 and CRF4. This is due to the fact that after 20 days the SRF2 formula breaks down into the water exposing more layers to desorption.

Other than for the first day the release of NO_3^- from NPK is significantly higher than the rest of the treatments during all the time of the study. In order to study the rates of release, the data on Table 4.28 was used to draw Figure 4.57.

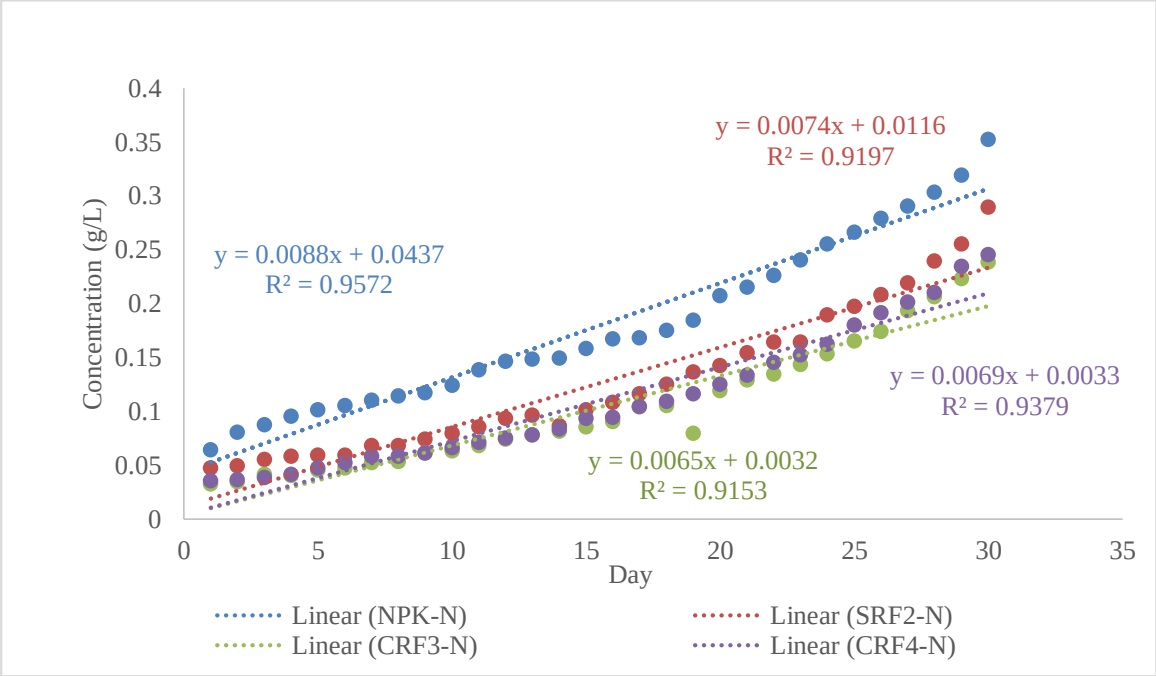

Figure 4. 57: Rate of release of NO_3^- in 70-30 treatments

The straight line representing NPK-N has a significantly higher rate of 0.0088$gL^{-1}day^{-1}$. There is also significant difference between the gradients of SRF2-N from those of CRF3-N and CRF4-N that are very close to each other. This trend supports the nature of release as was discussed earlier, that NPK dissolves into the soil solution when the NO_3^- in SRF2 desorbs through the pores slowly and even more slowly when it has to pass through a layer of a SAP coat. The rate of release of NO_3^- in SRF2 is 0.0074 $gL^{-1}day^{-1}$ which is higher than CRF3 with 0.0065 $gL^{-1}day^{-1}$. CRF4 has a slightly higher release capacity of 0.0069 $gL^{-1}day^{-1}$ than CRF3.This is due to the larger number of OH crosslinks in the starch-PVA than starch-GA that enables it to absorb a lot of water

before it desorbs it across the film into the solution. The nutrient release rates showed a linear relationship as in research of (Ding *et al.,* 2016).

This discussion supports data on XRD from Figure 4.10 whose argument that SRF2 with an intercalation ratio of 70 % CTAB to 30 % DMSO-modified clay is a better nano product than SRF1 subsequently making the coated CRF3 and CRF4 more superior to CRF1 and CRF2.

4.6.2 Nutrient retention and release capacity of $H_2PO_4^-$ for 70-30 formula.

Equations 4i and 4j on Appendix 31 were used to convert the absorbance on Appendix 6 into concentration in ppm into gL^{-1}. The analyzed data is recorded on Table 4.29.

Table 4. 29: Concentration of Phosphorus in for 70-30 formula

DAY	NPK-P ±SE	SRF2-P ±SE	CRF3-P ±SE	CRF4-P ±SE
1	0.017 ± 0.0001^{Ae}	0.015 ± 0.0002^{Bv}	0.009 ± 0.0002^{Dp}	0.012 ± 0.000^{Cu}
2	0.017 ± 0.0001^{Ae}	$0.016\pm0.001^{A*uv}$	0.010 ± 0.0002^{Cp}	0.013 ± 0.0000^{Bu}
3	$0.017\pm0.0001^{A*e}$	0.017 ± 0.0002^{Atu}	0.010 ± 0.0002^{Cp}	0.013 ± 0.0000^{Btu}
4	0.018 ± 0.0001^{Aabcd}	$0.018\pm0.000^{A*st}$	0.012 ± 0.0003^{Cop}	0.014 ± 0.0001^{Bstu}
5	$0.018\pm0.0002^{A*de}$	0.018 ± 0.0006^{Ast}	$0.012\pm0.000^{B*no}$	0.013 ± 0.000^{Brstu}
6	$0.018\pm0.0000^{A*de}$	0.019 ± 0.0000^{Ars}	$0.013\pm0.00^{B*mno}$	0.014 ± 0.0000^{Brst}
7	0.018 ± 0.0001^{Bde}	0.020 ± 0.0001^{Aqr}	0.013 ± 0.000^{Dmno}	0.014 ± 0.0000^{Cqrs}
8	0.019 ± 0.0001^{Bcde}	0.021 ± 0.0002^{Apq}	0.013 ± 0.000^{Dmno}	0.015 ± 0.0003^{Cqr}
9	0.019 ± 0.0000^{Bcde}	0.021 ± 0.0001^{Aop}	0.014 ± 0.000^{Dlmn}	0.016 ± 0.0000^{Cq}
10	0.020 ± 0.0001^{Bbcde}	0.022 ± 0.0001^{Ano}	0.015 ± 0.0001^{Dln}	0.018 ± 0.0007^{Cop}
11	0.025 ± 0.000^{Aabcde}	0.023 ± 0.000^{Bmn}	0.016 ± 0.0001^{Dkl}	0.017 ± 0.0003^{Cp}
12	0.024 ± 0.000^{Aabcde}	$0.024\pm0.00^{A*m}$	0.016 ± 0.0001^{Ckl}	0.019 ± 0.000^{Bnop}
13	0.025 ± 0.000^{Aabcde}	0.025 ± 0.0001^{Al}	0.017 ± 0.0002^{Cjkl}	0.019 ± 0.000^{Bmno}
14	0.026 ± 0.000^{Aabcde}	$0.026\pm0.00^{A*kl}$	0.018 ± 0.0000^{Cijk}	0.020 ± 0.0002^{Bmn}
15	0.027 ± 0.000^{Aabcde}	$0.026\pm0.0001^{A*k}$	0.019 ± 0.0000^{Cij}	0.020 ± 0.0002^{Blk}
16	$0.028\pm0.000^{A*abcde}$	0.028 ± 0.000^{Aj}	0.018 ± 0.0000^{Cijk}	0.021 ± 0.0001^{Bkl}
17	0.025 ± 0.0001^{Babcde}	0.029 ± 0.0001^{Aj}	0.019 ± 0.0000^{Cij}	0.022 ± 0.0003^{Bjk}
18	0.030 ± 0.000^{Aabcde}	$0.029\pm0.0006^{A*ij}$	0.020 ± 0.0003^{Chi}	0.023 ± 0.0000^{Bj}
19	0.035 ± 0.000^{Aabcde}	0.030 ± 0.0002^{Bi}	$0.022\pm0.002^{C*fg}$	0.023 ± 0.0001^{Cj}
20	0.038 ± 0.0040^{Aabcde}	0.032 ± 0.0000^{Bh}	0.021 ± 0.0000^{Dgh}	0.025 ± 0.0000^{Ci}
21	0.037 ± 0.0001^{Aabcde}	0.035 ± 0.0002^{Bg}	0.022 ± 0.0001^{Dfg}	0.026 ± 0.0001^{Chi}
22	0.035 ± 0.0002^{Aabcde}	$0.035\pm0.0002^{A*g}$	0.024 ± 0.0000^{Cef}	0.027 ± 0.0001^{Bgh}
23	0.036 ± 0.0004^{Aabcde}	$0.036\pm0.0002^{A*fg}$	0.024 ± 0.0009^{Cef}	0.028 ± 0.0003^{Bfg}
24	0.039 ± 0.0000^{Aabcd}	0.037 ± 0.0000^{Bef}	0.026 ± 0.0003^{Dde}	0.029 ± 0.0001^{Cef}
25	0.040 ± 0.0003^{Aabc}	$0.037\pm0.0002^{A*e}$	0.027 ± 0.0009^{Cd}	$0.030\pm0.s0003^{Bde}$
26	$0.040\pm0.0002^{A*ab}$	0.041 ± 0.0001^{Acd}	0.030 ± 0.0001^{Cc}	0.031 ± 0.0004^{Bcd}
27	0.039 ± 0.0000^{Babcd}	0.043 ± 0.0001^{Aab}	0.030 ± 0.0001^{Dc}	0.032 ± 0.0000^{Cc}
28	0.041 ± 0.0003^{Aab}	0.042 ± 0.0002^{Bbc}	$0.034\pm0.0001^{C*b}$	0.035 ± 0.0001^{Cb}
29	0.042 ± 0.0000^{Aa}	0.040 ± 0.0002^{Bd}	0.037 ± 0.0003^{Ca}	$0.036\pm0.0005^{C*b}$
30	0.045 ± 0.0002^{Aa}	$0.045\pm0.0002^{A*a}$	$0.038\pm0.0006^{B*a}$	0.038 ± 0.0003^{Ba}

Key: NPK is NPK fertilizer, SRF2 is 70-30 slow release fertilizer, CRF3 is starch-PVA coated SRF2, CRF4 is starch-GA coated SRF2, Mean values followed by the same capital letter(s) within the same column do not differ significantly from one another while mean values followed by the same small letter(s) within the same row do not differ significantly from one another (α=0.05, one-way ANOVA, Posthoc-Tukey-test). An asterisk (*) on a letter is used to show the lower value between values that are not significantly different in a row while the harmonic mean sample size, n=3.

The data on Table 4.29 shows an increase in release of $H_2PO_4^-$ from the 1st day for all the treatments until the peak at the 30th day. A comparison of day one and day 30 shows that $H_2PO_4^-$ in NPK increased from 0.0166 gL^{-1} to 0.0447 gL^{-1}, SRF2 increased from 0.0152 gL^{-1} to 0.0445 gL^{-1}, CRF3 increased from 0.0093 gL^{-1} to 0.0376 gL^{-1} and lastly CRF4 from 0.0122 gL^{-1} to a high of 0.0384 gL^{-1}. NPK had the largest release of $H_2PO_4^-$ for 21 of all the 30 days denoted by letter A. The relatively small difference between the release of $H_2PO_4^-$ from NPK and SRF2 over the 30 days could be explained by the strong interionic repulsions that form when $H_2PO_4^-$ is in the small interlayer distances. However the lower release in SRF2 than NPK during the 30 days can be attributed to the multilayer pores on the clay sheets as seen on the SEM picture of white clay on plate 4.2 and TEM on plate 4.4. The $H_2PO_4^-$ which is dispersed into the interlayer spaces desorbs through the surface of the nanolayers through these small pores as opposed to NPK that dissolves. The amount of $H_2PO_4^-$ that desorbs depends on the surface area of the multifunctional organoclay as discussed on Figure 4.18.

Both CRF3 and CRF4 have lower concentrations released than SRF2. This shows that the SAPs used are effective in enhancing a reduction in the release capacity of the products as was observed on Table 4.12 on water retention.

A comparison between CRF3 and CRF4 shows that CRF3 releases lower concentration than CRF4 which could be due to the larger, stronger OH crosslinks that form strong hydrogen bonds with the OH of the $H_2PO_4^-$ as is observed on Table 4.29. The data on Table 4.29 were used to draw the column of Figure 4.58.

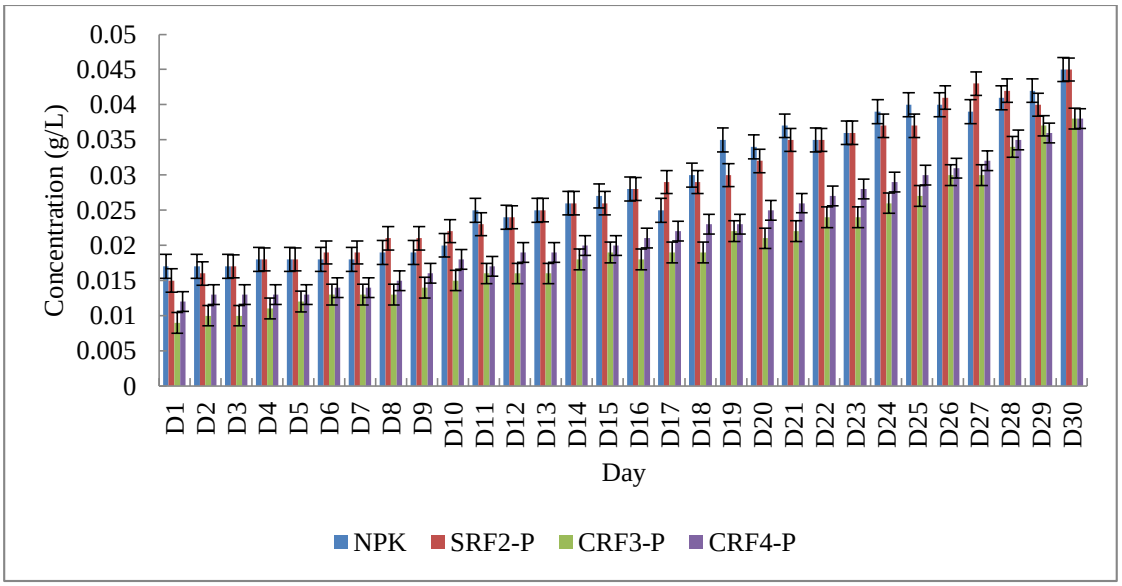

Figure 4. 58: Column for release of $H_2PO_4^-$ from 70-30 formula

The error bars on Figure 4.58 show that release of $H_2PO_4^-$ from NPK and SRF2 are not significantly different except for the 19th and 27th day. This collaborates (Amanda *et al.*, 2017) that the SRF formulation improve the release of phosphorus. The release of $H_2PO_4^-$ from CRF3 and CRF4 are not significantly different except for the 18th, 20th, 21st and 23rd day. The starch-PVA product shows lower concentrations released than starch-GA product up to around the 27th day when the two level up. The lower release of $H_2PO_4^-$ could be due to strong associations that are developed between it and the CTAB surfactant in the interlayer distances as was also noted by (Bronschat & Moore, 2007). The difference between starch-PVA and starch-GA effect reduces as the coating dissolves in water. The data also shows that starch-GA dissolves more rapidly that starch-PVA.

The data on Table 4.29 was used to draw a graph as Figure 4.59. The nutrient release rates showed a linear relationship as in research of (Ding *et al.*, 2016).

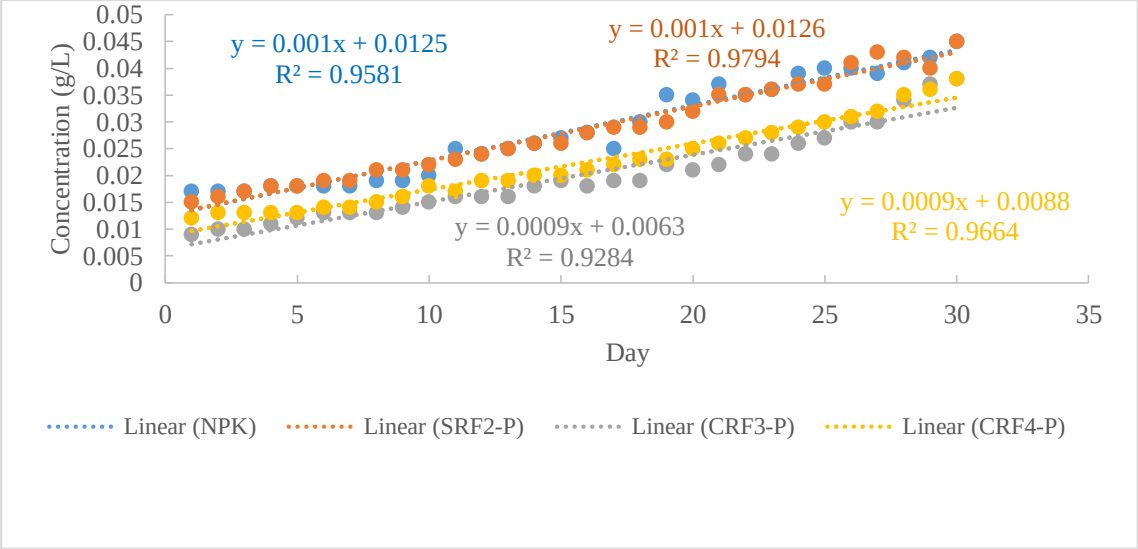

Figure 4. 59: Release of $H_2PO_4^-$ from SRF2 70-30 formulas

The rate of release of $H_2PO_4^-$ of both NPK and SRF2 is 0.001 gL^{-1} hence the lines of NPK and SRF2 on Figure 4.59 tend to superimpose. These two lines are spaced from the lines representing the coated products CRF3 and CRF4. The line graphs representing the coated products are parallel and with the same gradient though spaced from each other.

It is worth noting that amounts of $H_2PO_4^-$ dissolving out is smaller than the other nutrients since part of the $H_2PO_4^-$ is ionized into PO_4^{3-} and HPO_4^{2-} that were not studied by the UV analysis and also $H_2PO_4^-$ is strongly attracted to the K^+ reducing its release into solution. The rate of release of P-NPK is slightly higher than that of SRF2 which is slower due to the mode of release as previously discussed.

4.6.3 Nutrient retention and release capacity of Potassium for 70-30 formula

The Equations 4k and 4l on Appendix 31 were used to convert the absorbance on Appendix 7 into concentration in gL^{-1}. The analyzed data for the concentration of K^+ in gL^{-1} is recorded on Table 4.28 below.

Table 4. 30: Concentration of Potassium in 70-30 formula

DAY	NPK-K ±SE	SRF-K ±SE	CRF3-K ±SE	CRF4-K ±SE
1	0.020 ± 0.0001^{Ab}	0.019 ± 0.0002^{Br}	$0.019\pm0.0021^{B*n}$	0.020 ± 0.0002^{Ap}
2	0.022 ± 0.0003^{Ab}	0.020 ± 0.0004^{Br}	0.019 ± 0.0000^{Bmn}	0.019 ± 0.0001^{BCp}
3	0.023 ± 0.0003^{Ab}	0.020 ± 0.0004^{Br}	$0.020\pm0.0001^{B*mn}$	0.020 ± 0.0003^{Bop}
4	0.024 ± 0.0002^{Ab}	0.020 ± 0.0004^{Bq}	0.020 ± 0.0004^{Amn}	0.020 ± 0.0002^{Aop}
5	0.024 ± 0.0005^{Ab}	0.023 ± 0.0004^{ABq}	0.022 ± 0.0002^{Bkl}	0.022 ± 0.0001^{Bklm}
6	0.024 ± 0.0001^{Ab}	0.023 ± 0.0001^{ABp}	0.022 ± 0.0002^{Blm}	0.023 ± 0.0003^{ABno}
7	0.026 ± 0.0003^{Aab}	0.020 ± 0.0001^{Bop}	0.023 ± 0.0006^{Ckl}	0.024 ± 0.0000^{BCmn}
8	0.028 ± 0.0003^{Aab}	0.024 ± 0.0001^{Bmn}	0.024 ± 0.0002^{Bijk}	$0.024\pm0.0002^{B*jkl}$
9	0.029 ± 0.0002^{Aab}	0.027 ± 0.0005^{Bno}	$0.024\pm0.0000^{C*ijk}$	0.026 ± 0.0001^{Clm}
10	0.028 ± 0.0001^{Aa}	0.027 ± 0.0001^{Bmn}	$0.025\pm0.0001^{B*jkl}$	0.027 ± 0.0001^{Alm}
11	0.029 ± 0.0002^{Aab}	0.028 ± 0.0001^{Bm}	0.026 ± 0.0005^{Dghi}	0.027 ± 0.0000^{Chij}
12	0.031 ± 0.0003^{Aab}	0.029 ± 0.0000^{ABl}	0.027 ± 0.0002^{Chijk}	0.029 ± 0.0007^{BCijk}
13	0.032 ± 0.0001^{Aab}	0.029 ± 0.0002^{Al}	$0.027\pm0.0001^{A*ghij}$	0.030 ± 0.0002^{Aghij}
14	0.034 ± 0.0001^{Aab}	0.031 ± 0.0001^{Bk}	0.030 ± 0.0020^{Dghij}	0.030 ± 0.0001^{Cghij}
15	0.033 ± 0.0000^{Aab}	0.032 ± 0.0003^{Bk}	0.031 ± 0.0000^{Cfgh}	0.032 ± 0.0001^{Bghi}
16	0.036 ± 0.0030^{Aab}	0.034 ± 0.0001^{Bj}	0.032 ± 0.0010^{Cfghi}	0.033 ± 0.0001^{BCgh}
17	0.037 ± 0.0002^{Aab}	0.035 ± 0.0001^{ABj}	0.033 ± 0.0001^{Bfgh}	0.034 ± 0.0000^{ABg}
18	0.042 ± 0.0002^{Aab}	0.035 ± 0.0001^{Bi}	$0.034\pm0.0001^{C*f}$	0.035 ± 0.0002^{BCgh}
19	0.043 ± 0.0001^{Aab}	0.037 ± 0.0001^{Bi}	0.035 ± 0.000^{Df}	0.036 ± 0.0001^{Cgh}
20	0.050 ± 0.0002^{Aab}	0.039 ± 0.0002^{Bh}	0.036 ± 0.0002^{Dfg}	0.038 ± 0.0003^{Cghij}
21	0.049 ± 0.0002^{Aab}	$0.038\pm0.0001^{C*g}$	0.040 ± 0.0003^{Bde}	0.0374 ± 0.0003^{Cef}
22	0.052 ± 0.0001^{Aab}	0.041 ± 0.0000^{Bg}	0.036 ± 0.0005^{Ce}	0.0402 ± 0.0009^{Bdef}
23	0.053 ± 0.0002^{Aab}	0.046 ± 0.0010^{Bg}	0.040 ± 0.0001^{Cde}	0.0400 ± 0.0010^{Cde}
24	0.054 ± 0.0002^{Aab}	0.045 ± 0.0001^{Bf}	$0.042\pm0.0001^{C*cd}$	0.0431 ± 0.0000^{Cf}
25	0.056 ± 0.0002^{Aab}	0.046 ± 0.0001^{Ce}	0.047 ± 0.0010^{Dde}	0.0442 ± 0.0001^{Cc}
26	0.057 ± 0.0000^{Aab}	0.048 ± 0.0003^{Be}	0.041 ± 0.0001^{Dcd}	0.0465 ± 0.0001^{Cd}
27	0.058 ± 0.0002^{Aab}	0.050 ± 0.0001^{Bd}	0.044 ± 0.0006^{Dcd}	0.0477 ± 0.0000^{Cbc}
28	0.059 ± 0.0005^{Aab}	0.053 ± 0.0001^{Bc}	0.047 ± 0.0001^{Dbc}	0.0507 ± 0.0003^{Cab}
29	0.066 ± 0.0000^{Aab}	0.056 ± 0.0003^{Bb}	0.045 ± 0.0001^{Dab}	0.0535 ± 0.0001^{Ca}
30	0.064 ± 0.0000^{Aab}	0.059 ± 0.0001^{Ba}	0.053 ± 0.0001^{Da}	0.0566 ± 0.0000^{Ca}

Key: NPK is NPK fertilizer, SRF2 is 70-30 slow release fertilizer, CRF3 is starch-PVA coated SRF2, CRF4 is starch-GA coated SRF2, Mean values followed by the same capital letter(s) within the same column do not differ significantly from one another while mean values followed by the same small letter(s) within the same row do not differ significantly from one another (α=0.05, one-way ANOVA, Posthoc-Tukey-test). An asterisk (*) on a letter is used to show the lower value between values that are not significantly different in a row while the harmonic mean sample size, n=3.

The trend of concentration of K^+ released on Table 4.30 from the 1st day to the last day the analysis is similar to that of the other nutrients for all the treatments. For example the release from NPK was 0.02 gL^{-1} on the first day which increased to 0.064 gL^{-1} on the last day, similarly SRF1 increased from 0.0191 gL^{-1} to 0.0591 gL^{-1}, the one of CRF1 increased from 0.0186 gL^{-1} to 0.0532 gL^{-1} and lastly CRF4 release increased from 0.0204 gL^{-1} to 0.0566 gL^{-1}.

CRF3 and CRF4 released lower concentrations than both NPK and SRF2 for the 30 days. This is due to the SAP coating on the SRF2. Apart from developing a barrier between SRF2 and the water, it desorbs according to diffusion equilibrium between the K^+ ions in the product and those in the water.

Table 4.30 shows that CRF3 has the lowest release of nutrients in 23 of the 30 days. This suggests that the starch-PVA coating offers better slow release cover than the starch-GA coat due to its higher OH crosslinks. The points on Table 4.30 were used to draw a column to compare the quantitative difference in the products on daily basis as Figure 4.60.

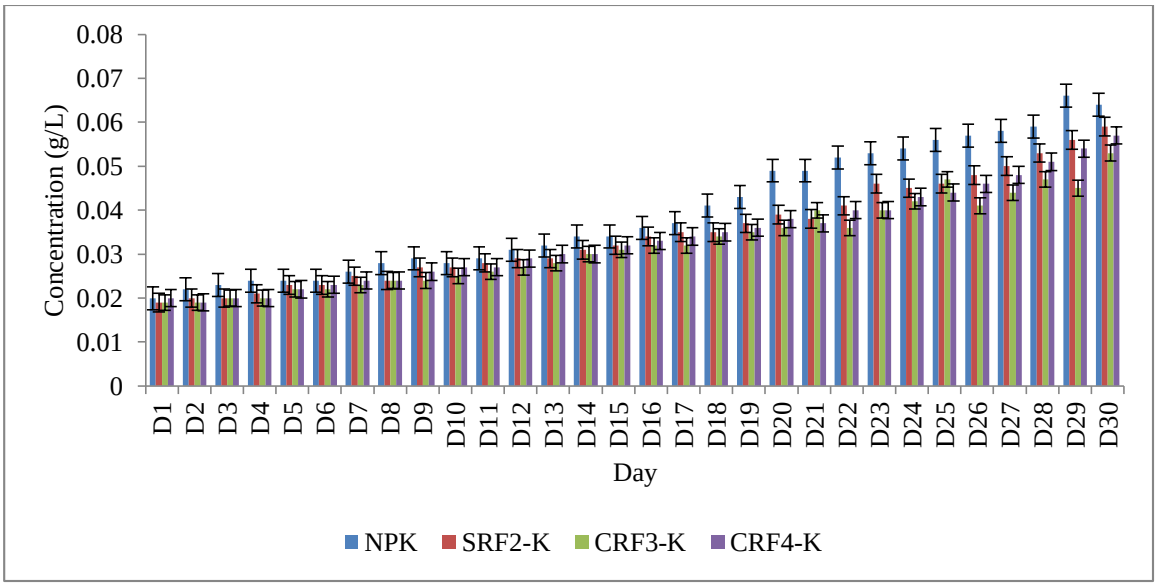

Figure 4. 60: Column for release of K^+ from 70-30 formula

The error bars on Figure 4.60 display release of K^+ from NPK that is significantly higher than the other treatments for 8th day, then from 18th day to the 29th day. So as the products dissolve into water, the difference between dissolving process of NPK and desorption one for SRF2, CRF3 and CRF4 is clearly demonstrated. The overall release of K^+ at 0.065gL^{-1} is lower than that of NO_3^- that is 0.35gL^{-1}. The lower release of K^+ could be attributed to the very strong attractions between K^+ and NO_3^-, $H_2PO_4^-$, in the interlayer distances. It could also be due to strong interactions between K^+ and the OH on the T-O, T-O-T sheets within the interlayers.

The data on Table 4.30 was also used to plot a graph to show the rate of release in the 30 days shown as Figure 4.61. The nutrient release rates showed a linear relationship as in research of (Ding *et al.*, 2016).

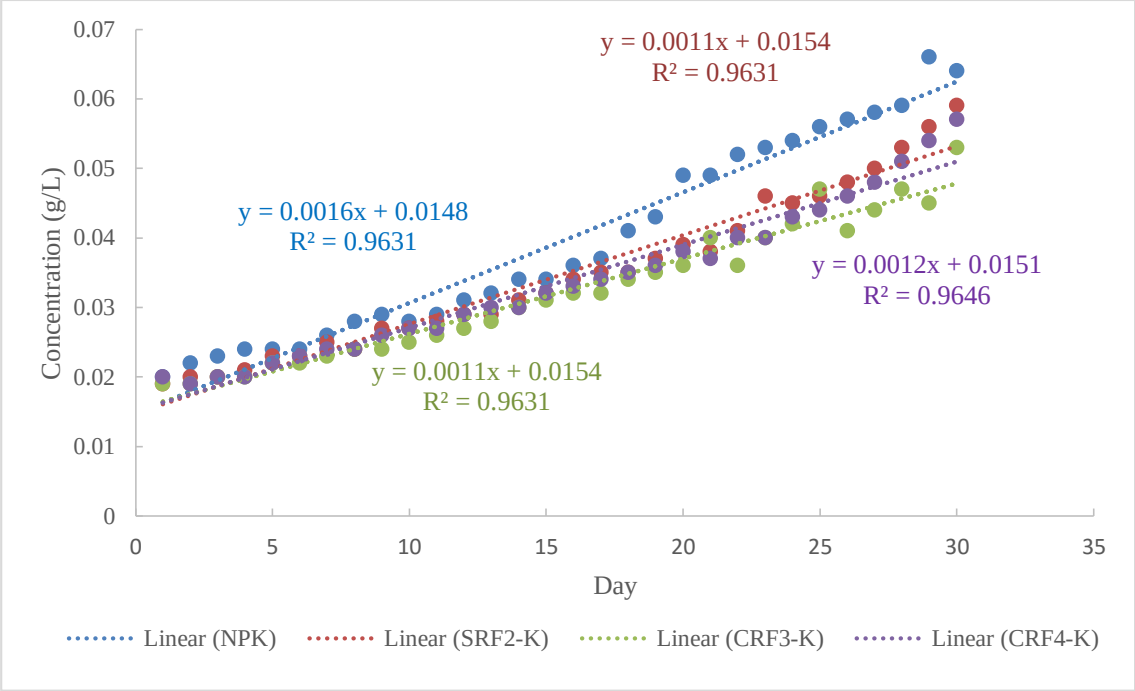

Figure 4. 61: Rate of release of K^+ in 70-30 formulas

Figure 4.61 illustrates that the rate of release of K^+ in SRF2 which is $0.0013gL^{-1}$ is lower than that of NPK which is $0.0016gL^{-1}$. K^+ is a small cation hence easily passes through the pores in the structure of the multifunctional organoclay. The positive on the nitrogen of CTAB generates a repulsion force to the K^+, which when coupled with the negative charge on TOT enhances drive to the TOT sheets enhancing desorption. Figure 4.61 shows a fairly gradual rise in the rate of release except for days 23 and 24. K^+ is soluble but is however strongly attracted to NO_3^- and $H_2PO_4^-$ which reduces the amount of the ion dissolving into the water from the product. However intercalation and encapsulation drastically reduces the release of K+ in water as is seen from the difference in the rate of NPK which is 0.0016 gL^{-1} and that of SRF2 which is 0.0013 gL^{-1}.

Figure 4.61 displays a rate value of $0.0011gL^{-1}$ for CRF3 that is not significantly different from that of CRF1 which is $0.001gL^{-1}$. However the starch-PVA coating on SRF2 has reduced the release from $0.0013gL^{-1}$ to $0.0011gL^{-1}$.

Figure 4.61 shows the rate of release of K^+ in CRF4 as $0.0012gL^{-1}$ which is not significantly different from that $0.001\ gL^{-1}$ of CRF2. The slightly higher rate in CRF4 points to slightly less cross-linked SAP of starch-GA as compared with starch-PVA. The effect of coating is also seen to generally reduce the dissolution of the nutrients.

4.6.4 Analysis of release of nutrients from in 70-30 formula

It is noted from Tables 4.28, 4.29 and 4.30 that the concentration of nutrients released into water increased until it peaked. The steady constant concentration of release of nutrients after day 30 showed that equilibrium had been achieved between the nutrients in the 1L solution and the formulas.

Table 4. 31: Statistical analysis of 70-30 Treatment

Treatments	NPK ±SE	SRF2 ±SE	CRF3 ±SE	CRF4 ±SE
NO_3^-	0.179 ± 0.0144^a	0.126 ± 0.0124^b	0.104 ± 0.0109^b	0.110 ± 0.0114^b
$H_2PO_4^-$	0.029 ± 0.0017^a	0.028 ± 0.0016^a	0.020 ± 0.008^b	0.022 ± 0.0014^b
K^+	0.039 ± 0.0026^a	0.035 ± 0.0021^a	0.032 ± 0.0018^a	0.034 ± 0.002^a

Key: NPK is NPK fertilizer, SRF2 is 70-30 slow release fertilizer, CRF3 is starch-PVA coated SRF2, CRF4 is starch-GA coated SRF2, mean values followed by the same small letter(s) within the same row do not differ significantly from one another (α=0.05, one-way ANOVA, Posthoc-Tukey-test) while the harmonic mean sample size, n=3.

Table 4.31 shows that SRF2 released lower concentration for all the treatments than NPK. This is expected since SRF2 desorbs the nutrients through pores in the surface of the clay mineral as seen on Figure 4.18 as opposed to NPK that simply dissolves.

The release capacity of SRF2 on Table 4.31 is higher than the coated formulas of CRF3 and CRF4. The SAP coating on the SRF2 absorbs and retains nutrients for longer period as discussed under Figure 4.10 on water absorbency.

Lastly CRF3 releases lower concentration of all the nutrients than CRF4 which supports the discussion on Tables 4.11 of water diffusivity and 4.12 of fickian factor.

4.6.5 Comparison of release of nutrients in 70-30 and 50-50 formulas

Tables 4.27 and 4.31 show the release of nutrients from the treatments for the 50-50 and 70-30 formulas respectively.

Table 4. 32: Comparison of 70-30 and 50-50

Treatment	NPK	SRF1	SRF2	CRF1	CRF3	CRF2	CRF4
NO_3^-	0.179± 0.014^{a}	0.160±0. 013^{abc}	0.126±0. 012^{bc}	0.157±0. 014^{abc}	0.1040± 0.011^{c}	0.16±0 .014^{ab}	0.1100± 0.011^{bc}
$H_2PO_4^-$	0.029± 0.002^{a}	0.027±0. 002^{ab}	0.0283± 0.009^{ab}	0.0224± 0.001^{ac}	0.0199± 0.002^{c}	0.023± 0.0^{abc}	0.0221± 0.002^{bc}
K^+	0.040± 0.003^{a}	0.036±0. 002^{a}	0.0350± 0.002^{a}	0.0320± 0.002^{a}	0.0320± 0.002^{a}	0.033± 0.002^{a}	0.0340± 0.0020^{a}

Key: NPK is NPK fertilizer, SRF2 is 70-30 slow release fertilizer, CRF3 is starch-PVA coated SRF2, CRF4 is starch-GA coated SRF2, mean values followed by the same small letter(s) within the same row do not differ significantly from one another (α=0.05, one-way ANOVA, Posthoc-Tukey-test) while the harmonic mean sample size, n=3.

The data on Table 4.32 shows that all treatments release less concentrations of nutrients than NPK. SRF2 releases 0.126 gL^{-1} NO_3^- which is less than 0.16 gL^{-1} released by SRF1 similarly SRF2 releases 0.035 gL^{-1} of K^+ which is slightly less than 0.036 gL^{-1} released by SRF1 which confirms the argument from the XRD that the SRF2 is better intercalated than SRF1. However SRF2 releases more $H_2PO_4^-$ than SRF1. This means conversion of the fertilizer into an SRF formula would improve availability of P known

to be a limiting element in all fertilizers (Amanda *et al.,* 2017). This trend is observed in CRFs in which the 70-30 CRFs release less NO_3^- and $H_2PO_4^-$ than the 50-50 formulas.

In conclusion the XRD data of SRF2 of Figure 4.10 suggests that the 70-30 formula is a better intercalated formula than 50-50 as is supported by a comparison on the Table 4.32. This informed the decision to use SRF2 in the optimization with a maize crop.

4.7 Analysis of the nutrients from the formulas into soils.

The maize yields have been decreasing in the past years due to continuous cropping, increased population pressure on the arable land, degradation of land resource and low investments into maize farming activities (Owino, 2010). Fertilizers are extensively used to improve the yield with little effect especially for small scale farmers. Studies show that phosphate absorption is increased under low pH in soils (Owino, 2010) though the DAP which is extensively used is known to increase acidity beyond levels of suitable absorption. It is also noted that N should be applied with P since N improves P uptake (Sangakhara & Cho, 2008).

4.7.1 Nitrates nutrients in soils of crops

Poor and declining soil fertility is a major challenge for crop production with nitrogen and phosphorus as most limiting elements (Kadiata & Lumpungu, 2003); (Tenning *et al.,* 2013). It is noted from research of (Onasanya *et al.,* 2009) that nitrogen contributes immensely to maize growth and yield. However crops take in often less than half of the nitrogen applied due to volatilization and nitrate leaching (Bouwman *et al.,* 2002); (Ngosong *et al.,* 2019). This increase in unused nitrogen causes soil degradation, nutrient imbalance, salinization and reduction in soil pH (Zhou *et al.,* 2013); (Zhong *et al.,* 2014). Sub-Saharan Africa averagely uses 10 kg/Ha as compared to 87 kg/Ha used

in developed countries (Bekunda *et al.*, 2010); (Ngosong *et al.*, 2019) hence being responsible for the lower maize yields. Other farmers often apply more nitrogen fertilizer than the minimum required for growth with negative effects (Ngosong *et al.*, 2019. Hence optimum nitrogen fertilization rates for maize are paramount (Ngosong *et al.*, 2019).

The study on the levels of unused nitrogen from SRF composite fertilizers during the 14 weeks in which maize crop actively absorbed nitrogen becomes necessary to avoid the negative effects discussed above. When the SRF granules come in contact with moist soil the nutrients are released through the membrane with help of molecular diffusion (Kaplan *et al.*, 2013).

Equations 4m, 4n and 4o on Appendix 31 were used to convert the absorbance as Appendix 8 into concentration in gL^{-1}. The analyzed data was recorded on Table 4

Table 4. 33: Concentration of nitrate from soil samples

TIME	FP ±SE	NPK ±SE	SRF2 ±SE	CRF3 ±SE	CRF4 ±SE
W2	2.92 ± 0.009^{Ba}	5.75 ± 0.003^{Ag}	2.77 ± 0.001^{Cf}	2.53 ± 0.001^{Eg}	2.64 ± 0.002^{Dg}
W4	2.88 ± 0.016^{Bab}	6.08 ± 0.000^{Af}	2.90 ± 0.002^{Be}	2.58 ± 0.001^{Df}	2.75 ± 0.001^{Cf}
W6	2.86 ± 0.018^{Dab}	6.16 ± 0.004^{Ae}	2.96 ± 0.002^{Ce}	2.77 ± 0.001^{Ee}	3.07 ± 0.002^{Be}
W8	2.83 ± 0.029^{Dbc}	6.41 ± 0.002^{Ad}	3.04 ± 0.001^{Bd}	2.96 ± 0.001^{Cd}	2.90 ± 0.001^{Cd}
W10	2.77 ± 0.002^{Ecd}	6.84 ± 0.002^{Ac}	3.12 ± 0.002^{Dc}	3.17 ± 0.002^{Cc}	3.29 ± 0.002^{Bc}
W12	2.74 ± 0.001^{Ed}	7.16 ± 0.000^{Ab}	3.66 ± 0.002^{Bb}	3.30 ± 0.007^{Db}	3.34 ± 0.010^{Cb}
W14	2.63 ± 0.002^{Ee}	7.56 ± 0.029^{Aa}	4.16 ± 0.037^{Ba}	3.45 ± 0.003^{Da}	3.66 ± 0.000^{Ca}

Key: W is time in weeks, FP= planted without fertilizer, NPK is NPK fertilizer, SRF2 is 70-30 slow release fertilizer, CRF3 is starch-PVA coated SRF2, CRF4 is starch-GA coated SRF2, mean values followed by the same capital letter(s) within the same column do not differ significantly from one another while mean values followed by the same small letter(s) within the same row do not differ significantly from one another (α=0.05, one-way ANOVA, Posthoc-Tukey-test) while the harmonic mean sample size, n=3.

There were five different treatments of NO_3^- which included a control without a fertilizer FP, a control containing an NPK conventional fertilizer, SRF2 and two CRFs which was similar to the research in (Ding *et al.,* 2016). Table 4.33 shows the concentration of NO_3^- in gL^{-1}. The amount of NO_3^- in the soils at start of optimization was 2.94 gL^{-1}. The trend on Table 4.33 for freely planted maize crop, FP reduced as duration increased. For instance the concentration of NO_3^- in the soils after 2 weeks of planting was 2.92 gL^{-1} which reduced over the 14 weeks to 2.64 gL^{-1}. This is expected since the nitrogen is absorbed by the plants with time without an equal rate of replenishment. This implies that the amount of nitrogen used by the plants was 0.307 gL^{-1} over the period of 14 weeks. It should also be noted that the soils are also generating some nitrogen within the 14 weeks which may assist in balancing the nitrogen lost to volatilization.

SRF2 showed an increase in the amount of NO_3^- released into the soils from 2.77 gL^{-1} in week 2 to 4.16 gL^{-1} in the 14^{th} week, CRF3 increased from 2.53 gL^{-1} in the second week to 3.45 gL^{-1} in the 14^{th} week and lastly CRF4 changed from 2.64 gL^{-1} in week 2 to 3.66 gL^{-1} in week 14. The increase in the concentration of NO_3^- in NPK, SRF2, CRF3, and CRF4 confirms evidence of excess NO_3^- that would cause severe pollution effects in the soils on farms. Table 4.33 shows that the tin planted with NPK had 7.56 gL^{-1} of unused NO_3^-, SRF2 released 4.16 gL^{-1} into its tin, CRF4 released 3.66 gL^{-1} and lastly CRF3 released 3.45 gL^{-1}. The amounts of nitrogen in the soils with SRF2, CRF3 and CRF4 at week 2 were lower than what was in the tins without a fertilizer. This could be because at two weeks the plants generate a stronger osmotic pressure due to presence of

a fertilizer at a higher equilibrium than the release causing a nutrient uptake from both the formula and the soil.

The lower concentration of released nutrient confirms that SRF2 is a slow release formula whose effect can be improved by coating with a superabsorbent polymer as is observed on plate 4.9 of some of the reclaimed formulas after the fourteen weeks.

If these products are used on large farms then the accumulated excess NO_3^- will leach into the surface water with severe pollution effects of acidity to the soil as seen on equation 4y.

$NO_3^- + H_2O \longrightarrow 2HNO_3 + O^{2-}$ …….. equation 4y.

The lower release concentration in SRF2 than NPK can be attributed to the slow release nature of the multifunctional nanocomposite. The NO_3^- which is dispersed into the interlayer distance as seen on TEM picture of plate 4.4 is primarily desorbed through the surface of the organoclay as discussed on Figure 4.18. This desorption is regulated by the surface pores and pore volumes of the clay minerals. The matrix in the interlayer will desorb by osmotic pressure caused by the roots of plants on need. In absence of the plant ecological need, the NO_3^- will adsorb and desorb through the micropores and mesopores forming equilibrium with the solution in the soils.

After the first 4 weeks and 2 days the maize crop looked closely alike in all the categories as seen on plate 4.9. As discussed earlier this maize show adequate uptake of nitrogen save for the FP crop. This is deduced from the colour of the leaves and stem (Zenawi & Mizan, 2019).

As the crop continues to grow the effect of fertilizer is observed in the crop that was not planted with any fertilizer as seen on plate 4.11 whose photo was taken from the back of the greenhouse.

Plate 4. 11: Maize crop at 5 weeks and tree days

The column on the left is maize crop planted without fertilizer, next to it is maize planted with NPK, followed by those planted with SRF2, CRF3 and lastly CRF4. The colour of leaves and stems on plate 4.10 of the NPK does not significantly differ from those of the other products which confirm the argument that the excess NO_3^- reported in NPK is a pollutant. The colour of the plant shows that at five weeks three days, there was sufficient quantities of NO_3^-. The crop in the first column is yellow with weak stems and shows depressed growth. The maize lacks sufficient concentration of nitrogen which is responsible for generating chlorophyll (Zenawi & Mizan, 2019). This means by the fifth week all the nitrogen that was in the soil is exhausted and there is very low replenishment. In another research optimal plant growth was evident when ammonium

nitrogen used was at a rate of 50% of the total amount of N applied (Muniz *et al.*, 2009).

The maize that were planted without any nutrient formulation show a depletion in the nitrogen concentration in the tins from 2.92 g to 2.64 g as opposed to the other samples that show increase in the nitrogen concentration as the maize crop grows as is evident on Table 4.32. This means as the nutrient formulation put in the soil was dissolving from the treatments at a higher rate than the absorption of the same by the plants. However Table 4.32 shows that SRF increases more rapidly than the NPK. This can be explained by the fact that as this formula dissolves, the interlayers break down releasing the nitrogen rapidly. On the other hand the columns of CRFs show that starch-PVA (Liu *et al.*, 2006) protects the SRF2 formula better than starch-GA. This is because starch-GA breaks down more quickly than starch-PVA as observed on Table 4.11 of water diffusivity. The data on Table 4.33 was used to draw columns of Figure 4.62.

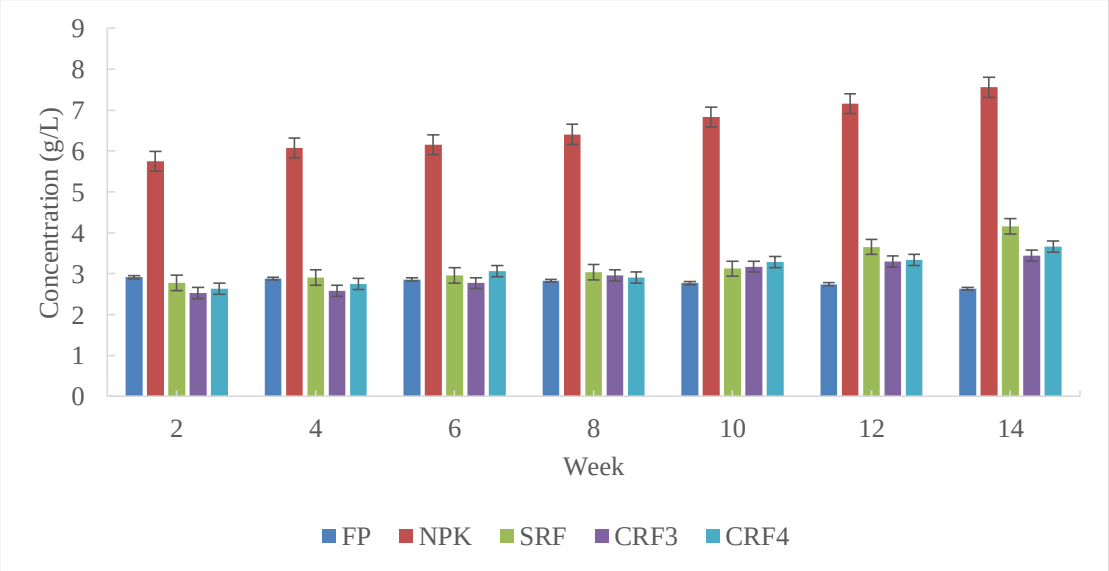

Figure 4. 62: Column for release of NO_3^- from the soil samples

Figure 4.62 shows that the amount of NO_3^- from NPK is significantly higher than the rest of the other treatments. The rest of the treatments do not differ significantly in release of NO_3^- except during week 14 in which SRF2 releases significantly higher concentration than CRF3 and CRF4. The difference arises from the nature in which the nutrients are released from the formulas. Whereas SRF2, CRF3 and CRF4 are releasing NO_3^- in an equilibrium manner set by the plant's osmotic pressure and the nutrients dispersed into the interlayers, the NPK releases the nutrients by dissolving into water. Figure 4.62 also shows that the amount of NO_3^- released from NPK increases with time a lot more than in the case of SRF2, CRF3 and CRF4 which is explained by the slow release nature of SRF2. The data on Table 4.33 was used to plot Figure 4.63.

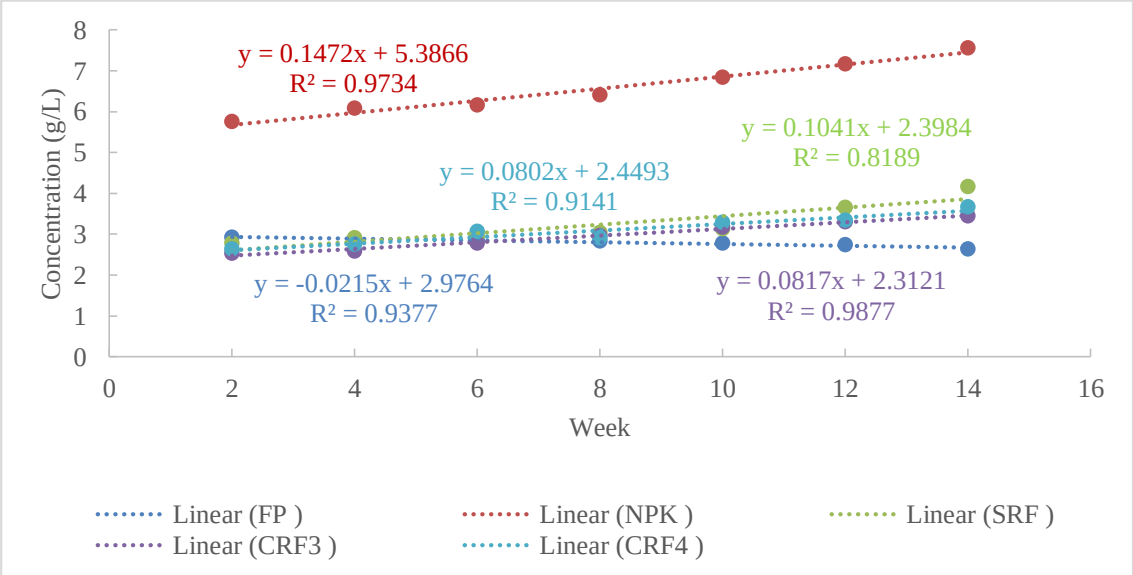

Figure 4. 63: Rate of release of NO_3^- into soils with crops

Figure 4.63 shows reducing rate of $-0.0215gL^{-1}wk^{-1}$ in the planting tin without fertilizer, FP. This implies that the plants are picking the NO_3^- that was initially in the soils without an equal rate of replacement. As discussed earlier NO_3^- is the major nutrient required for generation of chlorophyll that is key in manufacture of food for plant

growth. The column on the left hand side on plate 4.9 represents the tins that were planted without any fertilizer. The immediate column on the right represents the tins that were planted with NPK which has excess of 7.56 gL^{-1}as per Table 4.33. The difference in colour of the maize plant in the two columns on plate 4.10 confirms that nitrogen is responsible for the green coloration of maize because the maize crop that was planted without a fertilizer was yellow and hence starved of NO_3^-. The colour of the maize planted with SRF2 which is on the immediate right side of NPK shows a similar green colour to that of NPK. This shows that a single application of SRF2 can cover several applications of normal fertilizer formulas (Guertal, 2009).

Figure 4.63 shows the amount of NO_3^- released at a rate of 0.0817 $gL^{-1}wk^{-1}$ in CRF3 planting pot over the period of 14 weeks with r^2 of 0.9876. The amount of NO_3^- in the pot soil is significantly lower, 3.45gL^{-1} after 14 weeks lower than that in the pot with SRF2 that had 4.16 gL^{-1}. This shows that the S-PVA used as a SAP has reduced the release of N into the soils (Hongtao *et al.*, 2014).

Figure 4.63 shows the amount of NO_3^- released, 0.0802 $gL^{-1}wk^{-1}$ in the planting pot with CRF4. The Figure 4.64 however shows an irregular data picked at week 8 that could be attributed to the uneven coating of the starch-GA. The value 0.0078$gL^{-1}wk^{-1}$ is the lowest giving this product the best double effect for reduction of leachate from CRF4.

Figure 4.63 compares the amount of NO_3^- in the crop analysis over a period of 14 weeks which in turn shows the rate of absorption of NO_3^- from the products. There is increase in unused total nutrients. The trend shows increased total nutrients over the period of

study for all except in the treatment where no nutrient formulation was used. Such steady increase in the curves was also observed in the research of (Ding *et al.*, 2016) and that of (Tong *et al.*, 2018).

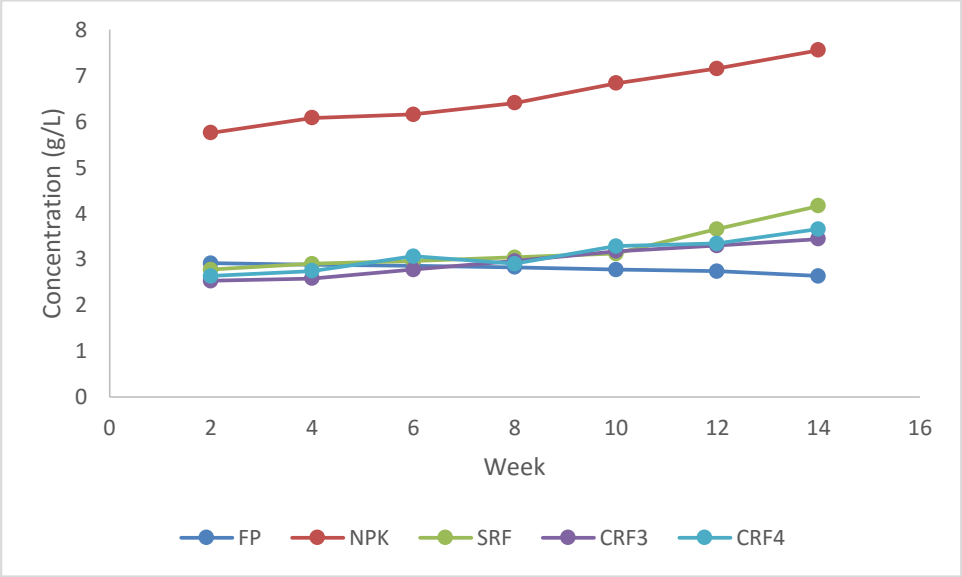

Figure 4. 64: Weekly rate of release of NO_3^- from treatments into soils

The Figure 4.64 shows a reduced linearity at week 7 and week 12. This could indicate that there is need of a nutrient enhancement if the crops have to grow and fruit.

The products SRF2, CRF3 and CRF4 have similar rates and amounts remaining in the containers increased with increase in weeks. The curve for NPK has a similar trend to SRF2, CRF3 and CRF4 but shifted to increased rate and much larger quantities of NO_3^- in the tins. The increase in NO_3^- is enhanced after the 11^{th} week for SRF2, CRF3 and CRF4. This increase is smaller in the containers with CRF3 followed by CRF4 due to the effect of the SAP coating. SRF2 discharges more NO_3^- into the soils from week 11 as the formula breaks down into smaller units.

The rate of release is dependent on PH, temperature (Basu *et al.*, 2010) and thickness of the coating (Tlustos *et al.,* 1994) as is evident on CRF3 on picture on plate 4.9, thus the rate of NO_3^- release is influenced by the soil conditions (Kaplan *et al.,* 2013) though in the greenhouse these conditions were controlled.

4.7.2 Phosphorus nutrients in soils of crops

This research observed that phosphorus is far less used nutrient as also in that of (Mirjana *et al.,* 2012). It was established in another research that crops used only 20% of the applied phosphorus in the first year of application (Megan *et al.,* 2012).

The equations 4p, 4q and 4r on Appendix 31 were used to convert the absorbance on Appendix 9 into concentration in gL^{-1}. The analyzed data was put on Table 4.34 as shown below.

Table 4. 34: Concentration of $H_2PO_4^-$ in soil samples in gL^{-1}

TIME	FP ±SE	NPK ±SE	SRF2 ±SE	CRF3 ±SE	CRF4 ±SE
W2	0.118 ± 0.001^{aE}	6.27 ± 0.000^{fA}	5.92 ± 0.000^{dB}	4.95 ± 0.001^{gD}	4.99 ± 0.001^{gC}
W4	0.116 ± 0.001^{aD}	6.31 ± 0.001^{fA}	5.99 ± 0.062^{dB}	5.12 ± 0.000^{fC}	5.20 ± 0.001^{Fc}
W6	0.097 ± 0.001^{bE}	6.70 ± 0.004^{eA}	6.20 ± 0.002^{cB}	5.26 ± 0.001^{eD}	5.36 ± 0.000^{eC}
W8	0.093 ± 0.002^{bE}	6.86 ± 0.000^{dA}	6.23 ± 0.000^{bcB}	5.42 ± 0.002^{dD}	5.63 ± 0.020^{dC}
W10	0.070 ± 0.005^{cE}	6.92 ± 0.027^{cA}	6.15 ± 0.002^{cB}	5.66 ± 0.026^{cD}	5.81 ± 0.003^{cC}
W12	0.055 ± 0.002^{dE}	7.09 ± 0.001^{bA}	6.31 ± 0.000^{abB}	5.73 ± 0.001^{bD}	5.96 ± 0.000^{bC}
W14	0.037 ± 0.002^{eE}	7.18 ± 0.010^{aA}	6.39 ± 0.005^{aB}	6.12 ± 0.001^{aD}	6.08 ± 0.002^{aC}

Key: W is time in weeks, FP= planted without fertilizer, NPK is NPK fertilizer, SRF2 is 70-30 slow release fertilizer, CRF3 is starch-PVA coated SRF2, CRF4 is starch-GA coated SRF2, Mean values followed by the same capital letter(s) within the same column do not differ significantly from one another while mean values followed by the same small letter(s) within the same row do not differ significantly from one another (α=0.05, one-way ANOVA, Posthoc-Tukey-test), while the harmonic mean sample size, n=3

There were five different treatments of $H_2PO_4^-$ which included a control without a fertilizer FP, a control containing an NPK conventional fertilizer, SRF2 and two CRFs which was similar to the research in (Ding *et al.,* 2016). The maize crop that was planted without any fertilizer, FP was a control that showed the approximate quantities of $H_2PO_4^-$ used in the soils. NPK formula was used as a control for the treatments; SRF2, CRF3 and CRF4.

Reduction in the concentration of $H_2PO_4^-$ released into the tins, from 0.118 gL^{-1} in week two to 0.037 gL^{-1} in the 14^{th} week is reflected in Table 4.34. It can be seen from Table 4.34 that the soils have very low concentrations of $H_2PO_4^-$ compared to the other nutrients. For instance W2 of FP had 0.118 gL^{-1} of $H_2PO_4^-$ as compared to 3.04 gL^{-1} for K^+ and 2.92 gL^{-1} for NO_3^{-1}. The reduction in concentration of $H_2PO_4^-$ from W2 to W14 is due to the higher rate at which $H_2PO_4^-$ is being absorbed by crop than that of regenerating the $H_2PO_4^-$ naturally in the soils. An analysis of the soils showed the concentration of $H_2PO_4^-$ as 0.119 gL^{-1} therefore the amount of $H_2PO_4^-$ used during the 14 weeks was 0.082 gL^{-1} which compares with the research of (Megan *et al.,* 2012).

Table 4.34 shows that NPK released the largest concentration of $H_2PO_4^-$ which was 7.18 gL^{-1} in the 14^{th}week followed by the SRF2 with 6.39 gL^{-1}. This is expected since the SRF2 formula releases the $H_2PO_4^-$ through the surface of the multilayer modified clay mineral as was discussed on Figure 4.18. The release of $H_2PO_4^-$ decreases when the SRF2 is coated with SAP. The OH crosslinks of the SAP interact with the OH of the $H_2PO_4^-$ through hydrogen bonds which causes an equilibrium that is only broken by both the osmotic pressure of the plant root and principles of diffusion. When the plant absorbs the $H_2PO_4^-$ in the solution, the concentration of the $H_2PO_4^-$ reduces forcing the

$H_2PO_4^-$ to diffuse from the crosslinks of the SAP into the water around the root zone, which in turn causes $H_2PO_4^-$ from the formula to diffuse into the crosslinks of the SAP. The data on Table 4.34 for SRF2, CRF3 and CRF4 provides evidence that in presence of adequate quantity of nutrients, the crop absorbs more $H_2PO_4^-$. Whereas the FP absorbs about 0.091 gL^{-1} NPK absorbs about 0.91 gL^{-1}. Figure 4.65 shows a column for the data on Table 4.34.

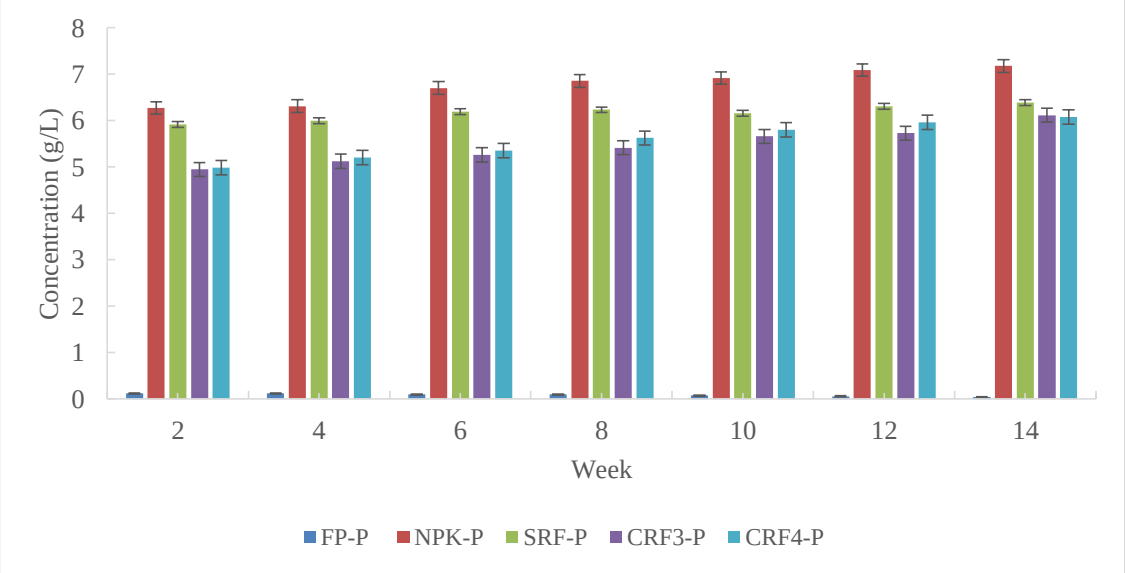

Figure 4. 65: Column for release of $H_2PO_4^-$ from the soil samples

The column for $H_2PO_4^-$ in FP is very short in all the weeks as seen on Figure 4.65. Both NPK and SRF2 discharge $H_2PO_4^-$ that is significantly higher than the rest of the treatments as seen from the error bars. The Figure 4.65 also summarises that CRF3 and CRF4 do not discharge significantly different quantity of $H_2PO_4^-$. The release of $H_2PO_4^-$ from NPK is significantly higher than the rest of the treatments. The concentrations of CRF3 and CRF4 are smaller in all the 14 weeks as is reflected in the Table 4.34. Generally CRF3 releases less $H_2PO_4^-$ then CRF4 due to the effectiveness of the coating as was discussed on Figure 4.11 of water diffusivity. The data on Table 4.34 was used to draw Figures 4.66 and 4.67 that compares the rate of release of the nutrients.

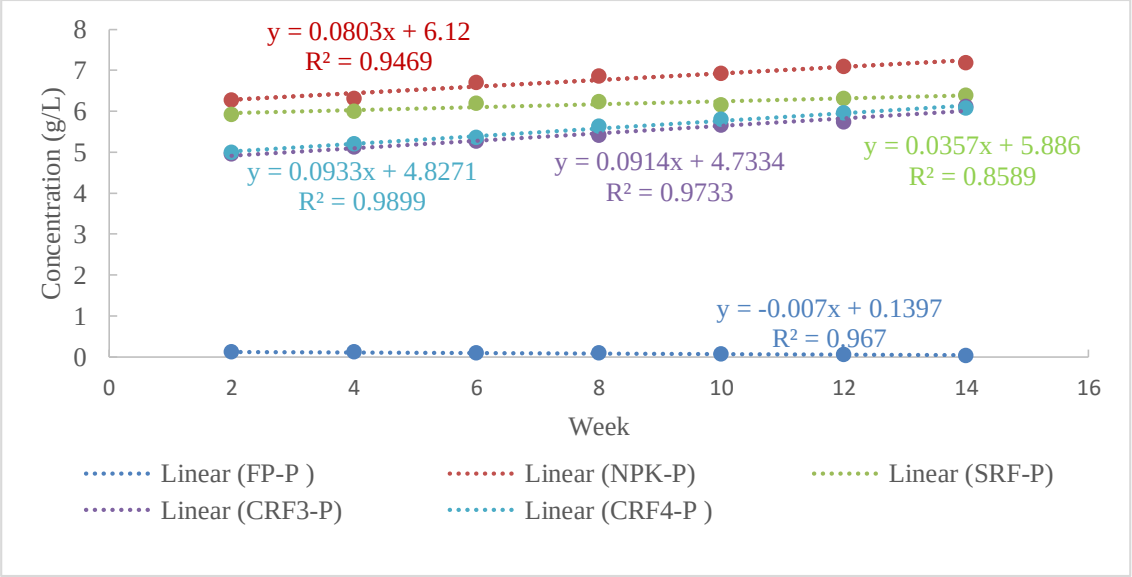

Figure 4. 66: Rate of release of $H_2PO_4^-$ into soils

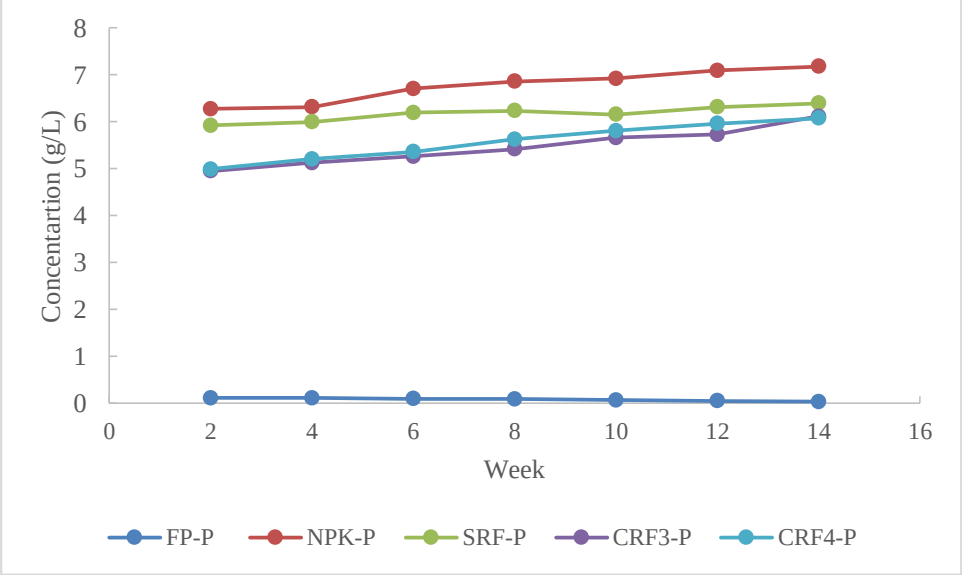

Figure 4. 67: Weekly rate of release of $H_2PO_4^-$ into soils

Figure 4.66 shows the rate at which $H_2PO_4^-$ is being reduced from the soils in the planting tin in which maize was planted without any nutrient formulation, FP. The rate of -0.007$gL^{-1}wk^{-1}$ indicates a reduction in the concentration of $H_2PO_4^-$ in the soils. The amount of $H_2PO_4^-$ in the soil is small as compared to NO_3^- and K^+. Figure 4.66 shows a rate of release of 0.091 $gL^{-1}wk^{-1}$ for CRF3 which is significantly higher than of NPK

and SRF2. This confirms the argument that the OH and the H_2O in the crosslink sacks attract the $H_2PO_4^-$ anion improving its release into the soils. This improves the available $H_2PO_4^-$ for the plant on need considering that $H_2PO_4^-$ is a limiting element in most $H_2PO_4^-$ fertilizers.

Figure 4.66 also shows a deposition of $H_2PO_4^-$ at 0.093 $gL^{-1}wk^{-1}$ from CRF4 into the soils in the tin. This value of deposition is not significantly different from that of CRF3. The soil attached to starch coating material can stimulate the soil microbes' activity degrading coating causing disintegration enhancing nutrient dissolution (Himmah *et al.*, 2018). This was observed in the CRF4 case in which all the coating from the reclaimed products did not have any coating as observed on picture on plate 4.9.

Figure 4.67 shows slight decrease in rate of release after the 8^{th} week for all treatments. This could mean that the soil's ability to regenerate $H_2PO_4^-$ is low as most of the available $H_2PO_4^-$ is strongly attached to the soil silicates due to reduction in the soil pH (Weeks & Gange, 2019). Increase in acidity is due to the deposition of H^+ from the $H_2PO_4^-$ into the soils.

Figure 4.67 shows $H_2PO_4^-$ from NPK increases sharply to the 6^{th} week after which there a steady slow increase towards week 14. This provides evidence that most of the $H_2PO_4^-$ released from the NPK is absorbed by the plants in the first 4 weeks which is probably the ecological maize plant need for $H_2PO_4^-$. The steep raise in the curve after the 4^{th} week represents the $H_2PO_4^-$ that is dissolved from the NPK but is not absorbed by the plant which would mean the plant has a reduced need for $H_2PO_4^-$. A similar research by

(Kaplan *et al.,* 2013) showed a $H_2PO_4^-$ uptake that peaked during the budding of chrysanthemum.

Previous research show that large proportions of phosphorus in soils is insoluble hence unavailable to plants (Singh & Kapoor, 1994); (Mirjana *et al.,* 2012). Mobility of the phosphate ion is low in most mineral soils hence scarcely leached into soils for absorption of plants (Mengel & Kiskby, 2001). However some bacteria like bacillus and pseudomones in soils at proper conditions solubilize the phosphates promoting plant growth (Joo *et al.,* 2004); (Poonguzhali *et al.,* 2008); (Mirjana *et al.,* 2012). The pH of the soils in the greenhouse soil was 7.1 as observed on Table 4.1, which fits in the pH 4.5 to 9.5 recommended in (Mirjana *et al.,* 2012) research for maize crop. After nitrogen, phosphorus is the most limiting nutrient for crop yields (Mirjana *et al.,* 2012) and is essential for maize growth and development (Wu *et al.,* 2005). In the research of (Mirjana *et al.,* 2012) plant growth promoting rhizobacteria (PGPR) was recognized as an important factor in sustainable agricultural production (Mrkovacki & Bjelic, 2011). PGPR was used to increase plant nutrition by increasing the nitrogen and phosphorus uptake through biofertilization (Caskmakci *et al.,* 2005). This would improve the levels of available phosphorus in the soils which would be seen as an increase in the Phosphorus levels on column of FP on Figure 4.65. Adaptations of bacteria to different soil properties and a broad range of pH and salinity may lead to better completion and crop survival (Mirjana *et al.,* 2012). Plate 4.11 is maize crop at 7 weeks

Plate 4. 12: Maize at 7 weeks and 3 days

The maize crop shows uniform green colour of the leaves and averagely equal sized stems. The leaves also do not show any sign of diseases. This therefore it means that the plant had adequate concentration of phosphorus (Zenawi & Mizan, 2019) which improved the root and stem development.

4.7.3 Potassium nutrients in soils of crops

The equations 4s, 4t and 4u on Appendix 31 were used to convert the absorbance of Appendix 10 into concentration in gL^{-1}. The analyzed data is recorded on Table 4.35.

Table 4. 35: Concentration of K^+ in the soil samples

TIME	FP ±SE	NPK ±SE	SRF2 ±SE	CRF3 ±SE	CRF4 ±SE
W2	3.04 ± 0.001^{aE}	5.80 ± 0.060^{Fa}	5.62 ± 0.000^{eB}	4.72 ± 0.003^{eD}	4.96 ± 0.001^{fC}
W4	2.90 ± 0.001^{bE}	5.97 ± 0.000^{efA}	5.68 ± 0.001^{eB}	4.46 ± 0.001^{fD}	5.33 ± 0.001^{eC}
W6	2.84 ± 0.000^{bD}	6.12 ± 0.000^{Ea}	5.91 ± 0.000^{dB}	4.93 ± 0.001^{dC}	6.11 ± 0.005^{dA}
W8	2.55 ± 0.000^{cE}	6.61 ± 0.001^{dB}	6.96 ± 0.000^{bA}	5.74 ± 0.001^{cD}	6.13 ± 0.019^{dC}
W10	2.63 ± 0.035^{cD}	7.27 ± 0.033^{cA}	6.83 ± 0.034^{cB}	6.38 ± 0.001^{bC}	6.38 ± 0.000^{cC}
W12	2.41 ± 0.028^{dD}	8.39 ± 0.054^{bA}	6.96 ± 0.044^{bB}	6.48 ± 0.036^{aC}	6.55 ± 0.060^{bC}
W14	2.31 ± 0.054^{dE}	9.27 ± 0.058^{aA}	7.13 ± 0.001^{aB}	6.41 ± 0.001^{bD}	6.89 ± 0.046^{aC}

Key: W is time in weeks, FP= planted without fertilizer, NPK is NPK fertilizer, SRF2 is 70-30 slow release fertilizer, CRF3 is starch-PVA coated SRF2, CRF4 is starch-GA coated SRF2, Mean values followed by the same capital letter(s) within the same column do not differ significantly from one another while mean values followed by the same small letter(s) within the same row do not differ significantly from one another (α=0.05, one-way ANOVA, Posthoc-Tukey-test), while the harmonic mean sample size, n=3.

There were five different treatments of K^+ which included a control without a fertilizer FP, a control containing an NPK conventional fertilizer and an SRF2 and two CRFs which was similar to the research in (Ding *et al.,* 2016). As seen in Tables 4.33 and 4.34, Table 4.35 shows decrease in the concentration of K^+ for FP from week 2 to week 14. This is expected because the maize crop uses K^+ at a higher rate than the soils can naturally replenish. For example the K^+ concentration in W2 for the maize crop grown without any fertilizer is 3.04 gL^{-1} and reduced to 2.31 gL^{-1} at end of week 14.

Table 4.35 shows that NPK release the highest concentration of K^+. After the 14^{th} week NPK released 9.27 gL^{-1}, followed by SRF2 with 7.13 gL^{-1}, CRF4 with for SRF2, 6.89 gL^{-1} and lastly CRF3 with 6.41 gL^{-1}. As previously discussed, the K^+ in SRF2 is desorbed through the pores of the multifunctional organoclay mineral while the coated materials release nutrients only in equilibrium with the SAP's solution. Figure 4.68 compares the release of K^+ into the soils using columns.

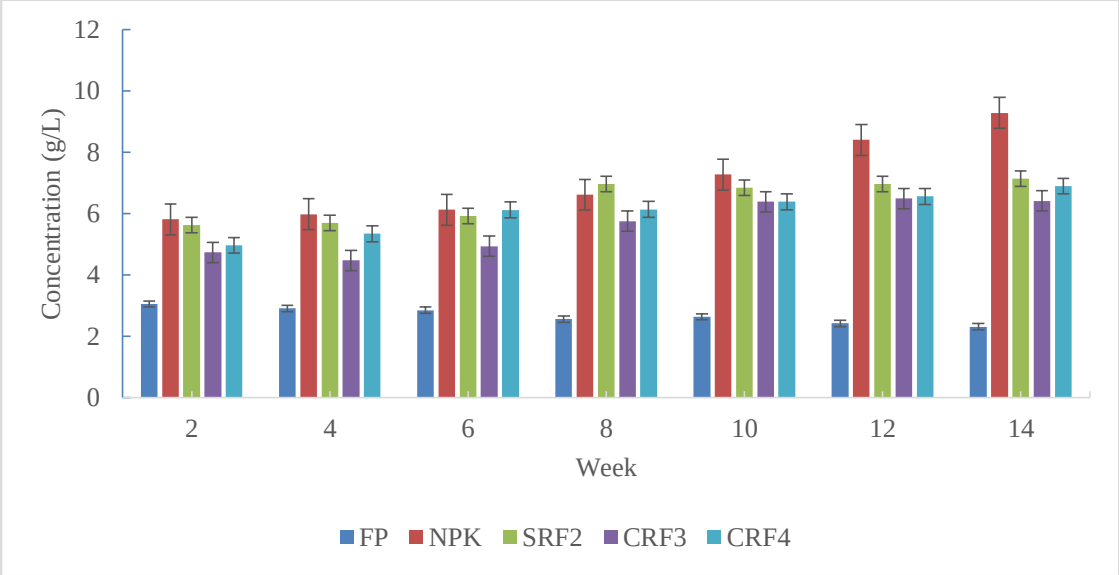

Figure 4. 68: Column for release of K^+ from the soil samples

The error bars on Figure 4.68 show that the amount of K^+ from NPK and SRF2 is not significantly different except for week 12 and 14. Figure 4.68 also indicates that CRF3 discharges less K^+ than CRF4 except for week 10. The K^+ concentration desorbed depends on the volume and size of the pores and the interaction of the K^+ with the anions in the interlayer distances. The small size of K^+ enhances desorption through the multilayer modified clay mineral. Figure 4.68 illustrates that from W8 to W14, the concentration of K^+ released from NPK increased by a larger value than in the SRF2. This can be explained by the slow release effect of the SRF2 in which the release is dependent on the need of the plant.

As seen on Figure 4.68, CRF3 released less potassium than CRF4 except for week 10 and week 12 which were equal. This is explained by the effectiveness of the starch-PVA coating, due to the large number of OH crosslinks that shifts the equilibrium of desorption towards the SAP. The data on Table 4.35 was used to draw a rate curve as Figure 4.68.

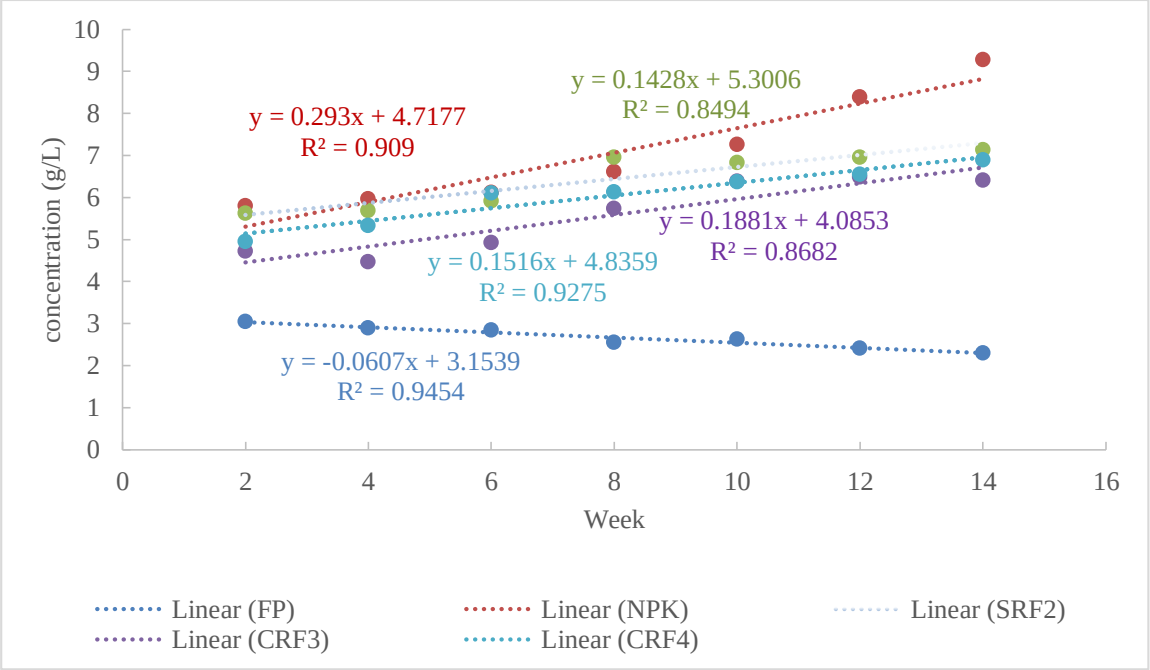

Figure 4. 69: Rate of release of K^+ into planting soils

Figure 4.69 shows a decrease in the rate of release from FP at -0.0607 $gL^{-1}week^{-1}$. This trend as explained earlier is expected since the maize crop uses the K^+ without replenishment of the nutrient. This compares well with a relationship of r^2=0.82 between potassium uptake and grain yield that was observed in the potassium plots with a good measure of soil potassium supplied to crops in the research of (Pathak *et al.*, 2003).

The rate of release of 0.188 $gL^{-1}week^{-1}$ for CRF3 on Figure 4.69 is higher than that of SRF2 of 0.143 $gL^{-1}week^{-1}$. This could be due to the attraction of the K^+ to the OH and H_2O of the starch-PVA causing an increase in the K^+ released.

As is observed on Figure 4.69, K^+ into maize tins with CRF4 has a slower rate of release than of CRF3 which could be due to the low number of crosslinks in CRF4 that reduces the amount of H_2O in the SAP that is responsible for attracting the K^+.

The trend of release of potassium is similar to the other nutrients, with CRF3 releasing least amount potassium. Figure 4.70 for NPK shows less steep increase in the first 6 weeks and rises steeply to 14th week. This means that most of the K^+ released into the soils was picked up by the maize plant in the first 6 weeks. Most of the K^+ released into the tins after week six, deposits as unused K^+. This could mean that the maize plant's need for K^+ reduces after 6 weeks as seen on plate 4.12 which does not show low resistance to conditions. The stems and leaves do not show any deficiency or general disease infestation (Wang *et al.*, 2016); (Rawat *et al.*, 2016).

Plate 4. 13: Maize crop at 9 weeks

It is evident from the stems and the leaves that the plants do not show any sort of stress or spots on the leaves that would point to disease infestation. The dry leaves show on

two of the stems is due to aging. This would then imply that the plants have sufficient quantities of potassium (Zenawi & Mizan, 2019).

The data on Table 4.35 was also plotted to show the day to day changes in the rate of release given on Figure 4.70.

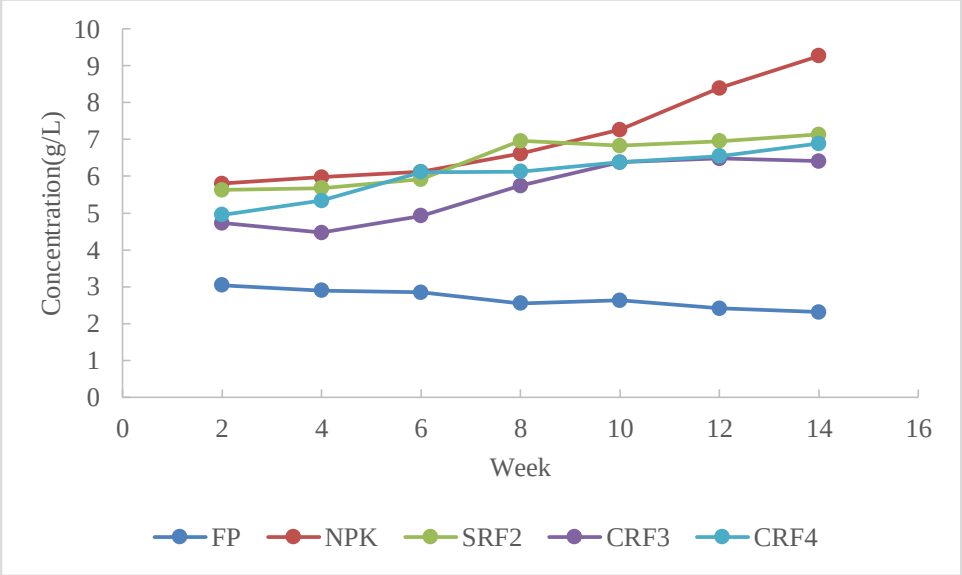

Figure 4. 70: Weekly rate of release of NO_3^- into soil

Figure 4.70 shows that FP decreased from 3.04 gL^{-1} to 2.31 gL^{-1} as the maize crop absorbs the K^+ from the soils, while NPK, SRF2, CRF3 and CRF4 increase from 5.80 gL^{-1} to 9.27 gL^{-1}, 5.62 gL^{-1} to 7.13 gL^{-1}, 4.73 gL^{-1} to 6.41 gL^{-1} and 4.96 gL^{-1} to 6.89gL^{-1} respectively. This trend that is similar to the one in the research of (Ding *et al.*, 2016).

The curves show that the product coated with starch-PVA loses K^+ at a slower rate than that with CRF4, which is also significantly slower than SRF2 for the first 6 weeks. This low rate of K^+ deposition is attributed to the slow release SRF2 coupled with the coating of the SAPs as was also noted by (Tarosiewicz & Tomaszewska, 2013). The rate of release of K^+ from NPK is significantly higher than the rest of the products due to its

unprotected release of the nutrient. After the 12th week there is steep increase in the rate of deposition of K^+ into the tins which is much higher than SRF2, CRF3 and CRF4.

The release in weeks 2, 4, 6 and 8 are not significantly different for NPK and SRF. However from week 10, NPK begins to dissolve more rapidly into the soils as seen on Figure 4.70. This could mean that the plants were utilizing more the potassium found in the soil which was exhausted by the 10th week (Satyanarayana *et al.,* 2011) (Singh *et al.,* 2013). This correlates with the research of (Kaplan *et al.,* 2013) that showed that their vegetable absorption of K^+ peaked during the blooming stage.

High acidity of soils could be caused by the oxidation of NH_4^+ to NO_3^- by soil bacteria releasing H^+ into soils (Ngosong *et al.,* 2019). Potassium availability is highest above soil pH 6.0 hence low pH decreases the soil's ability to keep supplying potassium to plants. Generally higher release rates for the N, P and K nutrients appear in PH 4-9 as was observed by (Ding *et al.,* 2016) which was adhered to by optimizing the release at pH 7.1 in this research.

Introduction of high holding rice, maize and wheat accelerated the depletion of potassium with low fertilizer replenishment (Timsina *et al.,* 2010). (Timsina *et al.,* 2010) observed a 30% reduction in 30 years in Bangladesh which is alarming (Islam *et al.,* 2016). The FP generally showed decrease of potassium from 3.04 gL^{-1} to 2.31 gL^{-1} as the maize crop absorbs the K^+ from the soils which correlates to the findings in research of (Islam *et al.,* 2016).

Most farmers have low K^+ fertilizer input due to its hidden effects on plant growth (Saleque *et al.,* 1998). It was believed that the soils of East Africa and by extension

Kenya were well supplied with K^+ hence did not need potassium based fertilizers a perception shared by a number of developing countries like Bangladesh (Islam & Muttaleb, 2016). Potassium depletion showed in a similar study in Guinea grass which showed higher potassium uptake from potassium available soils (Hussain *et al.,* 2015). Thus there is essential need for potassium to be supplied at an optimum dose and maintained to augment production and ensure improved quality crop (Satyanarayana *et al.,* 2011); (Singh *et al.,* 2013).

4.7.4 Comparison of nutrients in maize crop

The data on Table 4.36 helps us to establish the pollutants in the soils that are attributed to excessive use of fertilizers in the fields. Table 4.36 shows the means of concentrations of the formulas during the period of study.

Table 4. 36: Concentrations of nutrients in planting Tins of maize crops

Nutrients	NPK±SE	SRF2±SE	CRF3±SE	CRF4±SE
NO_3^-	6.564 ± 0.134^a	3.232 ± 0.103^b	2.966 ± 0.074^b	3.091 ± 0.076^b
$H_2PO_4^-$	6.762 ± 0.074^a	6.172 ± 0.035^b	5.465 ± 0.083^c	5.574 ± 0.084^c
K^+	7.062 ± 0.275^a	6.443 ± 0.139^a	5.590 ± 0.181^b	6.049 ± 0.141^{ab}

Key: FP= planted without fertilizer, NPK is NPK fertilizer, SRF2 is 70-30 slow release fertilizer, CRF3 is starch-PVA coated SRF2, CRF4 is starch-GA coated SRF2, mean values followed by the same capital letter(s) within the same column do not differ significantly from one another while mean values followed by the same small letter(s) within the same row do not differ significantly from one another (α=0.05, one-way ANOVA, Posthoc-Tukey-test), while the harmonic mean sample size, n=3

Like in previous discussions Table 4.36 shows that SRF2 released less nutrients into the soils than NPK. However statistically release of potassium from NPK and SRF2 does not show significant difference which could be due to the factory treatment on the commercial NPK used. Table 4.36 also confirms that starch-PVA is a more efficient

coating material than starch-GA due to the lowest release concentrations recorded for all the nutrients. The lower values of release from the CRFs is an indication that SAPs can be used to improve the slow release capacity of fertilizers. It should also be noted that when the SRF do not match the plant nutrient requirement, the plant growth reduces (Himmah *et al.,* 2018).

4.8 Testing of final work

4.8.1 Statistical testing of hypothesis

Tables 4.4 and 4.5 confirmed the composition of the white and black clays used in modification as 66.3% and 28.4% clay minerals respectively. SEM and TEM pictures on plate 4.1 and 4.4 confirmed surface pores and interlayer distances that were effectively intercalated by CTAB. Therefore the clay materials, intercalating surfactants and coating SAPs formed materials with sufficient physical and chemical properties to disperse NPK nutrients.

Table 4.21 and Table 4.22 show that water sorption into SAPs, release of N, P, K nutrients into deionized water, chemisorption of N, P, K nutrients from soils into maize plants do not indeed fit into the first order reactions

According to Table 4.35 SRF2 is statistically a slower release formula than NPK for NO_3^- and $H_2PO_4^-$ and the encapsulated CRF3 is a slower release formula than SRF2 in all the nutrients.

Lastly a comparison of release capacities of nutrients on Table 4.36 shows that the encapsulated SRF2 release lower nutrients than SRF2 for the nutrients $H_2PO_4^-$ and K^+

4.9.2 Quality control tests

NPK fertilizer is certified for use by KEBS and NEMA and has been in use over a period of time. The fact that SRF2 and its coated products release less nutrients into the soils according to Table 4.36, implies that the formed products passes quality control standard measures.

CHAPTER FIVE

CONCLUSION AND RECOMMENDATIONS

5.1 CONCLUSION

Clays used in this study had sufficient percentage clay minerals according to the XRD mineral assemblage characterization. The particle size and presence of pores on the surface of the clays were illustrated by BET isotherms and interlayers were observed on SEM and TEM pictures. The introduction of sodium ions modified the clay minerals alongside some intercalation as observed on XRD diffractograph of NaDp. The surfactants, DMSO and CTAB modified the clay minerals into organoclays and intercalated the clays as discussed from XRD crystallography and FTIR analysis. The study confirms by the overlay of diffractographs that the layers were pillared sufficiently enough to disperse in plant nutrients. The physicochemical analysis of starch-PVA and starch-GA prepared submit evidence that they are suitable coating materials.

The SAPs and release of NO_3^- , $H_2PO_4^-$ and K^+ into water fitted into pseudo first order reaction equation while sorption of NO_3^-, $H_2PO_4^-$ and K^+ into soils fitted into pseudo second order reaction equation.

Release of nutrients into water shows that SRF2 is slightly better intercalated and pillared than SRF1.

Maize crop optimization confirmed that SRF2 and CRFs performed equally well as NPK on growth of the maize crop but released less unused nutrients into soils.

5.2 RECOMMENDATION

This study recommends research into effect of pH on nutrient sorption into soils from SRFs throughout the growth of the maize plant.

This research recommends the use of this procedure to convert DAP into SRF in order to generate a formula for soils that have insufficient quantities of phosphorus.

Extensive research on intercalating surfactants be done in view of synthesizing surfactants that would achieve higher yield of intercalates with strong pillaring effect without obstructing dispersion of nutrients into the gallery.

It is also necessary to research on efficient and effective geometry of the SRF products that would provide optimum amount of the nutrient for maize crop.

REFERENCES

Abera T., Debele, T and Wegary, D. (2013) Effects of Varieties and Nitrogen fertilizer on Yield and Yield components of maize on Farm Field in Mid Altitude Areas of Western Ethopia,Hindawi- *International Journal of Agronomy* pp 1-14.

Abuh, M. A, Abia-Bassey, N, Udeinya, T. C, Nwannewuihe, H. U, Abong, A. A and Akpomie, K. G. (2014), Industrial Potentials of Adiabo Clay in Calabar Municipality of Cross River State. The pacific Journal of Science and Technology, 15(1) pp 63-74.

Ademba J. S., Kwach J. K., Esilaba A. O and Ngari S. M. (2015) The effects of phosphate fertilizers and manure of maize yield in south western Nyanza, Eastern *African Agricultural and Foresty Journal* pp 1-12.

Ahmed, S., Hassan, A. A., Salama, D. M., Abd El-Aziz, M. E and Mohamed S. A. A. E.(2019) Green Synthesis of Nanofertilizers and Their Application as a Foliar for Cucurbita pepo L, *Journal of Nanomaterials* 2019 pp1-11

Akbas F., Gunal, H and Acir, N. (2017) Spatial Variability of Soil Potassium and its relationship to Land use and Parent material, *Soil and Water Reserviours* **12**(4) pp 202-211.

Akenga, P., Salim, A., Onditi, A., Yusuf, A and Waudo, W. (2014) Determination of selected micro and macronutrients in sugarcane growing soils at Kakamega North District, Kenya. *IOSR Journal of Applied Chemistry* **7**(7) pp 34-41.

Alexandre, M. and Dubois, P. (2000), Polymer-layered silicate nanocomposites: Preparation, Properties and Uses of a new class of Materials. *Materials Science and Engineering* **28** pp 1-63.

AlvarezAcevedo, N. I., Rocha, M. C. G and Bertolino, L. C. (2017) Mineralogical characterization of natural clays from Brazilian Southeast region for Industrial applications.*Ceramica* 63 pp 253-262.

AlZahrani, S. M. (1999) Controlled Release Fertilizers, Modelling and Simulation, *International Journal of Engineering and Science* **37** pp 1299-1307.

Amanda. L. S., Arno. H. O and Maria. L. S, F. (2011). Influence of preferred orientation of Minerals in the Mineralogical Identification process by X-ray Diffraction. *International Nuclear Atlantic conference*, pp 1-11.

Amtmann A., Trouffland S and Armengand (2008) The effect of Potassium nutrition in pests and disease resistance in plants. *Physiology of plants* **133** pp 682-696.

Anabessa, Y and Juskiw, P. (2012) Review; Strategies to increase nitrogen use efficiency of spring barley, *Canadian Journal of Plant Science* **92**(4) pp 617-625.

Andala, D and Wachira, D. M (2015) Reversal of plasticity of leached kaolinitic clays in Mukurwe-ini-Kenya. *African Journal of Pure and Applied Chemistry* **9**(3) pp 1-10.

Anderson, J. M & Ingram, J. S. I. (1993) Tropical soil biology and fertility. A handbook of methods, CAB International,Wallingford, Oxon, UK).

Anita Srivastava and Rao, D. P. (2014),"Enhancement of seed germination and plant growth of wheat, maize, peanut and garlic using multiwalled carbon nanotubes", *Eur. Chem. Bull,* **3**(5) pp 502-504.

Aroke, U. O., Abdulkarim, A and Ogubunka, R. O. (2013) Fourier Transform Infrared Characterization of Kaolin, granite, bentonite and barite *ATBU Journal of Environmental Technology* **6**(1) pp 1-12.

Ashley, M. K., Grant, M and Grabor, A. (2006) Plant responses to potassium deficiencies: a role for potassium transport proteins, *Journal of experimental Biology* **51**(2) pp 425-436.

Auda J. B. (2017) Superabsorbent polymers, Polymer and Petrochemical Industries Department. *University of Babylon*

Aytung, A.K. (2014) Evaluation of structural properties of cellulose ether corn starch based on biodegradable films, *International Journal of Polymeric Material and Polymeric Biomaterials* **63** pp342-349.

Azeem, B., KuShaari K., Man, B., Basit, A., and Thanh, T. (2014) A review of materials and methods to produce cobrolled release coated urea fertilizers. *Journal of controlled release fertlizers* **181** pp 11-21.

Bamgbose, J. T. (2012) Equilibrium swelling and kinetic studies of highly swollen chitosan film. *Journal of chemistry and chemical Engineering*, **6** pp 272-283.

Bansiwal, A. K., Rayalu, S. S., Lbhasetwar, N. K., Juwarkar, A, A and Devotta, S. (2006), Surfactant Modified Zeolite (SMZ) as a slow Release fertilizer for phosphorus. *Agricultural Food Chemistry* **54**(13) pp 4773-4779.

Barrow, N. J. (2015) Soil phosphate chemistry and the P-Sparing effect of previuos phosphate applications, *Plant Soil* **397** pp 401-409.

Basak , B. B., Sharmistha, P and Datta1, S. C. (2012), Use of modified clays for retention and supply of water and nutrients , *current science.* **102**(9) pp 1272-1278.

Basu S. K., Kumar, N and Srivastava J. P. (2010) Modelling NPK release from spherically coated fertilizer granules, *Simulation, Modelling, Practice and Theory* **18** pp 820-835.

Bekunda, M., Sanginga, N and Woomer, P. L. (2010) Restoring soil fertility in SubSaharan Africa, *Advances in Agronomy* **108** pp 183-236.

Belmokhtar, A., Benyoucef, A., Zehhaf, A., Yahioui, A., Quijada, C and Morallon, E. (2012) Studies on the conducting nanocomposite prepared bypolymerization of 2-aminobenzoic acid with aniline from aquoues solutions in montimorillonite, *Synthetic metals* **162** pp1864-1870.

Benco, L., Tunega, D., Hafner, J and Lischka, H. (2001) Abnition Density Functional theory Applied to the Structure and Proton dynamics of clays **133** (6) pp 479-484.

Bhashar, J. S and Gopolalerishnarao, P. (2010) Fourier Transform Infrared Spectroscopic Chararcterization of Kaolinite from Assam and Megghalaya, Northeastern India. *Journal of Modern Physics.* **1**(1)pp 206-210.

Bohn, H. L, McNeal, B. L and O'Connor, G. A. (2001), Soil Chemistry, John Wiley and sons, 3rd Edition pp 129- 143.

Booze-Daniels, J. N and Schmidt, R. E. (1997), "Use of slow release Nitrogen fertilizers on roadside- A literature review", Dept of Crop and Soils Environmental Science Virginia Polytechnic Institute and State University **540** (231) pp-7175.

Borges, R., Baika, L. M., Grassi, M. T and Wypych, F. (2009) Mechanochemical conversion of Chrysotile/ K_2HPO_4 mixtures into potential suspension technique- A comparative study, *Journal of Colloid intersurface science* **330** pp 367-373.

Bouwman, A. F., Boumans, L. J and Batjes, N. H. (2002) Emissions of N_2O and NO from fertilized fields. Summary of available measurement data. *Global Biogeochemical cycles* **16**(4) pp 6-13.

Branauer, S., Emmett, P. H and Teller, E. (1939) Adsorption of gases and multimolecular layers, *Journal of the American chemical society* **60** pp 309-319.

Broschat, T. K and Moore, K. K. (2007) Release Rates of Ammonium-Nitrogen, Nitrate-Nitrogen, Phosphorus, Potassium, Manganese, Iron and Manganese from seven Controlled-Release Fertilizers, *Communication in Soil Science and Plant analysis*, **38** (7-8) pp 843-850.

Cairns, J. E., Hellin, J and Sonder *et al.,* (2013) Adapting maize production to climate change in sub-Saharan Africa, *Food Security* **5**(3) pp 345-360.

Cakmakci, R., Donmez, D., Aydin, A and Jahin, F. (2005) Growth promotion of plants by plant growth promoting rhizobacteria under greenhouse and 2 different field soil conditions. *Soil Biol. Biochem* **38** pp 1482-1487.

Chagas, J. O., Gomes, J. M., de Matos Cunha, I. S., de Melo, N. F. S., Fraceto, L. F., da Silva, G. A and Lobo F. A. (2018) Polymeric microparticles for modified release of NPK in agricultural applications, *Arabian Journal of Chemistry* **13** pp 1084-2095.

Chana, H and Yala, R. (2011) Nanotechnologies in Agriculture. New tools for Sustainable development. Trends in Food Science and Technology 22 pp 585-594.

Chana, H and Yala, R. (2011) Nanotechnologies in agriculture.New tools for sustainable development. *Trends in Food Science and Technology* **22**: pp 585-594.

Chen, L., Xie, Z., Zhiang, X., Chen X and Jing, X. (2008) Controlled Release of Urea encapsulated by starch-g-poly(1-lactide), *Carbohydrate polymers* **72** pp342-348.

Chuli, F., Benyoucef, A., Yahioui, A., Quijada, C and Morallon, E (2012). A conducting nanocomposite via intercalative polymerization of 2-methylaniline with aniline in montimorillonite cation exchanged. *Journal of polymer research* **19** pp 1-19.

Cifuentes, C. A. R., AvilaViatela, J. K and Rodriguez, M. J. P (2017) Revision of optimized Hydrogel Design for the Covering of NPK Fertilizers as a strategy for sustainable Development. *International Journal of ChemTech Research*, **10**(15) pp 1-8.

Corradini, E. M., Moura, R and Mattoso, L. H. C. (2010) A preliminary study of the incorporation of NPK fertilizer into chitosan nanoparticles, *Express polymer letters* 4 (5)(2010) pp 509-515.

Cozic, C., Picton, L., Garda, M. R., Marlhoux, F and LeCerf, D (2009) Polymer Testing Analysis of Arabic gum: Study of degradation and water desorption processes. *Food Hydrocoll*, **23**(7) pp1930-1943.

Csernatoni, F., Socaciu, C., Pop, M. R., Fetea, F and Bunchez, F (2013) Application of FTIR Spectroscopy for Fingerprinting Bioactive Molecules in Nutraceutical Promen comparatively with plant ingredients. *UASVM Foof Science and Technology* **70** (1) pp 68-69.

Cun-dian, G., Jun-Li, R., Shuai-yang, W., Run-Cang, S and Li-hong, Z. (2014) Preparation of Polyvinylalcohol/Xylan Blending Films with 1,2,3,4-Butane Tetracarboxylic acid as a New Plasticizer, Hindawi: Journal of Nanomaterials 2014 pp 1-9.

Daoub, R. M. A., Elmubrak, A. H., Misran, M., Hassan, E. A and Osman, M. E. (2018) Characterization and Functional Properties of some Natural Acacia. *Journal of Saudi Society of Agricultural Sciences*, **17** (3) pp 241-249.

Datta, S. C. (2011) Nanoclay Research in Agriculture, Environment and Industry. National sympozium on 'Applications of clay sciences, Agriculture Environment and Industry 18-19 February 2011. NBSS and LUP, Nangpur pp 71-73.

Daungtawan, F., Phattanarudee, S., Seetapan, N and Kiatkamjornwong, S. (2011) Acrylamide-itaconic acid Superabsorbent Polymers and Superabsorbent polymer/mica nanocomposites. *Polymers for Advanced Technologies*. **22**(5) pp 635-647.

DeRosa, M. C. 2010. Preparation of Functional Aptamer Films Using Layer-by-Layer Self-Assembly, *Biomacromolecules Journal* **10** pp 1149-1154.

Dietz, T., Foeken, D., Soeters, S and Klaver W. (2014), Agricultural dynamics and food security trends in Kenya, *Agro-Food Clusters in Africa (AFCA)* pp 1-64.

Ding, H., Zhang, Y. S., Li, W. H., Zheng, X. Z., Wang, M. K., Tang, L. N and Chen, D. L. (2016) Nutrients Release from a Novel Gel-Based Slow/Controlled Release Fertilizer, *Hindawi, Journal of Applied and environmental Soil Science*, **2016** pp1-13.

Donald, F. C. and Huey-Rong, H. (1960), Flocculation of selected Clays by various electrolytes, *Ninth National Conference on Clays and Clay minerals*, pp 269-275.

Dorovan, G and Casey. (1998) Soil fertility management in sub-Saharan Africa. *World bank Technical paper 408.*

Elliot M. (2010) Superabsorbent polymers *BASF* pp1-13.

Fahmid, P., Arifur R., Jahid, M. M. I., Mubarak, A. K and Saadat, A. H. M. (2010) Preparation and Characterization of starch/PVA Blend for Biodegradable Packaging Material, Advanced Materials Research 123(125) pp 351-354.

FAO. (2015) Current world fertilizer trends and outlook to 2015 *Rome, Italy*

Farida, M., Suraya, A. R and Mohd, K. Y (2014), Intercalation of Urea into Kaolinite for preparation of Controlled Release Fertilizer, *Chemical Industry and Chemical Engineering Quarterly*, **2**: 207-213.

Ferfera-harrar H., Aouaz, N and Dairi, D. (2015) Environmental-sensitive chitosan-g-polyacrylamide/carboxymethylcellulose superabsorbent composites for wastewater purification I. Synthesis and properties. *Polymer Bulletin* vol **73**(3) pp 815-840

Fujinuma, R., Balster, J., and Norman, M. (2009) An improved model of nitrogen release for surface applied controlled release fertilizer *Soil science society of America Journal* **73**(6) pp 2043-2050.

G'eminarda, J. C and Bouraya, D. H. (2005) Thermal conductivity associated with a head-head contact decorated by a liquid bridge.An experimental study based on the response of a chain subjected to thermal cycles. *Gayvallet Europian Physics* **48** pp 509-517.

Gao, C., Wang, X and Liu, S. (2014), "Highly efficient adsorption of ammonium onto palygorskite nanocomposite and evaluation of its recovery as a multifunctional slow-release fertilizer," *Chemical Engineering Journal* **252** pp 404–414.

Ghazali S., Jamani S., Noordin N and Tan K. M. (2017) Properties of controlled-Release- Water Retention Fertilizer Coated with Carbonaceous-g-poly (acrylic acid-co- acrylamide) superabsorbent polymer. *International Journal of chemical Engineering and applications* **8** (2) pp 141-147.

Gieseking, E. L. (1975), Soil Components Vol.2. Spinger-Verlag. New York. Inc. pp 98-100.

Goldstein, J. I. R., A.D.Jr.; Newberry, D.E.; Lyman, C.E.; Echlin, P.; Fiori, C.; Joy, D.C.; Lifshin, E. Scanning Electron Microscopy and X-ray Microanalysis,3rd Edition; Plenum: New York, 2003.

Grillo,R., Pereira, A.E.S., Nishisako C. S., de Lima, R., Ochlke K., Greiner, R and Fraceto L. (2014)Chitosan/tripolyphosphate nanoparticles loaded withparaquat herbicide: an environmentally safer alternative for weed control, *Journal Hazard Materials* **278** pp 163-171.

Grim, R. E. (1962), Applied Clay Mineralogy, McGraw-Hill Book Co., Inc., New York 136 pp 870-871.

Gu, Y. F, Zhang, Z. P., Tu, S. H and Lindstrom, K. (2009) Soil microbial biomass, crop yields and bacterial community structure as affected by long-term fertilizer

treatments under wheat-rice cropping. *Europian Journal of soil Biology*. **45** pp 239-246.

Guang-huo ,W and Qi-chun, Z. (2005) "Studies on nutrient uptake of rice and characteristics of soil microorganisms in a long-term fertilization experiments for irrigated rice", *Zhejiang Univ Sci B*. **6**(2) pp 147-152.

Guertal E. A., (2009) Slow release nitrogen fertilizers in vegetable production: A review, *Journal of Hort.Technology* **19** pp 16-91

Gulfam, N., Mohammad, S. K., and Uzma, K .(2014) Structural study of PVA composities with inorganic salts by X-Ray diffraction, *Journal of Pak Mater Society*, **3**(2) pp 66-70.

Gupta N., Gaurav S.S and Kumar A. (2013) Molecular basis of Aluminium toxicity in Plants: a review *American Journal of plant Sciences* **4**(12) pp 21-37.

Han, X., Chen, S and Hu, X. (2009), Controlled-release fertilizer encapsulated by starch/polyvinyl alcohol coating, *Desalination*, **240** pp 21-26.

Hanaji, M., Eltaib, M and Ahmad, B. (2000) Physical and chemical characterization of controlled release compound fertilizer. *Europian polymer Journal* **36**(10) pp 2018-2088.

Heinen, R. B., Ye, Q and Chaumont, F. (2009) Role of aquaporins in leaf physiology, *Journal of experimental Botany* **60** pp 2971-2985.

Himmah, N. I. F., Gunawan, D and Dawawan. (2018) Nutrient Release performance of starch Coated NPK Fertilizers and their effects on Corn Growth, *Journal of Soil Science and Agriclimatology* **15**(2) pp 104-114.

Ho, Y. S and McKay, G. (1998) A comparison of chemisorption kinetic models applied to pollutant removal on various sorbents, *Trans IChemE* **76** pp 331-340.

Ho, Y. S and McKay, G. (2002) Application of Kinetic Models to Sorption of Copper II on to Peat, *Adsorption Science and Technology*, **20**(2) pp 797-814.

Hongtao, Z., Yao L., Xiuli, D., Na, Y., YuLing, Z., YuLong, Z and Jianghui, D. (2014), Research Article Solubility Characteristics and Slow-Release Mechanism of Nitrogen from Organic-Inorganic Compound Coated Urea, *International Journal of Photoenergy* pp 1-7.

Hornyak, G. L. D., Tibbals, H. F and Rao, A. K. (2008) *Introduction to Nanoscience*; CRC Press: New York.

Hornyak, G. L. D., Tibbals, H. F and Rao, A. K. (2008) Introduction to Nanoscience; CRC Press: New York.

Hugo, D. G., Owuor, G., Cheryl, D., Ouma, J., Lutta, M and Danda, K (2005) The Maize Green Revolution in Kenya Revisted, *Journal of Agricultural and Development Economics* **2**(1) pp 32-49.

Hussain, A., Arshad, M., Ahmad, Z., Ahmad, H. T., Afzal, M., Ahmad M. (2015) Potassium fertilization and maize physiology. Potassium fertilization influences

growth physiology and nutrients uptake of maize (Zea MaysL.) *Cercet. Agronomy mold.* **XLVIII** pp 37-50.

Islam, A., Muttaleb, A. (2016) Effect of potassium fertilization on yield and potassium nutrition of Boro rice in a wetland ecosystem of Bangladesh, *Archieological Agronomy of soil science,* **62** pp1530-1540.

Islam, S., Timsina, J., Salim, M., Majumdar, K and Gathala, M. K. (2018) Potassium Supplying Capacity of Diverse soils and K- use efficiency of maize in south Asia. *Agronomy* **8**(121) pp1-22.

Jaber, F. (2012) New routes for synthesis of environmental friendly superabsorbent Polymers.MSc Thesis An-Najah National University

Jamaludin, J., Adam F., Abudul, R and Hassan, Z. (2017) Thermal studies on Arabic gum-carrgeenan polysaccharides film, *Chemical Engineering Research Bulletin* **19** pp 80-86.

Jamari, S., Ghazali, S and Yaacob, W. (2015) Effect of superabsorbent polymer composite filled carbon fiber towards the germination of abelmoschus esculentus. *Journal of Advanced Agricultural Technologies* **2** (2) pp156-159.

James,O. O., Adediran, M., Adekola, E. O., Odebunmi, E. O and Adekeye, J. I. D. (2008), Beneficiation and Characterization of a Bentonite from North Eastern Nigeria. *Journal of the North Carolina Academy of Science,* 124(4) pp 154-158.

Jeffery, D. R and Sinclair, T. R. (1998) The effect of pot size on growth and transpiration of maize and soya bean during water deficit stress, *Journal of Experimental Botany* 49(325) pp 1381-1386.

Jiang-Jen, L., Ying-Nan, C and Yi-Fen, L. (2010), Hydrophobic Modification of Layered Clays and Compatibility for Epoxy Nanocomposites, *Materials* **3** pp 2588-2605.

Jocksusch. S., Turro. N. J., Mitsukami. Y., Matsumoto M., Iwamura T., Lindner T., Flohr A and Massimo G. (2009) Photoinduced surface crosslinking of superabsorbent polymer particles. *Journal of Applied polymer Science* **111** pp 2163-2170.

Joo G. L., Kin Y. M., Lee I. J., Song K. and Rheek, S. (2004) Growth promotion of red pepper plag seedlings and the production of gibberellins by Bacillus cereus, Bacillus macrolides and Bacillus pumilus. *Biotechnology letters* **26** pp 487-491.

Jullien, M., Raynal, J., Kohler, E and Bildstein, O. (2005) Physicochemical Reactivity in Clay rich materials. Tools for safety assessment. *Oil and Gas Science and Technology* **60** pp107-120.

Kadiata, B. D and Lumpungu, K. (2003) Differential Phosphorus uptake and efficiency among selected nitrogen fixing tree legumes over time, *Journal of Plant nutrition* **26**(5) pp 1009-1022.

Kaiwen, C., Yern, C. C., Cheng, H. C., Sabariah, J and Nai-Shang, L. (2016) Prepartion and Characterization of Polyvinyl Alcohol- Chitosan Composite Films Reinforced with Cellulose Nanofiller. *Materials* **9** pp1-16.

Kaldenhoff, R., Ribons-Carbo, M., Flexas, J., Lovisolo, C., Heckwolf, M and Uehlein, N. (2008) Aquaporins and Plant water balance, *Plant cell Environment* 31 pp 658-666.

Kant, S and Kafkali, U. (2002) Potassium and abiotic stresses in plants. In: Pasrisha N S., Bansal S K (eds) Potassium for sustainable crop production. *Potash Institute of India, Gurgaon* pp 233-251.

Kaplan, L., Tlustos, P., Szakova, J and Najmanova, J. (2013)The influence of slow release fertilizers on potted chrysanthemum growth and nutrient consumption, *Journal of Plant soil environment* **59**(9) pp 385-391.

Kenyanya, O., Muthengia, J. and Mbuvi, H. (2013). Determination of potassium levels in intensive subsistence agricultural soils in Nyamira county, Kenya. *International Journal of Agriculture and Forestry* **3**(7) pp 294-302.

Khaldi M., Benyoucef A., Bousalem S., Yahiuoui A and Morallon E. (2014) Synthesis, characterization and conducting properties of nanocomposites of successifully intercalated 2- aminophenol with aniline in modified Montimorillonite. *Journal of inorganic and organometallic polymers and Materials* **24** pp 267-274.

Khandpur, R. S.(2007) Handbook of Analytical Instruments; McGraw Hill: New York.

Kharazmi, A., Faraji, N., Mat Hussin, R., Saion, E., Mat Ynus, M. W and Behzad, K (2015) Structural Optical Optothermal, Thermal Properties of Zn-PVA Nanofluids, *Journal of Nanotechnology* **6** pp 529-536.

Khelifa, I., Belmokhtar, A., Berenguer, R., Benyoucef, R and Morallon, E. (2018) Modified- clay nanocomposites: A study on spectral, thermal, morphological and Electrochemical characteristics, *Journal of molecular structure.* pp 1-22.

Khodakovskaya, M., Dervishi, E., Mahmood, M., Yang, X. U., Zhongrui, Li., Watanabe, F and Biris, A. S. (2009). Carbon nanotubes are able to penetrate plant seed coat and Dramatically affect seed germination and plant growth. *ACS Nano* **3** pp 3321-3227.

Kihanda, F. M. (1996) The role of farmyard manure in improving maize production in sub humid central highlands of central Kenya. *Ph D UK*.

KNBS, (2019), Population Distribution by Age, Sex and Administrative Units. Kenya Population and Housing Census **(1C).** pp 37

Komarneni, S. (2010). Potential of nanotechnology in Environmental Soil Science. I Proc. The 9th International Conference of the East and Southeast Asia Federation of soil sciences. *Science societies* pp 16-20.

Kornmann, X. (2000), Synthesis and Characterization of Thermoset- Clay Nanocomposites. Lulea University of Technology, Sweden .pp 8-48.

Kottegoda, N., Munaweera, I., Madusanka, N and Karunaratne, V. (2011) A green slow-release fertilizer composition based on urea-modified hydroxyapatite nanoparticles encapsulated wood. *Current Science,* **101** pp 73-78.

Lack, A. J and Evans, D. E. (2005) Instant notes in plant biology, *2nd edition Taylor and Francis. Oxford.*

LeBaron, P. C., Wang, Z and Pinnavair, T. J. (1999), Polymer layered Silicate nanocomposites: an overview. *Applied Clay Sciences,* **15** pp 11-29.

Liu, G., Shaopeng, W., Van de Ven, M., Molenaar, A and Besamusea, J. (2010) Characterization of Organic Surfactant on Montmorillonite Nanoclay to be used in Bitumen, *Journal of materials in civil engineering,* pp 794-795.

Liu, M and Gao, T. (2001) Preparation and swelling properties of crosslinked sodium polyacrylate. *Journal of Applied Polymer Science*, **82** pp 1515- 1520.

Liu, M. and Wu, L. (2008), "Preparation and properties of chitosan- coated NPK compound fertilizer with controlled-release and water-retention, *Carbohydrate Polymers*, **72**(2) pp 240– 247.

Liu, X. F., Zhao-bin., Fu-dao., Shu-ging, Z and Xu-sheng, H. E. (2005a). Study on adsorption and desorption properties on nano-kaolinite to nitrogen, phosphorus, potash and organic carbon. *Science Agriculture* **38** pp 102-109.

Mahendra, K. T., Alice, B., Dahryn, T., Gopal, N., Khemraj, B and Snehasia, J. (2015), Spectroscopic Characterization of Disodium Hydrogen Orthophosphate and

sodium Nitrate after Biofield Treatment *Journal of chromatographic separation Technique,* **6**(5) pp 1-5.

Majumdar, K., Zingore, S., Garcia, F and Johnston, A. M. (2017) Improving nutrient management for sustainable intensificationof maize. In: Achieving sustainable cultivation of maize; *Burleigh Dodas science publishing Sawston UK* **2** pp1-32.

Mandal, K. G., Hati, K. M and Misra, A. K. (2009) Biomas yield and energy analysis of soyabean production in relation to fertilizer-NPK and organic manure. *Biomass and bioenergy* **33** pp 1670-1679.

Manjunatha, S. B, Biradar, D. P and Aladakatti, Y. R. (2016). Nanotechnology and its applications in agriculture: A review. *Journal of Farm Sciences* **29**(1) pp 1-13.

Mano, J. F., Koniarova, D and Reis, R. L. (2003) Thermal properties of thermoplastic starch/synthetic polymer blends with potential biomedical applicability, *Journal of materials science in medicine* **14** pp 127-135

Marian J., Ignac B., Dusan L., Vojtech S., Dusan V and Dusan C. (2009).Terahertz Time-Domain Spectroscopy of selected Layered Silicates, *Clay and Clay minerals* **57**(4) pp 416-424.

Mark, F. (2001) *Optical Properties of Solids*; Oxford University Press: New York,

Marta, H., Cahyana, Y., Arifin, H. R and Khairani, L. (2019) Comparing the effect of four different thermal modifications on physicochemical and pasting properties of breadfruit(Artocarpus altilis)Starch, *International Food Research Journal* **26**(1) pp 269-276.

Masakuni, T., Yukihiro, T., Takeshi, T and Yasuhito, T. (2014) The Principles of Starch Gelatinization and Retrogradation, *Food and Nutrition Sciences* **5** pp 28-291.

Matson, P. A., Parton, W. J., Power, A. G and Swifft, M. J. (1997) Agricultural intensification and ecosystem properties *Science* **277** pp 504-509.

Maxim, R., Elshan, A., Alexey, R., Ales, B and Bulat, S. (2019) Mechanochemical preparation of slow release fertilizer based on Glauconite –urea complexes, *Minerals* **9** pp 1-10.

Meena, D., Joshi, K., Jat, S., Chinchmalatpure. R., Narjary, B., Sheoran, P and sharma, K. (2016) Changes in biological and chemical properties in saline soil amended with municipal solid waste composite and chemical fertilizers in a mustered-pearl millet cropping system, *CATENA* **140** pp 1-8.

Megan, S., Roy, B and Jayne, T. S. (2012) Are farmers underutilizing fertilizer? *International Association of Agricultural Economics (IAAF) Triennial Conference*- Brazil, 18-24 August 2012, pp 1-46.

Mengel, K and Kiskby, A. A. (2011) Principles of Plant Nutrition(5^{th} ad)Dordrecht Springer Netherlands hppt://dri.org/10.1007/978-94-010-1009-2.

Mikhailenko, M. A., Sharafutdinov, M. R., Kozlov, A.S., Kuznetsova, S. A., Shakhtshneider, T. P and Zolotarev, K. V. (2016) Study of arbinogalactan supramolecular structure using synchrotron radiation SAXS and terahertz laser ablation methods. *Physics Procedia* **84** pp 382-385.

Mikhailenko, M. A., Sharafutdinov, T. P., Eltsov, I. V., Kozlov, A.S., Kuznetsova, S. A., Karacharov, S. A and Bolyrev, V. V. (2016) Supramolecular architecture of betuline diacetate complexes with arabinogalactan from Lerix sibirica. *Carbohydrate polymers* **138** pp 1-7

Min, Y. L., Wang T., Zhang Y G., and Chen, Y. C. (2011) The synthesis of poly(p-phenylenediamine) microstructures without oxidant and their effective adsorption of lead ions. *Journal of materials chemistry* **21** pp 6683-6689.

Mirjana, J., Nastasija, M., Dragana, B., Dragana, J., Timea, H-J and Dragana, S. (2012) Effects of plant promoting rhisobacteria on maize in greenhouse and field trial *African journal of microbiology research* **6**(27) pp 5683-5690.

Mohamad, N., NorDadia, A. N., Jeefferie, A. R., and MohdFainiz, D. (2013) Effect of Chitosan gelatinization temperature om water absorption and water retention of Chitosan based Urea fertikizer, *International Journal of Automotive and mechanical engineering* **8** pp 1357-1366.

Mohan, S and Lakhwant, S. (2016) Vibrational Spectroscopic Study of Muscovite and Biotite Layers, *Indian Journal of Pure and Applied Physics* **54** pp 116-122.

Mohan, Y. M. (2006) Synthesis and swelling behavior of acrylamide potassium methacrylate superabsorbent co-polymers. *Journal of polymeric materials* pp1-23.

Mohd, F. O., Hazizzan,M. A., Mohd, F. A. R and Jamaliah, M. S. (2014) Thermal Properties of Polyproxylene/muascovite layered Silicate composite effects of organic modificationsand Compatibilisers, *Journal of Composite Materials*, 0(0)

pp 1-15

Mohsen. Q. and El-maghraby, A. (2010), Characterization and Assessment of Saudi Arabia clays, Raw materials at different areas, *Arabian Journal of Chemistry,* 3 pp 271-277.

Mokwunye, U and Bationo, A. (2002) Meeting the phosphorus needs of the soil and crops in West Africa. *CAB publishing,* Wellingford UK.

Montalvo, D., Degryse, F and Laughlin, M. J. (2015a) Natural colloidal P and its contribution to plant P uptake, *Environmental Science and Technology* **49** pp 3427-3424.

Moreno-Tovar, R., Yanez-Hernandez, O. A., Perez-Moreno, F., Rivera, J. J. C., Rivera, A and Lugo, R. V. (2017) Clays for brick manufacturing in Actopan, Hidalgo: Phusical, chemical and Mineralogy Characterization.*Materials Research* **20**(5) pp 1185-1192.

Mothe, C. G., and Rao, A. M. (2000) Thermal behavior of GUM Arabic in comparison with cashew gum, *Thermochim Acta,* **357-358** pp 9-13.

Mrkovacki and Bjelic. (2011) Plant growth promoting rhizobacteria(PGPR) and their effect on maize. *Field vegetation crop research* **48**(2) pp 305-312.

Mucheru-Muna, M., Mugendi, D., Kungu, J., Mugwe, J and Bationo, A. (2007) Effects of organic and Mineral fertilizer inputs in Maize yield and soil chemical properties in a maize cropping system in Meru south District Kenya *Agroforest systems* **69** pp 189-197.

Mulavolta, E. (1985) Potassium status of tropical and subtropical region soils. In: Munson R D(ed) Potassium in agriculture, *American society of Agronomy, Crop science society of America and Science society of America*, Madison pp 163-200.

Mwanda, C. O. (2008) A note on weed control in Machakos District, Kenya: Retrieved 5.5.2008 from http://atnesa.org.

Naderi, M. R and Danesh-Shahraki, A. (2013), "Nanofertilizers and their roles in sustainable agriculture", *International Journal of Agriculture and Crop Sciences* **19** pp 2229-2232.

Nafie, A. A., Elfatih, A.H., Al-Sayed, A and Mohamed, G. A. M (2012) Diode Laser (532nm)Induced Grafting of Poplyacrylamide onto Gum Arabic, *Journal of Physical Science* **23**(2) pp 43-53.

Nambiro, E. and Okoth, P. (2013), What factors influence the adoption of inorganic fertilizer by maize farmers? A case of Kakamega District, Western Kenya, *Scientific Research and Essays* **8**(5) pp 205-210.

Ngosong, C., Bongkisheri, V., Tanyi, C B., Nangnoa, L. T and Tening, A. S. (2019) Optimizing Nitrogen Fertilization Regimes for Sustainable Maize(Zea MaysL.) Production on the volcanic soils of Buea Cameroon. *Hindawi- Advances in Agriculture* pp 1-9.

Nguyen, T. N., Tang, L. H., Peng, J. K., Ni, Y. J and Chang, Y. N. (2015), Effects of Composite inorganic Fertilizer and Foliar spray of Multi-nutrients on Growth,

Yield and Quality of Cherry Tomato, *Journal of Agriculture science and Technology* **17** pp 1781-1788.

Ni, B., Liu, S., Xie, L and Wang, Y. (2011) Environmentally friendly slow release Nitrogen fertilizer. *Journal of Agriculture food and chemicals* **59** pp 10169-10175.

Njoka, E. N., Ochieng, O., Githumbi, J. M and Nderi, O. (2015) Characterization of Clays from Tharaka-Nithi county in Kenya for industry and Agricultural Applications, *African Journal of Environmental Science and Technology* 9(3) pp 228-243.

Ochieng, O (2016) Characterization and classification of clay minerals for potential applications in Rugi Ward-Kenya, *African Journal of Environmental Science and Technology* **10**(11) pp 415-436.

Olejnik, S., Poner, A, M and Quirk, J. P. (1970), The Intercalation of Polar Organic compounds into Kaolinite, *clay minerals* pp 422-434.

Omodi, A and Saigusa, M. (2000) Broadcast application versus band application of polyolefin coated fertilizer on green peppers grown on sandy soil, *Journal of Plants Nutrition* **23** pp 1485-1493.

Onasanya, R, Aiyelari, O., Onasanya, A., Nwilene, F and Oyelari. (2009) Effect of different levels of Nitrogen and Phosphorus fertiliz growth and yield of maize(Zea MaysL.)in southern Nigeria. *International Journal of Agriculture Research* **4** pp 400-407.

Osabar, V. N., Okafor, P. C., Ibe, K. A and Ayi, A. A. (2009), Characterization of clays in Udukpani, South eastern Nigeria. *African Journal of Pure and Applied Chemistry*, 3 pp 79-85.

Owino, C. O. (2009) Decreased row spacing as an option for increasing maize(Zea MaysL)Yield in trans Nzoia district. Kenya. *Journal of plant Breeding Crop Science* **1**(8) pp 281-283.

Owino, C. O. (2010) Fertilizer options for sustainable Maize (Zea Mays L) Production in the Trans Nzoia district in Kenya *African Journal of Agricultural Research* **5**(11) pp 1208-1212.

Pack, J. E., Hutchinson C. M and Simonne E. H. (2006) Evaluation of controlled-release fertilizers for northern Florida chip potato production, *Journal of Plant nutrition* **29**(7) pp 1301-1313.

Parthasarathy, G., Kunwar, A. C and Srinivasan, R. (2001). Occurance of Maganite-Rich Chalcedony in Deccan Flood Basalts, Killain Mahrashatra India. *Europian Journal of minerals* **13** (1) pp127-134.

Pathak, D. S., Aggarwal P, K., Rotter, R. D., Kalra, N., Bandyopadhaya, S. K., Prasad, S and Van Kenlen, H. (2003) Modelling the quantitative evaluation of soil nutrient supply, nutrient use efficiency and fertilizer requirements of wheat in Inia, *Nutrition cycl. Agroecosust.* **65** pp 105-113.

Peng, X., Ruixin, Ma and Wengli, L. (2020) Study of the crystal structure of coal kaolinite and non-coal kaolinite: insights from experiments and DET

simulations, *symmetry-mdpi* **12**(1125) pp 1-12.

Perez, S and Vergelati, C. (1997)"Solid State and Solution Fea-tures of Amylose and Amylose Fragments," *Polymer Bulletin*, **17**(2), pp. 141-148.

Perrenoud, S. (1990) Potassium and plant health, 2nd edition. *International potash institute*, *Bern* pp 8-10.

Perrin, T. S., Drost, D. T., Boettinger, J. L and Norton, J. M. (1998). Ammonium loaded clinophlolite. A slow release nitrogen fertilizer for sweet corn. *Plant Nutrients* 21 pp 515-530.

Pieter, S., Gustaaf, S and Dirk, S. (2015), Kaolinite Nanocomposite Platelets Synthesized by Intercalation and Imidization of Poly (Styrene-*co*-Maleic anhydride, *Materials*, **8** pp 4363-4388.

Pironon, J., Pelletier, M., DeDonate, P and Mosser-Ruck, R. (2003) Characterization of smectite and illite by FTIR spectroscopy of interlayer NH_4^+ cations, *Clay minerals* **38** pp 201-211.

Poongushali, S., Madhaiyan, M and Sa, T. (2008) Isolation and identification of phosphate solubilizing bacteria from chinese cabbage and their effect on growth and phosphorus volatilization of plants. *Journal of microbiology and Biotechnology* **18** pp 773-777.

Puge, A. L, Miller, R. H and Keeney, D.R (eds) (1982) Methods of soil analysis part 2, second edition. Soil science society of America. Inc. Madison, Wincosin, USA pp149-161.

Rahul, S., Aditya, M and Upender, P. (2017) Synthesis and Testing of Corn starch Based Biodegradable Plastic and Composite, *8th International Science, social science, Engineering and Energy conference* pp 1-6.

Rai, M and Ainah, I. (2012), Role of Nanotechnology in Agriculture with Special Reference to Management of insect Pests, *Applied microbiological Biotechnology*, **93** pp 287-293.

Rai, V., Acharya, S and Dey N. (2012) Implications of nanobiosensors in agriculture. *J. Biomaterials and nanobiotechnology* **3** pp 315-324.

Rameshaiah, G. N., Pallavi, J and Shabnam, S. (2015), *International Journal of Engineering Research and General Science* **3** (1) pp 2091-2730.

Rameshaiah, G. N., Pallavi, J and Shabnam, S. (2015), Nanofertilizers and nanosensors- Attempt for developing smart agriculture, *International journal of engineering research and general science*, **3**(1) pp 1-7/2091-2730.

Ramos Campos, E. V., de Oliveira, J. L., Goncalves, daSilva, C. M., Pascoli, M., Pasquoto T., Lima R., Abhilash, P. C., Fraceto, L. F. (2015) Polymeric and solid lipid nanoparticles for sustained release of cabendazim and tebuconazole in agricultuiral applications, *Science Rep* **5** pp

Rashidzadel, A., and Olad, A. (2014) Slow release NPK fertilizer encapsulated by NaAl-g-g-Poly-(AA-Co-AAm)/MMT superabsorbent nanocomposite. *carbohydrate polymers* V11**4**(19) pp269-278.

Rashizadeh, A., Olad, A and Reyhanitabas, A. (2015) Hydrogel/Clinoptilotide Nanocomposite coated Fertilizer Swelling, water Retention and Slow Release Fertilizer properties, *Polymer Bull*. **72** pp 2667-2684.

Rawat, J., Sanwal, P and Saxena, J. (2016) Potassium and its role in sustainable agriculture, *https//www.researchgate.net/publication/304537669*, pp 235-255.

Ray, A. K., Bird, P. B., Lacobucci, G. A and Clark, R. C. (1995) Functionality of Gum Arabic, Fractionation, Characterization and Evaluation of Gum fractions in Citrus oil emulsions and Model Beavarages. *Food Hydrocoll* **9** pp 123-131.

Rodriguez, J., Martin, M. J., Ruiz, A. M and Clares, B. (2016) Current encapsulation strategies of bioactive oils: from elementary and pharmaceutical perspectives *Food Rest Int*. **83** pp 41-59.

Rouquerol, J., Rouquerol, F and Sing, K. S. W. (1998) Absorption by powders and porous solids. *Academic press.* ISBN0080526012.

Sachan, A and Penumadu, D. (2007) Identification of microfabric of Kaolinite Clay mineral using X-ray Diffraction Technique. *Geotechnical and Geological Engineering*, **25** pp 603-616.

Sadeghi, M and Hossein-Zadeh. H. (2008) Synthesis and swelling behavior of Starch-Poly(Sodium Acrylate-co-Acrylamide) superabsorbent hydrogel. *Turkish Journal of Chemistry* **32** pp 375-388.

Sadeghi, M. (2012) Synthesis of a bio copolymer Carrageenan-g-Poly(AAm-co-1A)/montimorillonite superabsorbent hydrogel composite. *Brazilian Journal of Chemical engineering* **29**(2)pp

Salahuddin N., Ayad A. A., and Ali, M. (2008) Synthesis and characterization of polyaniline- organoclay nanocomposite. *Journal of applied polymer science* **107** pp 1981-1989

Saleque, M. A., Sha, P. K and Pnaullah, G. M. (1998) and Bhuiyan N I(1998)Response of wetland rice to potassium in farmers' fields of the Barind tract of Bangladesh. *Journal of plant nutrition* **21** pp 39-47.

Sarko A, J. Southwick and J. Hayashi. (1976) "Packing Analysis of Carbohydrates and Polysaccharides. 7. Crystal Struc-ture of Cellulose III and Its Relationship to Other Cellu-lose Polymorphs," *Macromolecules*, **9**(5), pp 857-863.

Sarwono, A. (2013) Improvement of hydrophobicity of Urea Modified Tapioca starch Film with lignin for Slow Release Fertilizer, *AMR*, **625** pp 350-354.

Satyanarayana, T., Kaushik, M., Biradav, D, P. (2011)New approaches and tools for site specific nutrient management with reference to potassium, *Karnataka Journal of Agricultural science* **6** pp 3597-3605.

Schaffazick, S. R., Guterres, S. S. U., Freitas, L. D and Pohmann, A. R. (2003) Physicochemical characterization and stability of polymeric nanoparticle syatemsfor drug administration, *Quimica Nova* **26** pp 726-737.

Schroeder, D. (1974) Relationships between soil potassium and potassium nutrition of plants. In: Potassium research and Agriculture production. *Proceedures of the 10th congress of the international potash institute* pp 53-63.

Shafaq, N., Muhammad, R. S., Madiha, R., Sadia, K and Hafiz, A. (2017) Production of clay polymers for fertilizer coating. *International Journal of Chemical and Biological Sciences.* **12** pp 122-129.

Shan, J., Sha, L and Wenhao, P (2011) PVA Hydogel Properties for Biomedical Application, *Journal of the Mechanical Behavior of Biomedical Materials*, **4**(7) pp 1228-1233.

Shavit, U., Shaviv, A., Shalit, G and Zaslavsky, D. (1997) Release characteristics of a new controlled release fertilizer, *Journal of Controlled Release* 43(2-3) pp 131-138.

Shaviv, A (2001) Advances in controlled release fertilizers, *Advances in Agronomy* **71** pp 1-49.

Siafu, I. S., Hee-Taik K, Egid, M., Pogrebnoi, A., Godlisten, S and Askwar, H. (2015), Encapsulated Urea-Kaolinite Nanocomposite for Controlled Release Fertilizer Formulations, *Journal of Chemistry* pp 1-17.

Silverstein, M. R. W., Francis, X. (1998) Spectrometric Identification of Organic Compounds, 6th Ed.; John Wiley & Sons, Inc.: New York.

Singh, S and Kapoor, K. (1994) Solubilization of insoluble phosphates by bacteria isolated from different sources. *Environmental Ecology* **12** pp 51-55.

Singh, V. K., Dwivedi, B. S., Buresh, R. J., Jat, M. L., Majumdar, K., Gangwar, B., Govil, V., Singh, S. K. (2013) Potassium fertilization in rice-wheat system across northern India, Crop performance and soil nutrients, *Agronomy Journal* **105** pp 471-481.

Sparks, D. L. (2000) Bioavailability of soil potassium. In: Sumner M E (ed)Handbook of soil science CRC press, Boca Raton pp D38-D52.

Subbarao, V, Kartheek, G and Sirisha, D. (2013), "Slow Release of Potash Fertilizer Through Polymer Coating", *International Journal of Applied science and engineering* **11** (1) pp 25-30.

Sulahuddin, N., Ayad, M. M and Ali M. (2008) Synthesis and characterization of poly-aniline organoclay nanocomposite. *Journal of applied polymer science* **107** pp 1981-1989.

Suppan, S. (2017) Applying nanotechnology to fertilizers; Rationales, research, risks and regulatory challenges pp 1-21.

Survar, M. (2012) Effects of potassium fertilization on population buildup or rice stem borers (lepidopteron pests) and rice (oryza sativa L.) yield *Journal of cereal oilseeds* **3** pp 6-9.

Tan, K. H. (2011), Principles of Soil Chemistry, 4th Edition, CRC press pp160-169.

Tenning, A., Foba-Tendo, J. N., Yakum-Ntaw, S. Y and Tchuenteu, F. (2013) Phosphorus fixing capacity of a volcanic soil on the slope of mount Cameroon, *Agriculture and Biology Journal of North America (ABJNA)* **4**(3) pp 166-173.

Thirunavukkarasu, M (2015) *Trends in Bioscience* **8**(13) pp 3261-3268.

Timsina, J., Jat M. L and Majumdar, K. (2010) Rice-maize systems of south Asia: Current status, future prospects and research priorities for nutrient management, *Plant Soil* **335** pp 65-85.

Tlustos P., Balik, J., Pavlikova D. (1994) The effect of fertilizer coating on the nutrient release from NPK fertilizers, *Plant Soil and Environment* **40** pp 219-229.

Tong, X., He, X., Dvan, H., Han, L and Huang, G. (2018) Evaluation of Controlled Release Urea on the Dynamics of Nitrate, Ammonium and its Nitrogen Release in Black Soils in Northern China, *International Journal of Environmental Resources and Public Health* **15**(119) pp 1-13.

Trenkel, M. E. (1997) Controlled-release and stabilized fertilizers in agriculture. *Int. Fertilizer Association, Paris* pp 243-318.

Trenkel, M. F. (2010) Slow Release and Stabilized fertilizers; an option for Enhancing Nutrient Release Use Efficiency in Agriculture(2nd ed),Paris, IFA, International Fertilizer Industry Association.

Trinh, T. H and KuShaari K(2016) Dynamic of Water Absorption in Controlled Release Fertilizer and its Relationship with the Release of Nutrient, *Procedia Engineering* **148** pp 319-326.

Trouffland, S., Mullen, W., Carson, T. R., Graham, I. A., Cruzier, A., Amtmann, A and Armengand, P. (2010) Potassium deficiency induces the biosynthesis of

oxylipins and glucosinolates in Arabidopsis thaliana. *RMC plant Biology*, **10**(1) pp172.

Trunschke, A. (2013), Surface area and pore size determination, Modern methods in Heterogeneous catalysis Research, pp 1- 52.

Utpalendu, K and Manika, P. (2013) Specific surface area and particle size distribution in clays and Shales. *Geophysical prospecting* **61** pp 341-362B.

Verbeken D., Dierckx S., Dewethinck K. (2003)Exudate gums: occurance, production and applications. *Applied microbiol Biotechnology* **63** pp 10-21.

Vila, M., Sánchez-Salcedo, S and Vallet-Regí, M. (2012). Hydroxyapatite foams for the immobilization of heavy metals: From waters to the human body, *Inorganica Chimica Acta*. **393** pp 24-35.

Wang, M., Zheng Q., Shen Q and Guo S. (2013) The critical role of potassium in plant stress response, *International Journal of Molecular Sciences* **144** pp 7370-7390.

Wang, W., Zhang. T and Wang, A. (2009). Preparation and swelling properties of Superabsorbent nanocomposites based on natural guar gum and organo-Vermiculite. *Journal of Applied Science* **46** pp 21-26.

Webb, P. A and Orr, C. (1997) *Analytical Methods in Fine Particles Technology*; Micromeritics Instrument Corporation: Norcross, GA.

Weeks, J. J and Gange, M. H. (2019) A review of the latest in phosphorus fertilizers technology: Possibilities and Pragmation, *Journal of Environmental Quality* pp 1-15.

Wegner, L. (2010) Oxygen transport in waterlogged plants. In:Mancuso S, Shabala S(eds)Water signaling and tolerance inplants: Springer, *Berlin/Heidelberg* pp 3-22.

Wijesinghe W. P. S. L. and Weerasinghe A. M. C. P. (2015), Development of nano fertilizers as Slow Release Fertilizers. Young Researchers' Forum – PGIS, *Sciscitator* **2** pp 28-29.

World population clock, (2019) www.worldometers info

Wu, L and Liu, M. (2008) Preparation and Properties of Chitosan-coated NPK Compound Fertilizer with Controlled Release and Water Retention, *Carbohydrate Polymers* **72**(2) pp 240-247.

Wu, L., Liu, M and Liang, R. (2008) Preparation and properties of double-coated slow Release NPK compound fertilizer with superabsorbent and water retention. *Bioresource Technology* **99** pp 547-554.

Wu, S. C., Caob , Z. H., Lib, Z. G., Cheunga, K. C., Wonga, M, H. (2005) Effects of biofertilizer containing N-fixer, P and K solubilizers and A. M fungi on growth of maize: a greenhouse trial. *Geoderma* **125** pp 155-166.

Xiaoyu, N., Yuejin, W., Zhengyan, W., Lin, W., Guannan, Q. and Lixiang, Y. (2013), A novel slow-release urea fertiliser: Physical and chemical analysis of its structure and study of its release mechanism, *Biosystems Engineering* **115** pp 274 -284.

Yadav, V. S., Sharma, T., Saxena, V. K. (2000) Dissolution kinetics of potassium from glauconitic sandstones in acid lixiviant, *International Journal of Mineral processes* **60** pp 15-36.

Yakaya, S., Suzi, S. J., Budarulzaman, N. A., Dahiru, A and Adamu N. A. (2017) Chemical composition and Particle size Analysis of Kaolin Path of science **3**(10) pp 1-4.

Yogita, K., Krishna, K, Warbade and SusheelKumar B. (2014), Primary Nutrients Determination in the Soil Using UV Spectroscopy, *International Journal of Engineering Research and Technology,* **2**(2) pp 198-204

Young-Chang, N., Youn-Mook, L., Hui-Jeon, G and Fun-Kyung, C. (2009) Preparation and characterization of PVA/PVP/glycerin/antibacterial agent hydrogels using γ-radiation followed by freeze-thawing, Korean Journal of Chemical Engineering 26(6) pp 1675-1678.

Zangi, R., Zhon, R and Berne, B. J. (2009) Urea's action on hydrophobic interactions. *Journal of American Chemical society*. **131** pp 1535-1541.

Zenawi, G and Mizan, A. (2019) Effect of Nitrogen fertilization on the growth and seed yield of Sesame(Sesame indicum L.), *International journal of Agronomy* pp 1-8.

Zhang, H. C., Duan, X. X. and Lian, H. (2010) Fertilizer application Manual. China agriculture Press, China pp 1-4.

Zhong, H., Wang, Q., Zhao et al.,(2014) Effects of different Nitrogen Application on soil Physical and Chemical properties and Yield in maize(Zea Mays L,), Agricultural sciences **5**(14) pp 1440-1447.

Zhou, J., Xia, F., Liu, X., He, Y., Xu, J and Brooke, P. C. (2013) Effects of nitrogen fertilizer on the acidification of two typical acid soils in south China, *Journal of Soils and sediments* **14**(2) pp 415-422.

Zohuriaan, M. J and Shokrolahi. (2004) Thermal studies on natural and modified gums, **23**(5) pp 575-597.

Zonova, E. (2018) Demographic transition in Japan: Prerequisites and consequences *Leiobeinandi: Gunnella borgeirsdottir* pp 1-23.

APPENDICES

Appendix 1 Table of rates of absorption from calibration curves

Nutrients	50-50	70-30	CROP
N	0.0265	0.0276	0.0223
P	0.0435	0.04	0.0308
K	0.0303	0.0296	0.0207

Appendix 2 Absorbance of NO_3^- at 450 nm

	Absorbance			
Day	NPK	SRF1	CRF1	CRF2
1	0.425,0.425,0.423	0.365,0.366,0.364	0.313,0.313,0.313	0.344,0.344,0.343
2	0.522,0.521,0.523	0.366,0.366,0.369	0.324,0.323,0.322	0.348,0.347,0.346
3	0.555,0.555,0.558	0.374,0.374,0.371	0.330,0.331,0.333	0.363,0.363,0.362
4	0.589,0.589,0.588	0.491,0.488,0.491	0.332,0.332,0.333	0.469,0.470,0.470
5	0.613,0.613,0.614	0.544,0.543,0.546	0.510,0.509,0.507	0.523,0.524,0.522
6	0.624,0.623,0.624	0.563,0.561,0.567	0.514,0.513,0.514	0.528,0.528,0.529
7	0.645,0.643,0.644	0.561,0.561,0.561	0.521,0.521,0.524	0.532,0.531,0.534
8	0.649,0.648,0.647	0.589,0.589,0.590	0.491,0.490,0.489	0.577,0.576,0.575
9	0.652,0.651,0.653	0.599,0.599,0.599	0.522,0.522,0.522	0.564,0.564,0.562
10	0.674,0.674,0.675	0.619,0.619,0.619	0.603,0.603,0.604	0.613,0.613,0.614
11	0.733,0.733,0.733	0.632,0.631,0.632	0.622,0.621,0.620	0.637,0.637,0.638
12	0.757,0.758,0.756	0.665,0.665,0.664	0.645,0.645,0.643	0.653,0.653,0.654
13	0.730,0.780,0.728	0.645,0.645,0.647	0.656,0.655,0.657	0.660,0.660,0.661
14	0.728,0.728,0.729	0.678,0.678,0.678	0.655,0.655,0.656	0.688,0.687,0.686
15	0.751,0.751,0.752	0.689,0.689,0.690	0.673,0.673,0.668	0.692,0.687,0.686
16	0.772,0.772,0.774	0.679,0.680,0.680	0.678,0.677,0.677	0.699,0.692,0.695
17	0.759,0.758,0.759	0.703,0.703,0.704	0.692,0.692,0.692	0.711,0.707,0.707
18	0.766,0.766,0.767	0.742,0.743,0.741	0.719,0.719,0.719	0.713,0.713,0.713
19	0.778,0.778,0.779	0.765,0.765,0.766	0.722,0.723,0.723	0.766,0.766,0.765
20	0.849,0.849,0.849	0.776,0.776,0.776	0.788,0.788,0.787	0.797,0.799,0.798
21	0.854,0.853,0.854	0.783,0.783, 0.784	0.801,0.799,0.800	0.833,0.827,0.815
22	0.869,0.868,0.870	0.690,0.780,0.807	0.754,0.754,0.754	0.812,0.803,0.788
23	0.891,0.892,0.890	0.790,0.790,0.789	0.801,0.801,0.779	0.811,0.811,0.803
24	0.911,0.911,0.910	0.790,0.790,0.787	0.812,0.801,0.794	0.817,0.810,0.805
25	0.916,0.916,0.913	0.791,0.789,0.789	0.819,0.817, 0.799	0.819,0.819,0.792
26	0.922,0.922,0.924	0.868,0.891,0.885	0.867,0.867,0.861	0.892,0.861,0.861
27	0.924,0.924,0.923	0.796,0.796,0.795	0.887,0.884,0.884	0.821,0.821,0.821
28	0.924,0.923,0.920	0.799,0.799,0.802	0.811,0.811,0.814	0.822,0.822,0.820
29	0.931,0.931,0.930	0.822,0.851,0.845	0.814,0.813,0.787	0.853,0.845,0.848
30	0.976,0.979,0.979	0.900,0.899,0.902	0.912,0.910,0.907	0.932,0.929,0.932

Appendix 3 Absorbance of $H_2PO_4^-$ in 50-50 samples

	Absorbance			
Day	NPK	SRF1	CRF1	CRF2
1	0.211,0.211,0.214	0.191,0.189,0.191	0.165,0.166,0.163	0.188,0.186,0.188
2	0.208,0.208,0.211	0.207,0.208,0.212	0.206,0.201,0.203	0.206,0.206,0.211
3	0.213,0.210,0.209	0.208,0.209,0.201	0.204,0.204,0.206	0.206,0.204,0.209

4	0.215,0.214,0.214	0.200,0.200,0.198	0.203,0.197,0.205	0.206,0.205,0.205
5	0.213,0.212,0.207	0.197,0.197,0.195	0.200,0.198,0.195	0.202,0.200,0.206
6	0.206,0.206,0.206	0.196,0.199,0.200	0.190,0.184,0.184	0.200,0.200,0.202
7	0.202,0.198,0.203	0.208,0.191,0.211	0.193,0.193,0.195	0.200,0.200,0.201
8	0.206,0.206,0.208	0.204,0.198,0.200	0.197,0.197,0.198	0.204,0.198,0.200
9	0.203,0.203,0.204	0.200,0.198,0.196	0.198,0.194,0.192	0.200,0.193,0.197
10	0.206,0.206,0.210	0.203,0.204,0.204	0.192,0.192,0.192	0.198,0.198,0.184
11	0.250,0.250,0.255	0.219,0.218,0.218	0.193,0.192,0.192	0.201,0.184,0.195
12	0.240,0.245,0.246	0.229,0.229,0.293	0.194,0.194,0.192	0.202,0.197,0.199
13	0.241,0.239,0.239	0.238,0.233,0.233	0.193,0.185,0.185	0.202,0.195,0.195
14	0.245,0.246,0.241	0.232,0.232,0.231	0.193,0.189,0.189	0.203,0.199,0.200
15	0.246,0.250,0.240	0.232,0.230,0.230	0.194,0.194,0.184	0.201,0.200,0.201
16	0.248,0.248,0.251	0.233,0.224,0.224	0.195,0.195,0.195	0.201,0.179,0.197
17	0.216,0.217,0.218	0.235,0.183,0.174	0.197,0.200,0.184	0.195,0.194,0.191
18	0.254,0.253,0.253	0.239,0.238,0.236	0.190,0.167,0.167	0.209,0.203,0.203
19	0.283,0.283,0.287	0.241,0.238,0.238	0.197,0.164,0.197	0.193,0.188,0.189
20	0.270,0.270,0.275	0.260,0.254,0.255	0.198,0.198,0.190	0.208,0.206,0.214
21	0.281,0.284,0.284	0.261,0.269,0.257	0.198,0.200,0.200	0.203,0.200,0.215
22	0.264,0.264,0.260	0.261,0.252,0.252	0.199,0.200,0.200	0.197,0.197,0.200
23	0.255,0.260,0.265	0.246,0.244,0.252	0.185,0.178,0.179	0.198,0.193,0.193
24	0.269,0.269,0.269	0.242,0.242,0.235	0.191,0.187,0.190	0.205,0.200,0.205
25	0.264,0.265,0.260	0.250,0.246,0.246	0.187,0.186,0.187	0.203,0.200,0.200
26	0.259,0.256,0.256	0.250,0.256,0.259	0.180,0.184,0.179	0.200,0.198,0.198
27	0.239,0.239,0.240	0.232,0.233,0.227	0.187,0.184,0.184	0.199,0.197,0.197
28	0.239,0.235,0.241	0.232,0.230,0.230	0.195,0.194,0.196	0.201,0.200,0.200
29	0.236,0.236,0.236	0.235,0.220,0.220	0.194,0.191,0.191	0.192,0.192,0.194
30	0.222,0.253,0.247	0.220,0.215,0.215	0.196,0.188,0.172	0.185,0.185,0.188

Appendix 4 Absorbance of K^+ for release sample 50-50

Day	NPK	SRF1	CRF1	CRF2
1	0.217,0.218,0.222	0.209,0.209,0.212	0.194,0.190,0.194	0.201,0.201,0.199
2	0.231,0.223,0.232	0.211,0.212.0.212	0.199,0.199,0.201	0.206,0.206,0.202
3	0.234,0.228,0.239	0.215,0.218,0.208	0.200,0.199,0.197	0.209,0.208,0.208
4	0.234,0.244,0.249	0.225,0.224,0.224	0.210,0.203,0.202	0.209,0.213,0.207
5	0.233,0.234,0.249	0.228,0.229,0.226	0.260,0.215,0.259	0.253,0.266,0.269
6	0.231,0.233,0.233	0.237,0.237,0.238	0.235,0.195,0.214	0.214,0.194,0.242
7	0.249,0.249,0.257	0.237,0.238,0.244	0.244,0.238,0.219	0.230,0.228,0.228

8	0.261,0.270,0.260	0.256,0.254,0.260	0.254,0.249,0.233	0.255,0.258,0.260
9	0.259,0.259,0.263	0.240,0.236,0.245	0.259,0.227,0.236	0.255,0.227,0.227
10	0.245,0.246,0.247	0.240,0.238,0.236	0.258,0.213,0.204	0.254,0.222,0.213
11	0.255,0.251,0.251	0.243,0.242,0.243	0.254,0.254,0.255	0.259,0.254,0.255
12	0.260,0.260,0.253	0.260,0.248,0.252	0.245,0.236,0.228	0.246,0.245,0.245
13	0.260,0.260,0.263	0.252,0.247,0.247	0.240,0.240,0.241	0.248,0.247,0.247
14	0.270,0.270,0.271	0.313,0.256,0.269	0.235,0.232,0.232	0.243,0.240,0.242
15	0.264,0.263,0.264	0.249,0.252,0.249	0.240,0.240,0.241	0.245,0.241,0.241
16	0.269,0.265,0.273	0.255,0.257,0.257	0.228,0.228,0.227	0.245,0.242,0.243
17	0.267,0.269,0.271	0.255,0.250,0.256	0.228,0.229,0.227	0.240,0.240,0.240
18	0.298,0.298,0.293	0.271,0.272,0.272	0.241,0.236,0.241	0.237,0.237,0.228
19	0.299,0.299,0.298	0.271,0.263,0.273	0.245,0.235,0.221	0.225,0.225,0.221
20	0.331,0.328,0.334	0.271,0.271,0.268	0.248,0.201,0.217	0.198,0.201,0.201
21	0.322,0.322,0.318	0.273,0.273,0.274	0.263,0.263,0.260	0.258,0.253,0.256
22	0.329,0.327,0.328	0.270,0.272,0.272	0.239,0.239,0.238	0.250,0.0250,0.25
23	0.319,0.319,0.316	0.263,0.263,0.261	0.238,0.238,0.238	0.253,0.253,0.253
24	0.320,0.317,0.315	0.263,0.270,0.266	0.249,0.248,0.247	0.226,0.229,0.225
25	0.318,0.318,0.315	0.269,0.264,0.265	0.228,0.225,0.231	0.253,0.253,0.259
26	0.310,0.309,0.309	0.258,0.258,0.254	0.227,0.227,0.232	0.216,0.232,0.239
27	0.302,0.301,0.304	0.260,0.254,0.254	0.225,0.225,0.224	0.237,0.234,0.237
28	0.294,0.289,0.296	0.261,0.260,0.260	0.229,0.230,0.230	0.239,0.239,0.244
29	0.312,0.312,0.313	0.282,0.282,0.281	0.230,0.228,0.228	0.229,0.233,0.234
30	0.290,0.290,0.290	0.279,0.279,0.286	0.229,0.227,0.232	0.219,0.218,0.223

Appendix 5 Absorbance of NO_3^- for 70-30 sample

	Concentration in g/L			
Day	Npk	Srf2	CRF3	CRF4
1	0.442,0.442,0.441	0.327,0.327,0.328	0.222,0.222,0.225	0.238,0.238,0.241
2	0.544,0543,0.544	0.331,0.338,0.324	0.226,0.325,0.323	0.241,0.243,0.237
3	0.578,0.578,0.581	0.362,0.364,0.371	0.271,0.272,0.265	0.256,0.257,0.248
4	0.614,0.613,0.612	0.372,0.376,0.376	0.263,0.259,0.259	0.264,0.266,0.265
5	0.639,0.638,0.639	0.376,0.375,0.376	0.283,0.283,0.283	0.284,0.303,0.284
6	0.650,0.648,0.650	0.361,0.366,0.373	0.296,0.296,0.286	0.332,0.311,0.323

7	0.671,0.670,0.671	0.398,0.425,0.422	0.318,0.318,0.316	0.352,0.352,0.350
8	0.676,0.675,0.674	0.400,0.402,0.400	0.315,0.315,0.317	0.347,0.347,0.347
9	0.679,0.678,0.680	0.430,0.429,0.432	0.355,0.356,0.357	0.353,0.353,0.354
10	0.702,0.702,0.703	0.445,0.445,0.446	0.364,0.340,0.362	0.371,0.371,0.371
11	0.763,0.763,0.763	0.466,0.464,0.465	0.386,0.381,0.359	0.392,0.392,0.395
12	0.788,0.789,0.797	0.498,0.498,0.498	0.400,0.400,0.399	0.404,0.398,0.404
13	0.760,0.813,0.758	0.502,0.5023,0.501	0.408,0.404,0.409	0.404,0.404,0.414
14	0.758,0.758,0.759	0.440,0.440,0.444	0.412,0.414,0.409	0.429,0.429,0.419
15	0.783,0.783,0.783	0.500,0.502,0.500	0.421,0.421,0.422	0.457,0.457,0.467
16	0.804,0.804,0.806	0.523,0.524,0.524	0.432,0.432,0.433	0.453,0.449,0.454
17	0.790,0.790,0.790	0.545,0.545,0.547	0.469,0.472,0.516	0.479,0.483,0.497
18	0.797,0.797,0.798	0.568,0.568,0.569	0.477,0.478,0.478	0.498,0.498,0.500
19	0.810,0.810,0.811	0.600,0.596,0.609	0.498,0.495,0.486	0.510,0.512,0.517
20	0.884,0.884,0.884	0.601,0.603,0.616	0.508,0.509,0.508	0.534,0.535,0.535
21	0.889,0.889,0.890	0.636,0.636,0.636	0.531,0.532,0.533	0.549,0.549,0.549
22	0.905,0.905,0.906	0.657,0.657,0.656	0.535,0.534,0.534	0.580,0.580,0.576
23	0.928,0.929,0.927	0.633,0.633,0.633	0.554,0.554,0.553	0.589,0.587,0.589
24	0.949,0.949,0.948	0.704,0.701,0.704	0.569,0.569,0.566	0.602,0.602,0.603
25	0.954,0.954,0.951	0.708,0.707,0.707	0.592,0.592,0.588	0.646,0.648,0.648
26	0.960,0.960,0.963	0.718,0.721,0.713	0.609,0.590,0.598	0.658,0.658,0.659
27	0.962,0.962,0.962	0.750,0.696,0.728	0.658,0.629,0.626	0.666,0.662,0.668
28	0.962,0.962,0.959	0.771,0.771,0.730	0.657,0.638,0.667	0.684,0.670,0.648
29	0.970,0.970,0.969	0.773,0.773,0.776	0.680,0.680,0.671	0.704,0.701,0.723
30	0.988,0.991,0.991	0.807,0.804,0.869	0.696,0.678,0.698	0.726,0.707,0.698

Appendix 6 Absorbance of $H_2PO_4^-$ 70-30 formula

	Concentration of $H_2PO_4^-$ in g/L			
Day	NPK	SRF2	CRF3	CRF4
1	0.194,0.194,0.194	0.184,0.178,0.176	0.109,0.106,0.113	0.144,0.144,0.144
2	0.191,0.191,0.194	0.189,0.189,0.185	0.106,0.112,0.114	0.145,0.144,0.144
3	0.195,0.193,0.192	0.193,0.201,0.192	0.112,0.11,0.104	0.146,0.147,0.147
4	0.198,0.197,0.199	0.198,0.196,0.197	0.132,0.127,0.122	0.148,0.147,0.152
5	0.196,0.195,0.191	0.195,0.204,0.184	0.135,0.130,0.133	0.143,0.141,0.144
6	0.190,0.190,0.190	0.197,0.198,0.198	0.138,0.148,0.127	0.147,0.148,0.148
7	0.185,0.182,0.186	0.204,0.202,0.199	0.136,0.135,0.138	0.148,0.148,0.149

8	0.189,0.189,0.191	0.202,0.205,0.205	0.137,0.132,0.132	0.151,0.152,0.142
9	0.187,0.187,0.188	0.212,0.208,0.208	0.139,0.142,0.142	0.153,0.153,0.154
10	0.189,0.189,0.193	0.214,0.212,0.212	0.145,0.150,0.145	0.164,0.164,0.185
11	0.230,0.230,0.234	0.214,0.217,0.226	0.148,0.151,0.152	0.162,0.160,0.169
12	0.220,0.229,0.226	0.218,0.217,0.214	0.149,0.149,0.152	0.167,0.171,0.174
13	0.222,0.220,0.220	0.221,0.224,0.224	0.150,0.143,0.148	0.170,0.170,0.170
14	0.226,0.226,0.222	0.226,0.226,0.218	0.155,0.155,0.155	0.173,0.173,0.168
15	0.226,0.230,0.220	0.224,0.222,0.223	0.158,0.158,0.159	0.174,0.169,0.169
16	0.228,0.228,0.231	0.228,0.231,0.231	0.148,0.148,0.147	0.175,0.173,0.174
17	0.198,0.199,0.200	0.229,0.229,0.230	0.149,0.150,0.150	0.176,0.176,0.183
18	0.234,0.233,0.233	0.227,0.217,0.233	0.151,0.148,0.155	0.179,0.179,0.179
19	0.261,0.260,0.264	0.231,0.226,0.226	0.154,0.151,0.154	0.177,0.176,0.175
20	0.248,0.248,0.252	0.234,0.233,0.233	0.156,0.156,0.156	0.183,0.182,0.182
21	0.258,0.261,0.261	0.245,0.243,0.247	0.159,0.159,0.157	0.185,0.184,0.184
22	0.243,0.243,0.239	0.241,0.235,0.239	0.163,0.163,0.164	0.186,0.184,0.184
23	0.235,0.237,0.244	0.235,0.237,0.237	0.164,0.165,0.148	0.185,0.185,0.190
24	0.247,0.247,0.248	0.233,0.233,0.233	0.165,0.165,0.159	0.187,0.184,0.184
25	0.244,0.244,0.239	0.230,0.230,0.226	0.169,0.170,0.153	0.189,0.184,0.184
26	0.238,0.235,0.235	0.242,0.242,0.241	0.179,0.177,0.177	0.181,0.182,0.189
27	0.220,0.220,0.220	0.245,0.245,0.243	0.172,0.170,0.171	0.183,0.183,0.184
28	0.220,0.217,0.221	0.230,0.230,0.227	0.186,0.184,0.184	0.187,0.188,0.189
29	0.217,0.217,0.217	0.210,0.208,0.207	0.189,0.186,0.191	0.189,0.181,0.181
30	0.204,0.232,0.227	0.220,0.217,0.222	0.189,0.188,0.180	0.187,0.190,0.192

Appendix 7 Absorbance of K^+ for the 70-30 sample

Day	NPK	SRF2	CRF3	CRF4
1	0.212,0.213,0.217	0.202,0.203,0.203	0.200,0.199,0.192	0.218,0.217,0.213
2	0.226,0.217,0.227	0.207,0.206,0.217	0.201,0.201,0.2	0.2,0.2,0.199
3	0.228,0.223,0.233	0.209,0.209,0.203	0.203,0.203,0.207	0.21,0.203,0.21
4	0.228,0.238,0.448	0.211,0.211,0.199	0.211,0.199,0.199	0.207,0.203,0.2
5	0.227,0.228,0.243	0.217,0.226,0.227	0.212,0.213,0.206	0.203,0.204,0.207
6	0.22,0.223,0.223	0.217,0.218,0.214	0.209,0.195,0.213	0.213,0.214,0.205
7	0.238,0.238,0.245	0.224,0.224,0.225	0.216,0.209,0.214	0.218,0.218,0.219
8	0.249,0.257,0.249	0.213,0.213,0.216	0.212,0.212,0.213	0.213,0.212,0.207
9	0.247,0.247,0.251	0.225,0.234,0.24	0.212,0.211,0.21	0.22,0.221,0.223
10	0.223,0.234,0.236	0.231,0.228,0.229	0.214,0.0216,0.201	0.222,0.225,0.225
11	0.243,0.239,0.239	0.232,0.232,0.232	0.216,0.219,0.214	0.223,0.222,0.223
12	0.247,0.247,0.241	0.232,0.233,0.233	0.217,0.217,0.219	0.225,0.225,0.241

13	0.248,0.248,0.250	0.231,0.227,0.232	0.247,0.203,0.204	0.229,0.235,0.234
14	0.256,0.256,0.258	0.234,0.234,0.233	0.227,0.226,0.226	0.229,0.23,0.23
15	0.251,0.250,0.251	0.237,0.24,0.234	0.231,0.229,0.229	0.234,0.237,0.237
16	0.256,0.251,0.259	0.241,0.241,0.243	0.233,0.233,0.23	0.236,0.237,0.235
17	0.253,0.255,0.257	0.242,0.241,0.241	0.234,0.234,0.209	0.239,0.238,0.238
18	0.282,0.282,0.277	0.238,0.237,0.237	0.232,0.231,0.231	0.233,0.237,0.235
19	0.283,0.283,0.282	0.238,0.238,0.241	0.231,0.23,0.23	0.237,0.236,0.235
20	0.313,0.311,0.316	0.251,0.247,0.248	0.229,0.228,0.232	0.24,0.235,0.241
21	0.304,0.304,0.3	0.233,0.234,0.233	0.244,0.239,0.243	0.232,0.227,0.229
22	0.31,0.309,0.309	0.246,0.237,0.243	0.217,0.213,0.207	0.244,0.266,0.227
23	0.301,0.301,0.298	0.261,0.261,0.26	0.229,0.228,0.228	0.236,0.234,0.217
24	0.313,0.31,0.308	0.256,0.257,0.258	0.239,0.239,0.238	0.248,0.246,0.043
25	0.31,0.31,0.308	0.251,0.25,0.249	0.261,0.259,0.259	0.244,0.242,0.243
26	0.303,0.302,0.302	0.252,0.254,0.257	0.219,0.218,0.218	0.245,0.245,0.246
27	0.295,0.294,0.297	0.255,0.255,0.254	0.228,0.223,0.218	0.242,0.242,0.242
28	0.287,0.282,0.29	0.26,0.0258,0.258	0.23,0.226,0.227	0.248,0.248,0.243
29	0.305,0.305,0.305	0.26,0.256,0.258	0.21,0.209,0.21	0.249,0.249,0.248
30	0.283,0.283,0.283	0.263,0.262,0.262	0.237,0.235,0.236	0.251,0.251,0.252

Appendix 8 Absorbance of NO_3^- from soil samples

Wk	FP	NPK	SRF2	CRF3	CRF4
2	0.109,0.108,0.109	0.214,0.214,0.215	0.103,0.103,0.103	0.094,0.094,0.095	0.098,0.097,0.099
4	0.108,0.107,0.106	0.226,0.224,0.227	0.108,0.108,0.107	0.096,0.095,0.096	0.102,0.101,0.102
6	0.107,0.105,0.107	0.229,0.229,0.23	0.110,0.111,0.111	0.103,0.103,0.102	0.114,0.114,0.113
8	0.106.0.106,0.106	0.238,0.238,0.239	0.113,0.113,0.112	0.108,0.108,0.107	0.108,0.108,0.107
10	0.103,0.103,0.103	0.254,0.254,0.255	0.116,0.117,0.114	0.118,0.118,0.117	0.122,0.122,0.122
12	0.102,0.102,0.102	0.266,0.266,0.267	0.136,0.136,0.136	0.123,0.122,0.122	0.124,0.125,0.124
14	0.098,0.099,0.097	0.282,0.282,0.279	0.156,0.152,0.156	0.128,0.128,0.128	0.136,0.136,0.135

Appendix 9 Absorbance of $H_2PO_4^-$ for soils

Wk	FP	NPK	SRF2	CRF3	CRF4
2	0.006,0.006,0,006	0.322,0.322,0.322	0.304,0.3,0.304	0.254,0.254,0.255	0.256,0.256,0.257
4	0.006,0.006,0.006	0.324,0.324,0323	0.308,0.313,0.301	0.263,0.264,0.262	0.267,0.265,0.267
6	0.005,0.005,0.006	0.344,0.345,0.344	0.318,0.318,0.319	0.270,0.27,0.271	0.275,0.275,0.276
8	0.005,0.005,0.004	0.352,0.352,0.353	0.320,0.321,0.321	0.278,0.278,0.279	0.288,0.288,0.291
10	0.004,0.003,0.004	0.358,0.354,0.354	0.316,0.317,0.316	0.292,0.292,0.289	0.298,0.298,0.297
12	0.003,0.003,0.003	0.364,0.364,0.365	0.324,0.324,0.325	0.294,0.295,0.293	0.306,0.306,0.304
14	0.002,0.002,0.003	0.368,0.68,0.37	0.328,0.329,0.328	0.314,0.313,0.312	0.312,0.313,0.311

Appendix 10 Absorbance for K^+ in soil sample

Wk	FP	NPK	SRF2	CRF3	CRF4
2	0.105,0.105,0.105	0.202,0.202,0.202	0.194,0.194,0.194	0.163,0.163,0.163	0.171,0.171,0.171
4	0.10,0.109,0.1	0.206,0.205,0.205	0.196,0.196,0.196	0.154,0.151,0.155	0.184,0.184,0.185
6	0.098,0.098,0.099	0.211,0.21,0.0214	0.204,0.2,0.206	0.170,0.171,0.169	0.211,0.211,0.210
8	0.088,0.087,0.088	0.228,0.227,0.227	0.240,0.244,0.239	0.198,0.198,0.199	0.212,0.210,0.21
10	0.092,0.088,0.092	0.252,0.248,0.251	0.238,0.235,0.237	0.220,0.221,0.22	0.220,0.221,0.221
12	0.085,0.082,0.082	0.288,0.293,0.287	0.242,0.2410.237	0.226,0.223,0.222	0.228,0.228,0.222
14	0.082,0.081,0.076	0.316,0.321,0.323	0.246,0.245,0.245	0.221,0.222,0.225	0.240,0.2350.238

Appendix 11 Gradients for calibration curves

Nutrient	Soils	70-30 water	50-50 water
N	0.0233	0.0276	0.0265
P	0.0308	0.04	0.0435
K	0.0207	0.0296	0.0303

Appendix 12 Water diffusivity for starch-PVA

Time	Time/ mins	Ln t	S-PVA	Mean	M_t/M_0	In $F(M_t/M_0)$
9.10	5	1.61	2.2,2,3,2.2	2.2	0.237	-1.44
9.15	10	2.30	2.6,2.7,2.6	2.6	0.279	-1.28
9.20	15	2.71	3.4,3.4,3.3	3.4	0.366	-1.01
9.25	20	3.00	3.6,3.6,3.8	3.6	0.387	-0.95
9.30	25	3.22	3.9,3.8,3.7	3.8	0.409	-0.89
9.35	30	3.40	3.9,3.9,3.8	3.9	0.419	-0.87
9.40	35	3.56	4.2,4.2,4.1	4.2	0.452	-0.79
9.45	40	3.69	4.2,4.2,4.1	4.2	0.452	-0.79
9.50	45	3.81	4.5,4.4,4.5	4.5	0.484	-0.73
9.55	50	3.91	4.6,4.6,4.5	4.6	0.495	-0.70
10.00	55	4.01	4.6,4.7,4.4	4.6	0.495	-0.70
10.05	60	4.09	4.7,4.7,4.5	4.7	0.505	-0.68
10.10	65	4.17	4.8,4.9,4.8	4.8	0.516	-0.66
10.15	70	4.25	4.9,5.0,4.9	4.9	0.527	-0.64
10.20	75	4.32	5.0,5.1,5.0	5.0	0.538	-0.62
10.25	80	4.38	5.2,5.1,5.0	5.1	0.548	-0.60
10.30	85	4.44	5.2,5.1,5.1	5.1	0.548	-0.60
10.35	90	4.50	5.1,5.1,5.1	5.1	0.548	-0.60

10.40	95	4.55	5.3,5.3,5.2	5.3	0.569	-0.56
10.45	100	4.61	5.6,5.5,5.4	5.5	0.591	-0.52
10.50	105	4.65	5.6,5.6,5.5	5.6	0.602	-0.51
10.55	110	4.70	5.7,5.7,5.6	5.7	0.613	-0.49
11.00	115	4.75	5.8,5.7,5.7	5.7	0.613	-0.49
11.05	120	4.79	6.0,5.9,5.9	5.9	0.634	-0.46
11.10	125	4.83	6.1,6.0,5.9	6.0	0.645	-0.44
11.15	130	4.87	6.0,6.0,6.1	6.0	0.645	-0.44
11.20	135	4.91	6.1,6.0,6.0	6.0	0.645	-0.44
11.25	140	4.94	6.2,6.2,6.2	6.2	0.667	-0.41
11.30	145	4.98	6.3,6.4,6.2	6.3	0.677	-0.39
11.35	150	5.01	6.3,6.4,6.3	6.3	0.677	-0.39
11.40	155	5.04	6.4,6.4,6.3	6.4	0.688	-0.37
11.45	160	5.08	6.6,6.5,6.5	6.5	0.699	-0.36
11.50	165	5.11	6.8,6.6,6.7	6.7	0.720	-0.33
11.55	170	5.14	6.9,6.7,6.8	6.8	0.731	-0.31
12.00	175	5.15	7.0,7.0,6.7	6.9	0.742	-0.30
12.05	180	5.19	7.1,7.0,7.0	7.0	0.753	-0.28
12.10	185	5.22	7.0,7.1,7.0	7.0	0.753	-0.28
12.15	190	5.25	7.1,7.1,7.0	7.1	0.763	-0.27
12.20	195	5.27	7.2,7.0,7.1	7.1	0.763	-0.27
12.25	200	5.30	7.3,7.1,7.0	7.2	0.774	-0.26
12.30	205	5.32	7.3,7.2,7.1	7.2	0.774	-0.26
12.35	210	5.35	7.4,7.3,7.3	7.3	0.785	-0.24
12.40	215	5.37	7.5,7.4,7.3	7.4	0.796	-0.23
12.45	220	5.39	7.4,7.3,7.3	7.3	0.785	-0.24
12.50	225	5.42	7.3,7.3,7.2	7.3	0.785	-0.24
12.55	230	5.44	7.4,7.4,7.2	7.3	0.785	-0.24
13.00	235	5.46	7.3,7.4,7.3	7.3	0.785	-0.24
13.05	240	5.48	7.3,7.5,7.2	7.4	0.796	-0.23
13.10	245	5.50	7.7,7.5,7.3	7.5	0.807	-0.21
13.15	250	5.52	7.8,7.8,7.9	7.8	0.839	-0.18
13.20	255	5.54	7.9,7.8,7.8	7.8	0.839	-0.18
13.25	260	5.56	7.8,7.9,8.0	7.9	0.849	-0.18
13.30	265	5.58	8.1,8.1,7.9	8.0	0.86	-0.15
13.35	270	5.60	8.1,8.1,8.0	8.1	0.871	-0.14
13.40	275	5.62	8.2,8.1,8.0	8.1	0.871	-0.14
13.45	280	5.63	8.2,8.2,8.2	8.2	0.882	-0.13
13.50	285	5.65	8.1,8.1,8.2	8.1	0.871	-0.14
13.55	290	5.67	8.1,8.2,8.1	8.1	0.871	-0.14
14.00	295	5.69	8.1,8.1,8.1	8.1	0.871	-0.14
14.05	300	5.70	8.3,8.4,8.3	8.3	0.893	-0.11
14.10	305	5.72	8.5,8.4,8.3	8.4	0.903	-0.10
14.15	310	5.74	8.5,8.6,8.6	8.6	0.925	-0.08
14.20	315	5.75	8.7,8.7,8.7	8.7	0.936	-0.07

14.25	320	5.77	8.8,8.7,8.7	8.7	0.936	-0.07
14.30	325	5.78	9.0,8.9,8.9	8.9	0.957	-0.04
14.35	330	5.80	9.1,9.0,8.9	9.0	0.968	-0.03
14.40	335	5.81	9.2,9.4,9.3	9.3	1	0
14.45	340	5.83	9.3,9.4,9.3	9.3	1	0
14.50	345	5.84	9.5,9.4,9.2	9.3	1	0

Appendix 13 Water diffusivity for starch-GA

Time	Time/ mins	Ln t	S-GA in tea bag/g	Mean mass, g	$F=M_t/M_0$ in teabags	Ln F	S-GA in water/g	Mean in water
9.10	5	1.61	2.2,2.2,2.1	2.2	0.48	-0.734	2.2,2.2,2.2	2.2
9.15	10	2.30	2.9,2.8,2.9	2.9	0.64	-0.446	2.3,2.3,2.2	2.3
9.20	15	2.71	3.0,3.1,3.0	3.0	0.67	-0.400	2.5,.2.4,2.3	2.4
9.25	20	3.00	3.0,3.0,3.0	3.0	0.67	-0.400	2.6,2.6,2.4	2.5
9.30	25	3.22	3.1,3.1,3.2	3.1	0.69	-0.371	2.5,2.5,2.4	2.4
9.35	30	3.40	3.1,3.0,3.1	3.1	0.69	-0.371	2.6,2.5,2.4	2.5
9.40	35	3.56	3.2,3.1,3.1	3.1	0.69	-0.371	2,4,2.3,2.2	2.3
9.45	40	3.69	3.4,3.3,3.3	3.3	0.73	-0.315	2.2,2.2,2.2	2.2
9.50	45	3.81	3.3,3.3.3,4	3.3	0.73	-0.315	2.2,2.3,2.3	2.3
9.55	50	3.91	3.5,3.4,3.3	3.4	0.76	-0.274	2.2,2.1,2.1	2.1
10.00	55	4.01	3.6,3.4,3.5	3.5	0.78	-0.249	2.2.,2.2,2.1	2.2
10.05	60	4.09	3.8,3.8,3.6	3.7	0.82	-0.198	2.1,2.1,2.1	2.1
10.10	65	4.17	3.7,3.7,3.8	3.7	0.82	-0.198	2.1,2.0,2.0	2.0
10.15	70	4.25	3.7,3.8,3.8	3.8	0.84	-0.174	2.0,2.0,2.0	2.0
10.20	75	4.32	3.9,3.8,3.8	3.8	0.84	-0.174	2.0,1.9,1.9	1.9
10.25	80	4.38	3.9,3.9,3.9	3.9	0.87	-0.139	1.9,1.9,1.8	1.9

10.30	85	4.44	4.0,4.0,4.0	4.0	0.89	-0.117	1.9,1.8,1.8	1.8
10.35	90	4.50	4.1,4.1,4.0	4.1	0.91	-0.094	1.8,1.7,1.7	1.7
10.40	95	4.55	4.2,4.2,4.2	4.2	0.93	-0.073	1.6,1.6,1.6	1.6
10.45	100	4.61	4.4,.4.3,4.3	4.3	0.96	-0.041	1.6,1.6,1.5	1.6
10.50	105	4.65	4.4,4.4,4.4	4.4	0.98	-0.020	1.5,1.5,1.4	1.5
10.55	110	4.70	4.5,4.4,4.5	4.4	0.98	-0.020	1.5,1.3,1.3	1.4
11.00	115	4.75	4.6,4.5,4.4	4.5	1.0	0	1.4,1.4,1.3	1.4

Appendix 14 XRD data for SRP

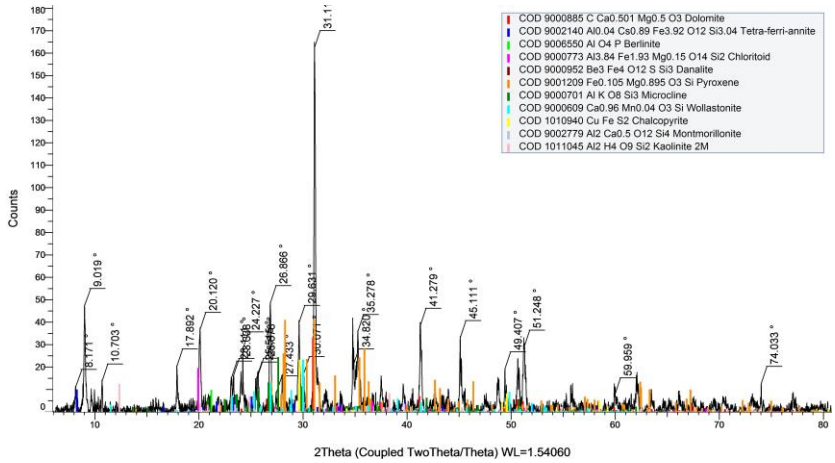

Appendix 15 Mineralogy diffractogram of white clay

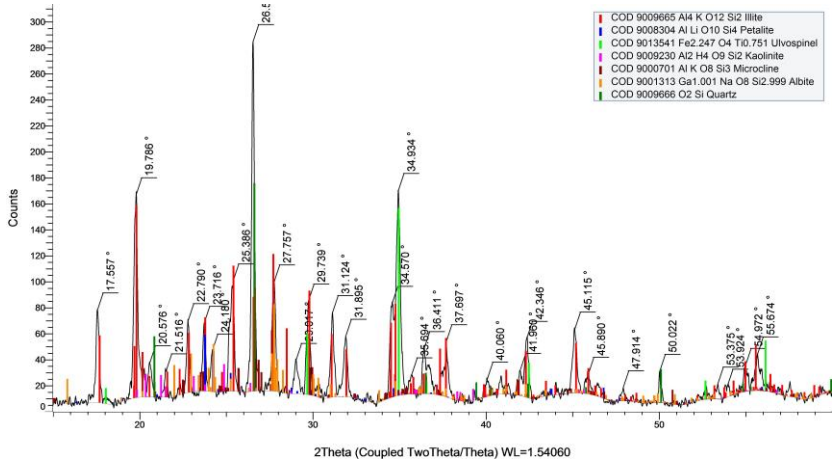

Appendix 16 Mineralogy diffractogram for black clay

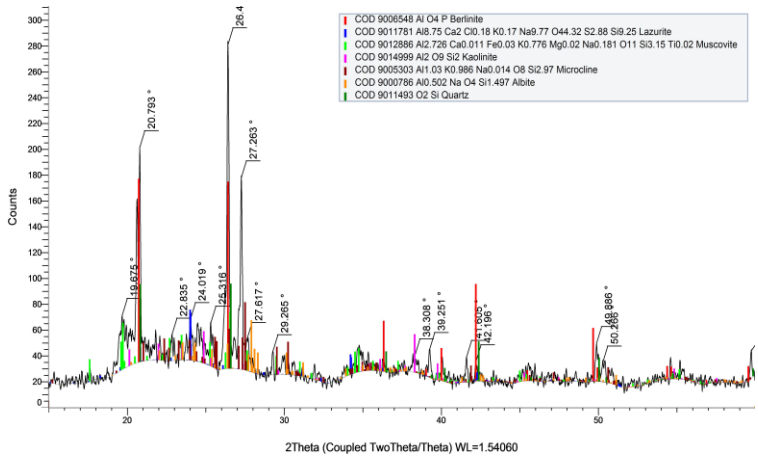

Appendix 17 d-spacings for kaolinite

Peak	d-valueÅ	2θ degree	Plane
Basal	7.191	12.3	001
	3.579	24.4	002
	2.395	37.6	003
	1.799	51.1	004
Prism	4.498	19.8	020
	4.386	20.3	‘110’
	2.566	35.1	130
	2.377	38.3	‘202’

Appendix 18 d-spacings for Muscovite

Peak	d-valueÅ	2θ	Plane
Basal	9.95	8.9	001
	4.97	17.8	002
	3.38	26.8	003
	2.55	35.0	004
Prism	4.40	20.1	010
	3.28	27.0	020
	1.98	46.0	030
	1.65	55.7	040

Appendix 19 d-spacing for Illite

Peak	d-valueÅ	2θ	Plane
Basal	10	8.7	001
	5.0	17.7	002
	3.3	26.8	003
	2.5	34.8	004

Appendix 20 Trends in mass of water absorbed

TIME	Mass of water SRF2	mass of water absorbed in CRF3	Mass of water absorbed in CRF4
D1	0	0	0
D3	0.46	1.8	0.4
D5	0.8	4.93	3.87
D7	1.26	8	6.73
D9	1.63	8.36	7.6
D11	2.36	8.56	7.83
D13	2.63	8.86	7.93
D15	2.73	9.3	8.07
D17	2.86	9.53	8.3
D19	3.06	9.73	8.43
D21	3.36	10.03	9.13
D23	3.76	10.3	9.13

D25	4.03	10.53	9.1
D27	4	11.4	9.43
D29	4.66	11.83	9.63
D31	4.83	12.3	9.8
D33	5.3	12.76	9.97

Appendix 21 Kinetics data for starch-PVA and starch-GA.

Time	t/qt	Mass SR1	(qe-qt) for SR1	In(qe-qt)	Time	Mass SR2	qe-qt SR2	In(qe-qt)	t/qt
10	7.89	1.267	6.033	1.797	10	0.867	1.733	0.55	11.53
20	11.99	1.667	5.633	1.729	20	1	1.6	0.47	20
30	16.07	1.867	5.433	1.692	30	1.067	1.533	0.427	28.12
40	18.46	2.167	5.133	1.636	40	1.333	1.267	0.237	30.01
50	19.48	2.567	4.733	1.555	50	1.4	1.2	0.182	35.71
60	22.79	2.633	4.667	1.541	60	1.733	0.867	-0.143	34.62
70	23.87	2.933	4.367	1.474	70	1.767	0.833	-0.183	39.62
80	25.81	3.1	4.2	1.435	80	1.9	0.7	-0.357	42.11
90	29.03	3.1	4.2	1.435	90	2.067	0.533	-0.629	43.54
100	28.57	3.5	3.8	1.335	100	2.367	0.233	-1.457	42.25
110	29.99	3.667	3.633	1.29	110	2.467	0.133	-2.017	44.59
120	30.51	3.933	3.367	1.214	120	2.6	0	∞	46.15
130	32.23	4.033	3.267	1.184					
140	33.33	4.2	3.1	1.131					
150	34.62	4.333	2.967	1.088					
160	35.3	4.533	2.767	1.018					
170	35.42	4.8	2.5	0.916					

180	35.76	5.033	2.267	0.819					
190	37.75	5.033	2.267	0.819					
200	38.97	5.133	2.167	0.773					
210	39.38	5.333	1.967	0.677					
220	41.51	5.3	2	0.693					
230	43.13	5.333	1.967	0.677					
240	45	5.333	1.967	0.677					
250	42.86	5.833	1.467	0.383					
260	44.07	5.9	1.4	0.336					
270	44.5	6.067	1.233	0.21					
280	45.16	6.2	1.1	0.095					
290	47.29	6.133	1.167	0.154					
300	47.37	6.333	0.967	-0.034					
310	47.21	6.567	0.733	-0.311					
320	47.53	6.733	0.567	-0.567					
330	47.14	7	0.3	-1.204					
340	46.58	7.3	0	∞					

Appendix 22 Data for Pseudo 1st and 2nd order for release of N from 50-50

Mins x10^3	t/qt NPK	Ln(q_e -q_t) NPK	t/qt SRF1	Ln(q_e-q_t) SRF1	t/qt CRF1	Ln(q_e-q_t) CRF1	t/qt CRF2	Ln(q_e-q_t) CRF2
1.44	22.5	-1.25	26.1	-1.31	30.5	-1.27	27.8	-1.26
2.88	35.8	-1.31	51.0	-1.32	57.8	-1.28	53.9	-1.27
4.32	49.4	-1.34	73.7	-1.33	82.9	-1.29	75.8	-1.28
5.76	60.9	-1.36	73.2	-1.41	108.1	-1.30	76.4	-1.35
7.20	71.6	-1.39	80.6	-1.45	862.3	-1.42	83.9	-1.39
8.64	86.8	-1.41	91.4	-1.47	100.4	-1.43	100.9	-1.40
10.08	78.2	-1.43	89.8	-1.49	96.4	-1.44	94.6	-1.41
11.52	101.2	-1.44	111.4	-1.51	134.0	-1.42	114.0	-1.45
12.96	110.6	-1.46	120.5	-1.53	138.2	-1.46	127.9	-1.45
14.40	116.0	-1.49	126.4	-1.56	129.7	-1.53	127.6	-1.51
15.84	114.5	-1.55	132.9	-1.59	135.2	-1.56	131.7	-1.54
17.28	118.0	-1.59	134.4	-1.63	138.6	-1.60	136.6	-1.57
18.72	126.3	-1.60	146.0	-1.63	143.7	-1.63	142.7	-1.59
20.16	135.8	-1.61	145.9	-1.68	150.7	-1.65	143.8	-1.63
21.60	137.1	-1.65	149.5	-1.72	153.5	-1.68	149.3	-1.66
23.04	138.3	-1.70	157.2	-1.73	157.8	-1.68	153.7	-1.69
24.48	145.4	-1.71	156.8	-1.78	159.4	-1.75	155.7	-1.73
25.92	148.0	-1.74	152.7	-1.87	157.7	-1.81	158.8	-1.76
27.36	149.1	-1.80	151.6	-1.95	160.6	-1.85	151.4	-1.87

28.80	139.4	-1.95	152.5	-2.00	150.2	-2.00	148.4	-1.96
30.24	140.9	-2.00	153.5	-2.06	150.3	-2.07	145.7	-2.06
31.68	140.1	-2.09	160.4	-2.07	161.5	-2.03	151.9	-2.07
33.12	137.9	-2.21	155.6	-2.20	154.8	-2.18	152.2	-2.15
34.56	135.7	-2.35	156.7	-2.27	154.1	-2.27	152.5	-2.23
36.00	135.6	-2.48	162.4	-2.35	152.8	-2.40	153.1	-2.30
37.44	134.4	-2.65	140.7	-2.85	143.4	-2.72	142.3	-2.63
38.88	133.9	-2.81	155.4	-2.60	139.7	-3.02	150.6	-2.56
40.32	133.2	-3.06	153.7	-2.78	151.4	-2.80	149.6	-2.73
41.76	130.8	-3.47	145.1	-3.27	151.3	-2.98	143.4	-3.12
43.20	122.9		133.5		132.2		129.1	-

Appendix 23 Data for Pseudo 1st and 2nd order for release of $H_2PO_4^-$ from 50-50

Minx10^3	t/qt NPK-P x10^3	Ln(qe-qt) NPK-P x10^3	t/qt SRF2-P	Ln(qe-qt) SRF2-P x10^3	t/qt CRF 1	Ln(qe-qt) CRF1 x10^3	t/qt CRF2	Ln(qe-qt) CRF2 x10^3
1.440	86.8	-3.57	96.6	-3.67	111.63	-3.84	98.63	-3.91
2.88	172.5	-3.58	172.5	-3.75	177.78	-4.0	174.55	-4.01
4.32	252.6	-3.59	257.2	-3.75	258.7	-4.03	257.2	-4.03
5.76	321.8	-3.62	321.8	-3.74	342.9	-4.03	338.8	-4.04
7.20	402.2	-3.62	431.1	-3.75	428.6	-4.03	418.6	-4.05
8.64	482.7	-3.62	502.3	-3.77	533.33	-4.0	496.6	-4.06
10.08	566.3	-3.62	556.9	-3.81	586.1	-4.06	566.3	-4.09
11.52	612.8	-3.65	633	-3.81	643.6	-4.1	633	-4.11
12.96	685.7	-3.66	704.3	-3.82	716	-4.11	708.2	-4.12
14.40	731	-3.69	742.3	-3.87	786.9	-4.12	782.6	-4.12
15.84	643.9	-3.91	743.7	-3.96	842.6	-4.16	838.1	-4.15
17.28	708.2	-3.9	688.5	-4.18	895.3	-4.19	914.3	-4.22
18.72	757.9	-3.91	773.6	-4.13	970.0	-4.19	940.7	-4.25
20.16	781.4	-3.97	822.9	-4.15	1002.9	-4.24	950.9	-4.31
21.60	812	-4.01	860.6	-4.19	1043.5	-4.28	990.8	-4.36
23.04	828.8	-4.08	910.7	-4.2	1056.9	-4.37	1071.6	-4.36
24.48	983.1	-3.92	1078.4	-4.04	1102.7	4.4	1102.7	-4.39
25.92	864	-4.21	919.2	-4.42	1246.2	-4.29	1066.7	-4.58

27.36	788.5	-4.61	940.2	-4.49	1205.3	-4.44	1179.3	-4.47
28.80	757.9	-5.01	891.6	-4.83	1166	-4.63	1090.1	-4.8
30.24	819.5	-4.85	884.2	-5.09	1167.6	-4.76	1128.4	-4.85
31.68	894.9	-4.68	920.9	-5.13	1177.7	-4.88	1174.6	-4.84
33.12	914.9	-4.77	960	-5.15	1314.3	-4.68	1217.7	-4.91
34.56	888.4	-5.15	996	-5.19	1261.3	-4.95	1175.5	-5.26
36.00	909.1	-5.28	967.7	-5.78	1281.1	-5.05	1192.1	-5.43
37.44	931.3	-5.38	940.7	-7.6	1323	-5.08	1203.9	-5.66
38.88	997.4	-5.15	1031.9	-5.92	1284.8	-5.45	1208.7	-5.99
40.32	995.6	-5.47	1028.6	-6.81	1218.1	-6.57	1185.9	-7.42
41.76	994.3	-5.91	1046.6	-7.82	1221.1	-8.11	1221.1	-7.82
43.20								

Appendix 24 Data for Pseudo 1st and 2nd order for release of K^+ from 50-50

Minx 10^3	t/qt NPK	Ln(qe-qt) NPK	t/qt SRF2	Ln(qe-qt) SRF2	t/qt CRF1	Ln(qe-qt) CRF1	t/qt CRF2	Ln(qe-qt) CRF2
1.44	70.9	-3.09	74.6	-3.16	80.9	-3.42	77.8	-3.5
2.88	133.3	-3.12	144.7	-3.17	152.4	-3.46	149.2	-3.52
4.32	195	-3.14	209.7	-3.19	225	-3.46	216	-3.55
5.76	187.6	-3.18	261.8	-3.22	285.2	-3.5	288	-3.57
7.20	301.3	-3.18	315.8	-3.24	292.7	-3.65	276.9	-3.8
8.64	361.5	-3.18	354.1	-3.28	392.7	-3.56	387.4	-3.63
10.08	387.7	-3.24	400	-3.31	411.4	-3.65	418.3	-3.7
11.52	411.4	-3.29	417.4	-3.37	443.1	-3.73	415.9	-3.86
12.96	451.6	-3.3	489.1	-3.34	489.1	-3.73	498.5	-3.78
14.40	519.9	-3.27	537.3	-3.35	567	-3.69	558.2	-3.78
15.84	542.5	-3.31	563.7	-3.39	538.8	-3.86	535.1	-3.95
17.28	566.6	-3.35	576	-3.45	617.1	-3.79	593.8	-3.93
18.72	588.7	-3.39	617.8	-3.46	641.1	-3.85	621.9	-3.98
20.16	596.5	-3.45	620.3	-3.53	692.8	-3.84	667.6	-3.98
21.60	654.6	-3.45	672.9	-3.51	701.3	-3.93	692.3	-4.04
23.04	649	-3.5	698.2	-3.58	765.5	-3.89	720	-4.1
24.48	668.9	-3.54	709.6	-3.6	789.7	-3.94	750.9	-4.12
25.92	624.6	-3.73	680.3	-3.74	773.7	-4.07	807.5	-4.09
27.36	634.8	-3.79	703.3	-3.77	809.5	-4.09	847.1	-4.1
28.80	583	-4.12	714.6	-3.84	870.1	-4.05	966.4	-3.96
30.24	612.2	-4.12	718.3	-3.92	750.4	-4.59	767.5	-4.67
31.68	605.7	-4.32	733.3	-3.98	831.5	-4.39	796	-4.71

33.12	630.9	-4.34	764.9	-3.99	842.8	-4.49	832.2	-4.96
34.56	635.3	-4.49	757.9	-4.12	813.2	-4.83	909.5	-4.61
36.00	638.3	-4.69	761.1	-4.23	888.9	-4.61	794.7	-5.68
37.44	654.6	-4.78	788.2	-4.24	885.1	-4.8	883.0	-5.05
38.88	666.9	-4.92	788.6	-4.37	897.9	-4.93	854.5	-5.71
40.32	684.6	-5.0	770.9	-4.65	872.7	-5.45	834.8	-7.6
41.76	636.6	-	705.4	-5.92	868.2	-6.03	855.7	-
43.20		-		-				

Appendix 25 Data for Pseudo 1st and 2nd order for release of NO_3^- from 70-30

Min x10^3	t/qt NPK	Ln(q_e-q_t) NPK	t/qt SRF2	Ln(qe-qt) SRF2	t/qt CRF3	Ln (qe-qt) CRF3	t/qt CRF4-N	Ln(qe-qt) CRF4
1.44	22.5	-1.250	30.6	-1.42	45	-1.58	41.1	-1.56
2.88	35.8	-1.310	58.8	-1.43	84.7	-1.59	80	-1.56
4.32	49.4	-1.340	78.6	-1.45	105.4	-1.62	113.7	-1.58
5.76	60.9	-1.360	99.0	-1.47	144.0	-1.62	140.5	-1.59
7.20	71.6	-1.390	121.6	-1.47	161.4	-1.64	154.2	-1.62
8.64	86.8	-1.410	146.4	-1.47	183.4	-1.66	166.8	-1.64
10.08	78.2	-1.430	147.6	-1.51	193.1	-1.68	174.4	-1.68
11.52	101.2	-1.440	170.7	-1.51	217.0	-1.69	197.3	-1.68
12.96	110.6	-1.460	174.7	-1.54	211.1	-1.73	212.8	-1.69
14.40	116.0	-1.490	183.2	-1.56	229.3	-1.74	219.5	-1.72
15.84	114.5	-1.550	186.8	-1.59	232.9	-1.77	222.5	-1.75
17.28	118.0	-1.590	186.8	-1.62	232.9	-1.81	231.3	-1.77
18.72	126.3	-1.600	195.8	-1.65	241.2	-1.83	240.9	-1.79
20.16	135.8	-1.610	233.3	-1.6	250.1	-1.85	241.7	-1.82
21.60	137.1	-1.650	214.3	-1.67	254.7	-1.88	233.1	-1.88
23.04	138.3	-1.700	212.4	-1.72	257.4	-1.91	246.2	-1.89
24.48	145.4	-1.710	210.5	-1.76	236.5	-2.01	236.1	-1.96
25.92	148	-1.740	207.5	-1.81	247.1	-2.02	236.9	-2.0
27.36	149.1	-1.800	200.7	-1.88	248.1	-1.84	235.5	-2.05
28.80	139.4	-1.950	203.1	-1.91	242.2	-2.13	230.8	-2.12
30.24	140.9	-2.000	196.9	-2.0	235.3	-2.21	228.1	-2.19
31.68	140.1	-2.090	193.1	-2.08	237.3	-2.26	219.2	-2.3
33.12	137.9	-2.210	202.2	-2.08	231.1	-2.36	217.5	-2.38
34.56	135.7	-2.350	183.2	-2.3	226.6	-2.49	213.9	-2.48
36.00	135.6	-2.480	182.7	-2.39	218.6	-2.61	199.6	-2.74

37.44	134.4	-2.650	180.1	-2.51	215.5	-2.74	196.2	-2.91
38.88	133.9	-2.810	177.7	-2.66	201.9	-3.09	194.2	-3.12
40.32	133.2	-3.060	167	-3.0	195.7	-3.44	191.8	-3.36
41.76	130.8	-3.470	163.8	-3.38	187.3	-4.2	178.7	-4.47
43.20	122.9		149.3	-	181.3		176.3	

Appendix 26 Data for Pseudo 1st and 2nd order for release of $H_2PO_4^-$ from 70-30

Min x10^3		t/qt NPK-P	Ln(qe-qt) NPK-P x10^3	t/qt SRF2	Ln(qe-qt) SRF2	t/qt CRF3	Ln(qe-qt) CRF3	t/qt CRF4	Ln(qe-qt) CRF4
1.44	1	86.8	-3.57	94.7	-3.53	154.8	-3.57	118	-3.64
2.88	2	172.5	-3.58	176.7	-3.61	299.1	-3.58	230.4	-3.67
4.32	3	252.6	-3.59	249.7	-3.62	450	-3.65	332.3	-3.69
5.76	4	321.8	-3.62	323.6	-3.63	500.9	-3.68	426.7	-3.68
7.20	5	402.2	-3.62	400	-3.66	585.4	-3.71	545.5	-3.71
8.64	6	482.7	-3.62	462	-3.69	664.6	-3.71	617.1	-3.73
10.08	7	566.3	-3.62	553.9	-3.73	824.4	-3.71	755.2	-3.74
11.52	8	612.8	-3.65	562	-3.76	872.7	-3.76	789	-3.78
12.96	9	685.7	-3.66	614.2	-3.80	906.3	-3.80	836.1	-3.88
14.40	10	731	-3.69	651.6	-3.85	947.4	-3.83	813.6	-3.86
15.84	11	643.9	-3.91	679.8	-3.87	996.2	-3.85	910.3	-3.92
17.28	12	708.2	-3.9	732.2	-3.93	1060.1	-3.86	929	-3.94
18.72	13	757.9	-3.91	751.8	-3.99	1134.6	-3.92	990.5	-3.98
20.16	14	781.4	-3.97	787.5	-4.01	1132.6	-3.97	1023.4	-4.01
21.60	15	812	-4.01	821.3	-4.10	1155.1	-3.93	1069.3	-4.06
23.04	16	828.8	-4.08	825.8	-4.15	1280	-3.97	1091.9	-4.13
24.48	17	983.1	-3.92	853	-4.17	1309.1	-4.01	1097.8	-4.17
25.92	18	864	-4.21	890.7	-4.25	1296	-4.15	1127	-4.20
27.36	19	788.5	-4.61	906	-4.38	1255.1	-4.12	1169.2	-4.31
28.80	20	757.9	-5.01	900	-4.63	1345.8	-4.19	1152	-4.40
30.24	21	819.5	-4.85	871.5	-4.65	1350	-4.29	1158.6	-4.48
31.68	22	894.9	-4.68	907.7	-4.76	1325.5	-4.31	1169	-4.60
33.12	23	914.9	-4.77	922.6	-4.85	1374.3	-4.43	1170.3	-4.68
34.56	24	888.4	-5.15	941.7	-4.95	1344.8	-4.53	1187.6	-4.82
36.00	25	909.1	-5.28	962.6	-5.68	1343.3	-4.89	1188.1	-4.95
37.44	26	931.3	-5.38	911	-6.73	1243.9	-4.92	1235.6	-5.12
38.88	27	997.4	-5.15	897.9	-6.12	1283.2	-5.66	1200	-5.63
40.32	28	995.6	-5.47	953.2	-5.45	1182.4	-6.81	1158.6	-5.84
41.76	29	994.3	-5.91	1036.2		1144.1		1176.3	-

43.20	30								

Appendix 27 Data for Pseudo 1st and 2nd order for release of K^+ from 70-30

Min $x10^3$	t/qt NPK	Ln(qe-qt) NPK	t/qt SRF2-K	Ln(qe-qt) SRF2-K	t/qt CRF3-K	Ln(qe-qt) CRF3-K	t/qt CRF4-K	Ln(qe-qt) CRF4-K
1.44	70.9	-3.09	74.6	-3.22	80.9	-3.36	77.8	-3.32
2.88	133.3	-3.12	144.7	-3.25	152.4	-3.39	149.2	-3.29
4.32	195	-3.14	209.7	-3.25	225	-3.41	216	-3.32
5.76	187.6	-3.18	261.8	-3.67	285.2	-3.42	288	-3.32
7.20	301.3	-3.18	315.8	-3.32	292.7	-3.46	276.9	-3.35
8.64	361.5	-3.18	354.1	-3.33	392.7	-3.47	387.4	-3.5
10.08	387.7	-3.24	400	-3.37	411.4	-3.51	418.3	-3.42
11.52	411.4	-3.29	417.4	-3.35	443.1	-3.53	415.9	-3.41
12.96	451.6	-3.3	489.1	-3.44	489.1	-3.54	498.5	-3.47
14.40	519.9	-3.27	537.3	-3.44	566.9	-3.57	558.1	-3.5
15.84	542.5	-3.31	563.7	-3.47	538.8	-3.62	535.1	-3.52
17.28	566.6	-3.35	576	-3.5	617.1	-3.65	593.8	-3.58
18.72	588.7	-3.39	617.8	-3.52	641.1	-3.68	621.9	-3.62
20.16	596.5	-3.45	620.3	-3.56	692.8	-3.75	667.6	-3.63
21.60	654.6	-3.45	672.9	-3.61	701.3	-3.81	692.3	-3.7
23.04	649	-3.5	698.2	-3.67	765.5	-3.86	720	-3.74
24.48	668.9	-3.54	709.6	-3.71	789.7	-3.87	750.9	-3.8
25.92	624.6	-3.73	680.3	-3.73	773.7	-3.96	807.5	-3.82
27.36	634.8	-3.79	703.3	-3.79	809.5	-4.01	847.1	-3.88
28.80	583	-4.12	714.6	-3.92	870.1	-4.08	966.4	-3.96
30.24	612.2	-4.12	718.3	-3.86	750.4	-4.29	767.5	-3.95
31.68	605.7	-4.32	733.3	-4.01	831.5	-4.06	796	-4.11
33.12	630.9	-4.34	764.9	-4.31	842.8	-4.33	792.3	-4.1
34.56	635.3	-4.49	757.9	-4.26	813.2	-4.47	909.5	-4.31
36.00	638.3	-4.69	761.1	-4.3	888.9	-5.13	794.7	-4.39
37.44	654.6	-4.78	788.2	-4.51	885.1	-4.43	883	-4.6
38.88	666.9	-4.92	788.4	-4.72	897.9	-4.69	854.5	-4.72
40.32	684.6	-5.0	770.9	-5.12	872.7	-5.02	834.8	-5.13
41.76	636.6	-	705.4	-5.63	868.2	-4.82	855.7	-5.7

43.20		-				-		0

Appendix 28 data for pseudo 1st and 2nd order reaction rates for NO_3^-

Time $x10^3$	$Ln(q_e-q_t)$ NPK	t/q_t $x10^3$ NPK	$Ln(q_e-q_t)$ SRF2 $x10^3$	t/q_t SRF2	$Ln(q_e-q_t)$ CRF3 $x10^3$	t/q_t $x10^{-3}$CRF3	$Ln(q_e-q_t)$ CRF4 $x10^3$	t/q_t $x10^{-3}$CRF4
20.16	5.900	3.506	3.300	7.278	-0.800	7.968	0.300	7.636
40.32	3.900	6.632	2.300	13.904	-1.500	15.628	-0.800	14.662
60.48	3.400	9.818	1.800	20.432	-4.000	21.834	-5.100	19.700
80.64	1.400	12.580	1.100	26.526	-7.300	27.243	-2.700	27.807
100.80	-3.300	14.737	0.400	32.308	-13.10	31.798	-9.700	30.638
120.96	-9.200	16.894	-6.900	33.049	-19.00	36.655	-11.400	36.216

Appendix 29 data for pseudo 1st and 2nd order reaction rates for $H_2PO_4^-$

Time $x10^3$	$Ln(q_e-q_t)$ NPK	t/q_t NPK	$Ln(q_e-q_t)$ SRF2	t/q_t SRF2	$Ln(q_e-q_t)$ CRF3	t/q_t CRF3	$Ln(q_e-q_t)$ CRF4	t/q_t CRF4
20.16	-0.940	3.215	-7.550	3.405	1.570	4.073	0.860	4.040
40.32	-1.390	6.390	-9.420	6.731	-1.00	7.875	-1.390	7.754
60.48	-7.550	9.027	-16.100	9.755	-1.500	11.498	-3.290	11.284
80.64	-11.400	11.755	-18.300	12.944	-3.570	14.878	-7.990	14.323
100.80	-13.500	14.567	-14.300	16.390	-7.990	17.809	13.100	17.349
120.96	-24.100	17.061	-25.300	19.170	-9.420	21.110	22.100	20.295

Appendix 30 Data for pseudo 1st and 2nd order reaction rates for K

Time $x10^3$	$In(q_e-q_t)$ NPK	t/qt $x10^3$ NPK	$In(q_e-q_t)$ SRF2	t/qt $x10^3$ SRF2	$In(q_e-q_t)$CRF	t/qt $x10^3$ CRF3	$In(q_e-q_t)$ CRF4	$t/qtx10^3$ CRF4
20.16	1.250	0.3476	0.41	0.3587	0.52	0.4271	0.660	0.4065
40.32	1.190	0.6754	0.37	0.7099	0.67	0.9040	0.440	0.7565
60.48	1.150	0.9882	0.20	1.0234	0.37	1.2268	0.250	0.9899
80.64	0.980	1.2200	-1.74	1.1586	-0.41	1.4049	0.280	1.3155

100.80	0.700	1.3865	1.20	1.4758	-2.27	1.5799	0.680	1.5799
120.96	-0.130	1.4417	1.73	1.7379	-	1.8667	1.090	1.8467

Appendix 31 Equations for conversion of absorbance into ppm the into gL^{-1}

Nutrient	50-50 formula	Eqtn	70-30 formula	Eqtn	Soils	Eqtns
NO_3^-	$\frac{yxvol1x1000}{Gxvol2xW}$	4a	$\frac{yxvol1x1000}{Gxvol2xW}$	4g	$\frac{Ax3}{GxVx1}$	4m
	$\frac{62x1.629xppm}{101x1000}$	4b	$\frac{62x1.629xppm}{101x1000}$	4h	$\frac{62x1.629xppm}{101x1000}$	4n
					$\frac{Ax3}{GxVx2}$	4o
$H_2PO_4^-$	$\frac{yxvol1x1000}{Gxvol2xW}$	4c	$\frac{yxvol1x1000}{Gxvol2xW}$	4i	$\frac{Ax3}{GxVx1}$	4p
	$\frac{97x1.403xppm}{136.09x1000}$	4d	$\frac{97x1.403xppm}{136.09x1000}$	4j	$\frac{97x1.403xppm}{136.09x1000}$	4q
					$\frac{Ax3}{GxVx2}$	4r
K^+	$\frac{yxvol1x1000}{Gxvol2xW}$	4e	$\frac{yxvol1x1000}{Gxvol2xW}$	4k	$\frac{Ax3}{GxVx1}$	4s
	$\frac{39x1.912xppm}{74.5x1000}$	4f	$\frac{39x1.912xppm}{74.5x1000}$	4l	$\frac{39x3.49xppm}{136.09x1000}$	4t
					$\frac{Ax3}{GxVx2}$	4u